DOT/FAA/CT-82/33-I

COMPUTER SIMULATION OF AN AIRCRAFT SEAT AND OCCUPANT IN A CRASH ENVIRONMENT

VOLUME I-TECHNICAL REPORT

David H. Laananen
Akif O. Bolukbasi
Joseph W. Coltman

March 1983

Final Report

U.S Department of Transportation
Federal Aviation Administration
Technical Center
Atlantic City Airport, N.J. 08405

NOTICE

This document is disseminated under the sponsorship of the Department of Transportation in the interest of information exchange. The United States Government assumes no liability for the contents or use thereof.

The United States Government does not endorse products or manufacturers. Trade or manufacturer's names appear herein solely because they are considered essential to the object of this report.

Technical Report Documentation Page

1. Report No.	2. Government Accession No.	3. Recipient's Catalog No.
DOT/FAA/CT-82/33-I		

4. Title and Subtitle	5. Report Date
COMPUTER SIMULATION OF AN AIRCRAFT SEAT AND OCCUPANT IN A CRASH ENVIRONMENT-VOLUME I - TECHNICAL REPORT	March 1983
	6. Performing Organization Code
7. Author(s) D. H. Laananen, A. O. Bolukbasi, and J. W. Coltman	8. Performing Organization Report No. TR 82401
9. Performing Organization Name and Address Simula Inc. 2223 S. 48th Street Tempe, Arizona 85282	10. Work Unit No. (TRAIS) 11. Contract or Grant No. DTFA03-80-C-00098
12. Sponsoring Agency Name and Address Federal Aviation Administration Technical Center Atlantic City Airport, New Jersey 08405	13. Type of Report and Period Covered FINAL September 1980 - September 1982 14. Sponsoring Agency Code ACT-330

15. Supplementary Notes

16. Abstract

A mathematical model of an aircraft seat, occupant, and restraint system has been developed for use in analysis of light aircraft crashworthiness. Because of the significant role played by the seat in overall system crashworthiness, a finite element model of the seat structure is included. The seat model can accommodate large plastic deformations and includes the capability for simulation of local buckling of bending members. Because the program has been written for use primarily by engineers concerned with the design and analysis of seat and restraint systems, an effort has been made to minimize the input data required to describe the occupant. This volume of the final report discusses development of the mathematical model of the occupant, the finite element seat analysis, validation, and organization of the computer program.

17. Key Words	18. Distribution Statement
Aircraft Computer Simulation Crashworthiness Restraint Systems Seats	Document is available to the U.S. public through the National Technical Information Service, Springfield, Virginia 22161

19. Security Classif. (of this report)	20. Security Classif. (of this page)	21. No. of Pages	22. Price
Unclassified	Unclassified	160	

Form DOT F 1700.7 (8-72)

FOREWORD

This report was prepared by Simula Inc. under Contract No. DTFA03-80-C-00098 with the Federal Aviation Administration (FAA) Technical Center, where L. M. Neri acted as Technical Monitor. Under the same contract, final modifications were made to both seat and occupant models, and validation was completed. The project had been originally initiated under a contract with the FAA Systems Research and Development Service and continued with the support of the Civil Aeromedical Institute.

The Simula Inc. Program Manager has been Dr. D. H. Laananen, and final modifications to the computer program have been developed by A. O. Bolukbasi and J. W. Coltman. Data for model validation have been provided by the Protection and Survival Laboratory, FAA Civil Aeromedical Institute, where a comprehensive test program was conducted under the leadership of R. F. Chandler, who has also provided valuable guidance throughout this project. J. Gillespie of the Flight Standards National Field Office, Oklahoma City, has also been of great assistance during program development and validation.

TABLE OF CONTENTS

TABLE OF CONTENTS (CONTD)

LIST OF ILLUSTRATIONS

LIST OF ILLUSTRATIONS (CONTD)

LIST OF ILLUSTRATIONS (CONTD)

LIST OF ILLUSTRATIONS (CONTD)

LIST OF ILLUSTRATIONS (CONTD)

LIST OF ILLUSTRATIONS (CONTD)

EXECUTIVE SUMMARY

Program SOM-LA (Seat/Occupant Model - Light Aircraft) has been developed for use in evaluating the crashworthiness of aircraft seats and restraint systems. It combines a three-dimensional dynamic model of the human body with a finite element model of the seat structure. It is intended to provide the design engineer a tool with which he can analyze the structural elements of the seat as well as evaluate the dynamic response of the occupant during a crash.

The occupant model consists of twelve masses that represent the upper and lower torso, neck, head, and two segments for each of the arms and legs. An optional model of the human body includes beam elements in the spine and neck, but is restricted to two-dimensional motion.

External forces are applied to the occupant by the cushions, floor, and restraint system. Interface between the occupant and seat is provided by the seat bottom cushion, back cushion, and an optional headrest. The restraint system can consist of a lap belt alone or combined with a single shoulder belt, over either shoulder, or a double-strap shoulder harness. A lap belt tiedown strap, or negative-G strap, can also be included. Each component of the restraint system can be attached to either the seat or the aircraft structure.

For two standard occupants, a 50th-percentile human male and a 50th-percentile (Part 572) anthropomorphic dummy, all dimensions and inertial properties required for simulation are stored within the program. For other occupants, these characteristics must be provided as input.

The seat structure is modeled using the finite element method of analysis, selected because it is not dependent on previous testing, and it has the flexibility to deal with a wide range of design concepts. The SOM-LA seat analysis includes triangular plate elements, three-dimensional beam elements, and spring elements. It has the capability to model large displacements, nonlinear material behavior, local buckling, and various internal releases for beam elements.

The digital computer program based on the occupant and seat models described above has been written entirely in FORTRAN to ensure a high degree of compatibility with various digital computer systems. During development, the program has been run on IBM, Univac, and CDC computer systems. Output data include occupant segment positions, velocities, and accelerations; restraint system and cushion forces; injury criteria; and details of contact between the occupant and the aircraft interior. Seat output includes nodal displacements, element stresses, and forces at the points of attachment to the aircraft structure.

Validation has been based on data from several series of deceleration sled tests conducted at the FAA Civil Aeromedical Institute (CAMI). The response of the combined occupant and seat models was verified by comparison with data from tests that utilized specially designed and fabricated seats with replaceable legs. The test conditions in that series were specifically selected to cause significant plastic deformation of the legs. Response of the occupant model, particularly to a vertical input acceleration, was validated using data from other test series conducted with a rigid seat and with a production energy-absorbing helicopter seat. The final phase of validation included simulation of dynamic tests of production general aviation seats. The tests are described in the report, and model predictions are compared with test data. The SOM-LA program is shown to be a potentially useful tool for analyzing the performance of a seat and restraint system in a crash environment.

1.0 INTRODUCTION

The design of crashworthy seats and restraint systems for aircraft presents a complex engineering problem, the solution of which can be greatly aided by sufficiently rigorous analytical techniques. The crash environment can vary widely from one accident to another, thus a great number of conditions must be evaluated to establish those critical to occupant survival. For example, the restraint system must limit the movement of the occupant sufficiently to eliminate the possibility of head strike on rigid cockpit structure. Also, the relatively low tolerance of the human body to accelerations in a direction parallel to the spine requires the consideration of vertical impact forces which are usually present and often significant in crashes of light fixed-wing aircraft and helicopters (reference 1). A very strong, rigid seat is not a truly valid solution, since it would not only incur serious weight penalties, but would transmit high vertical impact forces directly to the occupant. In light aircraft and helicopters, it is seldom practical to consider designing sufficient energy-absorbing capability into the lower airframe structure to protect against these vertical forces, as the crush space is generally not available. Rather, a crashworthy seat for these aircraft should include the capacity to absorb energy through controlled deformation in the vertical direction, thus reducing the accompanying loads.

In the initial design phases, it is desirable to evaluate, in some detail, existing seats and restraint systems in their surrounding cockpits, thus establishing existing weaknesses. It is then desirable to make modifications and to evaluate the effect of these modifications on improving the survivability of the system. These evaluations must be conducted for a great many of the possible crash environments, thus constituting a relatively large matrix. Testing is extremely expensive and requires a great deal of time, since design modifications must be developed and fabricated prior to testing. Therefore, an analytical technique, such as was developed in this program, is required.

A number of one-, two-, and three-dimensional mathematical models of the human body have been developed for crash survivability analysis. These models vary in complexity and possess from one to forty degrees of freedom. The simplest models have been developed primarily for prediction of injury to a single component or subsystem of the body, such as vertebral injury due to the vertical force that might be experienced in a crash or the firing of an ejection seat. Simulation of the three-dimensional response of the entire body requires many more degrees of freedom, but permits more general use. Most of the three-dimensional models have been developed for use in evaluation of automobile interior design with respect to injuries caused by secondary impacts, such as the three-dimensional models described in references 2 through 5. Seats have been represented in a very simple manner because in automobiles the role of the seat design in determining occupant survival is minimal. Therefore, a simulation model intended specifically for the aircraft application is required.

The development of a three-dimensional mathematical model of a light aircraft seat, occupant, and restraint system is described in this report. This model forms the basis for a simulation computer program that has been written specifically for use in crashworthy design and analysis of light aircraft seats and restraint systems, Program SOM-LA (Seat/Occupant Model-Light Aircraft). The program, which combines a finite element model of the seat structure with a lumped-parameter model of the aircraft occupant, has been organized so as to minimize the volume and complexity of input data and to focus on seat and restraint system design parameters.

This original model was described in a comprehensive technical report that was published by the FAA in 1975 (reference 6). A number of modifications have been made to the model since then to improve simulation quality and to provide increased capability and additional desirable output. In 1977, a testing program was initiated by the Civil Aeromedical Institute (CAMI) to provide

data for validation of the model. The validation effort pointed out areas, particularly in the seat structure model, where modifications to the program were required. Also, use of the program both by its developers and other organizations demonstrated the need for additional capabilities. Probably the most significant change to the program since publication of reference 6 has been the incorporation of a more general finite element seat model with capabilities of simulating large, inelastic deformations and crippling of hollow members. With respect to the occupant model, the program user now has the option of either a three-dimensional occupant made up of rigid segments or a two-dimensional model which has beam elements representing the spine and neck, thus providing greater capability for injury prediction.

Presented in this report are the details of the occupant and seat models, as well as the results of model validation. Operation of the computer program is described in Volume II of this report, Program SOM-LA User Manual.

2.0 OCCUPANT MODEL

The mathematical model includes a lumped-parameter representation of the vehicle occupant and a finite element seat. Interface between the seat and occupant is provided by seat cushions and a restraint system, which consists of a lap belt and, if desired, a single-strap or double-strap shoulder harness. A lap belt tiedown strap, or negative-G strap, can be added for simulation of a full, five-point restraint system. The response of the occupant and seat can be predicted for any given set of aircraft impact conditions, including the initial velocity and attitude and the input acceleration.

As mentioned in chapter 1.0, both a three-dimensional occupant model consisting of rigid links and a two-dimensional model with deformable spinal elements are included. This chapter provides a discussion of the development of both models, including details of the approach to formulating the equations of motion and of the technique used for their solution. Section 2.1 presents the three-dimensional model and section 2.2, the two-dimensional model. Subsequent sections cover aspects of the equations which apply to both models, specifically the body joint model, the treatment of external forces, and body dimensions and properties.

2.1 THREE-DIMENSIONAL OCCUPANT MODEL

The three-dimensional mathematical model of the aircraft occupant is made up of twelve rigid segments, as shown in figure 1. This number is thought to represent the minimum that will permit accurate, meaningful simulation of three-dimensional response. A greater number might possibly improve the accuracy of simulation but would, in turn, increase program execution cost. Arm and leg segments are included to enable prediction of injuries to these extremities. Although leg and arm injuries, in themselves, may not be as serious as head or chest injuries, they may prevent excape from a stricken aircraft and the potential hazard of post-crash fire.

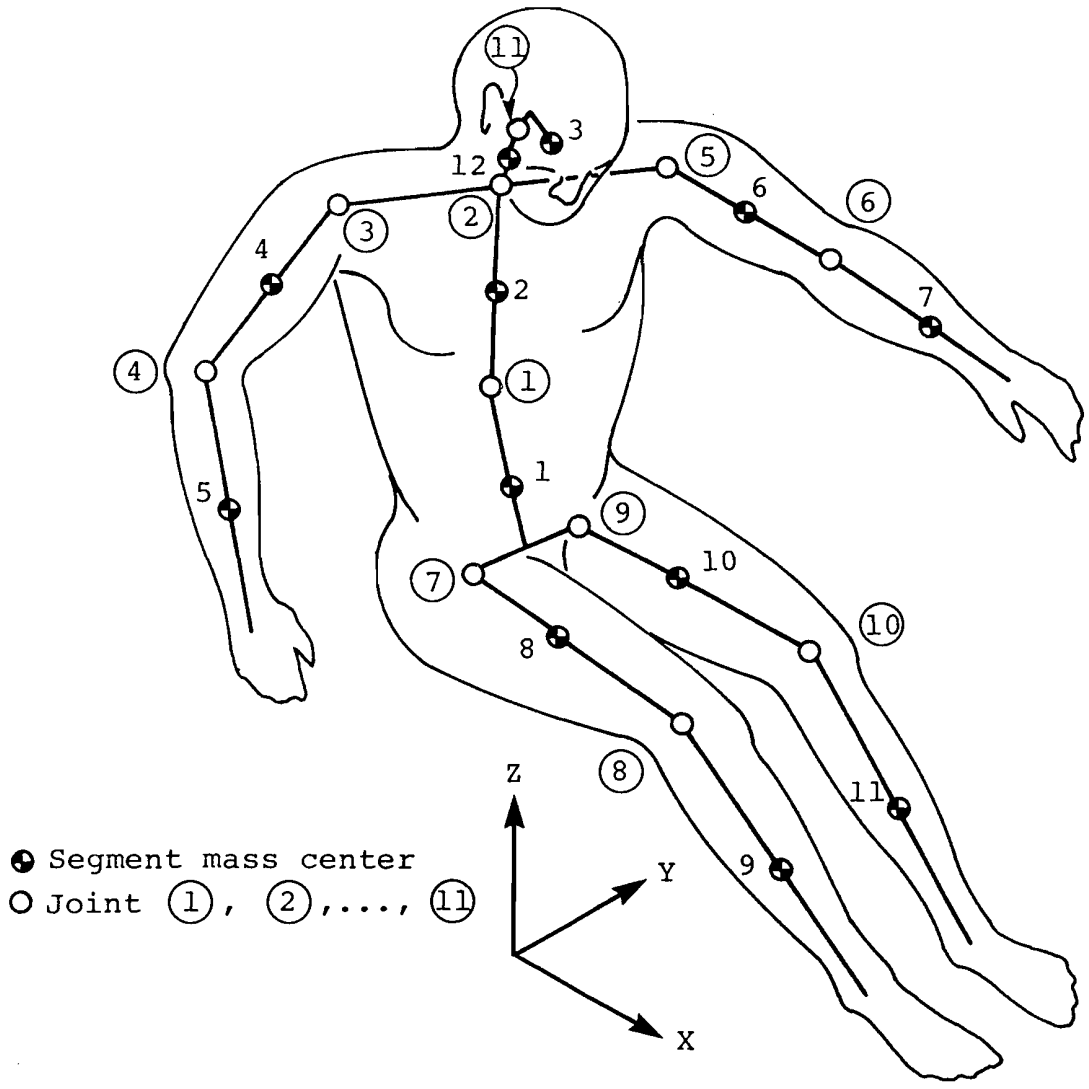

Figure 1. Twelve-segment (three-dimensional) occupant model.

Each of the body joints, with the exception of the elbow, knee, and head-neck joints, possesses three rotational degrees of freedom. Because of the hinge-type motion of a forearm or lower leg relative to an upper arm or thigh, respectively, the position of each of these segments is described by one additional angular coordinate, as is the position of the head relative to the neck. Therefore, the occupant system possesses a total of 29 degrees of freedom.

2.1.1 Coordinate Systems

Fixed at the center of mass of each of the 12 segments is a right-handed Cartesian coordinate system. For segment n (n = 1 2,..., 12) the local coordinate system is denoted by axes (x_n, y_n, z_n). Positive directions are defined such that when the body is seated as shown in figure 2, with the torso and head upright, the upper arms parallel to the torso, and the elbows and knees bent at right angles, positive x_n is directed forward, y_n to the left, and z_n upward.

In order to describe a general position of the body, it is necessary to relate the orientation of each segment (x_n, y_n, z_n) to the inertial system (X, Y, Z). The angular relationship between the local, segment-fixed coordinates and the inertial system can be expressed by the transformation

$$\begin{Bmatrix} X_n \\ Y_n \\ Z_n \end{Bmatrix} = \begin{bmatrix} \\ T^n \\ \\ \end{bmatrix} \begin{Bmatrix} x_n \\ y_n \\ z_n \end{Bmatrix} \qquad (1)$$

Because three angular coordinates can be used to define the rotation of a given segment, it is convenient to utilize a set of coordinates that will suffice as generalized coordinates in the formulation of the equations of motion. A system of Eulerian angles provides a convenient set of three independent angular coordinates. Assuming that the local (x_n, y_n, z_n) system is initially coincident with the inertial (X, Y, Z) system, the Euler angles are a series of three rotations, which, when performed in the proper sequence, permit the system to attain any orientation and uniquely define that position. The particular set of Euler angles selected for use here is illustrated in figure 3 and defined as follows:

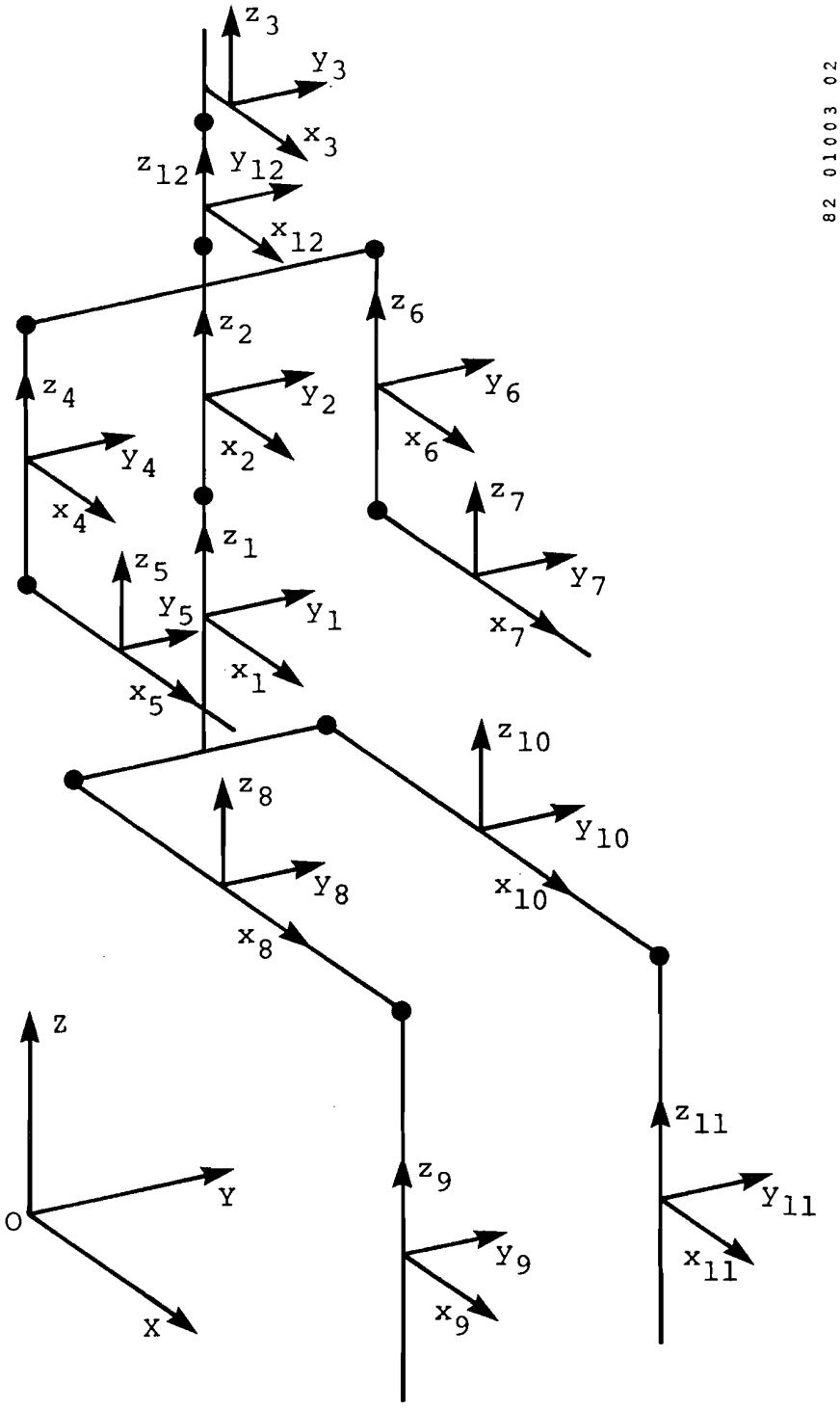

Figure 2. Segment-fixed local coordinate systems.

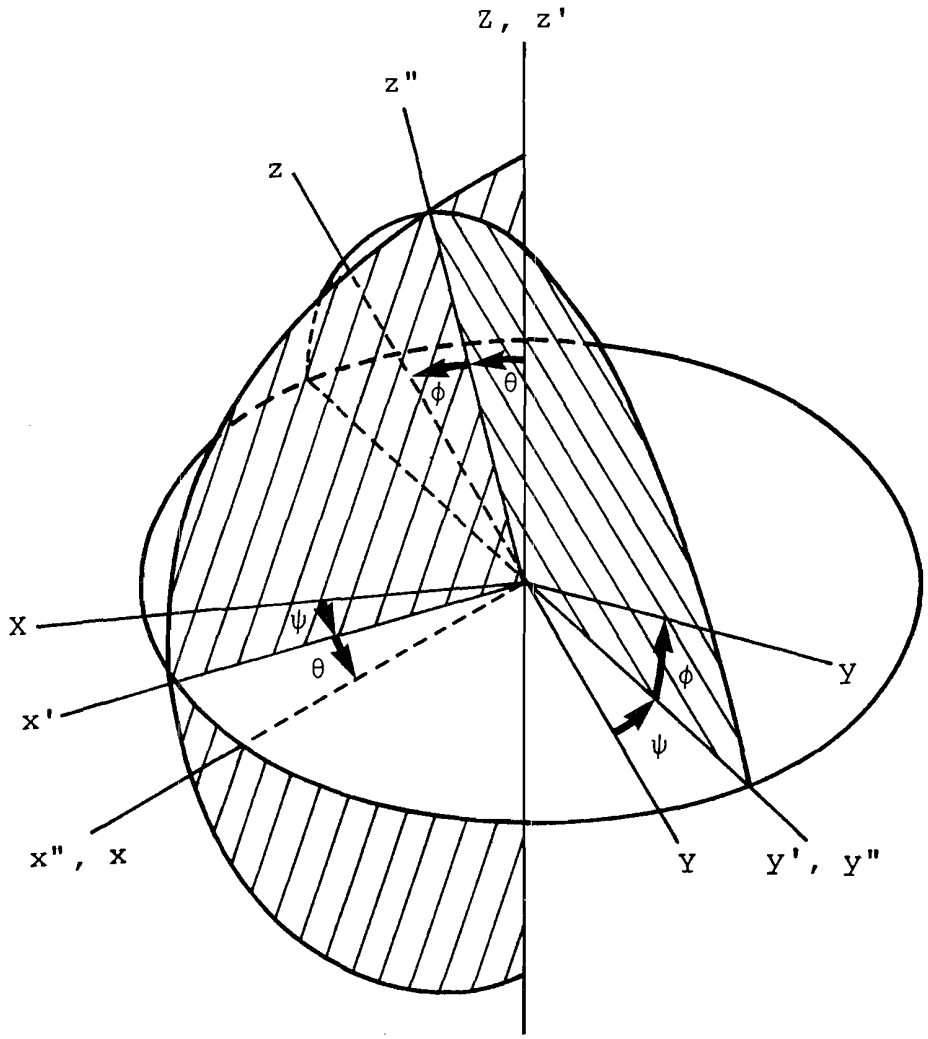

Figure 3. The Euler angles.

1. A positive rotation ψ about the Z-axis, resulting in the primed (x', y', z') system.

2. A positive rotation θ about the y'-axis resulting in the double-primed (x", y", z") system.

3. A positive rotation ϕ about the x"-axis resulting in the final (x, y, z) system.

In order to determine the elements of the transformation matrix $[T^n]$, it is necessary to consider the matrix equations that indicate the three individual rotations previously described above. Referring again to these definitions of ψ, θ, and ϕ, the following equations are obtained:

$$\begin{Bmatrix} X \\ Y \\ Z \end{Bmatrix} = \begin{bmatrix} \cos\psi & -\sin\psi & 0 \\ \sin\psi & \cos\psi & 0 \\ 0 & 0 & 1 \end{bmatrix} \begin{Bmatrix} x' \\ y' \\ z' \end{Bmatrix} \tag{2}$$

$$\begin{Bmatrix} x' \\ y' \\ z' \end{Bmatrix} = \begin{bmatrix} \cos\theta & 0 & \sin\theta \\ 0 & 1 & 0 \\ -\sin\theta & 0 & \cos\theta \end{bmatrix} \begin{Bmatrix} x'' \\ y'' \\ z'' \end{Bmatrix} \tag{3}$$

$$\begin{Bmatrix} x'' \\ y'' \\ z'' \end{Bmatrix} = \begin{bmatrix} 1 & 0 & 0 \\ 0 & \cos\phi & -\sin\phi \\ 0 & \sin\phi & \cos\phi \end{bmatrix} \begin{Bmatrix} x \\ y \\ z \end{Bmatrix} \tag{4}$$

Writing equations (2) through (4) in abbreviated form

$$\{R\} = [\psi]\ \{r'\}$$

$$\{r'\} = [\theta]\ \{r''\}$$

$$\{r''\} = [\phi]\ \{r\}$$

or

$$\{R\} = [\psi]\ [\theta]\ [\phi]\ \{r\} \tag{5}$$

where $\{R\}$ represents the components of a vector in the inertial system and $\{r\}$ represents the same vector in the final (x, y, z) system. Performing the matrix multiplications indicated in equation (5), the elements of the transformation matrix in equation (1) are obtained:

$$T_{11}^{n} = \cos\psi_n \cos\theta_n$$

$$T_{12}^{n} = \cos\psi_n \sin\theta_n \sin\phi_n - \sin\psi_n \cos\phi_n$$

$$T_{13}^{n} = \cos\psi_n \sin\theta_n \cos\phi_n + \sin\psi_n \sin\phi_n$$

$$T_{21}^{n} = \sin\psi_n \cos\theta_n$$

$$T_{22}^{n} = \sin \psi_n \sin \theta_n \sin \phi_n + \cos \psi_n \cos \phi_n$$

$$T_{23}^{n} = \sin \psi_n \sin \theta_n \cos \phi_n - \cos \psi_n \sin \phi_n$$

$$T_{31}^{n} = -\sin \theta_n$$

$$T_{32}^{n} = \cos \theta_n \sin \phi_n$$

$$T_{33}^{n} = \cos \theta_n \cos \phi_n$$

$$\text{for } n = 1, 2, 3, 4, 6, 8, 10 \qquad (6)$$

The additional constraint of hinge-type rotation, at the elbows and knees, requires the use of one additional angular coordinate to define the position of each of the forearm and lower leg segments. Referring to figure 4, the angular position of the forearm segments ($\ell = 5, 7$) is given by

$$\begin{Bmatrix} X_\ell \\ Y_\ell \\ Z_\ell \end{Bmatrix} = \begin{bmatrix} T^n \end{bmatrix} \begin{bmatrix} \sin\alpha_\ell & 0 & \cos\alpha_\ell \\ 0 & 1 & 0 \\ -\cos\alpha_\ell & 0 & \sin\alpha_\ell \end{bmatrix} \begin{Bmatrix} x_\ell \\ y_\ell \\ z_\ell \end{Bmatrix} \qquad (7)$$

and the lower leg segments (m = 9, 11) by

$$\begin{Bmatrix} X_m \\ Y_m \\ Z_m \end{Bmatrix} = \begin{bmatrix} T^n \end{bmatrix} \begin{bmatrix} \sin\alpha_m & 0 & -\cos\alpha_m \\ 0 & 1 & 0 \\ \cos\alpha_m & 0 & \sin\alpha_m \end{bmatrix} \begin{Bmatrix} x_m \\ y_m \\ z_m \end{Bmatrix} \qquad (8)$$

From equations (6) and (7), the elements of the transformation matrix for the forearms (segments 5 and 7) are written as:

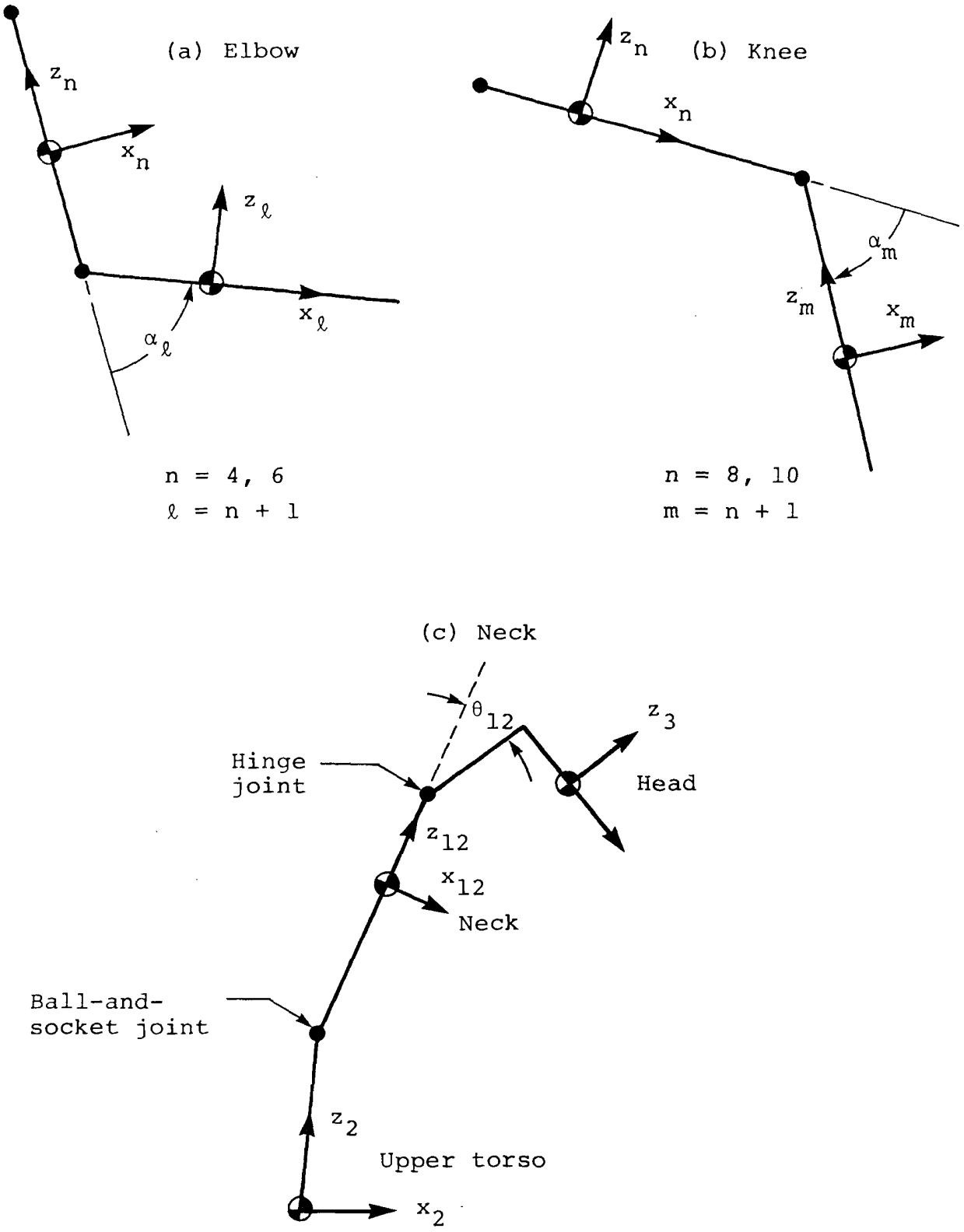

Figure 4. Definition of angular coordinates α for elbows, knees, and neck.

$$T_{11}^{\ell} = \cos\psi_n \cos\theta_n \sin\alpha_\ell - \cos\psi_n \sin\theta_n \cos\phi_n \cos\alpha_\ell$$
$$- \sin\psi_n \sin\phi_n \cos\alpha_\ell$$

$$T_{12}^{\ell} = \cos\psi_n \sin\theta_n \sin\phi_n - \sin\psi_n \cos\phi_n$$

$$T_{13}^{\ell} = \cos\psi_n \cos\theta_n \cos\alpha_\ell + \cos\psi_n \sin\theta_n \cos\phi_n \sin\alpha_\ell$$
$$+ \sin\psi_n \sin\phi_n \sin\alpha_\ell$$

$$T_{21}^{\ell} = \sin\psi_n \cos\theta_n \sin\alpha_\ell - \sin\psi_n \sin\theta_n \cos\phi_n \cos\alpha_\ell$$
$$+ \cos\psi_n \sin\phi_n \cos\alpha_\ell$$

$$T_{22}^{\ell} = \sin\psi_n \sin\theta_n \sin\phi_n + \cos\psi_n \cos\phi_n$$

$$T_{23}^{\ell} = \sin\psi_n \cos\theta_n \cos\alpha_\ell + \sin\psi_n \sin\theta_n \cos\phi_n \sin\alpha_\ell$$
$$- \cos\psi_n \sin\phi_n \sin\alpha_\ell$$

$$T_{31}^{\ell} = - \sin\theta_n \sin\alpha_\ell - \cos\theta_n \cos\phi_n \cos\alpha_\ell$$

$$T_{32}^{\ell} = \cos\theta_n \sin\phi_n$$

$$T_{33}^{\ell} = - \sin\theta_n \cos\alpha_\ell + \cos\theta_n \cos\phi_n \sin\alpha_\ell \qquad (9)$$

From equations (6) and (8), the elements of the transformation matrix elements for the legs (segments 9 and 11) are obtained:

$$T_{11}^{m} = \cos\psi_n \cos\theta_n \sin\alpha_m + \cos\psi_n \sin\theta_n \cos\phi_n \cos\alpha_m$$
$$+ \sin\psi_n \sin\phi_n \cos\alpha_m$$

$$T_{12}^{m} = \cos\psi_n \sin\theta_n \sin\phi_n - \sin\psi_n \cos\phi_n$$

$$T_{13}^{m} = -\cos\psi_n \cos\theta_n \cos\alpha_m + \cos\psi_n \sin\theta_n \cos\phi_n \sin\alpha_m + \sin\psi_n \sin\phi_n \sin\alpha_m$$

$$T_{21}^{m} = \sin\psi_n \cos\theta_n \sin\alpha_m + \sin\psi_n \sin\theta_n \cos\phi_n \cos\alpha_m - \cos\psi_n \sin\phi_n \cos\alpha_m$$

$$T_{22}^{m} = \sin\psi_n \sin\theta_n \sin\phi_n + \cos\psi_n \cos\phi_n$$

$$T_{23}^{m} = -\sin\psi_n \cos\theta_n \cos\alpha_m + \sin\psi_n \sin\theta_n \cos\phi_n \sin\alpha_m - \cos\psi_n \sin\phi_n \sin\alpha_m$$

$$T_{31}^{m} = -\sin\theta_n \sin\alpha_m + \cos\theta_n \cos\phi_n \cos\alpha_m$$

$$T_{32}^{m} = \cos\theta_n \sin\phi_n$$

$$T_{33}^{m} = \sin\theta_n \cos\alpha_m + \cos\theta_n \cos\phi_n \sin\alpha_m \qquad (10)$$

Segment 12, the neck, was added later. The hinge-type joint between the neck and the head is treated similarly to the knee joints, adding the generalized coordinate θ_{12}, as illustrated in figure 4.

Having developed the relationships expressed in the equations (1) through (10), the position of the occupant can be described by the following set of generalized coordinates:

$q_1 = X_1$	$q_{11} = \theta_3$	$q_{21} = \psi_8$
$q_2 = Y_1$	$q_{12} = \phi_3$	$q_{22} = \theta_8$
$q_3 = Z_1$	$q_{13} = \psi_4$	$q_{23} = \phi_8$
$q_4 = \psi_1$	$q_{14} = \theta_4$	$q_{24} = \alpha_9$

$$q_5 = \theta_1 \qquad q_{15} = \phi_4 \qquad q_{25} = \psi_{10}$$

$$q_6 = \phi_1 \qquad q_{16} = \alpha_5 \qquad q_{26} = \theta_{10}$$

$$q_7 = \psi_2 \qquad q_{17} = \psi_6 \qquad q_{27} = \phi_{10}$$

$$q_8 = \theta_2 \qquad q_{18} = \theta_6 \qquad q_{28} = \alpha_{11}$$

$$q_9 = \phi_2 \qquad q_{19} = \phi_6 \qquad q_{29} = \theta_{12}$$

$$q_{10} = \psi_3 \qquad q_{20} = \alpha_7 \qquad (11)$$

The above coordinates include the Cartesian coordinates of the mass center of segment 1 (X_1, Y_1, Z_1), selected as a reference point on the body, seven sets of Eulerian angles, and the five additional angular coordinates for the elbows, knees, and neck. Positions of the segment mass centers are presented in appendix A.

2.1.2 Lagrange's Equations

The response of the occupant system is described by Lagrange's equations of motion, which are written for the 29 generalized coordinates. The equations are developed according to

$$\frac{d}{dt}\left(\frac{\partial L}{\partial \dot{q}_j}\right) - \frac{\partial L}{\partial q_j} = Q_j \qquad (j = 1, 2, \ldots, 29) \qquad (12)$$

where L is the Lagrangian function

$$L = T - V \qquad (13)$$

t represents time, Q_j are the generalized forces not derivable from a potential function. (Forces that are derivable from a potential function are obtained from L, and T and V are the system kinetic and potential energies, respectively.)

Because the system being treated does not involve any velocity-dependent potentials, equation (12) can be written as

$$\frac{d}{dt}\frac{\partial}{\partial}\left(\frac{\partial T}{\partial \dot{q}_j}\right) - \frac{\partial T}{\partial q_j} + \frac{\partial V}{\partial q_j} = Q_j \qquad (j = 1, 2, \ldots, 29) \tag{14}$$

The system kinetic energy contains both translational and rotational parts:

$$T = \frac{1}{2}\sum_{n=1}^{12} M_n\left[(\dot{X}_n)^2 + (\dot{Y}_n)^2 + (\dot{Z}_n)^2\right] + \frac{1}{2}\sum_{n=1}^{12}\left(I_{x_n}\,\omega_{x_n}^{\,2} + I_{y_n}\,\omega_{y_n}^{\,2} + I_{z_n}\,\omega_{z_n}^{\,2}\right) \tag{15}$$

where M_n is the mass of segment n and I_{x_n}, I_{y_n}, and I_{z_n} are mass moments of inertia of segment n with respect to the local coordinate axes (x_n, y_n, z_n), assumed to be principal moments of inertia.

The absolute velocities of the 12 mass segments required for the translational kinetic energy must, of course, be written as functions of the generalized coordinates and generalized velocities in order to use equation (14). The angular velocity components (ω_{x_n}, ω_{y_n}, ω_{z_n}) seen in equation (15) are parallel to the local (x_n, y_n, z_n) coordinate systems. These angular velocity components cannot be used directly in Lagrange's equations because they do not correspond to the time derivatives of any set of coordinates that specify the position of the segment. They must be written as functions of the generalized coordinates, using the generalized angular velocities ($\dot{\psi}_n$, $\dot{\theta}_n$, $\dot{\phi}_n$), which are parallel to the axes Z, y_n', and x_n'', respectively.

An arbitrary angular velocity of segment n, $\underline{\omega}_n$, can be expressed as a function of the generalized angular velocities according to

$$\underline{\omega}_n = \dot{\underline{\psi}}_n + \dot{\underline{\theta}}_n + \dot{\underline{\phi}}_n \tag{16}$$

Referring to figure 3, $\dot{\underline{\psi}}_n$, $\dot{\underline{\theta}}_n$, and $\dot{\underline{\phi}}_n$ do not, in general, form a mutually perpendicular vector triad. ($\dot{\underline{\psi}}$ and $\dot{\underline{\phi}}$ are both perpendicular to $\dot{\underline{\theta}}$ but are not necessarily perpendicular to each other.) However, they can be considered as a nonorthogonal set of components of $\underline{\omega}$ since their vector sum is equal to $\underline{\omega}$. Summing the orthogonal projections of $\dot{\underline{\psi}}_n$, $\dot{\underline{\theta}}_n$, and $\dot{\underline{\phi}}_n$ on the (x_n, y_n, z_n) axes yields the angular velocity components required for the kinetic energy expression:

$$\begin{aligned}
\omega_{x_n} &= \dot{\phi}_n - \dot{\psi}_n \sin \dot{\theta}_n \\
\omega_{y_n} &= \dot{\psi}_n \cos \theta_n \sin \phi_n + \dot{\theta}_n \cos \phi_n \\
\omega_{z_n} &= \dot{\psi}_n \cos \theta_n \cos \phi_n - \dot{\theta}_n \sin \phi_n
\end{aligned} \tag{17}$$

The system potential energy is simply gravitational potential, which is written as

$$V = \sum_{n=1}^{12} M_n g \, (Z_n - Z_{n_o}) \tag{18}$$

where g is the acceleration due to gravity and Z_{n_o} is an arbitrary datum.

2.1.3 Matrix Equations

For the purposes of computation, the equations of motion are rewritten in the following form:

$$[A(q)] \{\ddot{q}\} = \{B(\dot{q},q)\} + \{P(q)\} + \{R(\dot{q},q)\} + \{Q(\dot{q},q)\} \tag{19}$$

where the elements of the inertia matrix [A] and the vector {B} are derived from the kinetic energy derivatives of Lagrange's equations. In other words,

$$\frac{d}{dt}\left(\frac{\partial T}{\partial \dot{q}_j}\right) - \frac{\partial T}{\partial q_j} = \sum_{k=1}^{29} A_{jk}\ddot{q}_k$$

$$- B_j \quad (\dot{q}_1, \dot{q}_2, \ldots, \dot{q}_{29}, q_1, q_2, \ldots, q_{29})$$

$$(j = 1, 2, \ldots, 29) \qquad (20)$$

The force vector {P} is derived from the system potential energy according to

$$P_j \quad (q_1, q_2, \ldots, q_{29}) = - \frac{\partial V}{\partial q_j} \quad (j = 1, 2, \ldots, 29) \qquad (21)$$

Both {R} and {Q} are vectors of generalized forces derived from the right-hand side of Lagrange's equations. The vector {R} describes the resistance of the body joints to rotation, discussed in detail in section 2.3; {Q} is the vector of generalized external forces, discussed in detail in section 2.4.

2.2 TWO-DIMENSIONAL OCCUPANT MODEL

In order to achieve economical program solutions for cases where occupant response is expected to be symmetrical with respect to the X-Z plane, a two-dimensional occupant model option was included in Program SOM-LA. This two-dimensional model was configured like the three-dimensional model shown in figure 1, with the exception of all joints being hinge-type joints. Because of the potential for vertebral injury in aircraft accidents that involve a significant vertical component of impact velocity, some measure of vertebral loading was considered desirable in the occupant model. The two-dimensional occupant model was configured to include beam elements in both the torso and neck, as shown in figure 5, replacing joints that exist in the three-dimensional

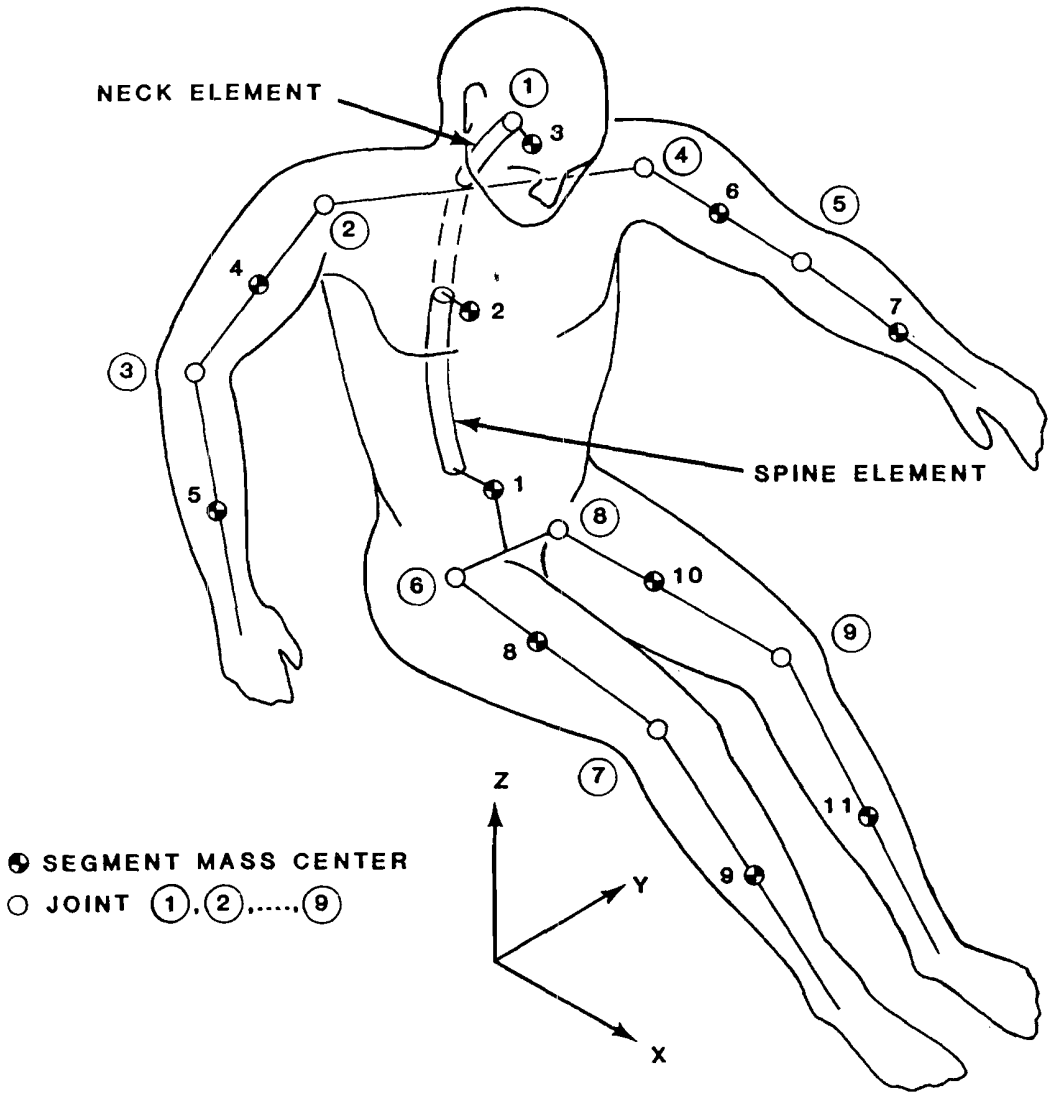

Figure 5. Eleven-segment (two-dimensional) occupant model.

model. The two-dimensional model has 11 degrees of freedom, as illustrated in figure 6. Simulation of purely vertical ($+G_z$) impact with the three-dimensional occupant model produced less bending of the torso than observed in tests with either dummies or human cadavers. Therefore, in order to produce the moments on the vertebral column that are induced by $+G_z$ acceleration in both human and dummy occupants, the mass centers of the torso segments,

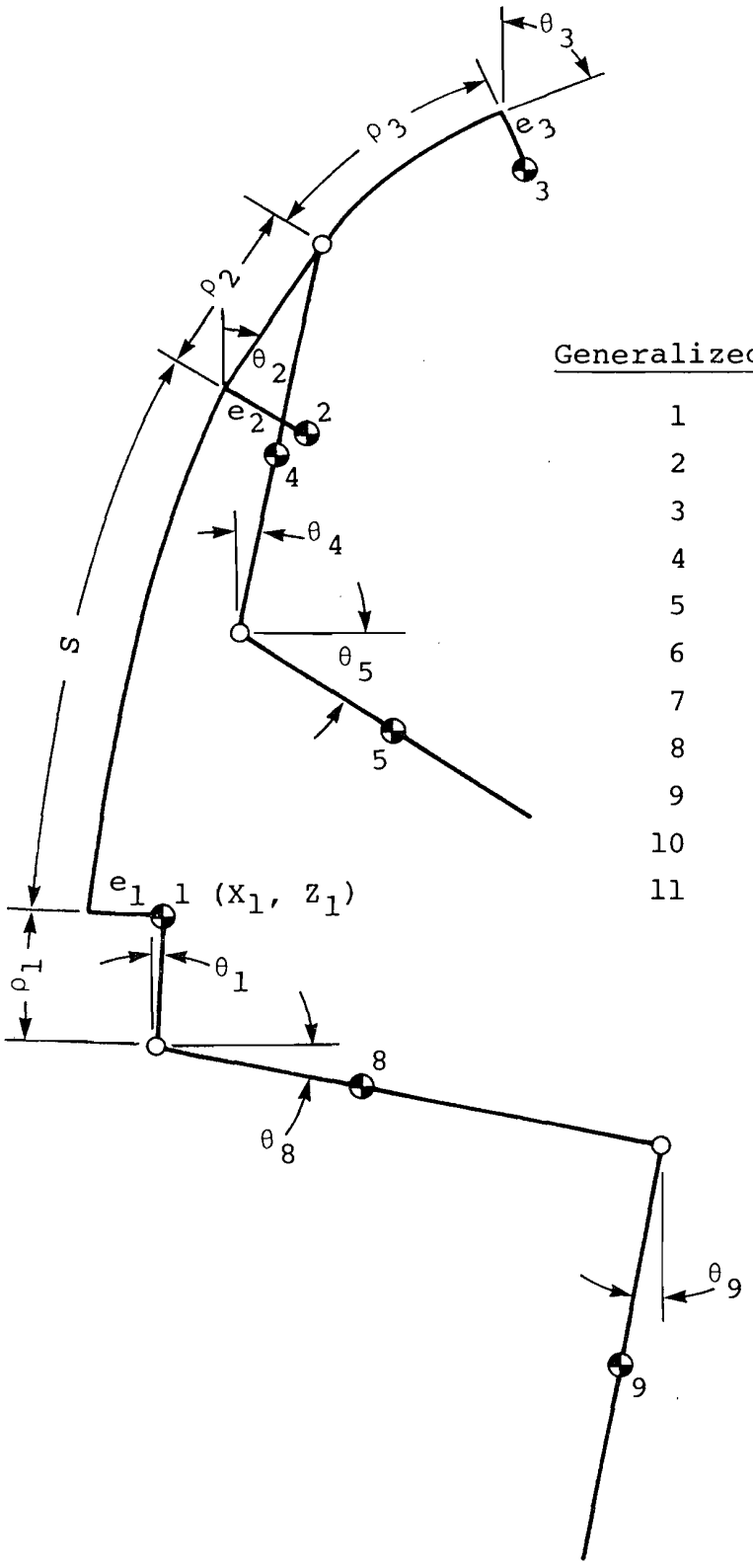

Generalized coordinates

1	X_1
2	Z_1
3	θ_1
4	S
5	θ_2
6	ρ_3
7	θ_3
8	θ_4
9	θ_5
10	θ_8
11	θ_9

Figure 6. Generalized coordinates for two-dimensional occupant model.

segments 1 and 2, are offset from the vertebral column by the dimensions e_1 and e_2, respectively. The dimension e_3, by which the center of mass of the head segment is placed forward of the neck, is used in both three-dimensional and two-dimensional models.

Development of the equations of motion for the two-dimensional occupant follows a procedure similar to that described in section 2.1 for the three-dimensional model. However, the procedure is simplified because the transformation between a local, segment-fixed coordinate system and the inertial system is dependent only on the angle θ. Transformations, therefore, take the form of equation (3). The position of the center of mass of segment 2, with respect to that for segment 1 and the position of the center of mass of segment 3, relative to segment 2, depend on the length and curvature of the beam elements in the spine and neck, respectively.

A detailed representation of the kinematics and mechanics of the spinal column would be complicated. The presence of the intervertebral disks leads to high flexibility in bending and high stiffness in compression. In addition, the column is tapered and possesses considerable initial curvature. A simplified model is incorporated into SOM-LA by using continuous beam elements for the neck and spine. These beam elements are intended to model the flexural, as well as axial, motion of the spine and neck and are subject to the following assumptions. The deformed beam elements take the shape of circular arc segments, therefore assuming flexure to be primarily due to the applied bending moment. This is equivalent to the assumption in beam theory that the span/depth ratio is large and that the modulus of elasticity and shear modulus are of the same order of magnitude so that shear deformation is negligible.

As illustrated in figure 7, The position of one end relative to the other in terms of arc length and angular coordinates at each end of the arc, is then given by

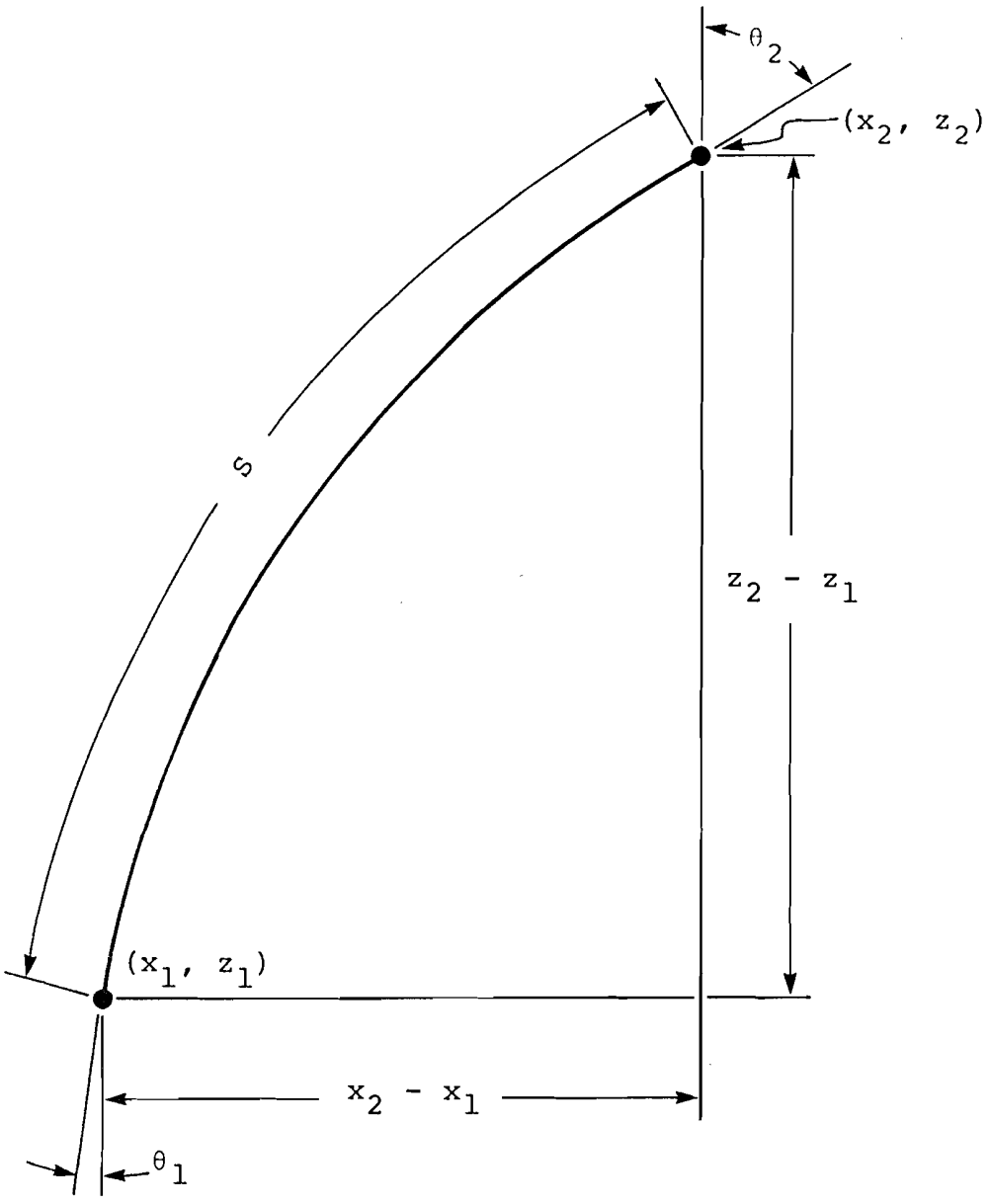

Figure 7. Position of segment 2 relative to segment 1.

$$x_2 - x_1 = 2\left(\frac{S}{\theta_2 - \theta_1}\right)\sin\left(\frac{\theta_2 - \theta_1}{2}\right)\sin\left(\frac{\theta_2 + \theta_1}{2}\right)$$

$$z_2 - z_1 = 2\left(\frac{S}{\theta_2 - \theta_1}\right)\sin\left(\frac{\theta_2 - \theta_1}{2}\right)\cos\left(\frac{\theta_2 + \theta_1}{2}\right) \quad (22)$$

Positions of the mass centers for the eleven body segments of the two-dimensional model are presented in appendix B.

2.3 JOINT RESISTANCE

The form of the joint resistance vector {R} in equation (19) depends on the user's selection of occupant type - either dummy or human. Although both joint models contain the same types of elements, a nonlinear torsional spring and a viscous torsional damper, the relative contributions of each of these elements determine the type of occupant.

The 11 body joints for the three-dimensional model, illustrated in figure 1, are defined as follows:

Joint 1 - Back, between 12th thoracic and 1st lumbar vertebrae

Joint 2 - Torso-neck, between 7th cervical and 1st thoracic vertebrae

Joint 3 - Right shoulder

Joint 4 - Right elbow

Joint 5 - Left shoulder

Joint 6 - Left elbow

Joint 7 - Right hip

Joint 8 - Right knee

Joint 9 - Left hip

Joint 10 - Left knee

Joint 11 - Head-neck, at occipital condyles

The angular displacement of joint i from its reference position (figure 2) is given by β_i. If (i_m, j_m, k_m) and (i_n, j_n, k_n) are triads of unit vectors in the local coordinate systems of two adjacent segments connected at joint i, as shown in figure 8, the joint angle is given by

$$\beta_i = \cos^{-1} (k_m \cdot k_n) \qquad (23)$$

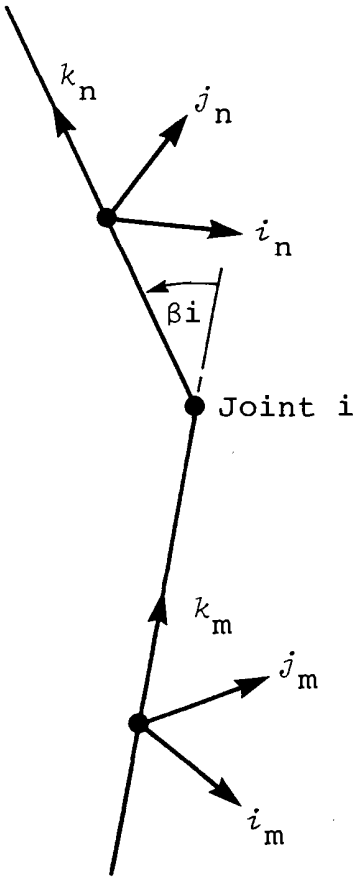

Figure 8. Joint angle β_i between segments m and n.

where $(k_m \cdot k_n)$ is the scalar product. Considering the geometry of the occupant model in the reference position, the β_i for the 11 joints are given by

$$\beta_1 = \cos^{-1} (k_1 \cdot k_2)$$

$$\beta_2 = \cos^{-1} (k_2 \cdot k_{12})$$

$$\beta_3 = \cos^{-1} (k_2 \cdot k_4)$$

$$\beta_4 = \alpha_5$$

$$\beta_5 = \cos^{-1} (k_2 \cdot k_6)$$

$$\beta_6 = \alpha_7$$

$$\beta_7 = \cos^{-1} (i_1 \cdot i_8)$$

$$\beta_8 = \alpha_9$$

$$\beta_9 = \cos^{-1} (i_1 \cdot i_{10})$$

$$\beta_{10} = \alpha_{11}$$

$$\beta_{11} = \cos^{-1} (k_3 \cdot k_{12}) \qquad (24)$$

If at each joint i, a moment M_i and a torsional damper with coefficient J_i act to resist motion of the joint, then the virtual work done on the system as each joint i undergoes a virtual displacement $\delta\beta_i$ is

$$\delta W = - \sum_{i=1}^{11} (M_i \ \delta\beta_i + J_i \ \dot{\beta}_i \ \delta\beta_i) \qquad (25)$$

Since the β_i are functions of the generalized coordinates q_j, the virtual displacements $\delta\beta_i$ can be expressed in terms of corresponding virtual displacements of the q_j. In general, such an expression would take the form

$$\delta\beta_i = \sum_{j=1}^{29} \frac{\partial\beta_i}{\partial q_j} \delta q_j \qquad (i=1, 2, \ldots, 11) \qquad (26)$$

where the partial derivatives $\partial\beta_i / \partial q_j$ are functions of the generalized coordinates. Substituting into equation (25) gives

$$\delta W = - \sum_{i=1}^{11} \sum_{j=1}^{29} (M_i + J_i \ \dot{\beta}_i) \frac{\partial\beta_i}{\partial q_j} \delta q_j \qquad (27)$$

Changing the order of summation, equation (27) can be written in the general form

$$\delta W = \sum_{j=1}^{29} R_j \, \delta q_j \tag{28}$$

where R_j are the generalized forces acting on the system. As seen in equation (19), the generalized forces are treated as two distinct types: joint resistance forces and external forces. Since the joint resistance terms are being treated here, the generalized joint forces referred to as R_j will be considered alone. Equation (28) becomes, more specifically

$$\delta W = \sum_{j=1}^{29} R_j \, \delta q_j \tag{29}$$

and, from equation (27), R_j can be written

$$R_j = - \sum_{i=1}^{11} (M_i + J_i \, \dot{\beta}_i) \frac{\partial \beta_i}{\partial q_j} \qquad (j=1, 2, \ldots, 29) \tag{30}$$

As mentioned earlier in this section, the type of occupant is determined by the relative contributions of M_i and J_i to the R_j terms. For the dummy joint, the resisting torque M_i is constant throughout the normal range of joint motion and increases rapidly along a third-order curve to a higher value at the limiting displacement β_{S_i}, as shown in figure 9. The normal values M_{D_i} are set equal to those resulting from the joint-tightening procedure of SAE Recommended Practice, Anthropomorphic Test Device for Dynamic Testing - SAE J963. That is, the body joints will just support a 1-G load in the reference (seated) position, with the exception of the torso joints, which will support a 2-G load. In addition to M_i, a small viscous damping term with constant J_i is included for energy dissipation.

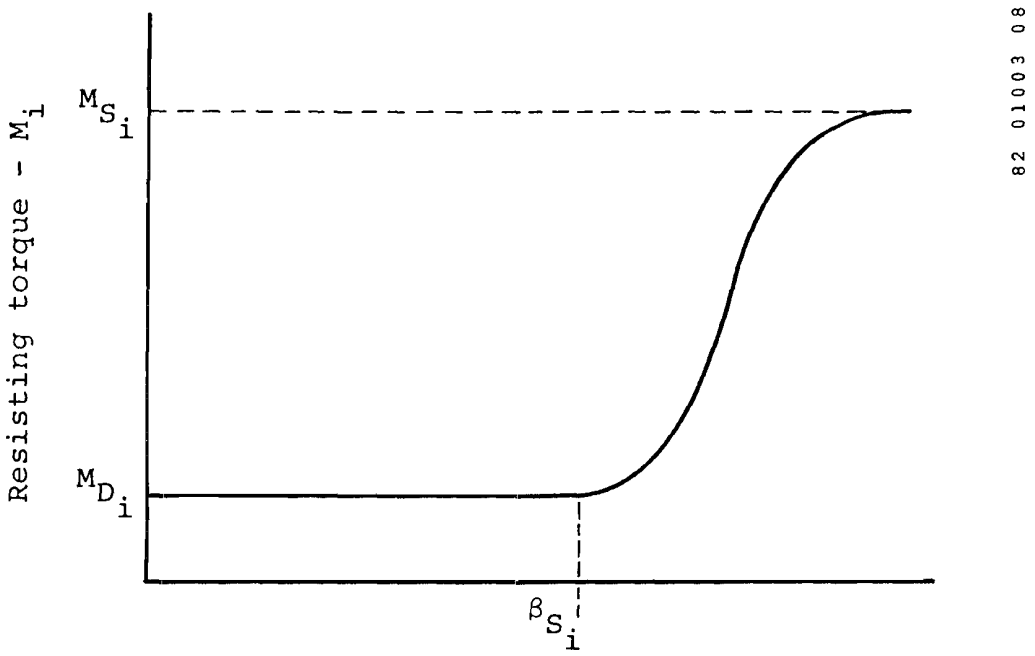

Figure 9. Dummy joint resisting torque.

The resistance of each human joint consists of up to three terms. The primary resisting force during normal joint rotation is a viscous damping term with constant coefficient J_i. In a manner similar to the case of the dummy, a resisting torque is applied at the limit of the joint range of motion, as shown in figure 10(a). An additional term used to simulate muscle tone is the moment M', which drops to zero after a small angular displacement from the initial position, provided that the crash deceleration is sufficient to overcome it (figure 10(b)).

For the two-dimensional model, the equations presented in this section are correct except that summations are performed for 8 joints and 11 degrees of freedom, rather than the 11 and 29 presented here, respectively.

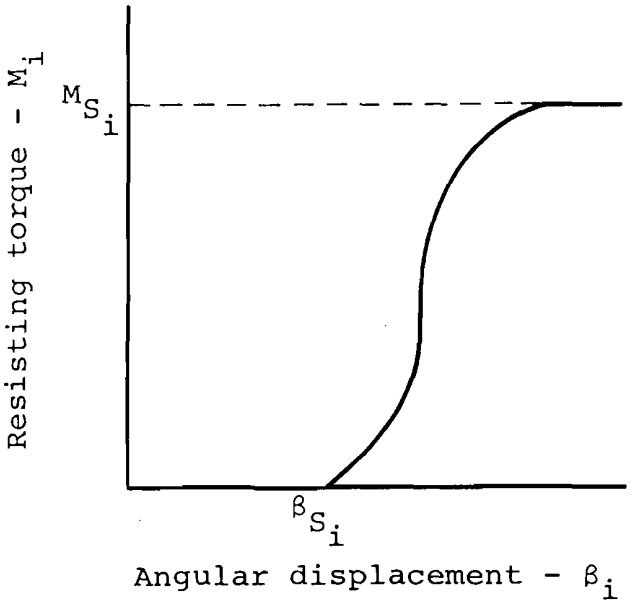

(a)

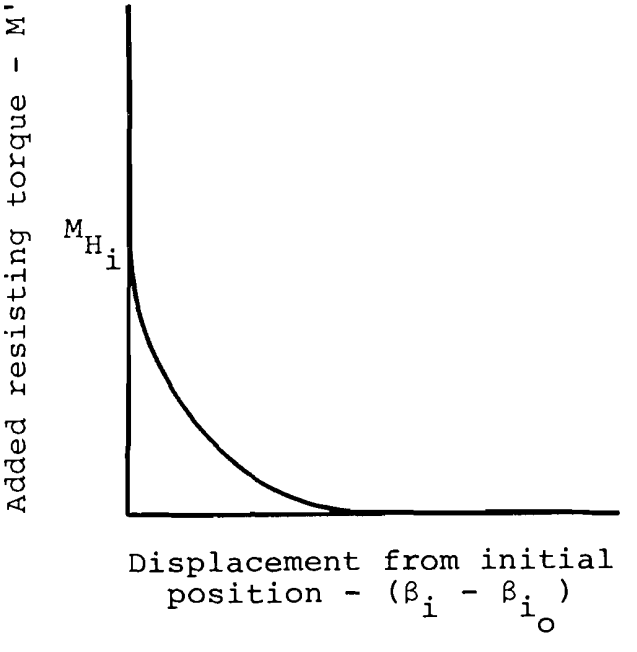

(b)

Figure 10. Human joint resisting torques: (a) displacement-limiting moment and (b) muscular resistance.

2.4 EXTERNAL FORCES

The vector of generalized external forces {Q} is developed in a manner similar to that discussed in the previous section for the joint resistance vector. Equations presented in this section include summations whose upper limits are correct for the three-dimensional model, with 12 segments and 29 degrees of freedom. The approach for the two-dimensional model is the same, except for the use of 11 segments and 11 degrees of freedom.

The resultant external force $\underline{F}_i$ acting on segment i is given by

$$\underline{F}_i = F_{X_i}\, i + F_{Y_i}\, j + F_{Z_i}\, k \tag{31}$$

where F_{X_i}, F_{Y_i}, and F_{Z_i} are components in the inertial (X, Y, Z) system. The absolute position of the point P_i on segment i, where the resultant force acts, can be represented by

$$\underline{r}_{P_i} = X_{P_i}\, i + Y_{P_i}\, j + Z_{P_i}\, k \tag{32}$$

As the resultant force applied to each segment i undergoes a virtual displacement δr_{P_i}, having components (δX_{P_i}, δY_{P_i}, δZ_{P_i}), the virtual work on the system done by the $\underline{F}_i$ is

$$\delta W = \sum_{i=1}^{12} \left(F_{X_i}\, \delta X_{P_i} + F_{Y_i}\, \delta Y_{P_i} + F_{Z_i}\, \delta Z_{P_i}\right) \tag{33}$$

Writing the virtual displacement components in terms of the generalized coordinates q_j:

$$\delta X_{P_i} = \sum_{j=1}^{29} \frac{\partial X_{P_i}}{\partial q_j}\, \delta q_j$$

$$\delta Y_{P_i} = \sum_{j=1}^{29} \frac{\partial Y_{P_i}}{\partial q_j} \delta q_j \qquad (34)$$

$$\delta Z_{P_i} = \sum_{j=1}^{29} \frac{\partial Z_{P_i}}{\partial q_j} \delta q_j$$

results in

$$\delta W = \sum_{j=1}^{29} \sum_{i=1}^{12} \left(F_{X_i} \frac{\partial X_{P_i}}{\partial q_j} + F_{Y_i} \frac{\partial Y_{P_i}}{\partial q_j} + F_{Z_i} \frac{\partial Z_{P_i}}{\partial q_j} \right) \delta q_j \qquad (35)$$

Using equation (28)

$$\delta W = \sum_{j=1}^{29} Q_j \, \delta q_j$$

yields the components of the generalized external force vector:

$$Q_j = \sum_{i=1}^{12} \left(F_{X_i} \frac{\partial X_{P_i}}{\partial q_j} + F_{Y_i} \frac{\partial Y_{P_i}}{\partial q_j} + F_{Z_i} \frac{\partial Z_{P_i}}{\partial q_j} \right) \qquad (36)$$

The external forces acting on the body segments can be characterized as either contact forces or restraint forces. These forces are discussed in further detail in the sections following.

2.4.1 Contact Forces

The contact forces applied to the occupant are those forces exerted by the cushions and floor, illustrated in figure 11. The forces of the seat back pass through the mass centers of the upper torso and head segments, and the normal forces applied to the legs by the seat bottom cushion pass through the mass centers of the thigh segments. The contact surface for the lower torso is not located at the mass center of that segment but is an ellipsoid whose major axis passes through both hip joints. The force of the back cushion

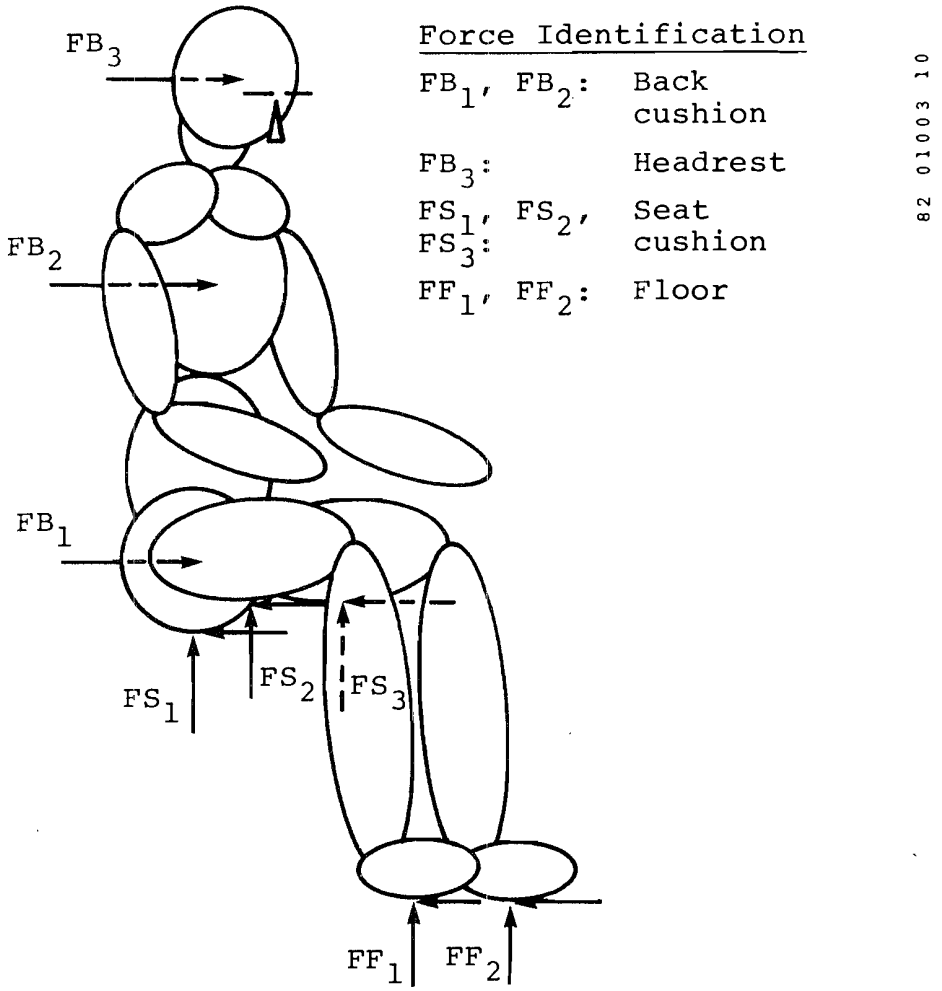

Figure 11. External forces of cushions and floor.

and the normal component of the seat bottom cushion force both pass through the center of this ellipsoid, i.e., through a point midway between the hips. The normal components of the floor and footrest forces are applied to the body at the lower ends of the leg segments.

Each of the forces mentioned above acts normal to the surface applying the force, or, in other words, its direction is determined by the plane of the surface, whether cushion or floor. As shown in figure 11, friction forces are also applied by the seat bottom cushion and the floor. The friction force is computed as the product of the coefficient multiplied by the normal force. It is applied in a direction opposite to the tangential component of relative

velocity between the occupant segment and the appropriate cushion or floor surface. In order to avoid abrupt changes in direction of the friction force, the force is reduced sinusoidally when the magnitude of the tangential velocity drops below a predetermined limit. (A limiting value of 1 ft/sec has produced satisfactory results in SOM-LA and is thus used by the program.)

All contact forces are calculated by first determining the penetration of a contact surface on the occupant into a surface with known force-deflection characteristics. Using the seat cushion force as an example, the pertinent dimensions of the seat and the parameters required to determine the penetration of the abdomino-pelvic segment (segment 1) into the cushion are illustrated in figure 12. X_P and Z_P are coordinates of the center of the contact surface of segment 1, and R_1 is the radius of the contact surface in the $(x_1 - z_1)$ plane. (Although this contact surface is an ellipsoid, cross-sections parallel to the $(x_1 - z_1)$ plane are circular. The dimensions of the contact surfaces will be discussed in section 2.5.) The position of the seat pan is defined by its height Z_S above the origin of the aircraft coordinate system and the angle θ_S that it makes with the aircraft $(X_A - Y_A)$ plane. The unloaded thickness of the seat cushion is t_e, and the loaded thickness under segment 1 is t. Summing the dimensions in the Z_A direction gives

$$Z_P = Z_S + (R_1 + t)/\cos \theta_S + X_P \tan \theta_s \tag{37}$$

Solving equation (37) for the cushion thickness,

$$t = (Z_P - Z_s) \cos \theta_s - R_1 - X_P \sin \theta_s \tag{38}$$

The deflection of the seat cushion is then

$$\delta_c = t_e - t \tag{39}$$

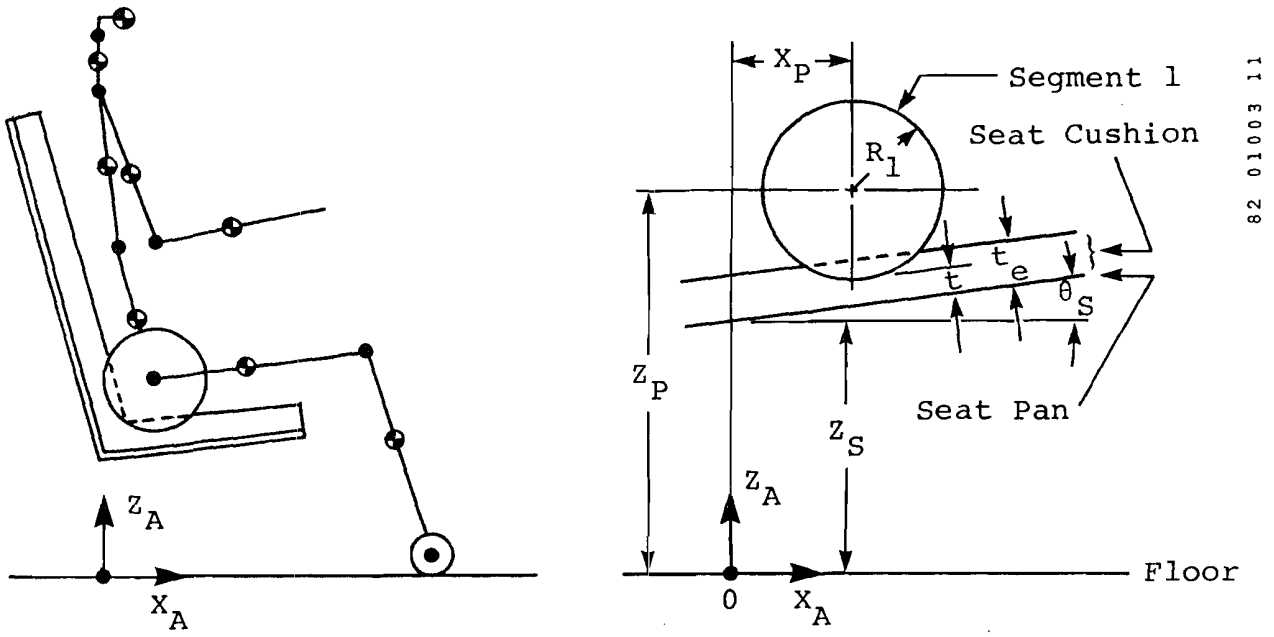

Figure 12. Seat cushion deflection.

and the force, which is assumed to act normal to the plane of the seat pan and pass through the center of curvature of the contact surface, is calculated from deflection according to

$$F_c = A(e^{b\delta_c} - 1) \tag{40}$$

To each normal force, a damping term is applied which is proportional to the deflection rate. The damping coefficient is based on the Rayleigh formulation in which the coefficient is proportional to both mass and stiffness according to

$$C = 2\beta m + \alpha K \tag{41}$$

For a multidegree-of-freedom system there will be a discrete damping coefficient associated with each characteristic mode. In a continuous system there will be an infinite number of coefficients, although several modes will generally dominate the dynamic solution. It was assumed for the formulation in SOM-LA that the damping ratio, ζ, was constant for all deformation modes of interest. This assumption greatly simplifies the solution of equation (41) because the

damping coefficient is not dependent on the system mass. Equation (41) can then be simplified to

$$C = 2K\alpha \tag{42}$$

where the stiffness K is the gradient of the cushion force-deflection curve, and α is a constant for the system.

The procedure used in SOM-LA to calculate the current value of the damping coefficient is based on the curent value of K, and the constant α which is determined from input data. The slope of the exponential load/deflection curve at deflection δ_c is

$$K = Abe^{b\delta_c} \tag{43}$$

The user supplies a damping coefficient, C_o, for the zero-deflection condition which the program uses to calculate α by applying equations (43) and (42), thereby resulting in

$$\alpha = \frac{Co}{2K_o} \tag{44}$$

The constant, α, and the current gradient of the cushion load-deflection curve, K, are used at each time step to determine the instantaneous cushion damping coefficient from equation (42).

2.4.2 Restraint System Forces

The method used in calculating the forces exerted on the body by the restraint system differs considerably from that described in the preceding section for the contact forces. The primary reason for this difference is that the restraint forces do not act at any fixed points on the occupant, but, rather, the points of application vary with the restraint system geometry.

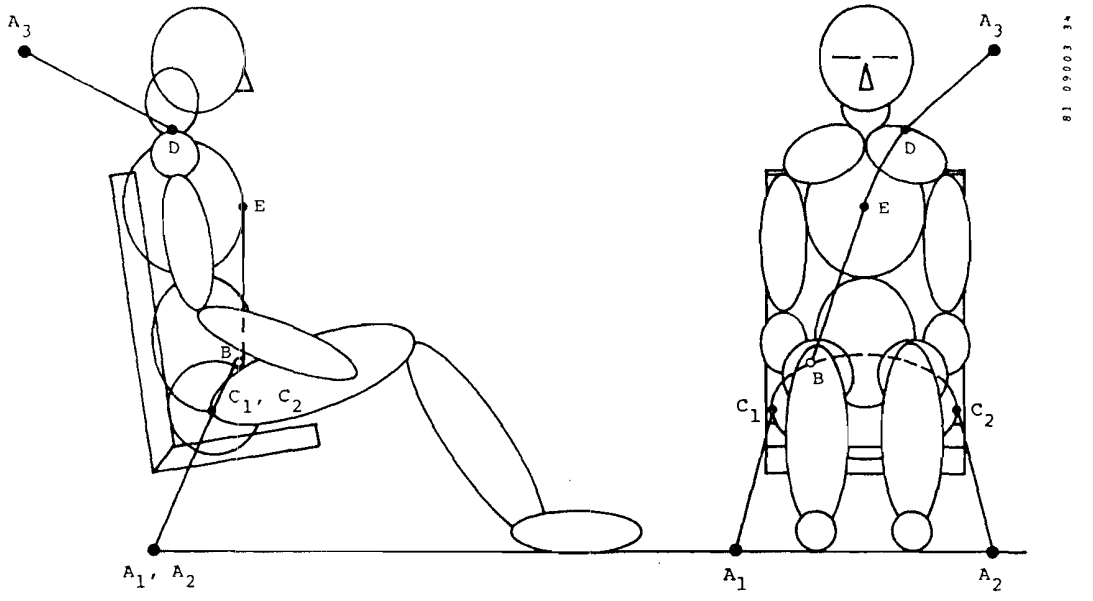

Figure 13. Restraint system configuration variables.

Although other configurations can be selected by the user, a restraint system consisting of a lap belt and diagonal shoulder strap will be used as an example. The restraint loads are transmitted to the occupant model through ellipsoidal surfaces fixed to the upper and lower torso segments. These surfaces are shown in figure 13. The locations of the anchor points A_1, A_2, and A_3 are determined by user input along with the webbing properties. The buckle B for a single shoulder belt is located according to an input parameter which specifies the distance from the appropriate point, in this case A_1, along the path of the lap belt. For a double-strap shoulder harness, the buckle is placed on the abdominal contact surface between its intersections with the thigh surfaces.

The ellipsoidal surfaces are described by

$$x_1^2/a_1^2 + y_1^2/b_1^2 + z_1^2/c_1^2 = 1 \qquad (45)$$

for the lower torso, where

$$a_1 = R_1$$

$$b_1 = L_H$$

$$c_1 = R_1$$

and

$$x_2^2/a_2^2 + y_2^2/b_2^2 + z_2^2/c_2^2 = 1 \qquad (46)$$

for the upper torso, where

$$a_2 = R_2$$

$$b_2 = L_2/2$$

$$c_2 = L_2/2$$

and these body dimensions are defined in section 2.5.

The restraint forces are determined in the same manner for both the upper and lower torso. First, the belt loads are calculated from the displacements of the torso segments, and the resultant force on each segment is then applied at the point along the arc of contact between the belt and the ellipsoidal surface where the force is normal to the surface.

Explaining this procedure in further detail for the restraint system configuration shown in figure 13, for any position of the occupant, the coordinates of the left shoulder, the hips, and the buckle connection B are calculated in the aircraft reference frame. The length of each side of the lap belt is equal to the

sum of the free length in a straight line from an anchor point (A_1 or A_2) to the outermost point on the hip contact surface (C_1 or C_2) added to the length of an arc from that point on the hip to the buckle (B). The shoulder belt length is computed as the sum of the distance from the anchor point (A_3) to a point of tangency on the top of the shoulder contact surface (D), the distance from the buckle to the extreme anterior (forward) point on the ellipsoidal chest surface (E), and the length of an arc over the chest surface between points D and E. If the length of the belt segment should exceed the equilibrium (zero load) length calculated initially, then there is some tensile force in the belt. The resultant force on each segment is the vector sum of the belt forces. Friction between the shoulder belt and chest along the length of the belt is taken into account by reducing the load in the belt between the chest and buckle by a constant fraction of the load in the free length between the anchor point and the body surface. The resultant force on the lower or upper torso segment may be written generally as

$$\underline{F} = F_x\, i + F_y\, j + F_z\, k \tag{47}$$

where F_x, F_y, and F_z are components in the local, segment-fixed coordinate system.

To find the point on the segment where $\underline{F}$ is normal to the surface, consider first the equation of an ellipsoid:

$$x^2/a^2 + y^2/b^2 + z^2/c^2 = 1 \tag{48}$$

which may also be expressed in functional form as

$$f\ (x, y, z) = x^2/a^2 + y^2/b^2 + z^2/c^2 - 1 \tag{49}$$

where the ellipsoid can be regarded as the level surface f=0 of the function. At any point (x, y, z) on the surface, the gradient of f is normal to the surface. The gradient is given by

$$\text{grad } f = (2x/a^2)\ i + (2y/b^2)\ j + (2z/c^2)\ k \tag{50}$$

and at the point of application of the resultant force, grad f is collinear with $\underline{F}$. Making use of the proportionality between the components of the two vectors,

$$\begin{aligned} F_x &= Cx/a^2 \\ F_y &= Cy/b^2 \\ F_z &= Cz/c^2 \end{aligned} \tag{51}$$

where C is an arbitrary constant. Solving equation (51) for the coordinates (x, y, z) and substituting into equation (48)

$$\left(\frac{F_x a^2}{C}\right)^2 \frac{1}{a^2} + \left(\frac{F_y b^2}{C}\right)^2 \frac{1}{b^2} + \left(\frac{F_z c^2}{C}\right)^2 \frac{1}{c^2} = 1 \tag{52}$$

$$\left(\frac{F_x a}{C}\right)^2 + \left(\frac{F_y b}{C}\right)^2 + \left(\frac{F_z c}{C}\right)^2 = 1 \tag{53}$$

which leads to

$$\begin{aligned} C^2 &= F_x^2 a^2 + F_y^2 b^2 + F_z^2 c^2 \\ C &= \pm \sqrt{F_x^2 a^2 + F_y^2 b^2 + F_z^2 c^2} \end{aligned} \tag{54}$$

the point of application of $\underline{F}$ is then

$$\begin{aligned} x &= F_x a^2/C \\ y &= F_y b^2/C \\ z &= F_z c^2/C \end{aligned}$$

with

$$C = -\sqrt{F_x^2 a^2 + F_y^2 b^2 + F_z^2 c^2} \tag{55}$$

The negative sign on C can be explained by the fact that each coordinate in the local system is opposite in sign to the corresponding component of the resultant force, or

$$\begin{aligned} x &> 0 \text{ if } F_x < 0 \\ y &> 0 \text{ if } F_y < 0 \\ z &> 0 \text{ if } F_z < 0 \end{aligned} \tag{56}$$

The capability of the belt's point of application of resultant belt loads to move relative to the torso surfaces allows simulation of the "submarining" under the lap belt.

2.5 OCCUPANT DIMENSIONS AND INERTIAL PROPERTIES

Characteristics required by the occupant model for each of the segments are the length, mass, center of mass location, and moments of inertia. Also required are the axial and flexural stiffnesses and damping coefficients for both vertebral elements, as well as compliance characteristics for the chest and abdomen. It is assumed that, for each segment, a line connecting the joints is a principal axis, so that the required moments of inertia are all principal moments. For each torso element, of the two-dimensional model, the center of mass may, in general, be offset from the spine as shown in figure 6. Moments of inertia are then moments with respect to axes located at the mass center. Final data required to describe the occupant are radii of 26 contact surfaces, which are ellipsoids and spheres.

For two "standard" occupants, a 50th-percentile human male and a 50th-percentile anthropomorphic (Part 572) dummy, all the required data are stored within the program. For other nonstandard

occupants, the above-described data must be provided as input. The human data are based on the U.S. Air Force drawing board manikin (reference 7), whose dimensions were extracted by the FAA Civil Aeromedical Institute and tabulated with appropriate inertial properties in reference 8. Dummy dimensions and characteristics were obtained from reference 9.

Most of the dimensions and inertial properties used in SOM-LA were taken from references 8 and 9, but because fewer segments are used in the mathematical model, some properties needed to be combined. That is, in the model, the hands are combined with the lower arms, the feet with the lower legs, and the mid torso with the lower torso. The distance from the wrist pivot to the mass center of the hand was added to the lower arm length; a contact sphere centered on the end of this link accounts for the remaining reach of the hand. Similarly, the distance from the ankle pivot to the foot center of mass was added to the lower leg length, and a contact sphere was sized to provide the correct distance between the knee pivot and the floor. Composite mass center locations and moments of inertia were calculated for the lower torso, lower arms, and lower legs.

2.5.1 Body Segment Dimensions

The basic dimensions of the occupant segments that are required in writing the equations of motion are illustrated in figure 14. The lengths of the segments are, in most cases, effective "link lengths" between joint centers, rather than standard anthropometric dimensions based on external measurements. These lengths, for the standard 50th-percentile occupants, are presented in table 1.

For segments other than the torso segment, the distance of the mass center of segment n from the end nearest the body reference point (m_1) is ρ_n. The distance between the mass center and the far end is given by

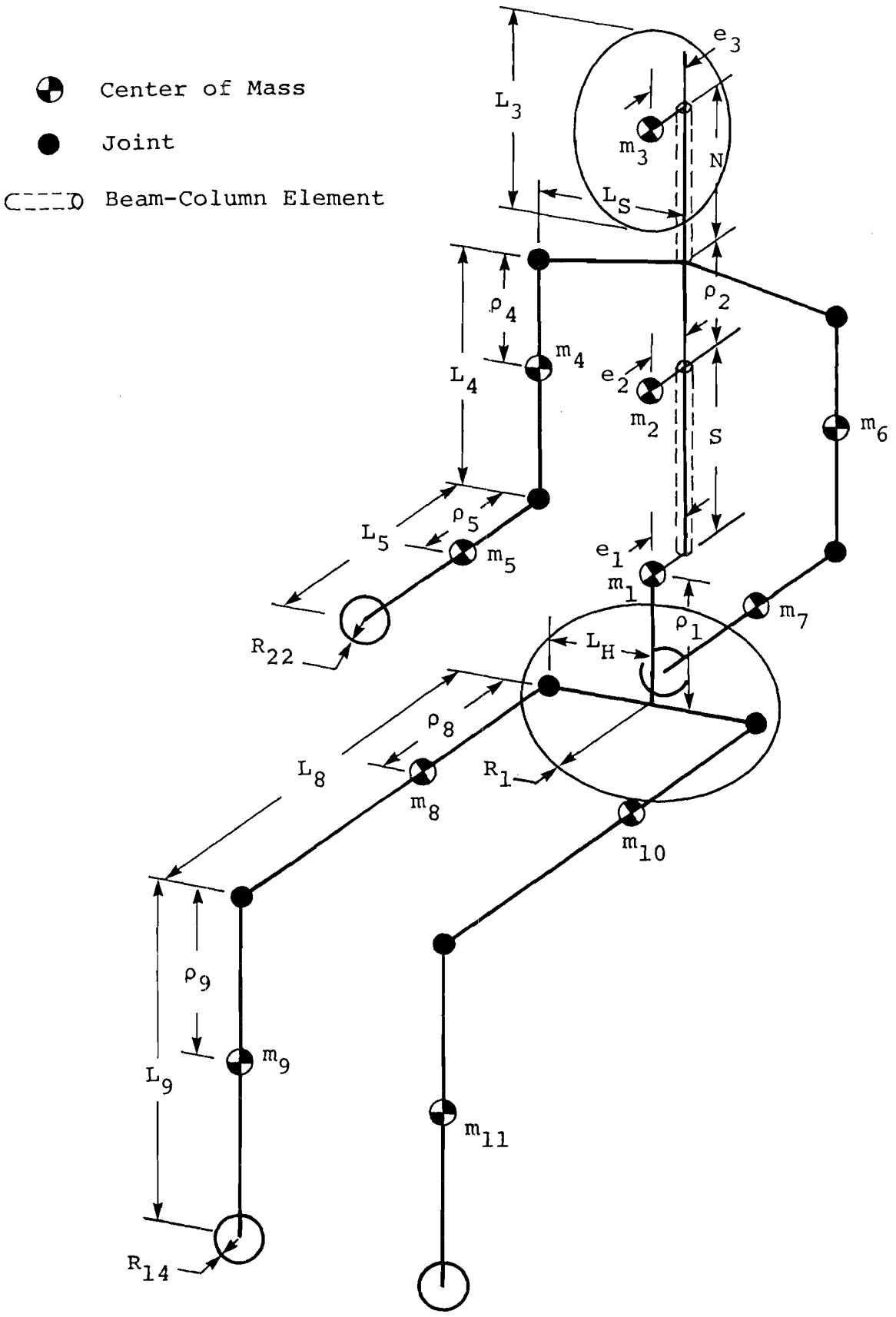

Figure 14. Program SOM-LA body segment dimensions.

TABLE 1. BODY SEGMENT LENGTHS (IN.)

Segment	50th-Percentile Aircrewmember (reference 8)	Part 572 Dummy (reference 9)
Lower Torso, L_1	9.44	10.5
Upper Torso, L_2	13.1	11.5
Neck, N	5.10	4.88(2)
Head, L_3	8.50(1)	8.35(2)
Upper Arm, L_4	11.6	11.3
Lower Arm, L_5	14.8(3)	13.3(3)
Upper Leg, L_8	17.1	16.5
Lower Leg, L_9	18.4(3)	18.0(3)
Spine, S	12.4(3)	10.85(3)
Seated Height	37.0(3)	36.0(3)

(1) Scaled from manikin drawing.
(2) Scaled from Part 572 drawing.
(3) Calculated.

$$\bar{\rho}_n = L_n - \rho_n \tag{57}$$

Note that the lengths of the torso segments, L_1 and L_2, are not used in the two-dimensional model shown in figure 5 although they are used to generate contact surface ellipsoids for the graphics display. However, the center of mass distances, ρ_1 and ρ_2, and the spinal length, S, are used and

$$L_1 + L_2 = \rho_1 + \rho_2 + S \tag{58}$$

Also, the seated height is equal to

$$R_1 + \rho_1 + S + \rho_2 + N + L_3/2 \qquad (59)$$

where R_1 is the radius of the pelvic contact ellipsoid in the mid-sagittal plane, N is the neck length, and L_3 is the head segment length (z-direction, approximately menton to top of head, in anthropometric terms).

2.5.2 Body Segment Weights and Center of Mass Locations

Body segment weights and axial locations of centers of mass for the two standard occupants are presented in table 2. The dimensions e_1 and e_2, by which the torso mass centers are offset from the spine were determined to be 0.20 and 0.70 in., respectively, based on simulation of vertical ($+G_z$) tests. A value of 1.17 in. for the corresponding dimension for the head, e_3, is based on Part 572 dummy drawings.

2.5.3 Body Segment Moments of Inertia

Body segment moments of inertia are presented in table 3. As indicated, moments of inertia with respect to lateral (y) axes were taken from references 8 and 9 for the standard human and dummy occupants, respectively. The moments of inertia with respect to the segment x- and z-axes were determined using approximations to segment geometry. The torso and head segments were approximated by ellipsoids. Assigning appropriate anthropometric dimensions to the ellipsoid axes, ratios I_x/I_y and I_z/I_y were calculated for unit mass. These ratios, multiplied by the I_y from reference 8 or 9, gave values of I_x and I_z for the torso and head segments. The identical procedure was used for the extremities, except that these segments were approximated by solid circular cylinders.

TABLE 2. BODY SEGMENT WEIGHTS AND CENTER OF MASS LOCATIONS

Segment	Weight (lb)		Center of Mass Location (in.)	
	50th-Percentile Aircrewmember (reference 8)	Part 572 Dummy (reference 9)	50th-Percentile Aircrewmember (reference 8)	Part 572 Dummy (reference 9)
Lower Torso	31.3	28.6	2.50(1)	4.17(1)
Upper Torso	55.0	42.0	7.60(1)	6.55(1)
Neck	2.34	1.98	1.93	2.44
Head	9.35	10.1	5.57	5.05
Upper Arm	8.78(2)	9.70(2)	6.02	4.72
Lower Arm (including hand)	8.34(2)	9.70(2)	7.07(1)	6.26(1)
Upper Leg	43.4(2)	43.4(2)	8.46	8.35
Lower Leg (including foot)	21.2(2)	19.0(2)	9.06(1)	11.0(1)
TOTAL	179.7	164.5		

(1) Calculated.
(2) Combined weight for two appendages.

TABLE 3. BODY SEGMENT MOMENTS OF INERTIA (lb-in.-sec^2)

Segment	I_x	I_y		I_z
		50th-Percentile Aircrewmember (reference 8)	Part 572 Dummy (reference 9)	
Lower Torso	4.03	1.19	0.760	2.323
Upper Torso	2.37	3.29	0.926	1.70
Neck	-	0.019	0.0177	-
Head	0.160	0.199	0.266	0.233
Upper Arm	0.131	0.120	0.135	0.022
Lower Arm (including hand)	0.105	0.254	0.185	0.195
Upper Leg	0.212	1.41	1.22	0.873
Lower Leg (including foot)	1.28	1.17	0.994	0.505

2.5.4 Body Contact Surfaces

Twenty-six surfaces are defined on the body for calculation of external forces exerted on the occupant by the seat cushions or restraint system and for prediction of impact between the occupant and the cockpit interior. These surfaces are ellipsoids, cylinders and spheres, as shown in figure 15. The dimensions of these surfaces, listed in table 4, were obtained from anthropometric data in references 8 and 9 or scaled off the drawings of the manikin and dummy. The surfaces and the dimensions required for their description are illustrated in detail in figure 16.

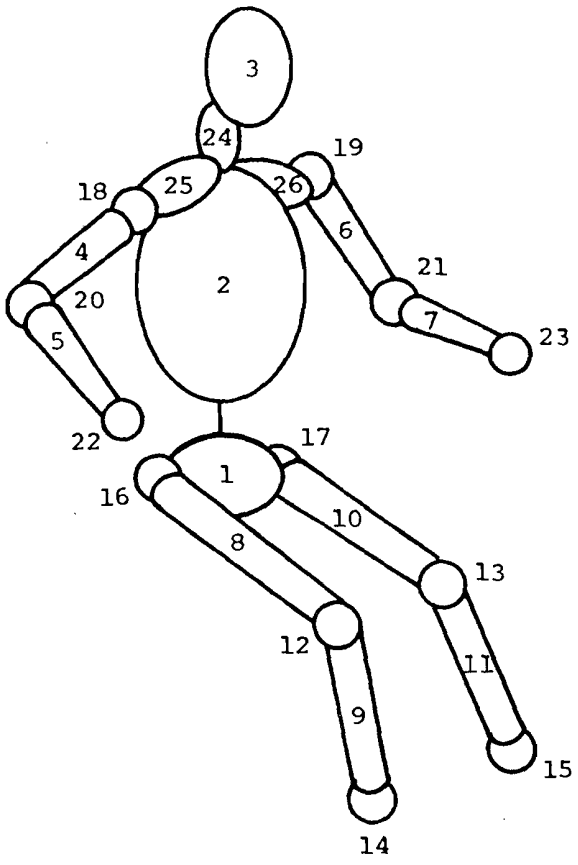

Surface Identification

1. Lower Torso
2. Upper Torso
3. Head
4. Right Upper Arm
5. Right Forearm
6. Left Upper Arm
7. Left Forearm
8. Right Thigh
9. Right Lower Leg
10. Left Thigh
11. Left Lower Leg
12. Right Knee
13. Left Knee
14. Right Foot
15. Left Foot
16. Right Hip
17. Left Hip
18. Right Shoulder Joint
19. Left Shoulder Joint
20. Right Elbow
21. Left Elbow
22. Right Hand
23. Left Hand
24. Neck
25. Right Shoulder
26. Left Shoulder

Figure 15. Occupant Contact Surfaces.

2.5.5 Joint Rotation

The results of several studies on the limits of human joint motion have been published. Two of these studies, in particular, were examined for applicability to the occupant model. First of all, Dempster's (reference 10) data on link lengths and inertial properties were used, as discussed in preceding sections, so it was considered appropriate to include his joint data here. Glanville and Kreezer (reference 11) presented limits of joint motion for both voluntary and forced rotation; their results appear, along

TABLE 4. BODY CONTACT SURFACE RADII (IN.)

Contact Surface	50th-Percentile Aircrewmember (scaled from manikin)	Part 572 Dummy (scaled from drawing)
Lower Torso	4.00	4.50
Upper Torso	5.00	4.50
Neck(1)	2.00	2.00
Head(2)	3.75	3.44
Upper Arm	2.10	1.95
Lower Arm	1.65	1.85
Upper Leg	3.28	3.10
Lower Leg	2.23	2.30
Hip(3)	3.56	3.56
Shoulder(4)	2.00	2.00
Foot	1.60	1.60

(1) Neck circumference divided by 2 π.
(2) Head length (anterior-posterior).
(3) Hip breadth (sitting)/2 - hip link length (L_H).
(4) Shoulder breadth/2 - shoulder link length (L_S).

with Dempster's, in table 5. Definitions of the various joint motions are illustrated in figure 17. Also included in table 5 are the rotations required for the Part 572 anthropomorphic dummy.

All of the rotations possible in the mathematical model are included in table 5 and figure 17, but some are, naturally, more important than others in determining permissible ranges of motion for the model. For the head, ventriflexion (B) is certainly the most important component of motion for frontal impact. Dorsiflexion (A) may also be important for frontal impact, but

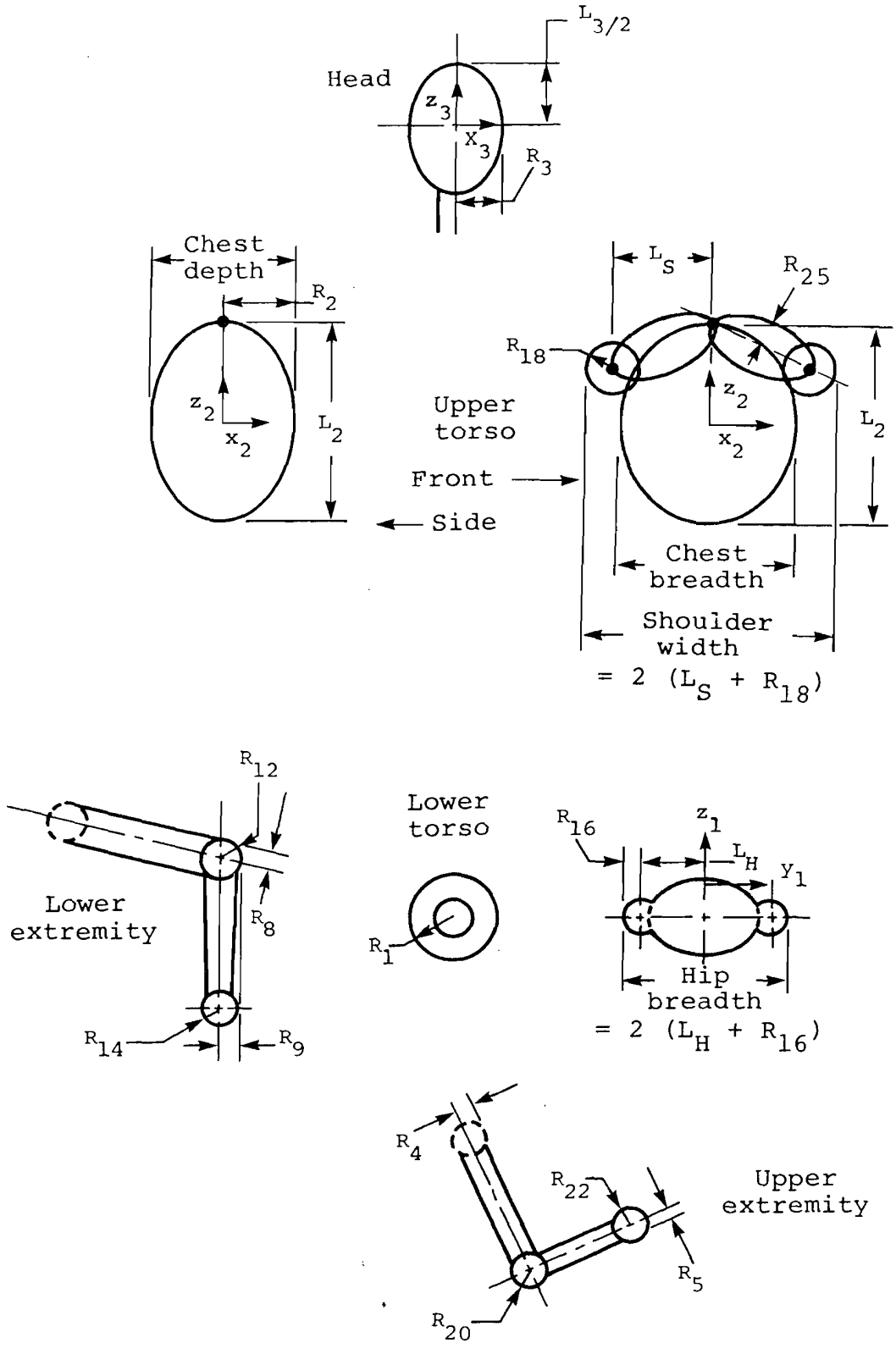

Figure 16. Body contact surface dimensions.

TABLE 5. RANGE OF JOINT ROTATION

Body Component Motion	Symbol	Motion Description	Measured Rotation - Deg			
			Human			
			Glanville and Kreezer[11]			
			Voluntary	Forced	Dempster[10]	Part 572 Dummy
Head - With Respect to Torso	A	Dorsiflexion	61	77	-	60
	B	Ventriflexion	60	76	-	60
	C	Lateral Flexion	41	63	-	40
	D	Rotation	78	63	-	70
Upper Arm - At Shoulder	E	Abduction (Coronal Plane)	130	137	134	135
	F	Flexion	180	185	188	180
	G	Hyperextension	58	69	61	60
Forearm - At Elbow	H	Flexion	141	146	142	135
Thigh - At Hip	I	Flexion	102	112	113	120
	J	Hyperextension	45	54	-	45
	K	Medial Rotation	-	-	39	50
	L	Lateral Rotation	-	-	34	50
	M	Adduction	-	-	31*	10
	N	Abduction	71	79	53*	50
Lower Leg - At Knee	P	Flexion	125	138	125	135
Long Axis of Torso	Q	Flexion	-	-	-	40
	R	Hyperextension	-	-	-	30
	S	Lateral Flexion	-	-	-	35
	T	Rotation	-	-	-	35

*Transverse plane.

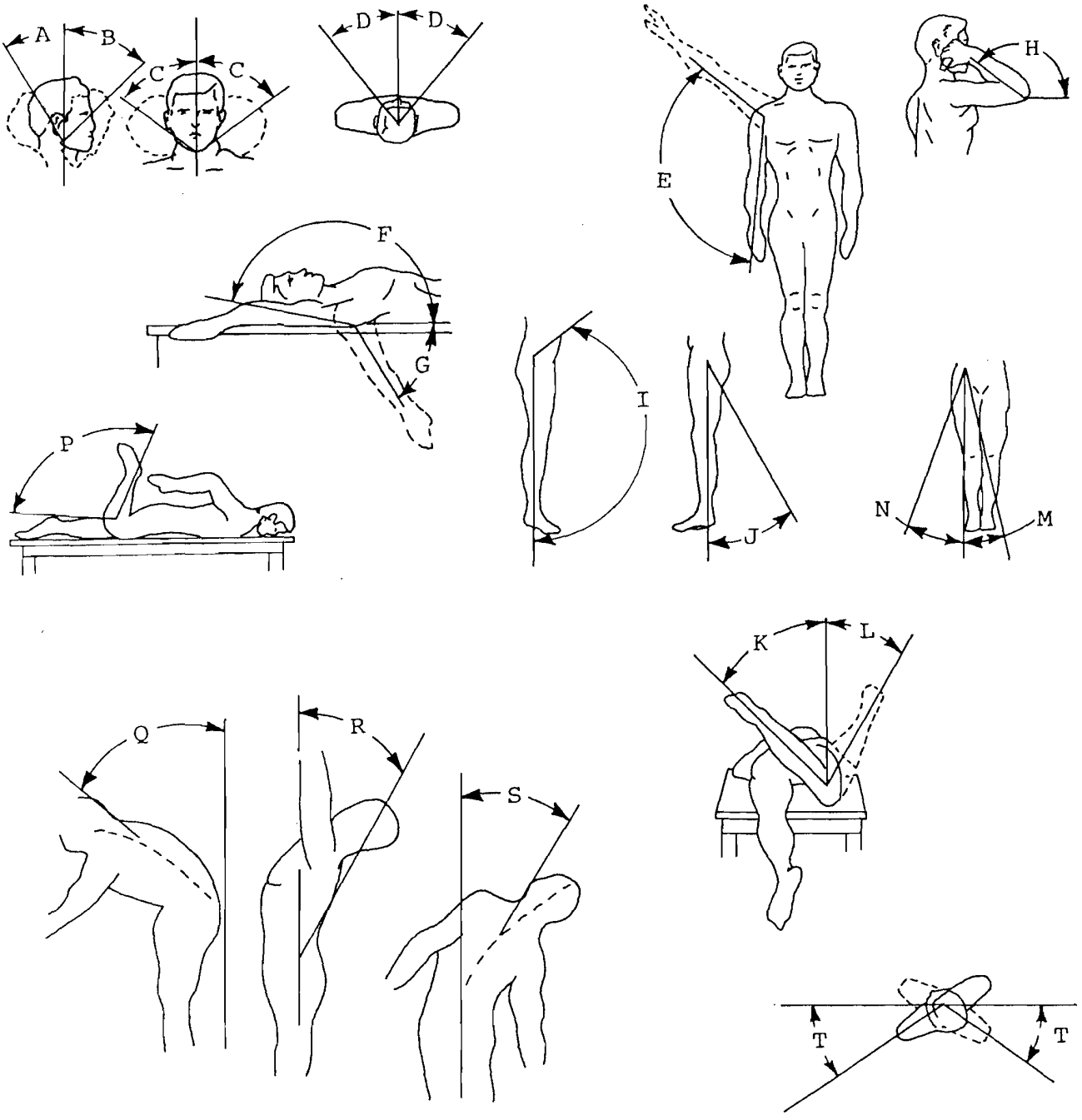

Figure 17. Motion diagrams.

the angles reported are sufficiently close to those for ventriflexion to be considered the same. Lateral flexion (C) is certainly less important since a pure lateral impact of an aircraft would be rare indeed, and rotation (D) will have an insignficant effect on model response. Therefore, the limiting rotation β_{S_i}

(see section 2.3) for the neck joint (i = 2) has been taken as the limit for voluntary ventriflexion, or 60 degrees. This angle can be found in table 6, along with the limiting angles for the other body joints. For all of the other angles, flexion is the most significant component for the type of motion that can usually be expected to take place in a crash environment. Therefore, the limiting angles were all taken as the limits for voluntary flexion. Note that, for the hip joint, the reference position of the body used in the mathematical model includes 90-degree flexion. Therefore, this amount has been subtracted from the angle reported in table 5, which is defined relative to the standard anatomical reference position. Since the seated position appears to aid in flexion of the hip joint, the largest angle in the table, the one given by the Part 572 specifications, was used in determining β_{S_7} which is thus given by $\beta_{S_7} = 120° - 90° = 30°$.

TABLE 6. JOINT LIMITING ANGLES

Joint	Location	Angle - β_{S_i} (deg)
1	Back	40
2	Neck	60
3, 5	Shoulder	180
4, 6	Elbow	142
7, 9	Hip	30
8, 10	Knee	125

2.5.6 Body Stiffnesses

The lumbar spine and neck of the two-dimensional model possess exponential stiffness characteristics, in the form of equation (40), for both axial and rational deformation. Exponential stiffness characteristics for the abdomen and chest are used to soften the input force-deflection values for the lap belt and shoulder belt, respectively.

3.0 SEAT MODEL

The seat structure is modeled using the finite element method of analysis. This method has been selected because it is not reliant on previous testing, and it has the flexibility to deal with a wide range of design concepts. The specific finite element formulation used in the program is based on the WRECKER II program, developed at the ITT Research Institute (reference 12).

The SOM-LA seat analysis includes triangular plate elements, three-dimensional beam elements, and spring elements. It has the capability to model large displacements, nonlinear material behavior, local buckling, and various internal releases for beam elements. The large displacement formulation separates the element displacement field into a rigid body rotation and translation associated with a local coordinate system that moves with the element and small element distortions relative to the current position of the element coordinate system. This formulation can accommodate extremely large rotations and deflections with accuracy depending on the size of the elements relative to the curvature of the structure. Nonlinear material formulation is based on a uniaxial elastic-plastic stress-strain law for beam and spring elements and a biaxial elastic-plastic stress-strain law (Von Mises yield criterion) for plate elements. Internal releases for beam elements include shear (transverse sliding joint), moment (transverse hinge joint), thrust (axial sliding joint) and torque (axial hinge joint) releases. Also, a simple local buckling model for thin-walled tubes subjected to axial compressive and/or bending loads was incorporated into the program. This model simulates the reduction in bending rigidity of the tube as the cross section distorts during local buckling.

3.1 SOLUTION PROCEDURE

The solution procedure is based on formulation of equations of quasi-static equilibrium for the finite element model in an incremental form according to

$$\underline{K}_T \left(\bar{u}_{i+1} - \bar{u}_i\right) = \begin{cases} \bar{F}^E_{i+1} - \bar{F}^E_i & \text{if } \left(\bar{F}^E_{i+1} - \bar{F}^E_i\right) > 0 \\ 0 & \text{if } \left(\bar{F}^E_{i+1} - \bar{F}^E_i\right) \leq 0 \end{cases} \tag{60}$$

where $\underline{K}_T$ = Tangent stiffness matrix

$\bar{F}^E_i$ = External forces applied at i^{th} solution time step

$\bar{u}_i$ = Displacements (or rotations) at i^{th} solution time step.

The external forces, $\bar{F}^E$, including restraint system loads, occupant loads on the seat pan and seat back, and seat support reactions are treated as static loads on the seat structure. The mass of the seat structure is neglected, since in most simulations it will be a small percentage of the total occupant weight, and the seat structure is assumed to be in a quasi-static equilibrium with the applied external forces $\bar{F}^E$.

During the part of the simulation when the external forces on the seat structure are increasing, $\left(\bar{F}^E_{i+1} - \bar{F}^E_i\right) > 0$, the incremental displacements, $(\Delta\bar{u} = \bar{u}_{i+1} - \bar{u}_i)$, are obtained from equation (60). The total displacement of the seat structure is obtained by summation of the incremental displacements. However, when the external load(s) are decreasing, $\left(\bar{F}^E_{i+1} - \bar{F}^E_i\right) \leq 0$, the elastic unloading of the seat structure is neglected and the incremental displacement is assumed to be zero, $(\Delta\bar{u} = \bar{0})$, since in most simulations elastic deformations will be small compared with plastic deformations.

The tangential stiffness matrix $\underline{K}_T$ depends on the state of stress of the seat structure and varies with time during the simulation.

Therefore, it must be recomputed, assembled and inverted at selected time steps during the solution. The major computational effort is the inversion of $\underline{K}_T$, which requires NB^2 multiplications where B is the semibandwidth and N is the number of degrees of freedom.

3.2 COORDINATE SYSTEMS

Three different coordinate systems are used to describe the finite element model of the seat structure. They are global, nodal, and element coordinate systems.

The global coordinate system (x, y, z) is fixed in space and serves as an inertial frame of reference.

A nodal coordinate system $(\bar{\bar{x}}, \bar{\bar{y}}, \bar{\bar{z}})$ is attached to each node. The orientation of nodal axes $(\bar{\bar{x}}, \bar{\bar{y}}, \bar{\bar{z}})$ with respect to the global axes at any time is established by the components of three vectors $\bar{n}_1$, $\bar{n}_2$, $\bar{n}_3$ which remain fixed along the nodal axes $(\bar{\bar{x}}, \bar{\bar{y}}, \bar{\bar{z}})$, respectively, as the node translates and rotates. If these three unit vectors $\bar{n}_1$, $\bar{n}_2$, $\bar{n}_3$ form the columns of a 3 x 3 matrix $\underline{N}$, then any vector $\bar{v}$ can be transformed from nodal to global coordinate system by the following time-dependent transformation

$$\bar{v}_G = \underline{N}\, \bar{v}_N \tag{61}$$

An element coordinate system $(\hat{x}, \hat{y}, \hat{z})$ is attached to each element and serves to define the rigid body rotation and translation of the element. The orientation of element axes $(\hat{x}, \hat{y}, \hat{z})$ with respect to the global axes at any time is established by the components of three vectors $\bar{e}_1$, $\bar{e}_2$, $\bar{e}_3$ which remain fixed along the element axes $(\hat{x}, \hat{y}, \hat{z})$, respectively, as the element translates and rotates. If these three unit vectors $\bar{e}_1$, $\bar{e}_2$, $\bar{e}_3$ form the columns of a 3 x 3 matrix $\underline{E}$, then any vector $\bar{v}$ can be transformed from element to global coordinate system by the following time dependent transformation:

$$\bar{v}_G = \underline{E}\, \bar{v}_E \tag{62}$$

For triangular plate elements, the $\hat{z}$-axis is defined by the normal to the plane formed by the three corner nodes, and the $\hat{x}$-axis, by a line bisecting the angle at a selected node (I), as shown in figure 18.

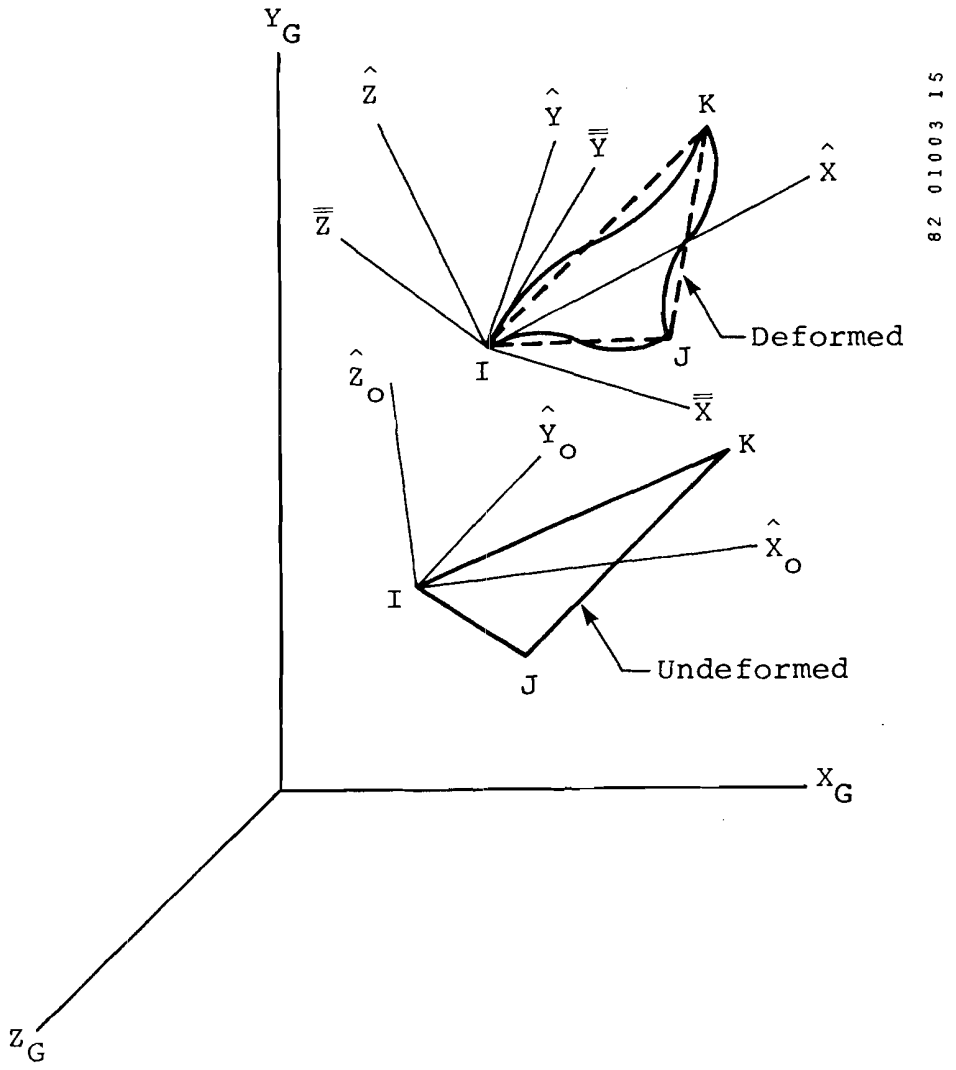

Figure 18. Three-dimensional plate element (from reference 12).

For beam elements (figure 19) the $\hat{x}$-axis is defined by a line connecting the end points of the beam, and the $\hat{y}$-axis, by a line normal to the $\hat{x}$-axis and lying in a plane containing both the

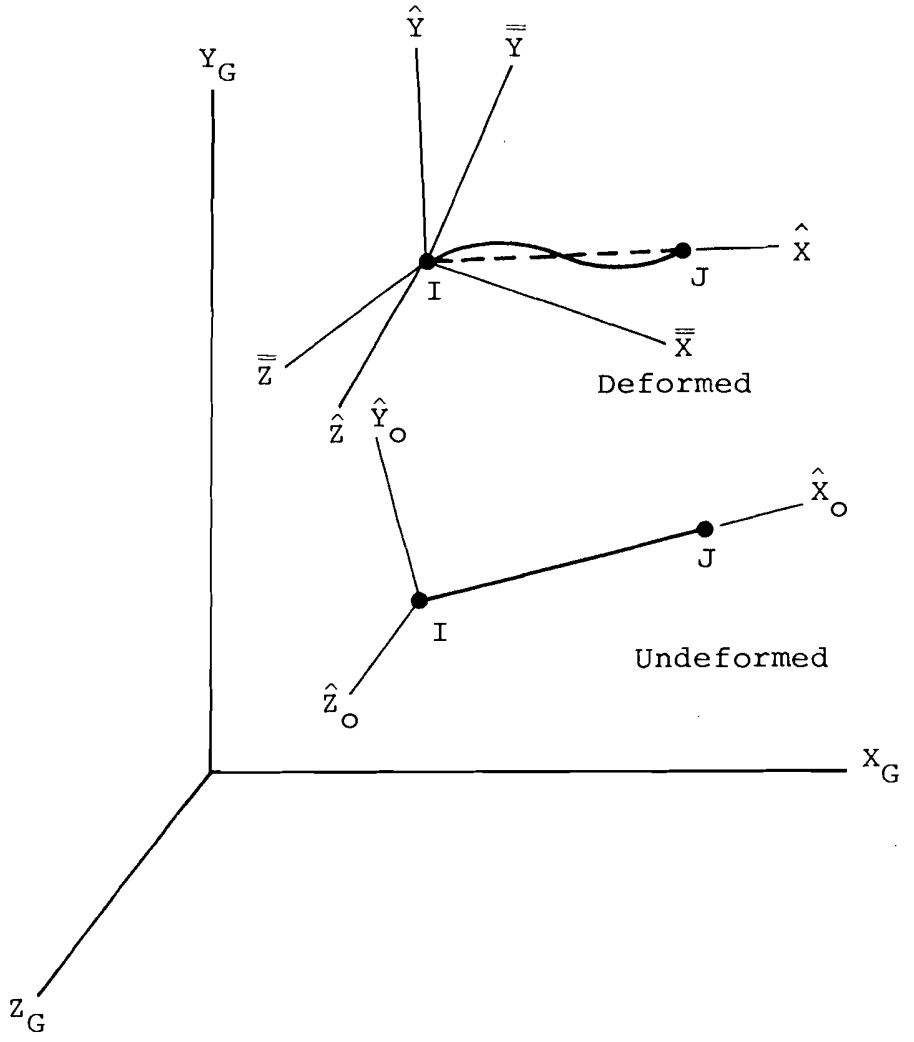

Figure 19. Three-dimensional beam element (from reference 12).

coordinate reference point and $\hat{x}$-axis. The remaining $\hat{z}$-axis is determined as a normal to $\hat{x}$- and $\hat{y}$-axes by the right-hand rule.

For spring elements, only one element axis is required, and it is defined by a line joining the end points of the spring.

3.3 ELEMENT FORMULATION

Large displacement formulation separates the element displacement field into rigid body rotation and translation and small element distortion relative to the current position of the element

coordinate system. After the rigid body motion is removed, it is possible to use the classical small deformation finite element formulations. Consequently, extremely large rotations and translations can be accommodated with accuracy depending on the size of the elements relative to the deformed curvature of the structure.

3.3.1 Beam Element

The beam element is based on the conventional small-deflection formulation involving cubic displacement fields for transverse displacements and linear displacements for axial and torsional displacements.

From the principle of virtual work, the general form of the beam element tangent stiffness matrix (reference 12) is given by

$$\underline{K}_T = \int_V \underline{D}^T \underline{C} \underline{D} \, dV \tag{63}$$

where $\underline{K}_T$ = Element tangent stiffness matrix

$\underline{D}$ = Matrix that relates element strains to nodal displacements

$\underline{C}$ = Constitutive matrix that relates stresses and strains.

For linear elastic beams, the form of the equation given in equation (63) results in the classical 12 x 12 elastic beam stiffness matrix shown in figure 20.

Where

A = area of cross section

E = modulus of elasticity

I = moment of inertia

G = modulus of rigidity

J = torsion constant

L = length of member

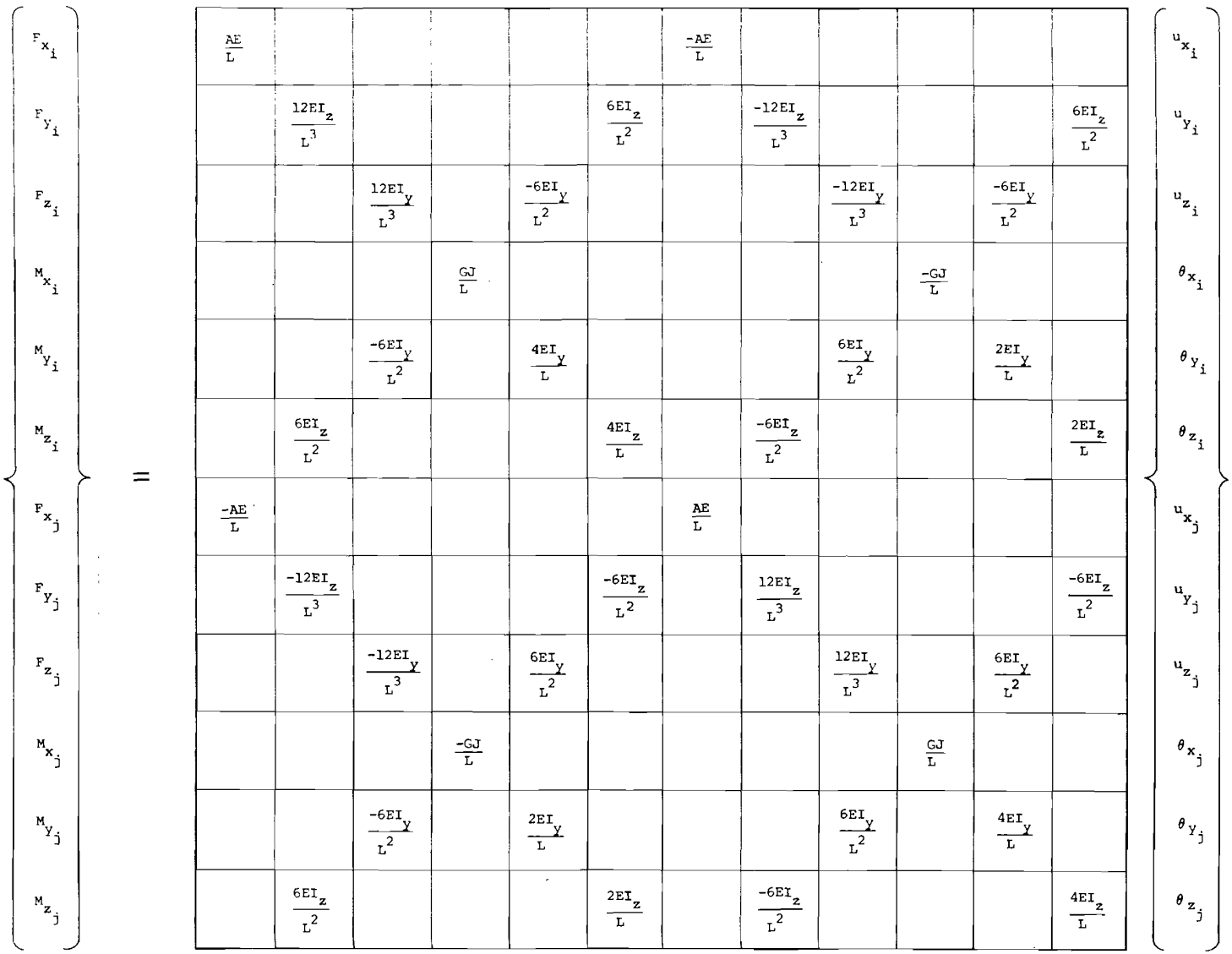

Figure 20. Elastic three-dimensional beam stiffness matrix.

M_{x_i}, (M_{y_i}), (M_{z_i}) = moment about x, (y), (z) at node i

F_{x_i}, (F_{y_i}), (F_{z_i}) = force in x, (y), (z) direction at node i

θ_{x_i}, (θ_{y_i}), (θ_{z_i}) = rotation about x, (y), (z) axis at node i

u_{x_i}, (v_{y_i}), (w_{z_i}) = x, (y), (z) component of displacement at node i

For nonlinear materials the constitutive matrix $\underline{C}$ is given by

$$\underline{C} = \frac{\Delta\sigma}{\Delta\varepsilon} \tag{64}$$

where $\Delta\sigma$ = incremental stress

$\Delta\varepsilon$ = incremental strain.

Using the cubic shape functions for the transverse displacements and linear shape functions for axial and torsional displacements in matrix $\underline{D}$ it can be shown that (reference 12)

$$\underline{K}_T = \frac{1}{\ell^4} \int_0^{\ell} \begin{bmatrix} \alpha\ell^2 & -\beta_z\ell f_2 & \beta_y\ell f_2 & -\beta_z\ell f_1 & \beta_y\ell f_1 \\ & \delta_z f_2^2 & -\delta_x f_2^2 & \delta_z f_3 & -\delta_x f_3 \\ & & \delta_y f_2^2 & -\delta_x f_3 & \delta_y f_3 \\ & & & \delta_z f_1^2 & -\delta_x f_1^2 \\ & & & & \delta_y f_1^2 \end{bmatrix} d\ell \tag{65}$$

where ℓ = element length

$f_1 = 6x - 2\ell$

$f_2 = 6x - 4\ell$

$$f_3 = f_1 f_2$$

$$\alpha = \int_A \frac{\Delta\sigma}{\Delta\varepsilon}\, dA$$

$$\beta_y = \int_A y \frac{\Delta\sigma}{\Delta\varepsilon}\, dA, \quad \beta_z = \int_A z \frac{\Delta\sigma}{\Delta\varepsilon}\, dA$$

$$\delta_x = \int_A yz \frac{\Delta\sigma}{\Delta\varepsilon}\, dA, \quad \delta_y = \int_A y^2 \frac{\Delta\sigma}{\Delta\varepsilon}\, dA,$$

$$\delta_z = \int_A z^2 \frac{\Delta\sigma}{\Delta\varepsilon}\, dA \qquad (66)$$

The integrals defined in equations (65) and (66) are calculated numerically through the cross section and along the length of the beam element. The integration is piecewise linear through the depth and linear along the length.

3.3.2 Spring Element

The spring element is a one-dimensional element, and its tangent stiffness matrix is a degenerate case of that of the beam element described in section 3.3.1.

The element stiffness matrix is given by

$$\underline{K}_T = \begin{bmatrix} k & -k \\ -k & k \end{bmatrix} \qquad (67)$$

where k is a spring constant that depends on the state of stress.

3.3.3 Plate Element

Triangular plate element formulation is based on small-deflection linear plate theory involving a linear displacement field for mid-plane deformations and a cubic displacement field for plate bending deformations (reference 13).

Node point degrees of freedom are two in-plane displacements u_x and u_y, and two rotations θ_x and θ_y. Nodal rotations normal to the plane of the plate, θ_z, are not admitted. The out-of-plane displacements u_z are zero, since the x-y element coordinate plane is established by the deformed position of the nodes.

The development of the tangent stiffness matrix for plates is similar to the development for beams. The general form of the plate element stiffness matrix is the same as equation (63)

$$\underline{K}_T = \int \underline{D}^T \, \underline{C} \, \underline{D} \, dV$$

where $\underline{C}$ = constitutive matrix that relates the biaxial stresses and strains

$$\underline{C}^T = \begin{bmatrix} \frac{\Delta\sigma_{xx}}{\Delta\varepsilon_{xx}} & \frac{\Delta\sigma_{yy}}{\Delta\varepsilon_{yy}} & \frac{\Delta\sigma_{xy}}{\Delta\varepsilon_{xy}} \end{bmatrix}$$

$\underline{D}$ = Matrix that relates element strains to nodal displacements.

Triangular plate element elastic stiffness matrix is given in reference 13.

For nonlinear materials, the stiffness matrix must be calculated by numerical integration based on the current state of stress and the plate strain-displacement relations. This development given in reference 12 is as follows:

The plate strains can be written as a combination of the membrane strains ε^0_{ij} and curvature functions κ_{ij} in the form

$$\varepsilon = \begin{Bmatrix} \varepsilon_{xx} \\ \varepsilon_{yy} \\ \varepsilon_{xy} \end{Bmatrix} = \begin{Bmatrix} \varepsilon^0_{xx} \\ \varepsilon^0_{yy} \\ \varepsilon^0_{xy} \end{Bmatrix} - z \begin{Bmatrix} \kappa_{xx} \\ \kappa_{yy} \\ \kappa_{xy} \end{Bmatrix} \qquad (68)$$

or,
$$\bar{\varepsilon} = \underline{\phi}\ \bar{u} - z\ \underline{\psi}\ \bar{\theta}$$

where $\bar{u}$ = in-plane displacements

$\bar{\theta}$ = plate corner rotations

$\underline{\phi}$ = matrix of membrane strain functions (reference 13)

$\underline{\psi}$ = matrix of curvature functions (reference 12).

The complete strain-displacement transformation matrix $\underline{D}$ has the form

$$\underset{\sim}{D} = \begin{bmatrix} \underline{\phi} & 0 \\ 0 & -z\underline{\psi} \end{bmatrix} \tag{69}$$

When this form of $\underline{D}$ is introduced into the stiffness matrix integral equation (63), it results in

$$\underline{K}_T = \begin{bmatrix} \underline{K}_{uu} & \underline{K}_{u\theta} \\ \underline{K}_{\theta u} & \underline{K}_{\theta\theta} \end{bmatrix} \tag{70}$$

where
$$\begin{aligned} \underline{K}_{uu} &= \int_V \underline{\phi}^T\ \underline{C}\ \underline{\phi}\ dV \\ \underline{K}_{u\theta} &= \int_V z\ \underline{\phi}^T\ \underline{C}\ \underline{\phi}\ dV \\ \underline{K}_{\theta u} &= \int_V z\ \underline{\psi}^T\ \underline{C}\ \underline{\phi}\ dV \\ \underline{K}_{\theta\theta} &= \int_V z^2\ \underline{\psi}^T\ \underline{C}\ \underline{\phi}\ dV \end{aligned} \tag{71}$$

These may be further written in terms of area and thickness integrals as

$$\underline{K}_{uu} = \int_A \underline{\phi}\, \underline{C}_{uu}\, \underline{\phi}^T \, dA$$

$$\underline{K}_{u\theta} = -\int_A \underline{\phi}^T\, \underline{C}_{u\theta}\, \underline{\psi} \, dA \qquad (72)$$

$$\underline{K}_{\theta u} = -\int_A \underline{\psi}^T\, \underline{C}_{\theta u}\, \underline{\phi} \, dA$$

$$\underline{K}_{\theta\theta} = \int_A \underline{\psi}^T\, \underline{C}_{\theta\theta}\, \underline{\psi} \, dA$$

where

$$\underline{C}_{uu} = \int_{-h/2}^{h/2} \underline{C} \, dz$$

$$\underline{C}_{u\theta} = \underline{C}_{\theta u} = \int_{-h/2}^{h/2} z\, \underline{C} \, dz \qquad (73)$$

$$\underline{C}_{\theta\theta} = \int_{-h/2}^{h/2} z^2\, \underline{C} \, dz$$

The matrices $\underline{C}_{uu}$, $\underline{C}_{u\theta}$, and $\underline{C}_{\theta\theta}$ in equation (73) are integrated numerically by trapezoidal rule. For elastic materials $\underline{C}_{u\theta}$ vanishes and hence

$$\underline{K}_{u\theta} = \underline{K}_{\theta u} = \underline{0}$$

The integrals in equation (72) are then evaluated by numerical quadratures. These integrations involve cross section integrations carried out each time the stiffness matrix is created.

3.4 INTERNAL RELEASES IN BEAM ELEMENTS

Internal releases for beam elements include shear (transverse sliding joint), moment (transverse hinge joint), thrust (axial sliding joint) and torque (axial hinge joint) releases. Combinations of

these releases are possible, e.g., a ball joint is formed by two transverse hinge joints in two different directions. Depending on the type of internal release, the original beam element stiffness matrix is modified for force and moment releases at specified locations within the element.

For axial sliding and hinge joints, the original joint stiffness is ignored. For other types of releases stiffness matrix modifications, formulated in reference 12, are developed below. Referring to figure 21, let the release be located at a distance "a" from the i^{th} end, and "b" from the j^{th} end. It is assumed that the original stiffness matrix $\underline{K}$ relating end rotations (ϕ_i, ϕ_j) and moments (M_i, M_j) of the element is known. The moment M_D and shear V_D at the joint are shown in figure 21.

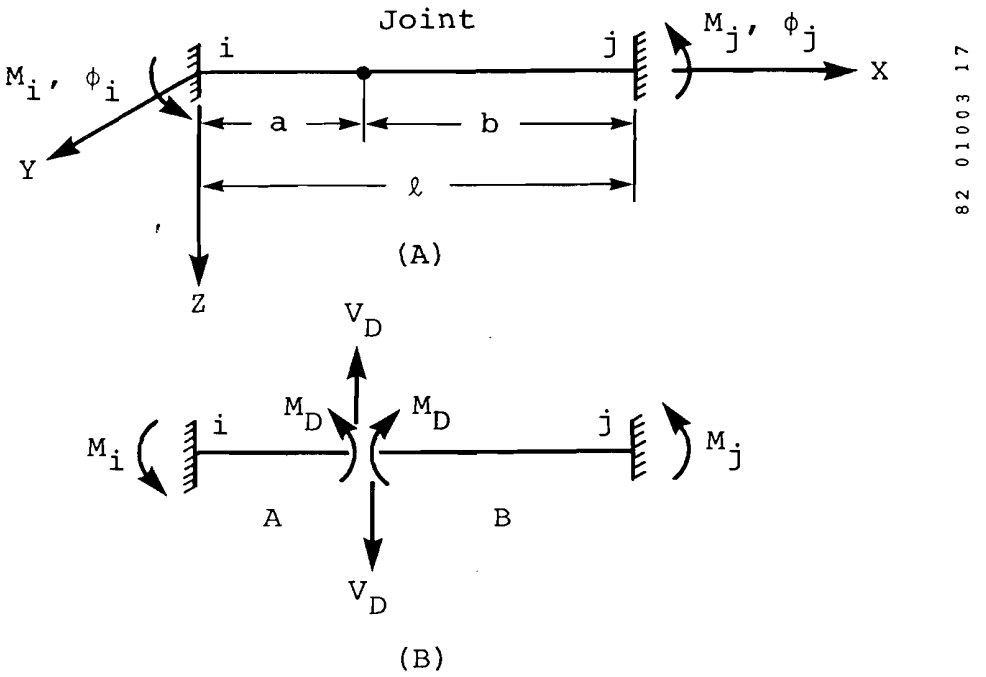

Figure 21. Beam element internal releases (from reference 12).

To satisfy the equilibrium on parts of the beam to the left and right of the joint, a relationship between end moments $\overline{S}_{ij} = (M_i \; M_j)$ and the forces $\overline{S}_D = (M_D \; V_D)$ at the joint is developed

$$\bar{S}_{ij} = \underline{T}\ \bar{S}_D \tag{74}$$

where

$$T = \begin{bmatrix} -1 & (-1)^n a \\ 1 & (-1)^n b \end{bmatrix}$$

and

$$n = \begin{cases} 1 \text{ if } S_{ij} \text{ is in z-direction} \\ 2 \text{ if } S_{ij} \text{ is in y-direction} \end{cases}$$

The relationship between the forces and the displacements $\bar{\delta}_D^T = (0_D, v_D)$ will be

$$\bar{S}_D = \underline{K}_D\ \bar{\delta}_D \tag{75}$$

Let $\underline{K}_D$ be of the form

$$\underline{K}_D = \begin{bmatrix} D_{ii} & D_{ij} \\ D_{ji} & D_{jj} \end{bmatrix}$$

It can be shown that

$$\underline{K}_D = \underline{T}^{-1}\ \underline{K}\ (\underline{T}^{-1})^T \tag{76}$$

The reverse transformation also holds that

$$\underline{K} = \underline{T}\ \underline{K}_D\ \underline{T}^T \tag{77}$$

At a transverse hinge joint no moment can be transmitted about the released axis, hence $M_D = 0$. Substituting $M_D = 0$ into equation (75), the reduced stiffness matrix $\underline{K}_D'$ is

$$\underline{K}_D' = \begin{bmatrix} 0 & 0 \\ 0 & D_{jj} - D_{ij}\ D_{ji}/D_{ii} \end{bmatrix} \tag{78}$$

Then the modified beam element stiffness matrix can be obtained from equation (77)

$$\underline{K}' = \underline{T}\ \underline{K}'_D\ \underline{T}^T \tag{78a}$$

At a transverse sliding joint no shear can be transmitted along the released axis, hence $V_D = 0$. Substituting $V_D = 0$ into equation (75), the reduced stiffness matrix $\underline{K}'_D$ is

$$\underline{K}'_D = \begin{bmatrix} D_{ii} - D_{ij}\ D_{ji}/D_{jj} & 0 \\ 0 & 0 \end{bmatrix} \tag{79}$$

Equation (73a) is also valid for this case.

In addition to the stiffness matrix, beam element end moments must also be modified. The shear forces and moments at the joint can be expressed in terms of end shear forces and moments by solving for $\overline{S}_D$ from equation (74).

$$\overline{S}_D = \underline{T}^{-1}\overline{S}_{ij} \tag{80}$$

To implement a joint, apply $-M_D$ to the member at the joint, set $V_D = 0$ but allow θ_D. Solve equation (75) for θ_D and v_D in terms of M_D. Solve equation (75) for M_D in terms of M_i and M_j. Combining the results with equation (74), the effect of the release $-M_D$ on S_{ij} is given by

$$\begin{bmatrix} M_i \\ M_j \end{bmatrix}' = \left(\begin{bmatrix} 1 & 0 \\ 0 & 1 \end{bmatrix} + T/\ell \begin{bmatrix} b & -a \\ b\ D_{ji}/D_{ii} & -a\ D_{ji}/D_{ii} \end{bmatrix} \right) \begin{bmatrix} M_i \\ M_j \end{bmatrix} \tag{81}$$

To implement a sliding joint, apply $-V_D$ to the member at the joint, set $\theta_D = 0$ but allow v_D and use the same procedure as for a hinge. Modified end forces take the form

$$\begin{bmatrix} M_i \\ M_j \end{bmatrix}' = \left(\begin{bmatrix} 1 & 0 \\ 0 & 1 \end{bmatrix} + T/\ell \begin{bmatrix} D_{ij}/D_{jj} & D_{ij}/D_{jj} \\ 1 & 1 \end{bmatrix} \right) \begin{bmatrix} M_i \\ M_j \end{bmatrix} \qquad (82)$$

3.5 MATERIAL NONLINEARITIES

Nonlinear material formulation is based on uniaxial elastic-plastic stress-strain law for beam and spring elements and bi-axial elastic-plastic stress-strain law (Von Mises yield criterion) for plate elements.

The computational procedure for a biaxial stress field for plates is presented in reference 12 and is based on the work of Hartzman and Hutchinson, (reference 14), as specialized for small strain and plane stress conditions. The current stress state at a point in the plate is established as follows; Let the prior stress state of the point under consideration be σ_{xx}^0, σ_{yy}^0, σ_{xy}^0 and a small increment in strain from the prior state to the current state be $\Delta\varepsilon_{xx}$, $\Delta\varepsilon_{yy}$, $\Delta\varepsilon_{xy}$. First a tentative, current stress state, $\bar{\bar{\sigma}}_{xx}$, σ_{yy}, σ_{xy} is calculated as though the strain increment were completely elastic.

$$\begin{aligned} \bar{\bar{\sigma}}_{xx} &= \sigma_{xx}^0 + \frac{E}{1-\nu^2} (\Delta\varepsilon_{yy} + \nu\Delta\varepsilon_{yy}) \\ \bar{\bar{\sigma}}_{yy} &= \sigma_{yy}^0 + \frac{E}{1-\nu^2} (\Delta\varepsilon_{yy} + \nu\Delta\varepsilon_{xx}) \qquad (83) \\ \bar{\bar{\sigma}}_{xy} &= \sigma_{xy}^0 + G\ \Delta\varepsilon_{xy} \end{aligned}$$

where E = Modulus of Elasticity

G = Shear Modulus

ν = Poisson's Ratio

An effective stress, $\bar{\bar{\sigma}}_e$, to determine whether plastic flow has taken place during the strain increment is calculated using the Von Mises criterion

$$\bar{\bar{\sigma}}_e = (\bar{\bar{\sigma}}_{xx}^2 - \bar{\bar{\sigma}}_{xx}\,\bar{\bar{\sigma}}_{yy} + \bar{\bar{\sigma}}_{yy}^2 + 3\bar{\bar{\sigma}}_{xy}^2)^{1/2} \tag{84}$$

If $\bar{\sigma}_e$ is less than the prior effective stress σ_e^0 at which yielding occurred, elemental loads are decreasing and the tentative stresses calculated ($\bar{\bar{\sigma}}_{xx}$, $\bar{\bar{\sigma}}_{yy}$, $\bar{\bar{\sigma}}_{xy}$) are the correct values of the current stress values (σ_{xx}, σ_{yy}, σ_{xy}). If $\bar{\bar{\sigma}}_e$ is greater than the prior effective stress σ_e^0, at which yielding occurred, tentative stresses calculated must be modified to account for the plastic behavior. Hartzman and Hutchinson (reference 14) have shown that the true value of the current effective stress will be

$$\sigma_e = \frac{\sigma_e^0 + (\frac{H'}{3G})\,\bar{\bar{\sigma}}_e}{1 + (\frac{H'}{3G})} \tag{89}$$

where $$H_i' = \frac{(E)(E_{pi})}{E - E_{pi}} \qquad i = 1, 2$$

and E_{pi} = Plastic modulus (figure 22)

The current state of stress is then given by

$$\sigma_{xx} = \frac{1}{1 + 3\lambda}\,[\bar{\bar{\sigma}}_{xx} + \lambda(\bar{\bar{\sigma}}_{xx} + \bar{\bar{\sigma}}_{yy})]$$

$$\sigma_{yy} = \frac{1}{1 + 3\lambda}\,[\bar{\bar{\sigma}}_{yy} + \lambda(\bar{\bar{\sigma}}_{xx} + \bar{\bar{\sigma}}_{yy})] \tag{86}$$

$$\sigma_{xy} = \frac{1}{1 + 3\lambda}\,\bar{\bar{\sigma}}_{xy}$$

where λ is given by

$$\lambda = \frac{1}{3}\left(\frac{\bar{\bar{\sigma}}_e}{\sigma_e} - 1\right) \tag{87}$$

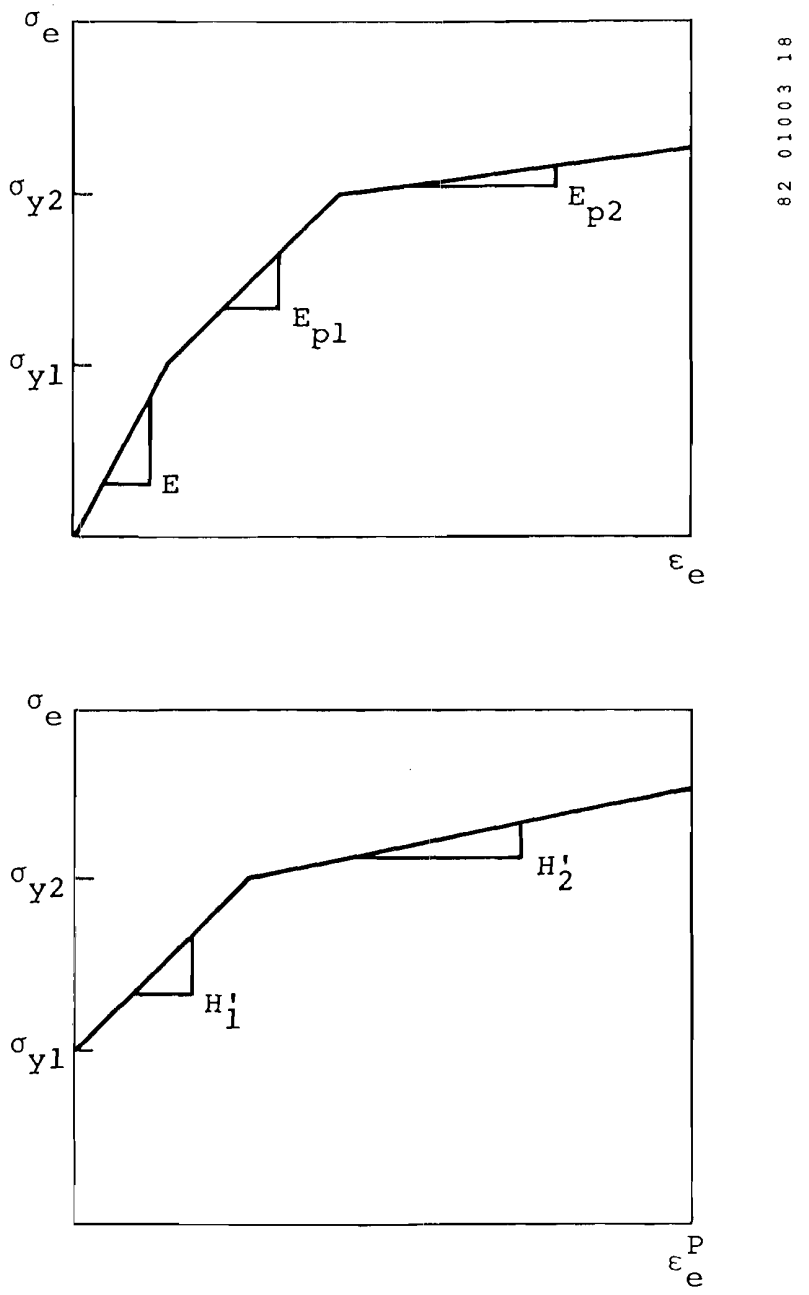

Figure 22. Trilinear stress-strain relation.

The extension of the formulation presented to uniaxial stress field for beam and spring elements is straightforward with $\sigma_{yy} = \sigma_{xy} = 0$.

3.6 LOCAL BUCKLING OF BEAM ELEMENTS

Local buckling is one of the failure modes of thin-walled tubes, typically used in light aircraft seats, when subjected to axial compressive and/or bending loads. Evaluation of the results of dynamic tests of seat-occupant systems have indicated that the local buckling of thin-walled tubes have a significant effect on the response of the seat-occupant system. Therefore, a simple local buckling model for thin-walled tubes was incorporated into the program.

Local buckling is traditionally expressed in terms of a moment-bending curvature diagram as shown in figure 23.

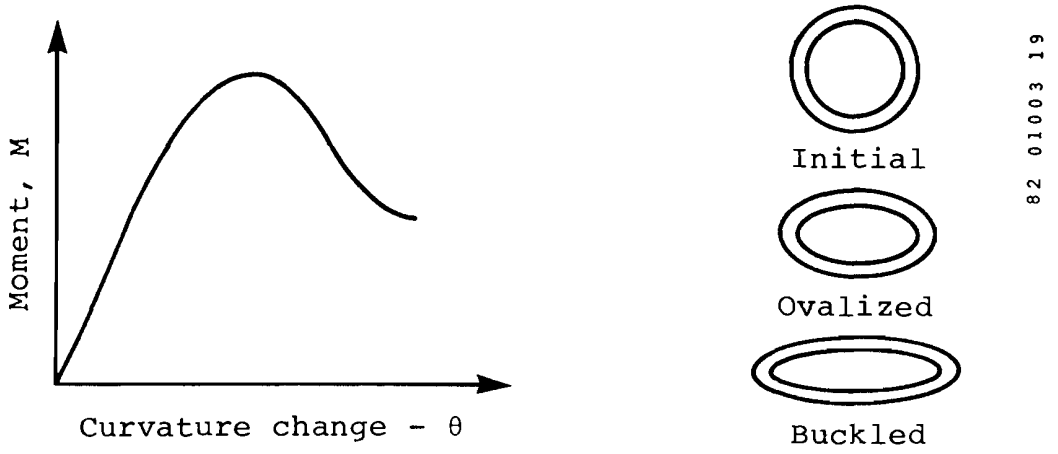

Figure 23. Moment capability versus curvature of a thin-walled circular tube.

The cross section goes through several stages of deformation as the structure bends. Although during this cross-section distortion axial stresses redistribute themselves, it was proposed in reference 15 that the reduced bending rigidity is most strongly related to the loss of lateral moment arm of the axial forces.

For a circular tube under uniform compression the stress, σ_L, at which local buckling starts is given in reference 16 as

$$\sigma_L = K_c E(\frac{t}{D}) \tag{88}$$

where $0.4 < K_c < 1.2$ (recommended values)

E = modulus of elasticity

t = wall thickness of the tube

D = diameter of the tube.

It was also proposed in reference 16 that for tubes subjected to bending, the local buckling stress, σ_L, as a function of material and geometry, can be taken as that for a circular tube under uniform axial compression, since in bending, a significant portion of the circumference is subjected to a relatively uniform compression field. However, dynamic tests of seat-occupant systems have indicated that the thin-walled circular tubes have suffered local buckling at stress levels much below that predicted by equation (88). This was partly due to the fact that the bending stresses have exceeded the yield point and the tubes have also suffered plastic deformation.

To account for plasticity as well as the cross-sectional properties, an empirical relation, equation (89) was used in the program to predict the local-buckling stress

$$\sigma_L = \sigma_y - (\frac{K}{E})(\frac{D}{t}) \tag{89}$$

where σ_L = local buckling stress

σ_y = yield stress

K = local buckling coefficient

t = wall thickness of the tube

D = diameter of the tube*.

The cross sections of beam elements are defined as thin-walled plate segments by specifying their end points and thickness as part of the input data (figure 24). The tangent stiffness matrix for nonlinear beam elements is then computed by evaluating the integrals given in equation (66) by Gaussian quadrature over the plate segments defining the beam cross section.

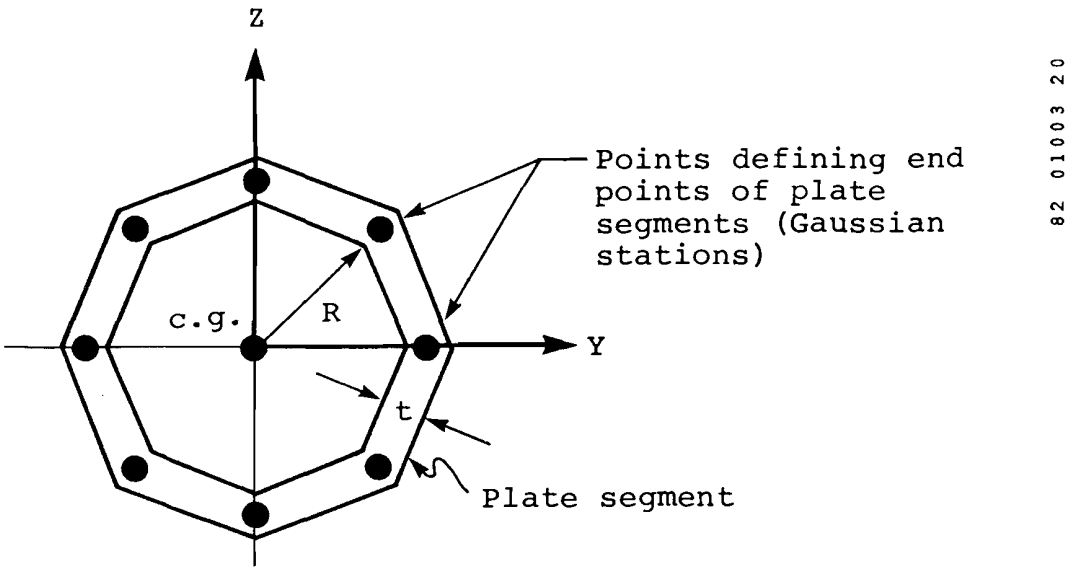

Figure 24. Circular tube cross section defined by eight thin-walled plate segments.

The program computes the stresses at all Gaussian stations across the cross section at each end of the beam elements. These stresses are then compared with the local buckling stress, σ_L, computed from equation (89) for each beam element. If any of the compressive stresses at the Gaussian stations exceed σ_L, the deformation

*For rectangular tubes the diameter of a circumscribing circular tube is used.

of the cross section is modeled by modifying the radial location of that Gaussian station using the following expression

$$R_{i+1} = \left(\frac{\sigma_L}{|\sigma_{i+1}|} \right)^K R_i \quad \text{if} \quad |\sigma_{i+1}| > \sigma_L \tag{90}$$

where R_i = radial location of the Gaussian station at time step i

σ_L = local buckling stress

σ_{i+1} = compressive stress at the Gaussian station at time step i+1

K = local buckling constant (0.50 recommended).

Consequently, reduced bending rigidity of the cross section due to the decrease in the lateral moment arm of axial forces during local buckling can be modeled.

4.0 SIMULATION COMPUTER PROGRAM

The digital computer program based on the occupant and seat models described in chapters 2 and 3 is called Seat/Occupant Model - Light Aircraft (SOM-LA). It has been written entirely in FORTRAN to ensure a high degree of compatibility with various digital computer systems. During development, the program has been run on IBM, UNIVAC, and CDC computer systems.

The elements of the program can be considered in terms of three general operations:

- Input and initialization
- Solution
- Output

which are summarized below and discussed in detail in the sections following. The general flow of the program is illustrated in figure 25. Input data describing the occupant and crash conditions are read first. If the user requests output of the prediction of impact between the occupant and the aircraft interior, the coordinates defining the cockpit surfaces are read. Finally, the seat data, either simple dimensions describing a rigid seat model or detailed design data for the finite element seat analysis, are provided. Based on the input data, the values of constants, such as occupant dimensions and properties are calculated, and the initial position of the occupant is determined.

The solution loop is entered for the first time with the aircraft initial velocity and the occupant initial position. At each subsequent entrance to the loop, the current aircraft displacement, velocity, and acceleration components are calculated. The equations of motion for the occupant are set up and solved. If a finite element seat model is being used, the forces applied to the seat, such as the cushion forces, are provided to the seat

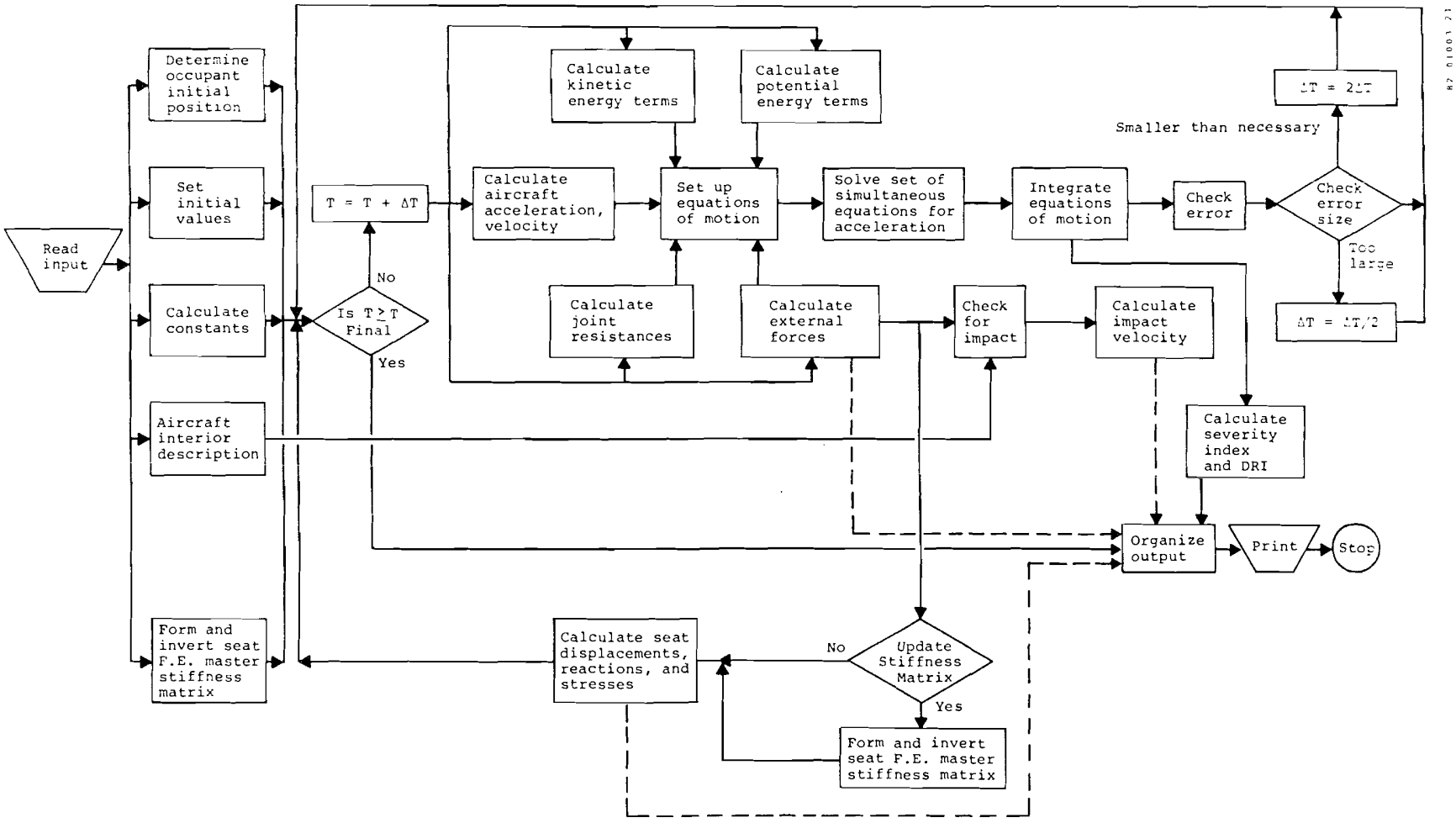

Figure 25. Program flow chart.

routines for computation of seat displacements. At time increments equal to a predetermined print interval, the output variables requested by the user are stored for printing after completion of the solution.

4.1 PROGRAM INPUT

Input data are read by the program in the following seven blocks:

1. Simulation and output control information
2. Cockpit description (optional)
3. Cushion properties
4. Restraint system description
5. Crash conditions
6. Occupant description
7. Seat design information.

4.1.1 Simulation Control Information

The first block of data contains the information required for controlling execution of the program. The initial time step for integration of the equations of motion, the total length of simulation, the number of cases to be run, the system of units (SI or English), selection of two-or three-dimensional occupant, and identification of the desired output are provided here.

4.1.2 Cockpit Description

For prediction of impact between the occupant and the cockpit interior, ten plane surfaces are used to describe the cockpit. As shown in figure 26, six of these surfaces are normal to the X_A - Z_A plane and four are normal to the Y_A - Z_A plane. The first five planes can be used to describe the environment of a crewseat, in which case they represent the firewall, instrument panel, and windscreen, or, for analysis of a passenger seat,

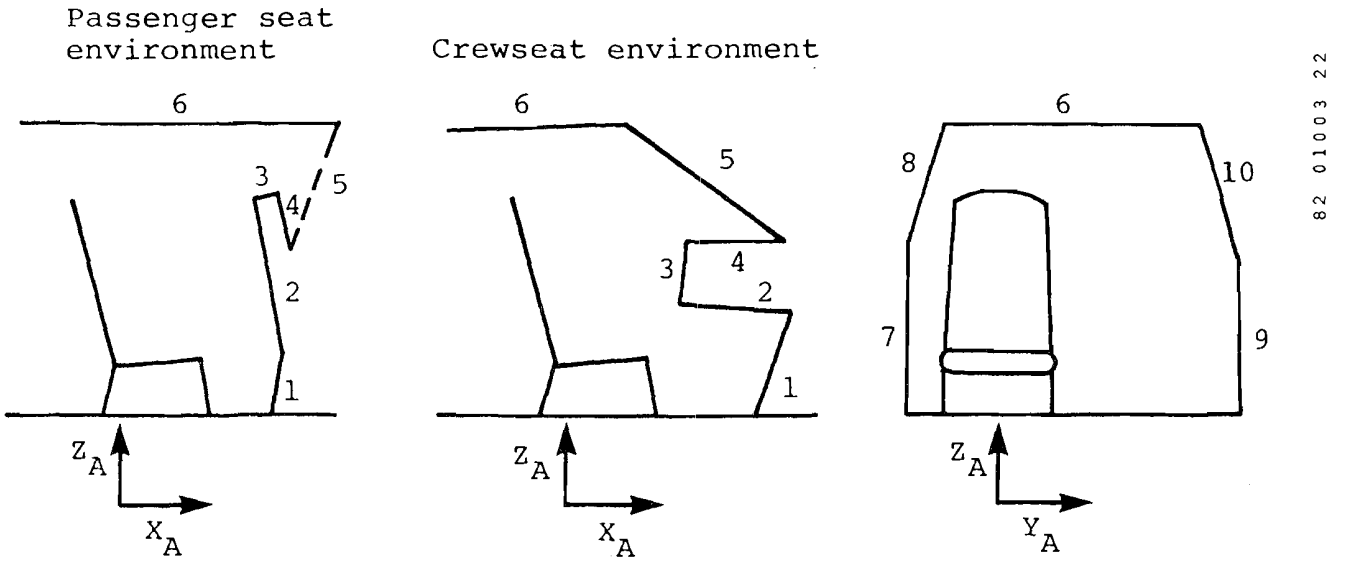

Figure 26. Planar surface approximation to aircraft interior.

they can be rearranged to describe a seat back. Input data include X and Z coordinates to define planes 1-6 and Y and Z coordinates for planes 7-10.

4.1.3 Cushion Description

Cushion load-deflection characteristics are described by an exponential function, whose coefficients are provided as input data. The equilibrium (zero load) thickness for both the seat and back cushions are also given. The cushion damping coefficient for zero deflection described in section 2.4.1 is also entered.

4.1.4 Restraint System Description

The restraint system used in the simulation may consist of a lap belt alone or combined with a single- or double-strap shoulder harness. A lap belt tiedown (negative -G) strap can also be included. The webbing force-elongation curve is approximated by three linear segments, which are described by input of points on

the curve. The force is computed by linear interpolation in this table, as described in section 4.3.1. The slack in the webbing is also provided by input in units of length.

The anchor points for the lap belt, shoulder harness, and tiedown strap are located by input of rectangular coordinates in the aircraft reference system. For a double-strap shoulder harness, the buckle, or point of connection to the lap belt, is assumed located on the mid-point of the lap belt. If a tiedown strap is included in this case it also connects to the other restraint system components at the buckle. For a single shoulder belt, which may pass over either the left or the right shoulder, an input parameter locates the buckle by the length of webbing between the buckle and the lap belt anchor point. This length may be zero if the buckle attaches directly to a rigid anchor point.

4.1.5 Crash Conditions

The aircraft crash conditions are defined by the initial velocity and attitude and the acceleration as a function of time. Six components of velocity are required: three translational in the aircraft coordinate system (V_{X_A}, V_{Y_A}, V_{Z_A}) and the yaw, pitch, and roll rates ($\dot{\psi}_A$, $\dot{\theta}_A$, $\dot{\phi}_A$). Each of the six acceleration components, which define the acceleration of the aircraft coordinate system, is described by sixteen points in time and acceleration. An example of an approximation to an actual acceleration pulse is illustrated in figure 27. Although many of the higher frequency oscillations observed in the actual pulse probably contribute little to the overall response of the occupant, the use of a large number of points reduces the effect of the investigator's subjectivity in the approximation.

4.1.6 Occupant Description

Because it has been assumed that the principal user of this program is interested primarily in the seat or restraint system, a

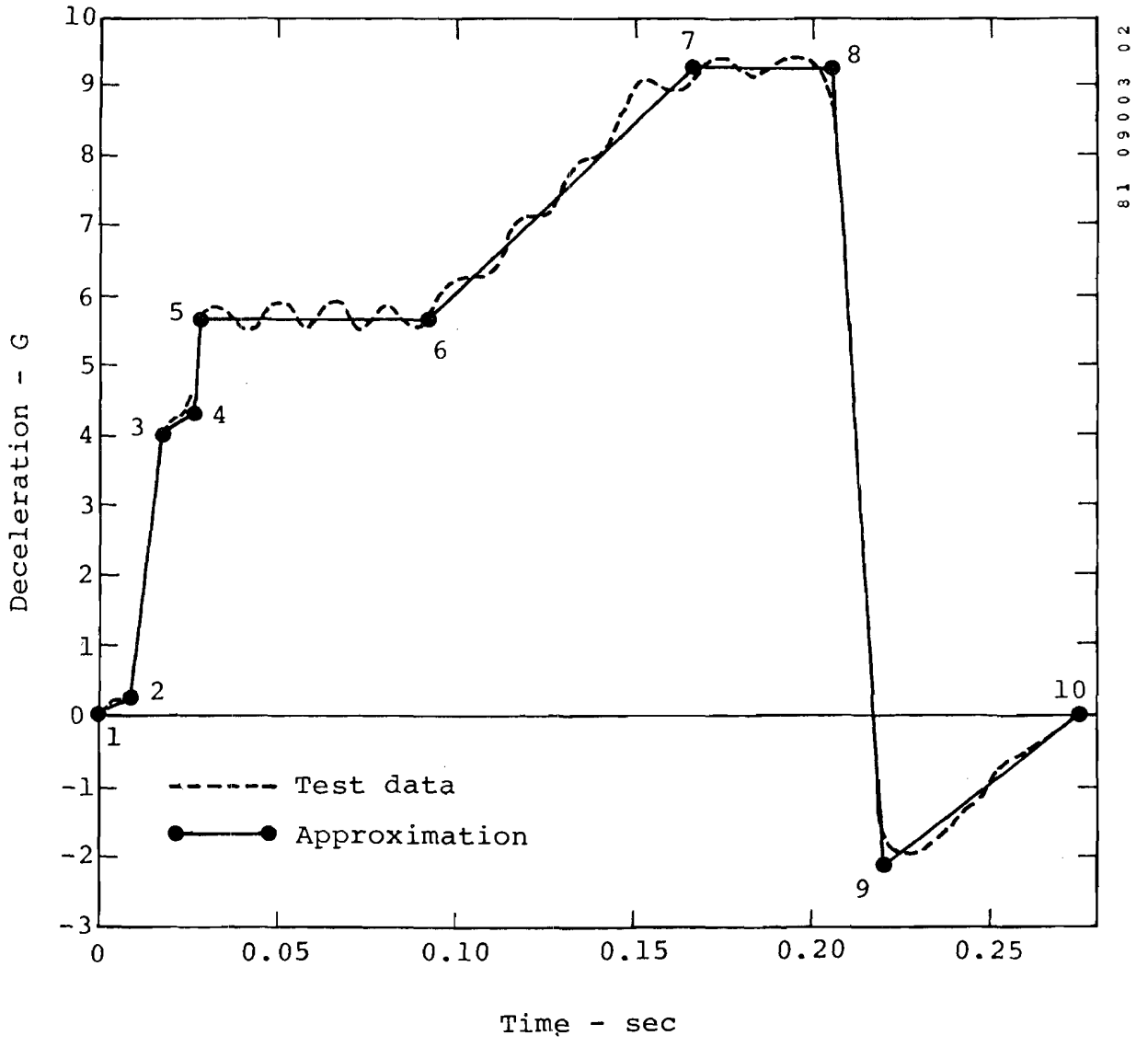

Figure 27. Piecewise approximation to aircraft acceleration component.

minimum of information is required to describe the occupant. Data for standard human and dummy occupants, as described in section 2.5, are stored within the program. Additional data must be provided for nonstandard occupants.

4.1.7 Seat Design Information

The input data required to describe the seat consist of nodal coordinates, material properties, cross-section geometries, element

locations, and attachment conditions, as described earlier. For possible use in restraint system or cabin configuration analyses where detailed seat response may not be important or seat design unknown, a rigid seat model can be selected. Input data for the rigid seat option consist only of locations of the seat pan and seat back.

4.2 OCCUPANT INITIAL POSITION

The initial position of the aircraft occupant is computed from the input parameters shown in figure 28. It is assumed that the occupant is seated symmetrically with respect to the aircraft (X_A - Z_A) plane or, equivalently, that the segment-fixed y_n-axes are all parallel to the Y_A-axis. The angular coordinates γ_i (i = 1, 2, 3, 4) define the rotation of segments 1-4 relative to the Z_A axis and, because of the symmetry condition, segment 6 is parallel to segment 4. Positive angles are shown in figure 28 although γ_1 and γ_2 are usually negative, considering the torso to be approximately parallel to an aftward-sloping seat back. The angle γ_5 describes the position of the forearms relative to the upper arms, and is the initial value of α_5 and α_7. The distance X_H is the initial X-coordinate of the heels (the inferior ends of segments 9 and 11). The procedure described below consists of seating the occupant in such a position that static equilibrium is achieved among the forces exerted by the seat cushion, floor, and either the restraint system or the back cushion.

The first step in determining the initial position for the three-dimensional occupant involves calculating the Euler angles for the torso, head, and arm segments, since this procedure does not require consideration of the forces due to the cushions and floor. Because the input parameters illustrated in figure 28 define the position of the occupant in the aircraft coordinate system, the orientation of the aircraft must be described in the inertial system. For an aircraft in level flight with zero pitch, roll, and yaw, it is assumed that the aircraft coordinate axes (X_A, Y_A, Z_A)

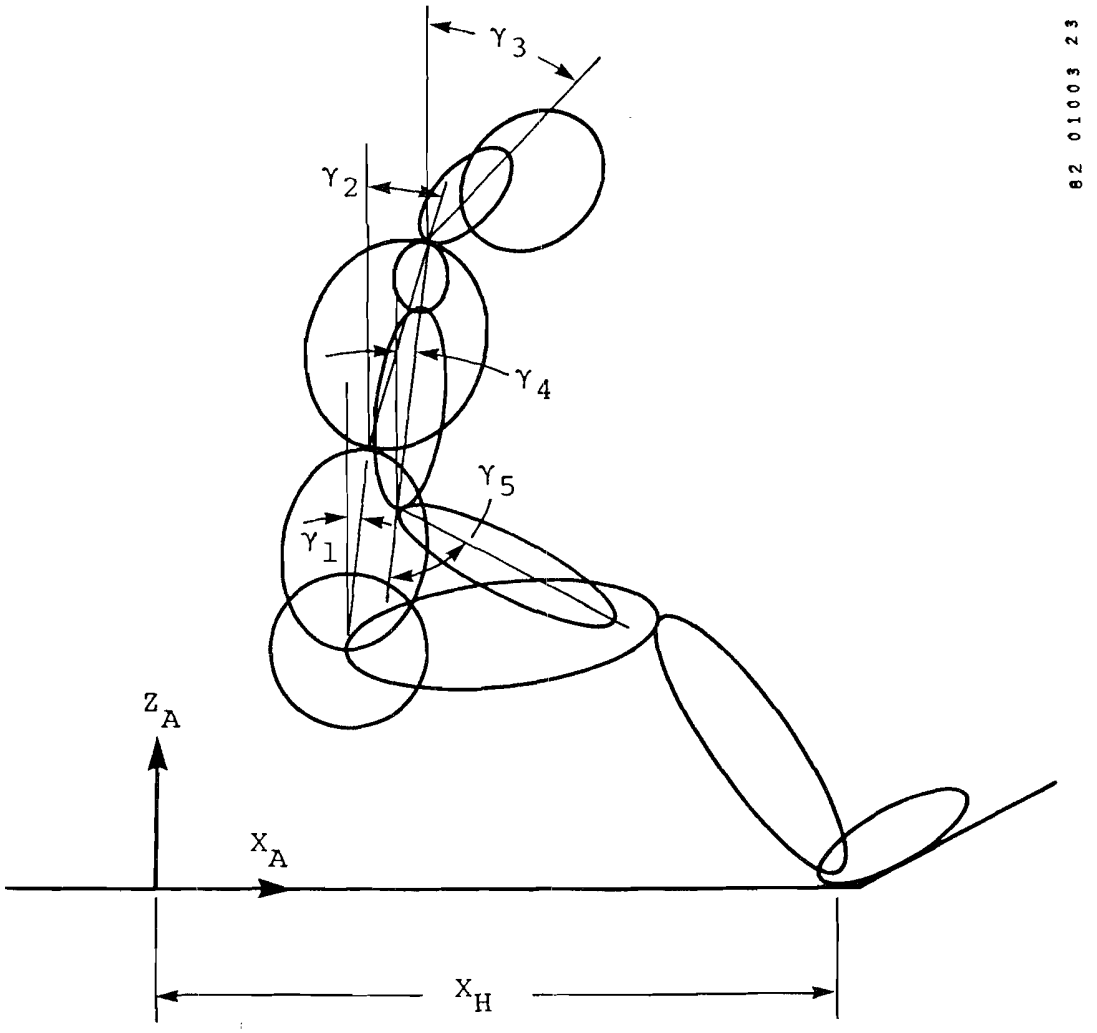

Figure 28. Initial position input parameters.

are parallel to the fixed coordinate axes (X, Y, Z) at the initial time (t = 0). A general orientation of the aircraft reference frame is obtained by the same sequence of rotations defined in section 2.1.1 for the body segments. Defining the rotations

ψ_A : Yaw

θ_A: Pitch

ϕ_A: Roll

the orientation of the aircraft relative to the inertial system is described by the coordinate transformation

$$\begin{Bmatrix} X \\ Y \\ Z \end{Bmatrix} = \begin{bmatrix} A \end{bmatrix} \begin{Bmatrix} X_A \\ Y_A \\ Z_A \end{Bmatrix} \tag{91}$$

where the elements of [A] are

$$A_{11} = \cos \psi_A \cos \theta_A$$

$$A_{12} = \cos \psi_A \sin \theta_A \sin \phi_A - \sin \psi_A \cos \phi_A$$

$$A_{13} = \cos \psi_A \sin \theta_A \cos \phi_A + \sin \psi_A \sin \phi_A$$

$$A_{21} = \sin \psi_A \cos \theta_A$$

$$A_{22} = \sin \psi_A \sin \theta_A \sin \phi_A + \cos \psi_A \cos \phi_A$$

$$A_{23} = \sin \psi_A \sin \theta_A \cos \phi_A - \cos \psi_A \sin \phi_A$$

$$A_{31} = -\sin \theta_A$$

$$A_{32} = \cos \theta_A \sin \phi_A$$

$$A_{33} = \cos \theta_A \cos \phi_A \tag{92}$$

The rotation of body segment n relative to the aircraft, remembering that the symmetry condition requires that y_n is parallel to Y_A, is described by

$$\begin{Bmatrix} X_{A_n} \\ Y_{A_n} \\ Z_{A_n} \end{Bmatrix} = \begin{bmatrix} \cos \gamma_n & 0 & \sin \gamma_n \\ 0 & 1 & 0 \\ -\sin \gamma_n & 0 & \cos \gamma_n \end{bmatrix} \begin{Bmatrix} x_n \\ y_n \\ z_n \end{Bmatrix} \tag{93}$$

Combining equations (91) and (93) results in the angular relationship between the local coordinate system of segment n and the inertial system expressed by the following transformation, which is a function of the input γ_n and the aircraft pitch, roll, and yaw:

$$\begin{Bmatrix} X_n \\ Y_n \\ Z_n \end{Bmatrix} = \begin{bmatrix} B^n \end{bmatrix} \begin{Bmatrix} x_n \\ y_n \\ z_n \end{Bmatrix} \tag{94}$$

where $[B^n]$ is given by

$$[B^n] = \begin{bmatrix} A \end{bmatrix} \begin{bmatrix} \cos \gamma_n & 0 & \sin \gamma_n \\ 0 & 1 & 0 \\ -\sin \gamma_n & 0 & \cos \gamma_n \end{bmatrix} \tag{95}$$

so that its elements are

$$B^n_{11} = A_{11} \cos \gamma_n - A_{13} \sin \gamma_n$$

$$B^n_{12} = A_{12}$$

$$B^n_{13} = A_{11} \sin \gamma_n + A_{13} \cos \gamma_n$$

$$B^n_{21} = A_{21} \cos \gamma_n - A_{23} \sin \gamma_n$$

$$B^n_{22} = A_{22}$$

$$B^n_{23} = A_{21} \sin \gamma_n + A_{23} \cos \gamma_n$$

$$B^n_{31} = A_{31} \cos \gamma_n - A_{33} \sin \gamma_n$$

$$B^n_{32} = A_{32}$$

$$B^n_{33} = A_{31} \sin \gamma_n + A_{33} \cos \gamma_n \qquad (96)$$

Comparison of equation (94) with equation (1) points out that the transformation matrices $[T^n]$ and $[B^n]$ are equivalent. Because $[T^n]$ is a function of Euler angles for segment n, equating the elements of $[T^n]$ and $[B^n]$ through

$$[T^n] = [B^n] \qquad n = 1, 2, 3, 4, 6, 8, 10 \qquad (97)$$

permits calculation of the initial values of the generalized coordinates from input parameters γ_n and ψ_A, θ_A, and ϕ_A. The procedure as used in Program SOM-LA is outlined below.

First θ_n is determined as follows:

$$T^n_{31} = B^n_{31} \text{ or } -\sin \theta_n = B^n_{31}$$

which gives

$$\theta_n = \sin^{-1} (-B^n_{31}) \qquad (98)$$

The cosine is then found by

$$\cos \theta_n = \cos [\sin^{-1} (-B^n_{31})]$$

so that ψ_n can be determined:

$$T_{11}^n = B_{11}^n \text{ or } \cos \psi_n \cos \theta_n = B_{11}^n$$

gives

$$\psi_n = \cos^{-1} (B_{11}^n/\cos \theta_n) \tag{99}$$

and, for determination of ϕ_n,

$$T_{33}^n = B_{33}^n \text{ or } \cos \theta_n \cos \phi_n = B_{33}^n$$

gives

$$\phi_n = \cos^{-1} (B_{33}^n/\cos \theta_n) \tag{100}$$

Equations (98) through (100) are used for segments 1, 2, 3, and 4; the symmetry requirement provides the Euler angles for segment 6, which are equal to those for segment 4. At this point the generalized coordinates q_4 through q_{20} have been determined. The next step involves seating the occupant and calculating X_1, Y_1, and Z_1 (q_1, q_2, and q_3) from static equilibrium.*

Because the problem of seating the occupant is statically indeterminate, certain simplifying assumptions are made. The first assumption, which is approximately correct for typical seating positions, is that 15 percent of the occupant's weight is supported by the floor. In other words, 85 percent is supported by the seat cushion and, depending on the aircraft attitude, the restraint system or the back cushion.

*Note that the computation of Euler angles is required only for the three-dimensional occupant model. For the two-dimensional model, the corresponding generalized coordinates are obtained directly from input data.

A first approximation to the initial position is made for the assumption of level flight ($\theta_A = \psi_A = \phi_A = 0$). The cushion forces act on the body as shown in figure 29, where it is assumed that 15 percent of the occupant weight is supported by the floor, as discussed in the preceding paragraph. Summing forces gives

$$F_{X_A}: \quad F_B \cos \theta_B - F_S \sin \theta_S = 0$$

$$F_{Z_A}: \quad F_B \sin \theta_B + F_S \cos \theta_S = W' \tag{101}$$

which can be solved for the cushion forces:

$$F_S = W' \cos \theta_B / \cos (\theta_B - \theta_S)$$

$$F_B = W' \sin \theta_S / \cos (\theta_B - \theta_S) \tag{102}$$

Dimensional considerations permit the coordinates of point P to be written as functions of the thicknesses t_S and t_B of the compressed seat and back cushions, respectively.

$$Z_P = Z_S + (R_1 + t_S)/\cos \theta_S + (X_P - X_S) \tan \theta_S$$

$$X_P = X_S + (R_1 + t_B)/\cos \theta_B - (Z_P - Z_S) \tan \theta_B \tag{103}$$

which can be solved for X_p and Z_p to give

$$X_P = X_S - f_1 \sin \theta_B + f_2 \cos \theta_S$$

$$Z_P = Z_S + f_1 \cos \theta_B + f_2 \sin \theta_S \tag{104}$$

where

$$f_1 = (R_1 + t_S)/\cos (\theta_B - \theta_S)$$

$$f_2 = (R_1 + t_B)/\cos (\theta_B - \theta_S)$$

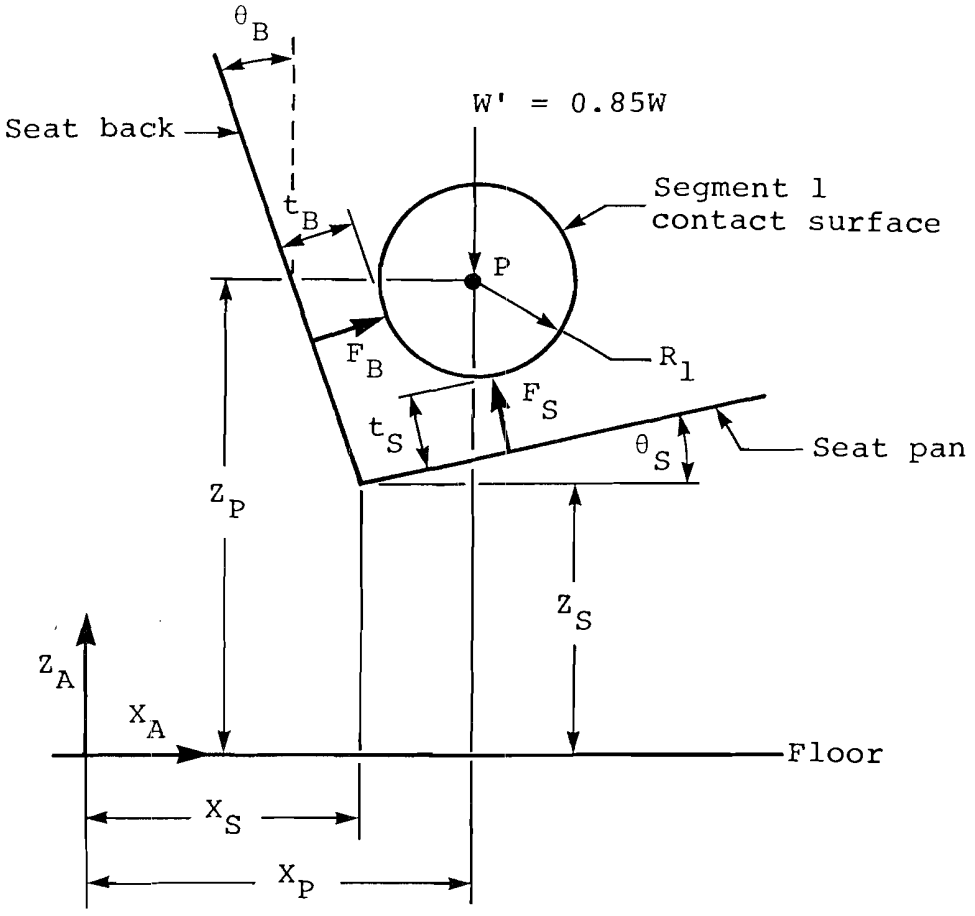

Figure 29. Forces acting on occupant torso (level flight).

Since the force-deformation characteristics of the cushions are known from input data, the compressed thicknesses t_S and t_B can be calculated from equation (102). These values, when used in equation (104), give the coordinates of point P for the first approximation of level flight. The equilibrium (zero-load) lengths of the lap belt and shoulder belt(s) are calculated for the body in this position.

Next, the aircraft is rotated to the attitude specified by the input conditions of pitch, roll, and yaw. Nose-up pitch will tend to load the back cushion, and the analysis will be the same as that described above for level flight, except that the W' vector in figure 29 will have a component in the X_A direction.

Nose-down pitch, on the other hand, will tend to load the restraint system. An iterative procedure is used to determine the correct position for this case. Referring to figure 30, summing forces gives a set of transcendental equations

$$F_{X_A}: \quad W' \sin \theta_A - F_S \sin \theta_S - F_L \cos \theta_L = 0$$

$$F_{Z_A}: \quad -W' \cos \theta_A + F_S \cos \theta_S - F_L \sin \theta_L = 0 \tag{105}$$

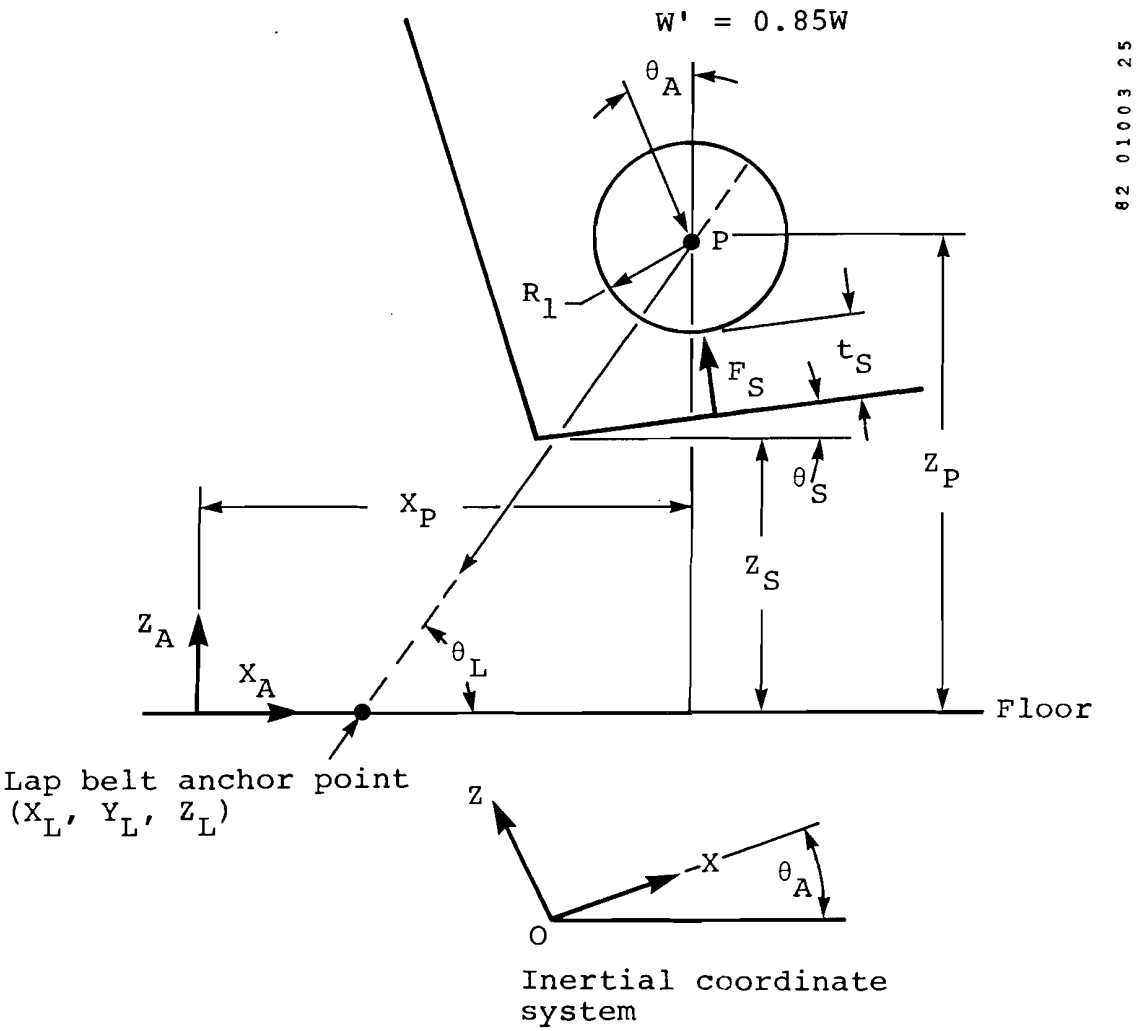

Figure 30. Forces acting on occupant torso (nose-down attitude).

where θ_L is the angle between the floor and the projection of the lap belt on the $X_A - Z_A$ plane. An initial estimate to θ_L is made using the body position calculated by equation (104) for the level flight assumption. The angle is defined according to

$$\theta_L = \sin^{-1} \left[(Z_P - Z_L) / \sqrt{(X_P - X_L)^2 + (Z_P - Z_L)^2} \right] \quad (106)$$

The forces in the seat cushion F_S and the lap belt F_L are determined using this value of θ_L in equation (105). From the input force-deformation characteristics for the seat cushion and lap belt, the deformations δ_S and δ_L are calculated. These deformations are used to determine new values of X_P and Z_P; this procedure amounts to permitting the body to further compress the seat cushion and slide forward into the lap belt. Following through the procedure, the new length for one side of the lap belt is

$$L_L = L_{Le} + \delta_L \quad (107)$$

where L_{Le} is the equilibrium length. The new value of X_P is given by

$$X_P = X_L + \left[(L_L - L_H)^2 - (Y_P - Y_L)^2 \right]^{1/2} \cos \theta_L \quad (108)$$

where L_H is one-half the hip breadth and Y_P is the Y-coordinate of the right hip in the aircraft system. The new value of Z_P is computed for the new cushion thickness t_S using equation (103), which is repeated here for continuity:

$$Z_P = Z_S + (R_1 + t_S)/\cos \theta_S + (X_P - X_S) \tan \theta_S$$

The new occupant position, determined by equations (108) and (103) is used in equation (106) to recalculate the lap belt angle θ_L, and the procedure is repeated until two consecutive values of X_P differ by less than 5 percent. The coordinates of the mass center of segment 1 (X_1, Y_1, Z_1) are then calculated from X_P, Y_P, and Z_P.

At this point the generalized coordinates for the upper body have been determined. The final task will be to determine the coordinates for the legs. Referring to figure 31, the angles γ_8 and θ_k can be found from simple geometric relationships among the dimensions shown. The Euler angles ψ_8, θ_8, and ϕ_8 are obtained from γ_8 by using equations (98) through (100), and the corresponding coordinates for segment 10, by symmetry. The knee angles are given by

$$\alpha_m = \pi - \theta_k \qquad m = 9, 11 \tag{109}$$

to complete the initialization of the generalized coordinates.

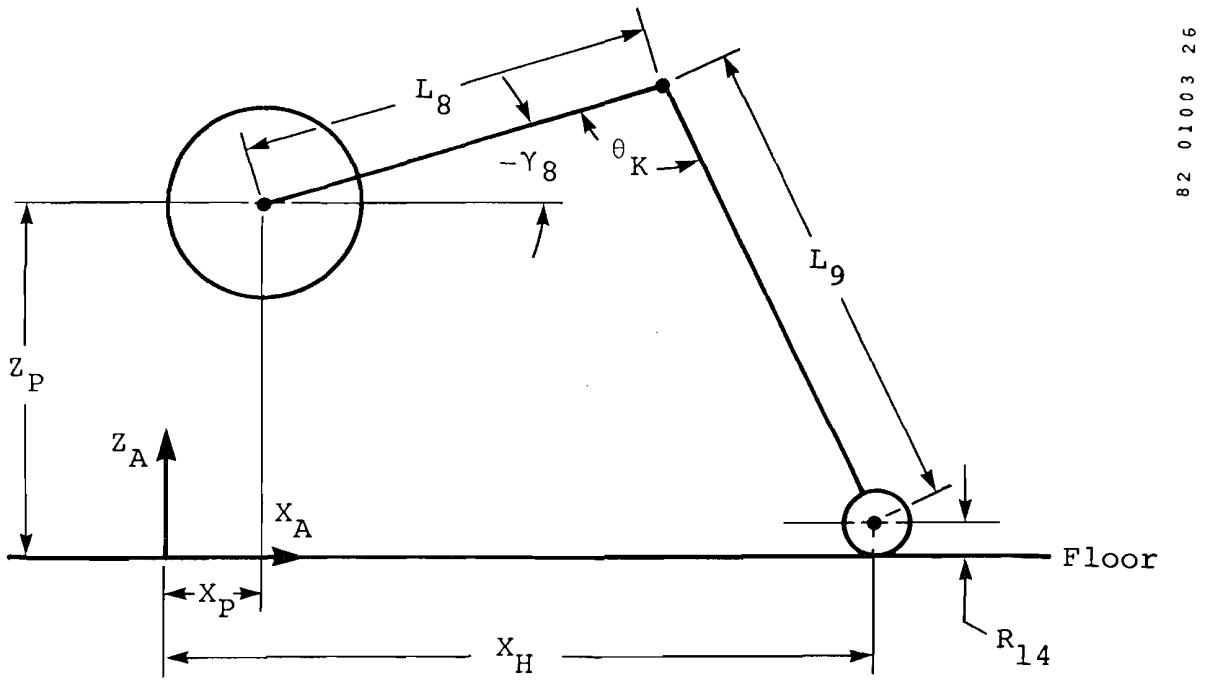

Figure 31. Leg position.

4.3 PROGRAM SOLUTION PROCEDURE

The first operation in each solution step includes the calculation of new values for the aircraft acceleration components and their subsequent integration to obtain aircraft velocity and

displacement components. Then the matrix form of the equations of motion, using equation (19)

$$[A(q)]\ \{\ddot{q}\} = \{B(\dot{q},q)\} + \{P(q)\} + \{R(\dot{q},q)\} + \{Q(\dot{q},q)\}$$

are set up for solution and solved, as discussed below.

4.3.1 Setup of Equations of Motion

The elements of [A], {B}, {P}, and {R} are calculated using the current values of the generalized coordinates and velocities. The elements of {Q}, which is the vector of generalized external forces, are calculated, as discussed in section 2.3. The external forces depend on displacements of the aircraft, which determine the motion of the seat, floor, and restraint system anchor points relative to the body. From these displacements new deflections of the cushions, floor, and restraint system are calculated.

4.3.2 Solution of Equations of Motion

The system of equations is solved for the generalized accelerations by first combining the vectors on the right-hand side:

$$[A]\ \{\ddot{q}\} = \{B'\} \tag{110}$$

where $\{B'\} = \{B\} + \{P\} + \{R\} + \{Q\}$

and solving for $\{\ddot{q}\}$ using Crout decomposition followed by Forsythe-Moler elimination.

The resulting set of N second-order differential equations have the general form

$$\ddot{q}_j = f_j\ (t,\ \dot{q}_1,\ \dot{q}_2,\ldots,\ \dot{q}_N,\ q_1,\ q_2,\ldots,\ q_N)$$
$$q_j\ (t=0) = q_{j0}\ \dot{q}_j\ (t=0) = \dot{q}_{j0} \qquad j = 1,\ 2,\ldots,\ N \tag{111}$$

where N, the number of degrees of freedom, is 12 for the two-dimensional model and 29 for the three-dimensional model.

These equations can be rewritten as 2N first-order equations having the general form

$$\dot{y}_j = f_j\ (t,\ y_1,\ y_2, \ldots,\ y_N,\ q_1,\ q_2, \ldots,\ q_N)$$

$$\dot{q}_j = y_j \tag{112}$$

$$y_j\ (t=0) = \dot{q}_{j0} \qquad q_j\ (t=0) = q_{j0}$$

Numerical integration of this set of equations is accomplished, using the Adams-Moulton predictor-corrector method with a variable step size. This method uses the difference equations

$$y^{(p)}_{j,n+1} = y_{j,n} + \frac{h}{24}\ (55f_{j,n} - 59f_{j,n-1} + 37f_{j,n-2} - 9f_{j,n-3}) \tag{113}$$

as the predictor and

$$y^{(c)}_{j,n+1} = y_{j,n} + \frac{h}{24}\ (9f^{(p)}_{j,n+1} + 19f_{j,n} - 5f_{j,n-1} + f_{j,n-2}) \tag{114}$$

as the corrector. Starting values are provided by the classical fourth-order Runge-Kutta method. Input data includes upper and lower error bounds for the solution. Error bounds for each variable are calculated and compared at each step with the difference between the predicted value $y^{(p)}_j$ and the corrected value $y^{(c)}_j$. If this difference exceeds the upper bound for any j, the step size is halved. If this difference is less than the minimum error bound for all j and for three successive steps, the step size is doubled. Halving the step size is accomplished by interpolation of past data, whereas doubling is effected by alternate selection of past data. The solution can be run with a fixed step size by making the upper and lower error bounds prohibitively large and small, respectively, or by using equal values for the maximum and minimum step size which are also included among input data.

4.4 PROGRAM OUTPUT

Output data consist of ten blocks of information that are selected for printing by user input. The data include time histories of the variables, which are simply sorted during the solution at predetermined print intervals as follows:

1. Occupant segment positions in the aircraft coordinate system (X, Y, Z, pitch, and roll).
2. Occupant segment velocities in the aircraft coordinate system (X, Y, and Z).
3. Occupant segment accelerations in the segment-fixed coordinate systems (x, y, z, and resultants).
4. Restraint system loads.
5. Cushion loads.
6. Aircraft displacement, velocity, and acceleration.
7. Injury criteria.
8. Details of contact between the occupant and the aircraft interior.
9. Seat structure nodal forces.
10. Seat structure element stresses.

Printer plots are provided for occupant segment accelerations, restraint system loads, and cushion loads. The option of two different filters is also provided for the occupant segment accelerations and cushion loads.

Two of the above blocks of output data will be discussed in further detail.

4.4.1 Impact Prediction

For prediction of impact between the occupant and the cockpit interior, 26 surfaces are defined on the body. These surfaces were illustrated in figure 15, and their dimensions discussed in section 2.5.

The distance between each of these occupant contact surfaces and the aircraft cockpit surfaces is calculated during execution of the program. When contact occurs between an occupant surface and a contact surface, the time and relative velocity of impact are computed and stored for printing. The impact conditions determined in this way can be used in evaluation of injury potential for a given cockpit configuration.

4.4.2 Injury Criteria

The injury criteria used in the program were selected as the most suitable for aircraft crash analysis. SOM-LA output can be used to determine the potential for injury to three regions of the body: head, vertebral column, and thorax. Each of these is discussed in the remainder of this chapter.

4.4.2.1 Head Injury. An accepted criterion for head injury is the Severity Index (SI) developed by C. W. Gadd (references 17 and 18), which is calculated for the head and chest according to

$$SI = \int_{t_o}^{t_f} a^n \, dt \qquad (115)$$

where a = acceleration in G as a function of time

n = weighting factor, 2.5 for head impacts

t = time in seconds.

Although Gadd used uniaxial acceleration in his validation of the Severity Index, Federal Motor Vehicle Safety Standard 208 requires the use of resultant acceleration. A tolerable SI value of 1000 is accepted for frontal impact of the head, and a value of 1500, for distributed, or noncontact accelerations (reference 19).

Also, the Head Injury Criterion (HIC) contained in Federal Motor Vehicle Safety Standard 208 is calculated according to

$$HIC = \max \left(\frac{1}{t_2 - t_1} \int_{t_1}^{t_2} a\,dt \right)^{2.5} (t_2 - t_1) \qquad (116)$$

where a is the resultant head acceleration in G and t_1 and t_2 are any two points in time (sec) during the crash event. A tolerable value of 1000 is accepted for the HIC.

4.4.2.2 Thoracic Injury. Although chest deflection is commonly accepted as the preferred tolerance criterion, it is not presently predicted by SOM-LA.

FMVSS 208 currently specifies as acceptable an acceleration pulse which ". . . shall not exceed 60 G except for intervals whose cumulative duration is not more than 3 msec," where the acceleration is the resultant measured at the center of gravity. This acceleration is printed by SOM-LA. Previously, FMVSS 208 had applied a Severity Index to the chest acceleration pulse. This index was calculated in exactly the same manner as the head Severity Index discussed previously, and the limit of 1000 was the same as that for the head. SOM-LA also prints this SI for the thorax.

4.4.2.3 Vertebral Injury. For determination of the potential of vertebral injury, the SOM-LA two-dimensional occupant model has beam elements in the lumbar spine and neck. Axial forces and bending moments are output for these segments. Tolerable force levels for the lumbar spine have not yet been established. However, based on cadaver tests, references 20 and 21 have published tolerable bending moments for the neck such as 1700 in.-lb in flexion (forward bending) and 500 in.-lb ft-lb in extension (rearward bending), respectively.

The dynamic response index (DRI) is also computed by SOM-LA as a measure of the probability of spinal injury due to a vertical acceleration parallel to the spine (reference 22).

In this model, the response of the body to acceleration parallel to the spine is modeled by a single lumped-mass, damped-spring system as shown in figure 32, or, in other words, the total body mass that acts on the vertebral column to cause deformation is represented by the single mass. In general, the motion of the system shown in figure 31 obeys the relationship

$$\frac{d^2\delta}{dt} + 2\zeta\omega_n \frac{d\delta}{dt} + \omega_n{}^2 \delta = \ddot{Z} \qquad (117)$$

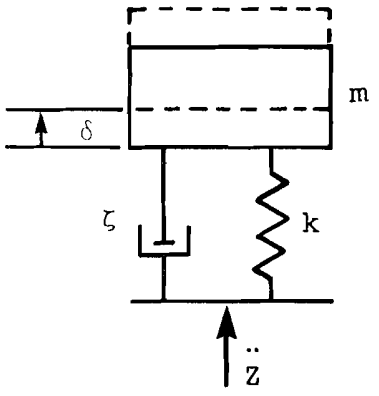

m = mass (lb-sec^2/in.)
δ = deflection (in.)
ζ = damping ratio
k = stiffness (lb/in.)
$\ddot{Z}$ = acceleration input (in./sec^2)

82 01003 27

$$*DRI = \frac{\omega_n{}^2 \delta_{max}}{g}$$

ω_n = natural frequency of the analog = $\sqrt{k/m}$ (rad/sec)

*Dynamic Response Index

g = 386 in./sec^2

Figure 32. Model used for prediction of spinal injury (from reference 22).

The solution, the deflection δ, is representative of the deformation of the spine, and the last term of the left-hand side of equation (117), divided by the gravitational acceleration, is the DRI. The properties used in the model were derived from tests involving human subjects and cadavers. For example, the spring stiffness k was determined from tests of human cadaver vertebral segments; damping ratios were determined from measurements of mechanical impedance of human subjects during vibration and impact. The acceleration input, $\ddot{Z}$, is the component of seat pan acceleration parallel to the vertebral column.

Equation (112) is solved for δ simultaneously with the occupant equations of motion, using the constants $\zeta = 0.224$ and $\omega_n = 52.9$ rad/sec. The DRI is then calculated at each step by

$$DRI = \omega_n^2 \delta / g \tag{118}$$

5.0 MODEL VALIDATION

Validation has been based on data from several series of deceleration sled tests conducted at the FAA Civil Aeromedical Institute (CAMI). The response of the combined occupant and seat models has been verified by comparison with data from tests that utilized specially designed and fabricated seats that had replaceable legs. Test conditions were selected to cause significant plastic deformation of the legs. Response of the occupant model, particularly to a vertical input acceleration, was validated using data from other test series that conducted with a rigid seat and with a production energy-absorbing helicopter seat. These tests are described in further detail in the remainder of this chapter.

5.1 SIMPLE SEAT STRUCTURES

Two series of deceleration sled tests were performed at CAMI specifically to provide data for validation of Program SOM-LA. The tests utilized an Alderson VIP-50 dummy in forward-facing test seats. The test program is described in reference 23, which includes a summary of measured data from all the tests.

The first series of tests used a rigid seat pan and seat back assembly, supported by solid, rectangular cross-section legs and seat back hinges. The second series of validation tests used a similar rigid seat pan and back, braced at a 90-degree included angle, as illustrated in figure 33. The seat legs were 1-in. diameter, 0.068-in. wall thickness 1010 steel tubing, pin jointed at the bottom, and fixed at the seat. Cushions were 1-in. thick Ensolite pads on the seat pan and back, and the restraint system consisted of a conventional nylon lap belt attached to the seat pan with a double shoulder belt that was anchored to the seat back and fitted to the buckle at the center of the lap belt. For all tests, the belts were adjusted to a snug fit with all slack removed. For each of these seat designs, two impact-vector orientations were used. The first orientation provided pure

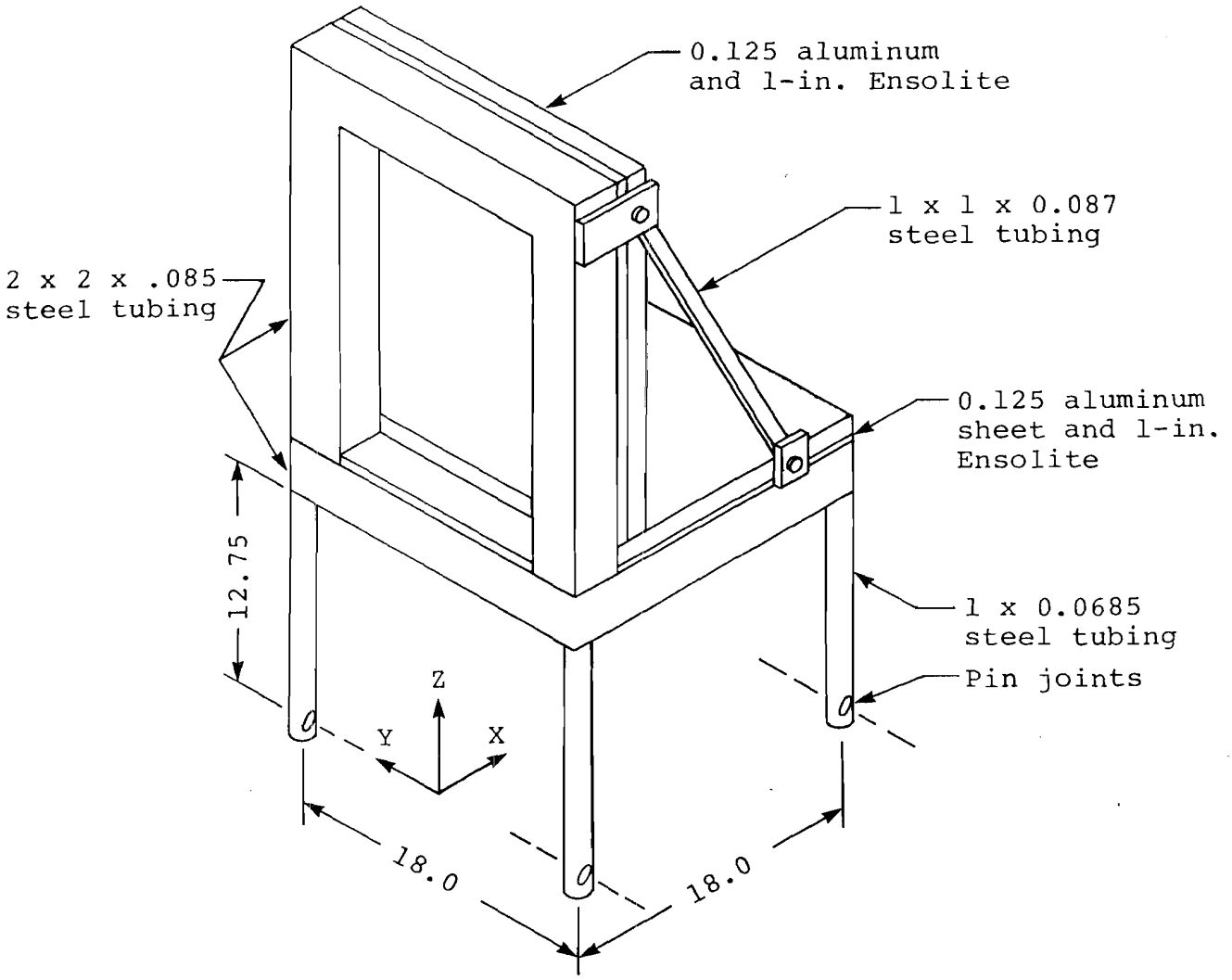

NOTE: All dimensions in inches.

Figure 33. CAMI Series 2 test seat.

forward-facing ($-G_x$) acceleration. The second orientation provided combined longitudinal ($-G_x$) and vertical ($+G_z$) acceleration by reorienting the seat system so that the impact vector fell 60 degrees below the floor plane of the seat. For the seat design with tubular legs, eight static tests and 58 dynamic tests, which used acceleration levels of 5.4 G and 9.5 G, were conducted. For the dynamic tests, the lower acceleration level produced minimal plastic deformation of the seat legs without significant cross section change, while the higher acceleration level produced

marked plastic deformation with localized buckling and cross sectional change at the fixed end. For the tests with the angled floor, acceleration levels of 13.5 G and 22 G were required to produce similar results. The impact velocity for all of these tests was approximately 44 ft/sec.

5.1.1 Low-Deceleration Tests

The first set of test conditions considered is that of the low-deceleration, forward-facing series. Pre- and posttest photographs from one of the 10 tests are shown as figures 34 and 35. The permanent deformation at the top of the legs can be seen in the latter photograph. The trapezoidally shaped input deceleration is shown in figure 36. This case is treated in detail as an example in Volume II - SOM-LA User Manual.

Predicted dummy accelerations, restraint system loads, and forward displacement of the seat pan are compared in figures 37 through 41 with the mean of data measured in 10 tests.

5.1.2 Higher-Deceleration Tests

A second series of forward-facing tests used the sled deceleration shown in figure 42. As shown in the posttest photograph of figure 43, a much greater forward displacement of the seat structure was achieved through plastic deformation and local buckling of the legs at their connection to the seat pan. Predicted response is compared in figures 44 through 48 with the mean of data from 10 tests.

5.2 ENERGY-ABSORBING SEAT TESTS

As part of a U.S. Army-sponsored research program, a number of sled tests were conducted at CAMI using a production crewseat for the Sikorsky UH-60A Black Hawk helicopter. The seat, described in detail in reference 24, consists of a bucket which supports the

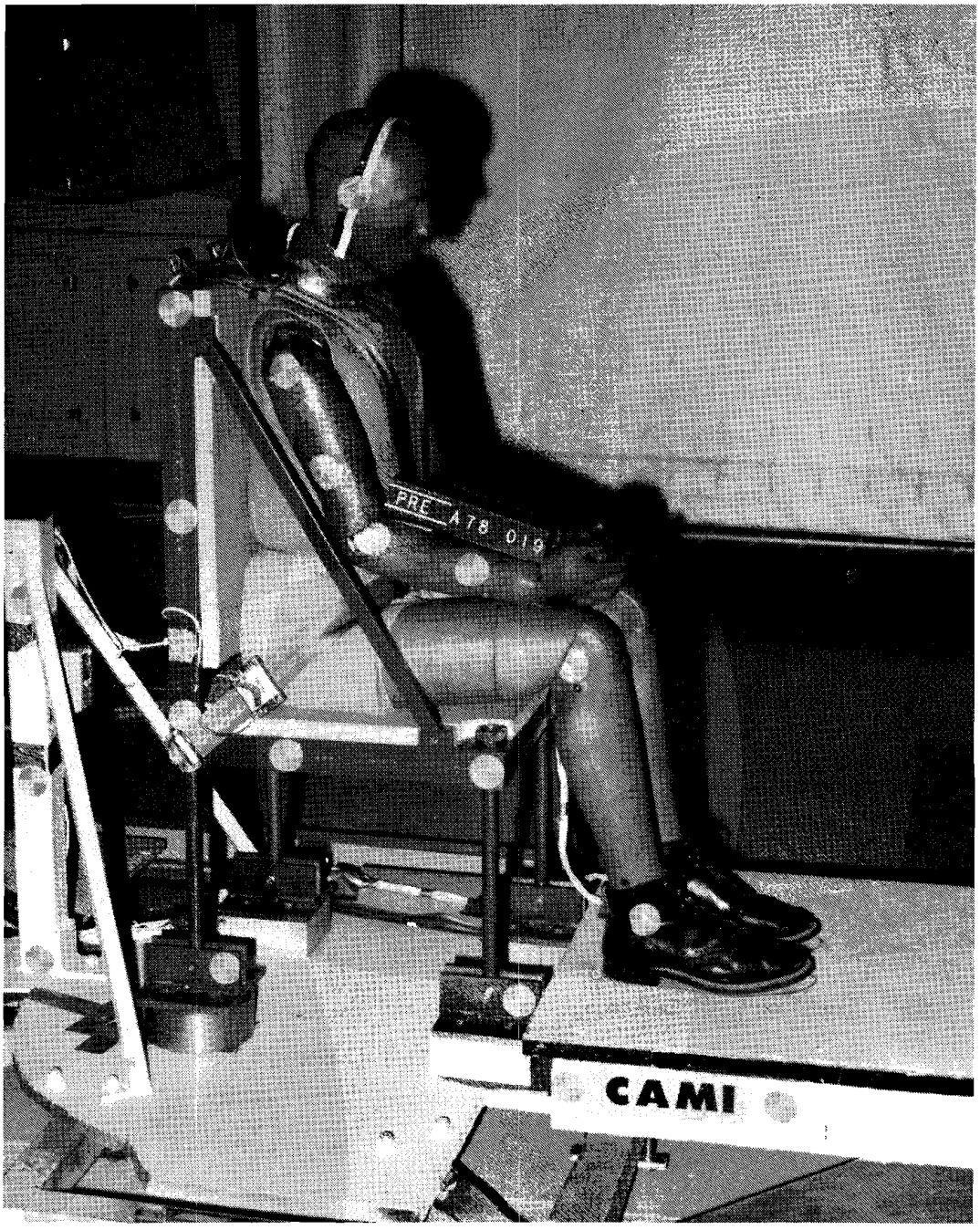

Figure 34. CAMI Series 2, low-deceleration, forward-facing test, pretest.

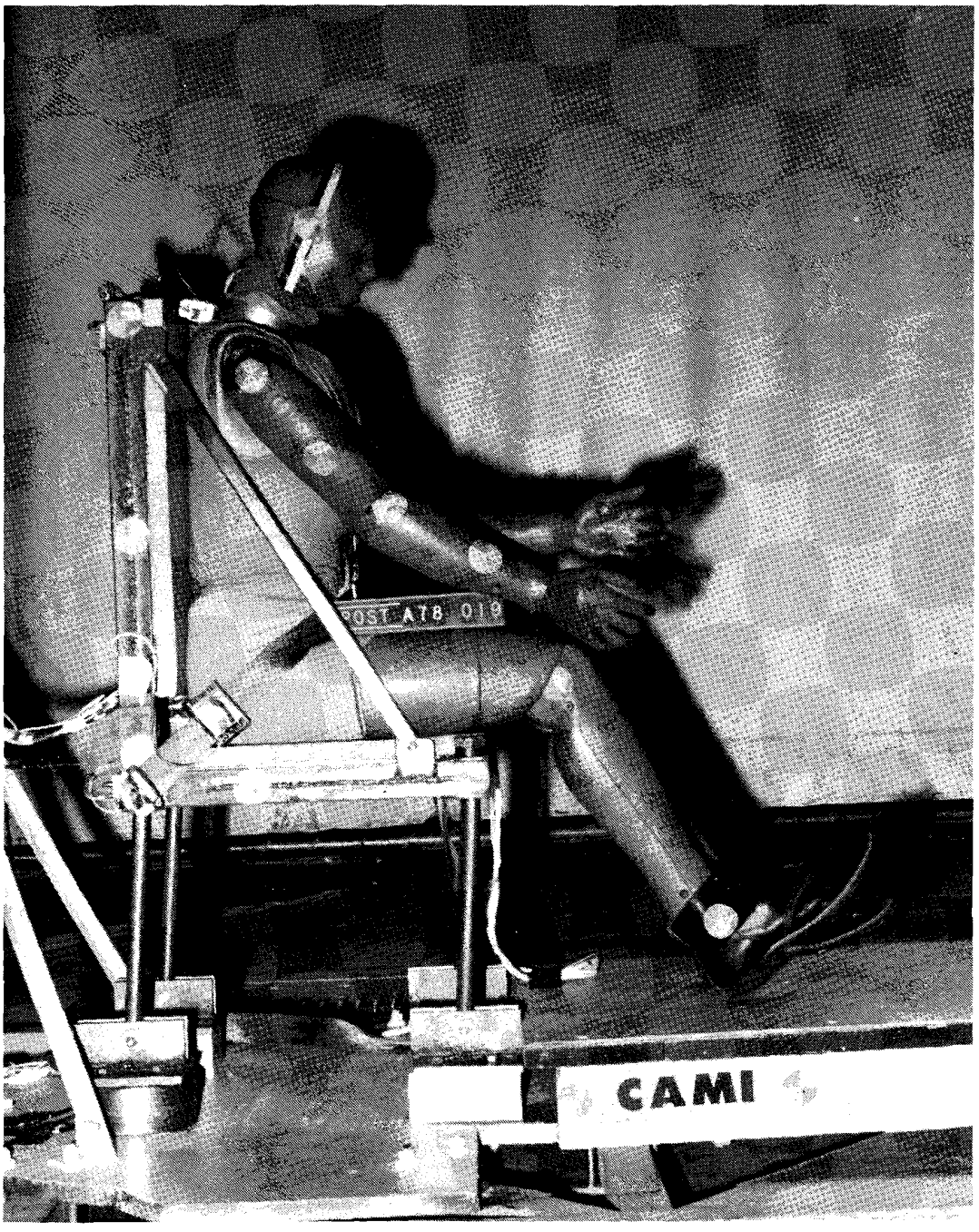

Figure 35. CAMI Series 2, low-deceleration, forward-facing test, posttest.

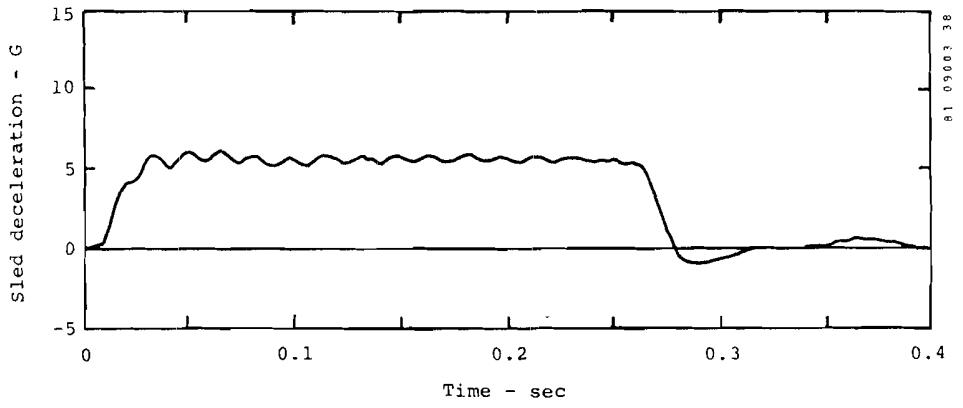

Figure 36. Sled deceleration, CAMI Series 2, low-deceleration, forward-facing tests.

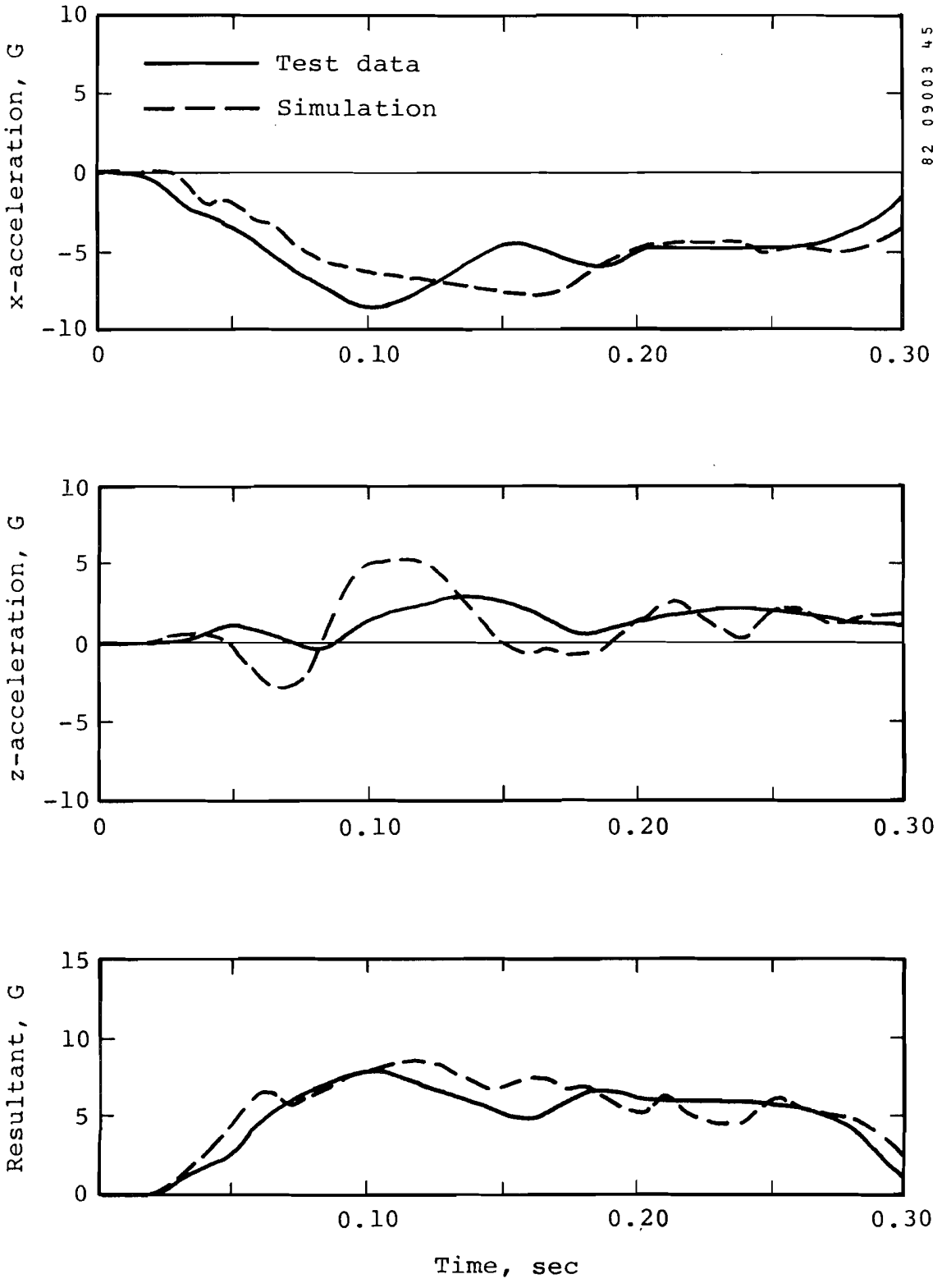

Figure 37. CAMI validation Series 2, low-deceleration, forward-facing tests, dummy pelvis acceleration.

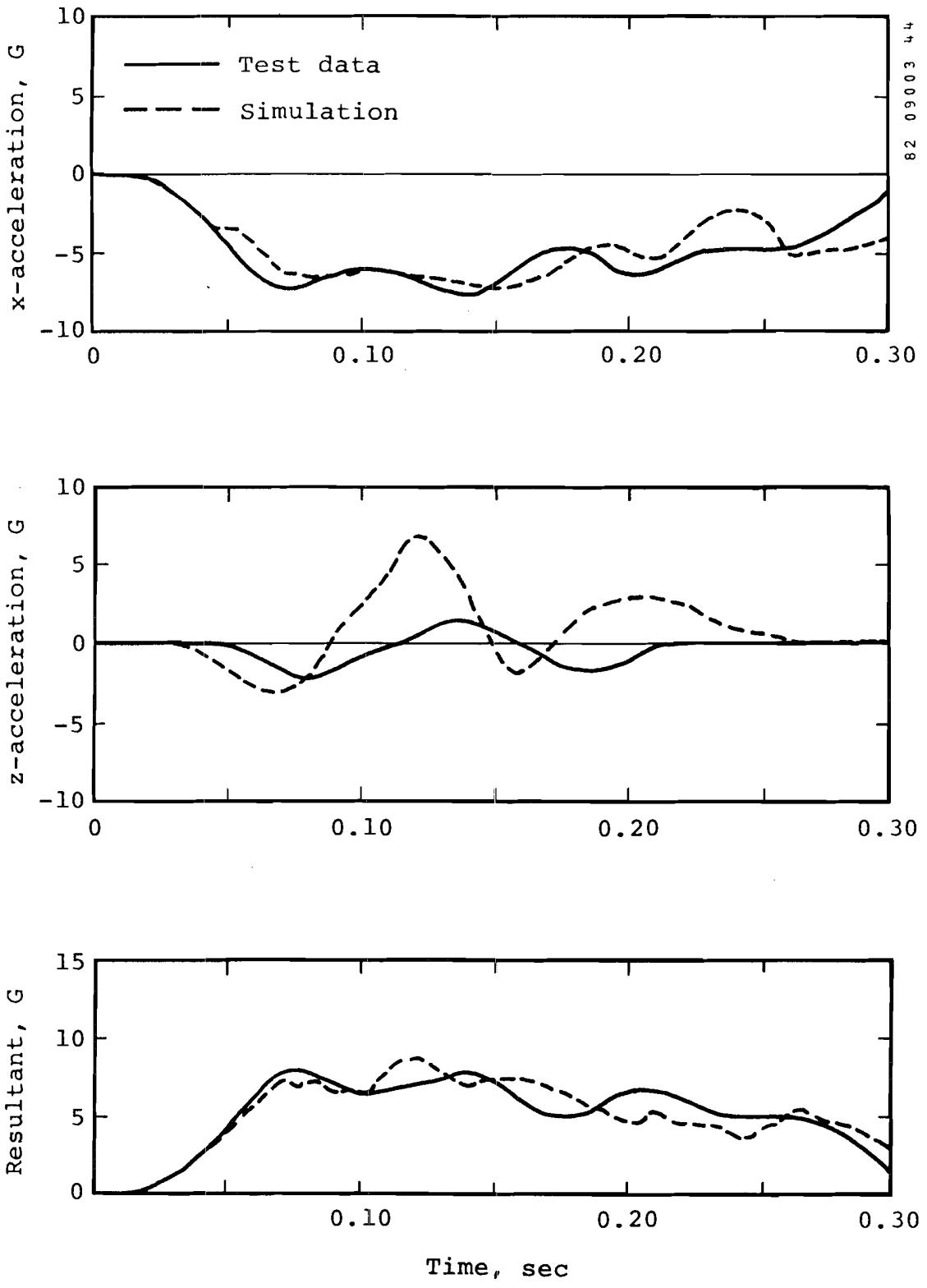

Figure 38. CAMI validation Series 2, low-deceleration, forward-facing tests, dummy chest acceleration.

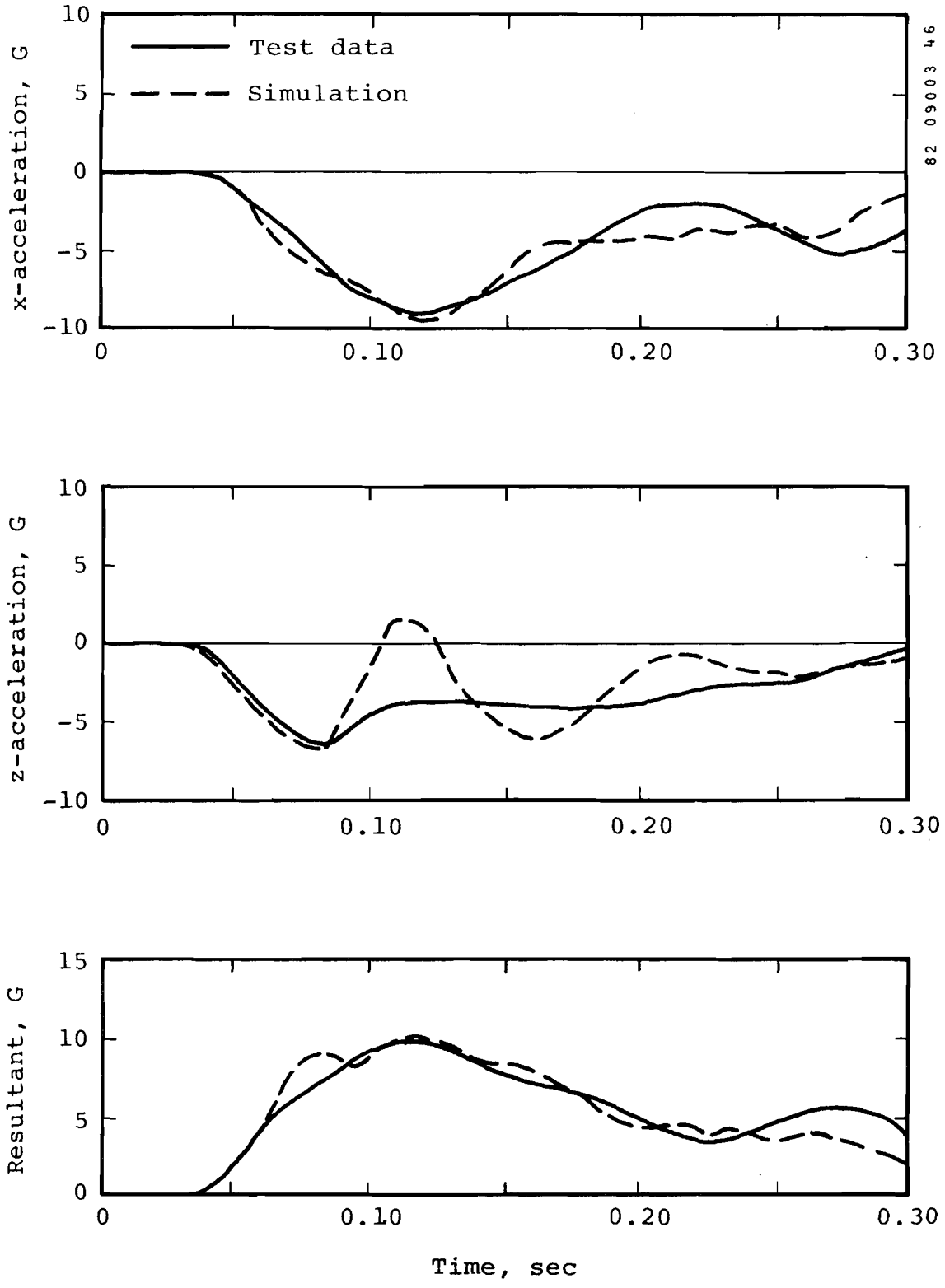

Figure 39. CAMI validation Series 2, low-deceleration, forward-facing tests, dummy head acceleration.

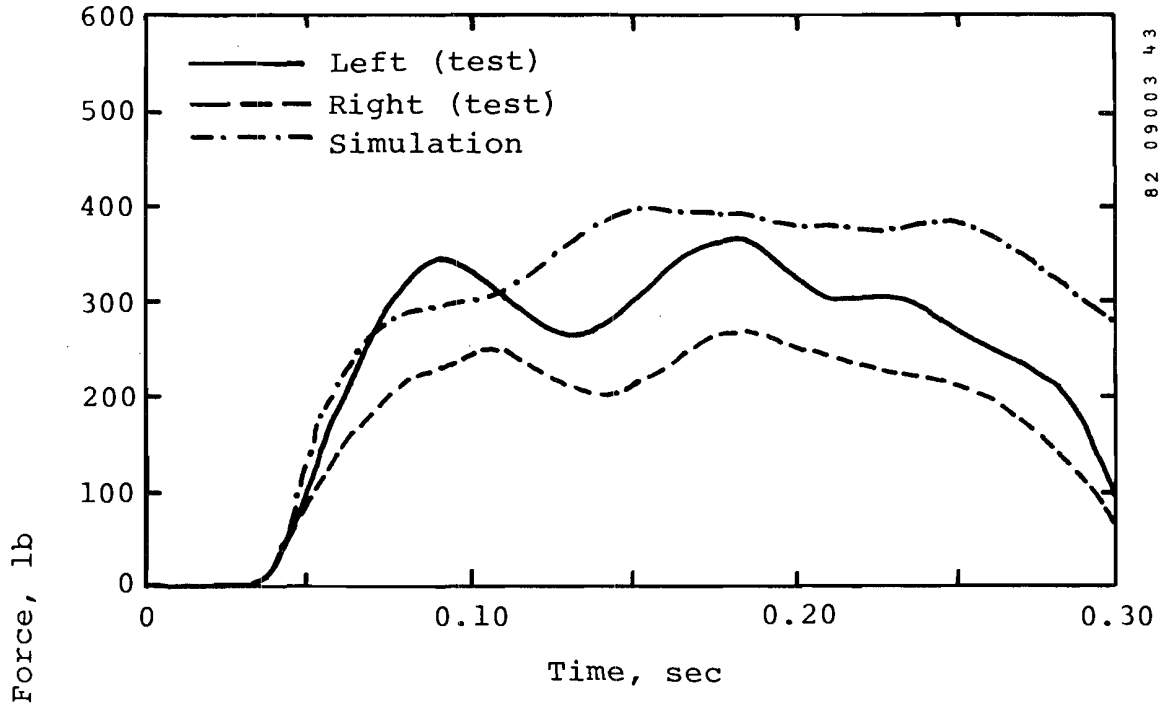

(a) Lap belt

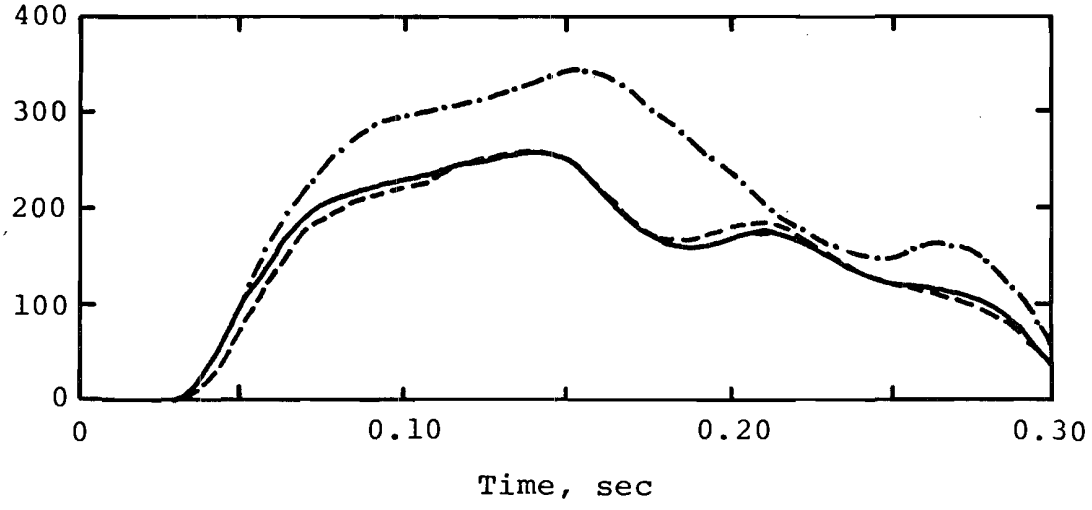

(b) Shoulder belts

Figure 40. CAMI validation Series 2, low-deceleration, forward-facing tests, restraint system loads.

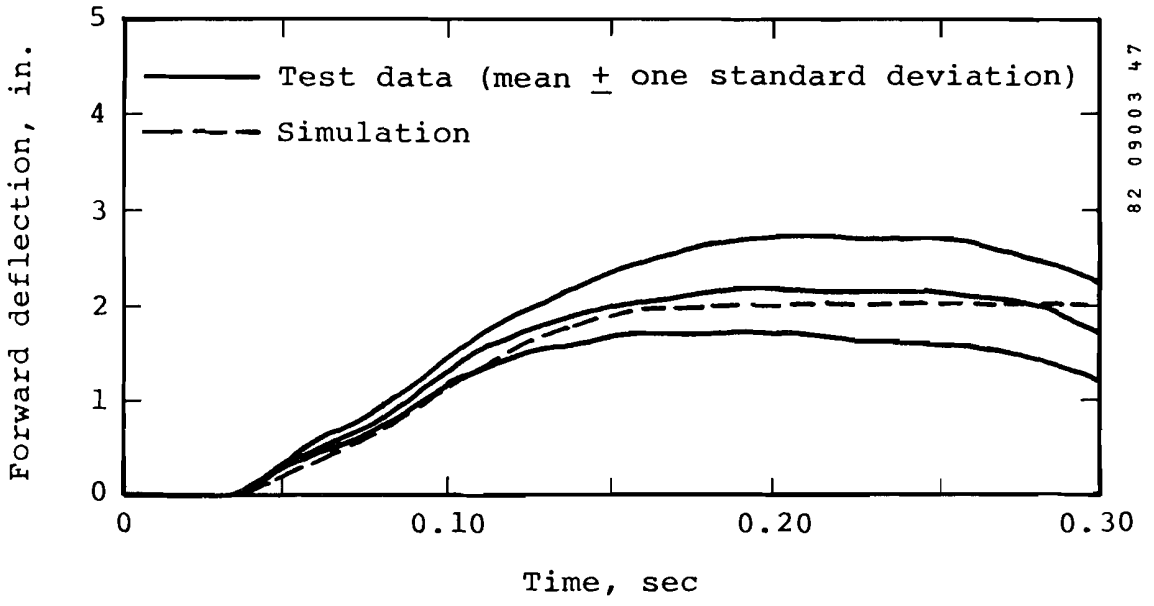

Figure 41. CAMI validation Series 2, low-deceleration, forward-facing tests, seat forward displacement.

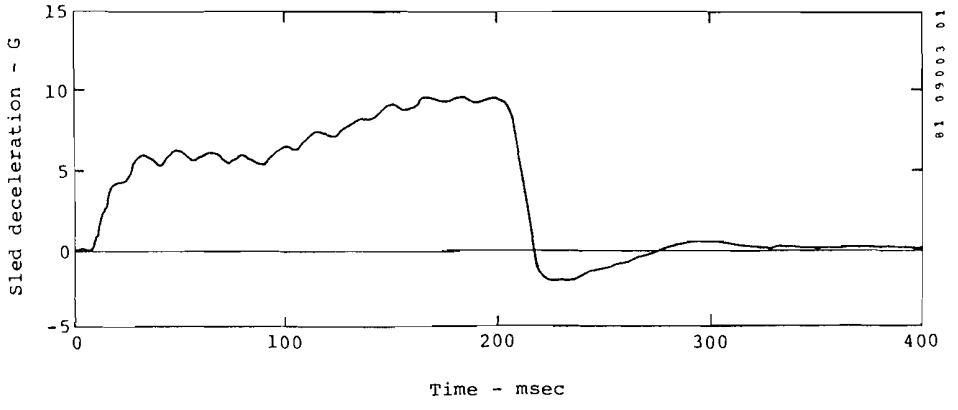

Figure 42. Sled deceleration, CAMI Series 2, higher-deceleration, forward-facing tests.

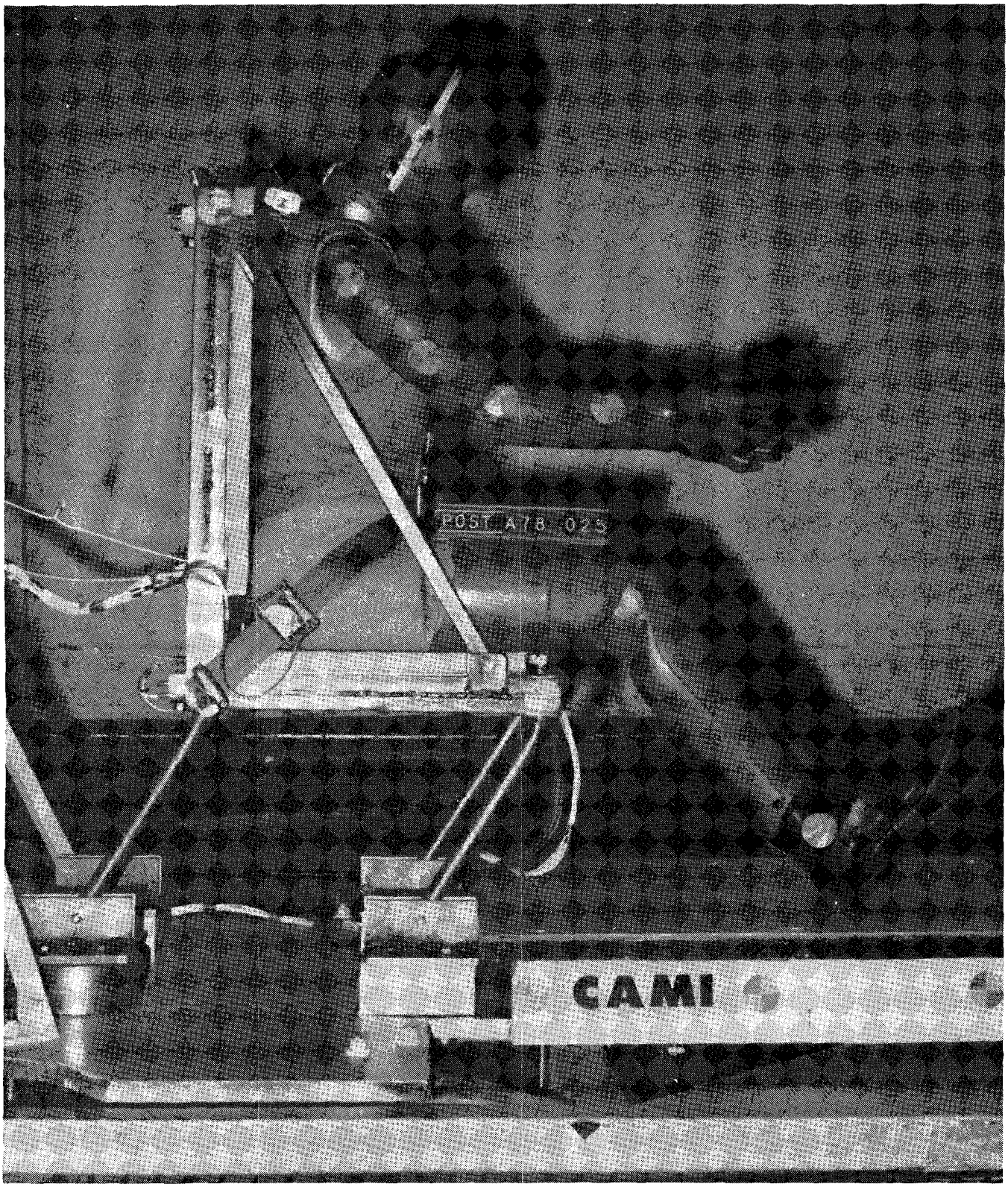

Figure 43. CAMI Series 2 forward-facing test, posttest.

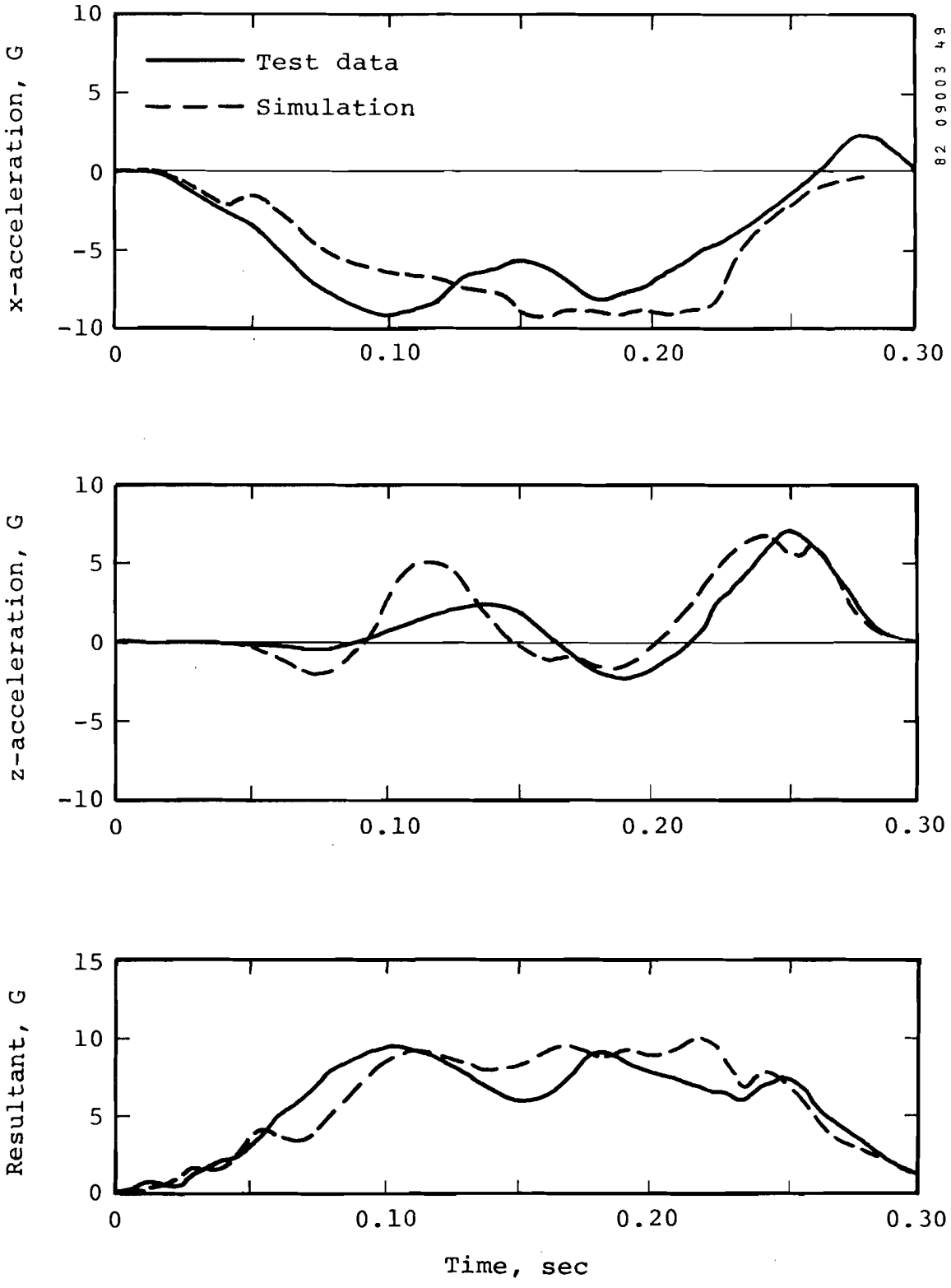

Figure 44. CAMI validation Series 2, higher-deceleration, forward-facing tests, dummy pelvis acceleration.

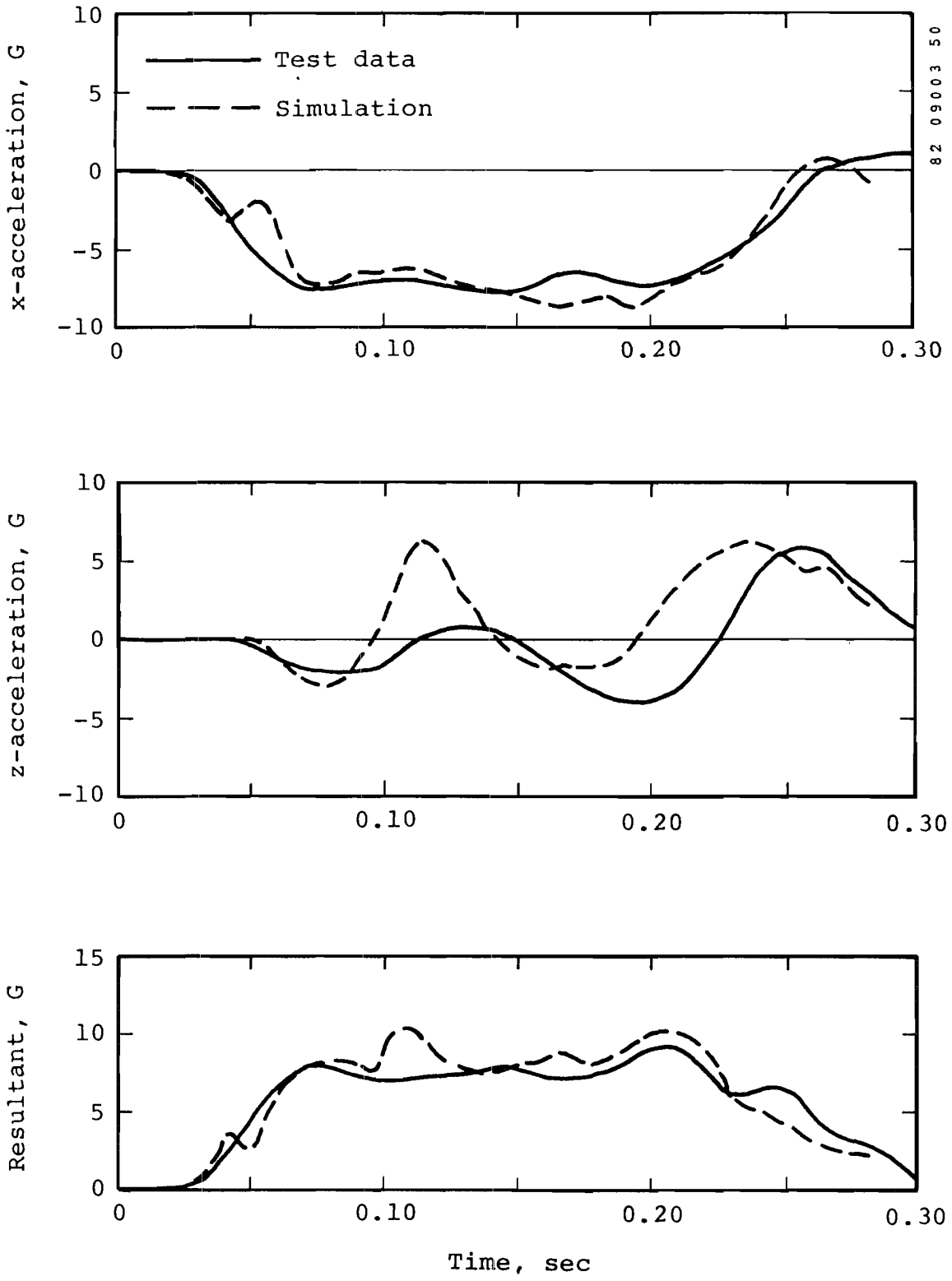

Figure 45. CAMI validation Series 2, higher-deceleration, forward-facing tests, dummy chest acceleration.

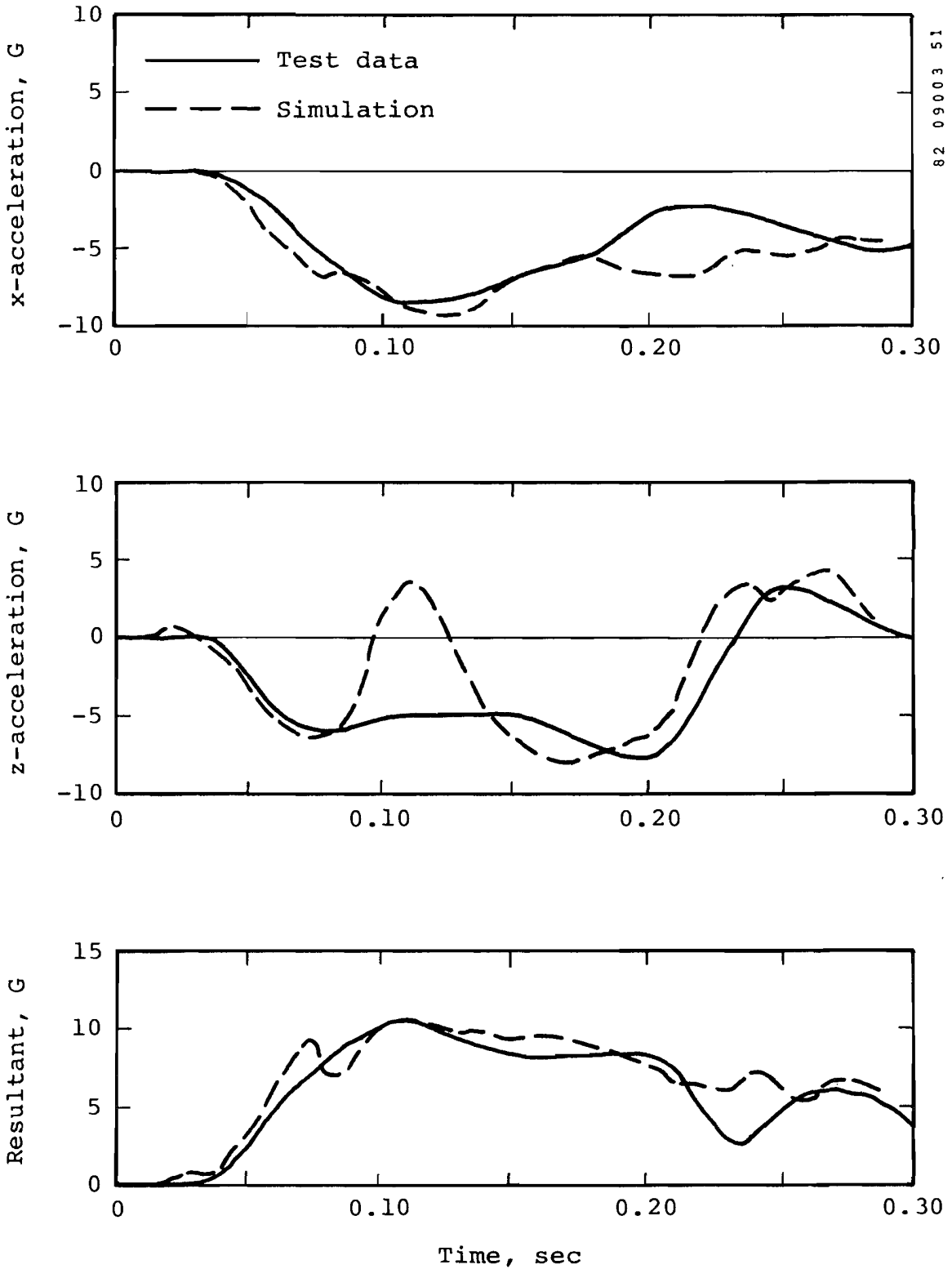

Figure 46. CAMI validation Series 2, higher-deceleration, forward-facing tests, dummy head acceleration.

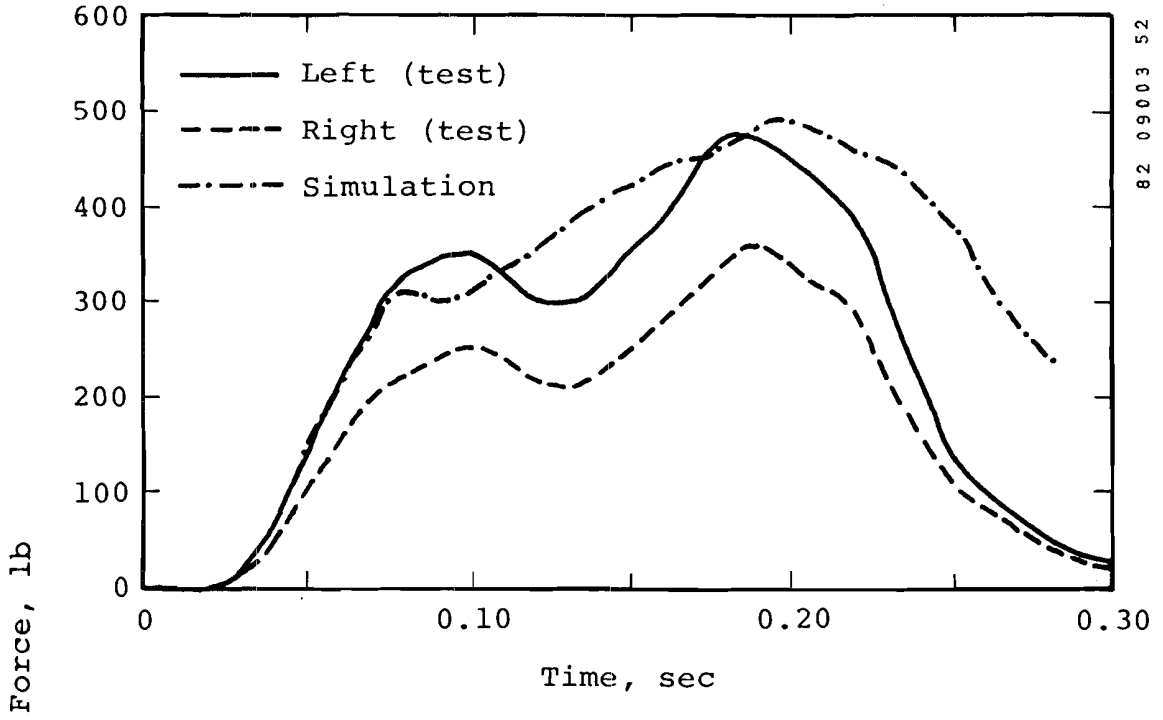

(a) Lap belt

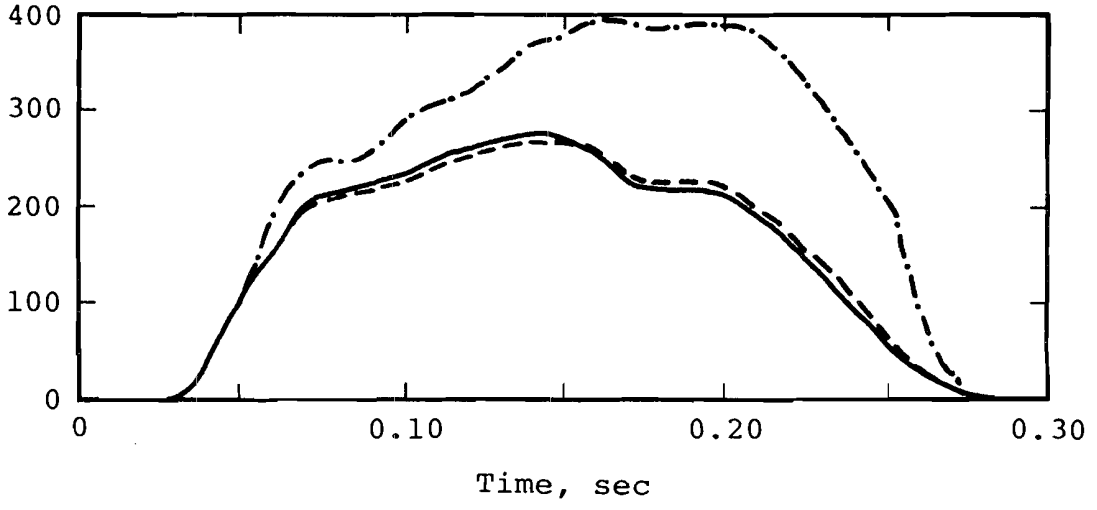

(b) Shoulder belts

Figure 47. CAMI validation Series 2, higher-deceleration, forward-facing tests, restraint system loads.

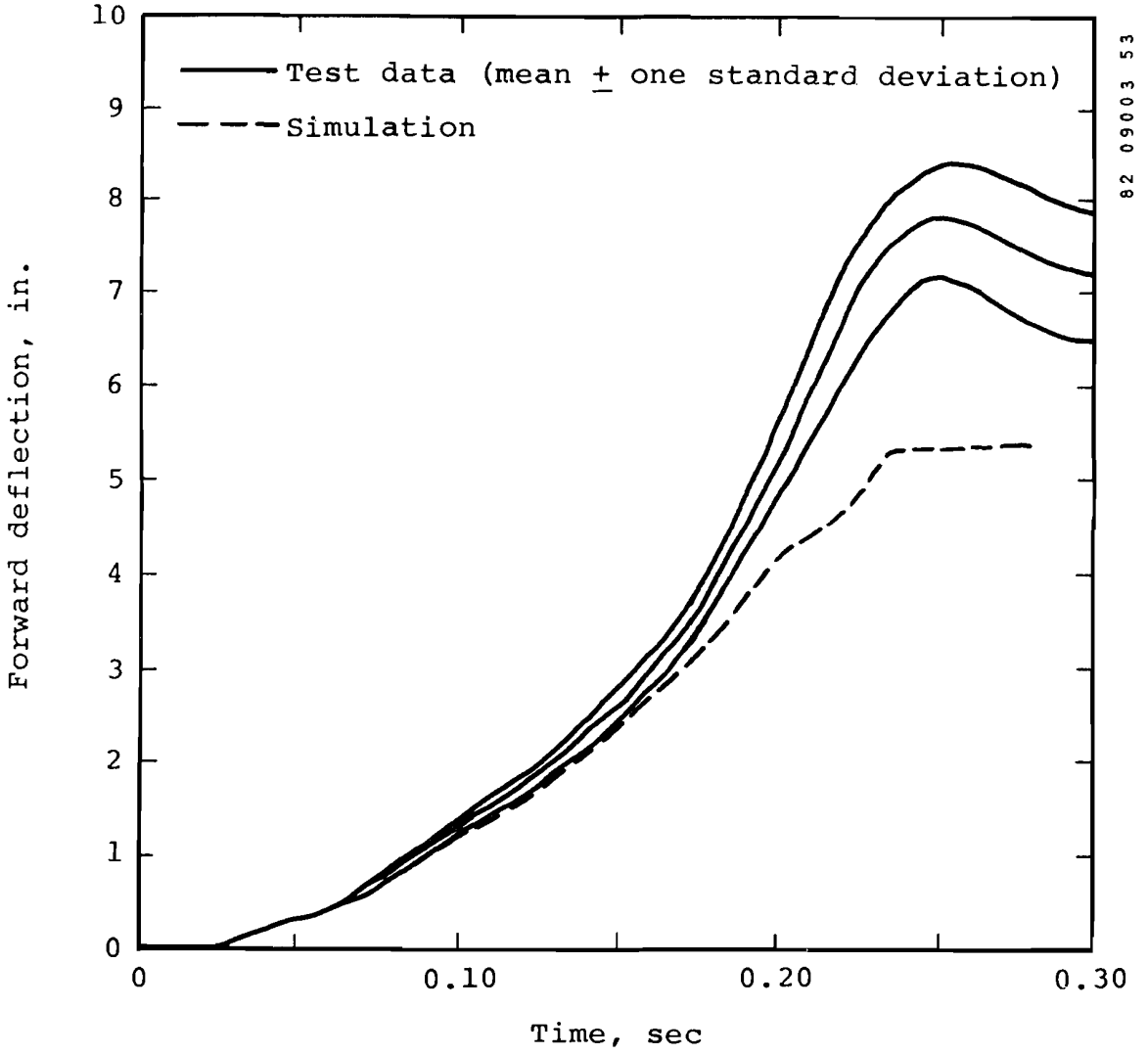

Figure 48. CAMI validation Series 2, higher-deceleration, forward-facing tests, seat forward displacement.

occupant and to which the restraint system is attached and a frame mounted on the aircraft floor. Principal functional members of the frame are two vertical (or nearly vertical) guide tubes along which the bucket can move, controlled by one or more energy-absorbing devices. Vertical inertial crash loads force the seat bucket down the guide tubes against the resistance of the energy absorbers, producing an energy-absorbing stroke in that direction. For most efficient use of the stroke distance available between the bucket and the floor, energy absorbers are designed

to stroke at constant load, that load being determined by design criteria based on human tolerance to $+G_z$ acceleration.

In order to simulate a nearly vertical impact on the horizontal sled, the seat z-axis was pitched forward 17 degrees from the plane of the sled, as shown in figure 49. A pretest view of the dummy positioned in the seat is presented in figure 50, where the fixture simulating the aircraft floor can be seen. (The Black Hawk helicopter has a well beneath each crewseat to permit additional stroke, so that a minimum of 12 in. and a maximum of 17 in. can be attained, depending on the seat's vertical adjustment position.) The dummy was flexed forward at the waist for positioning in the seat, and its lower torso was pushed firmly against the back cushion. The five-point restraint system was installed, and the lap belt was tightened. With the inertia reel unlocked, the shoulder harness was tightened using its adjusters, and a preload was applied to the reel. The dummy's feet were taped to the footrest, which was supported on a six-axis load cell. For the test used in SOM-LA validation, the impact velocity was 43.5 ft/sec, and the sled deceleration, with a peak of 41.5 G, was as shown in figure 51.

The pelvic structure of the 50th-percentile Part 572 dummy used in the test had been modified to include a six-axis load cell at the base of the lumbar spine (reference 25). Forces were thus measured in the dummy spine as well as in the footrest. Accelerations were measured in the dummy pelvis, chest, and head, and on the seat. Seat stroke was also measured using a displacement transducer.

The two-degree-of-freedom seat model was used in simulating this test. The energy absorber force-deflection characteristics were based on data from static and dynamic tests of these components. The seat's rotational stiffness was based on a static test of the system (reference 24).

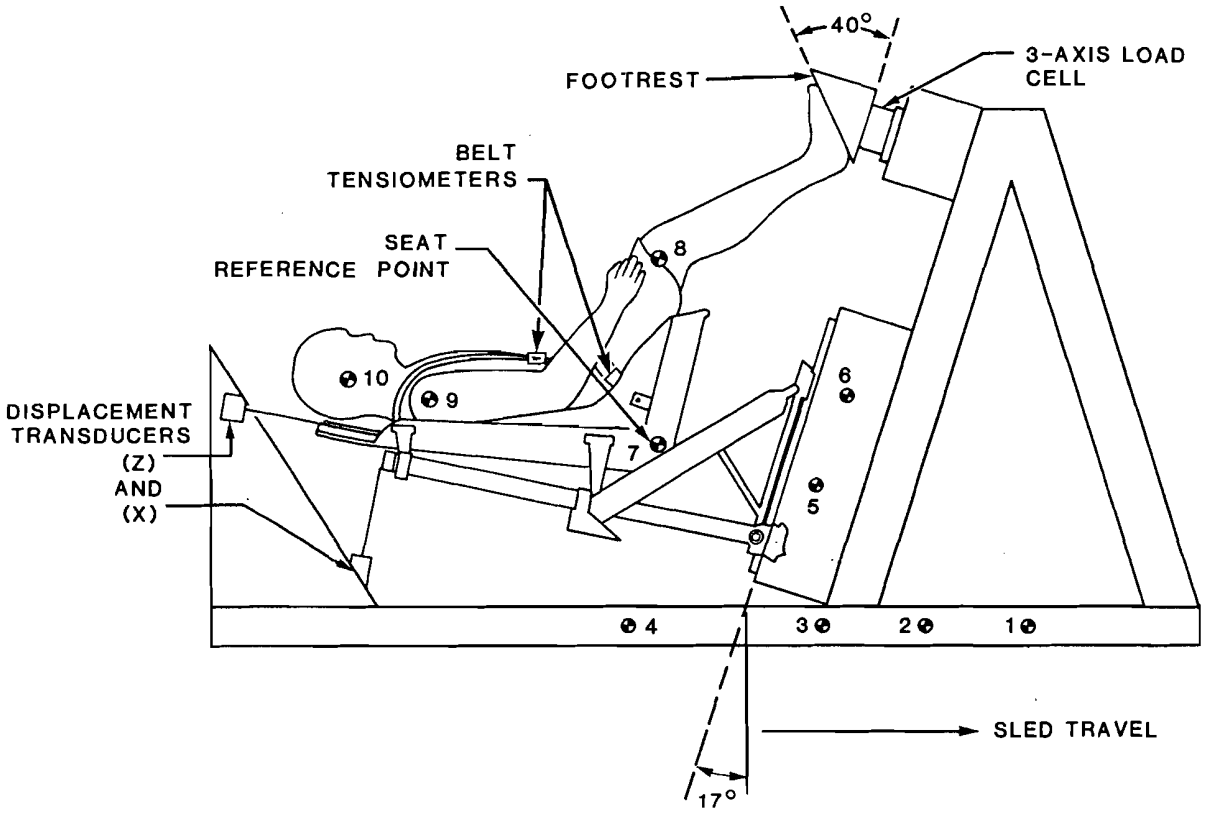

Figure 49. Test configuration for CAMI tests with energy-absorbing helicopter seat.

Comparisons of predicted accelerations, seat stroke, and forces with measured data are presented in figures 52 through 61.

5.3 RIGID SEAT TESTS

As part of the same U.S. Army-sponsored program mentioned in section 5.2, a number of tests were conducted with various dummies in a rigid seat whose seat pan and back formed a right angle with respect to each other, as shown in figure 62 (where a 95th-percentile dummy is shown). No cushions were used, and the plywood seat pan was supported by a six-axis load cell. The four-point restraint system used automotive-type nylon webbing, the vertical (z) axis of the seat was aligned with the velocity vector, in other words, horizontal for the sled impact. For the test with the modified Part 572 dummy, the sled deceleration is shown in figure 63.

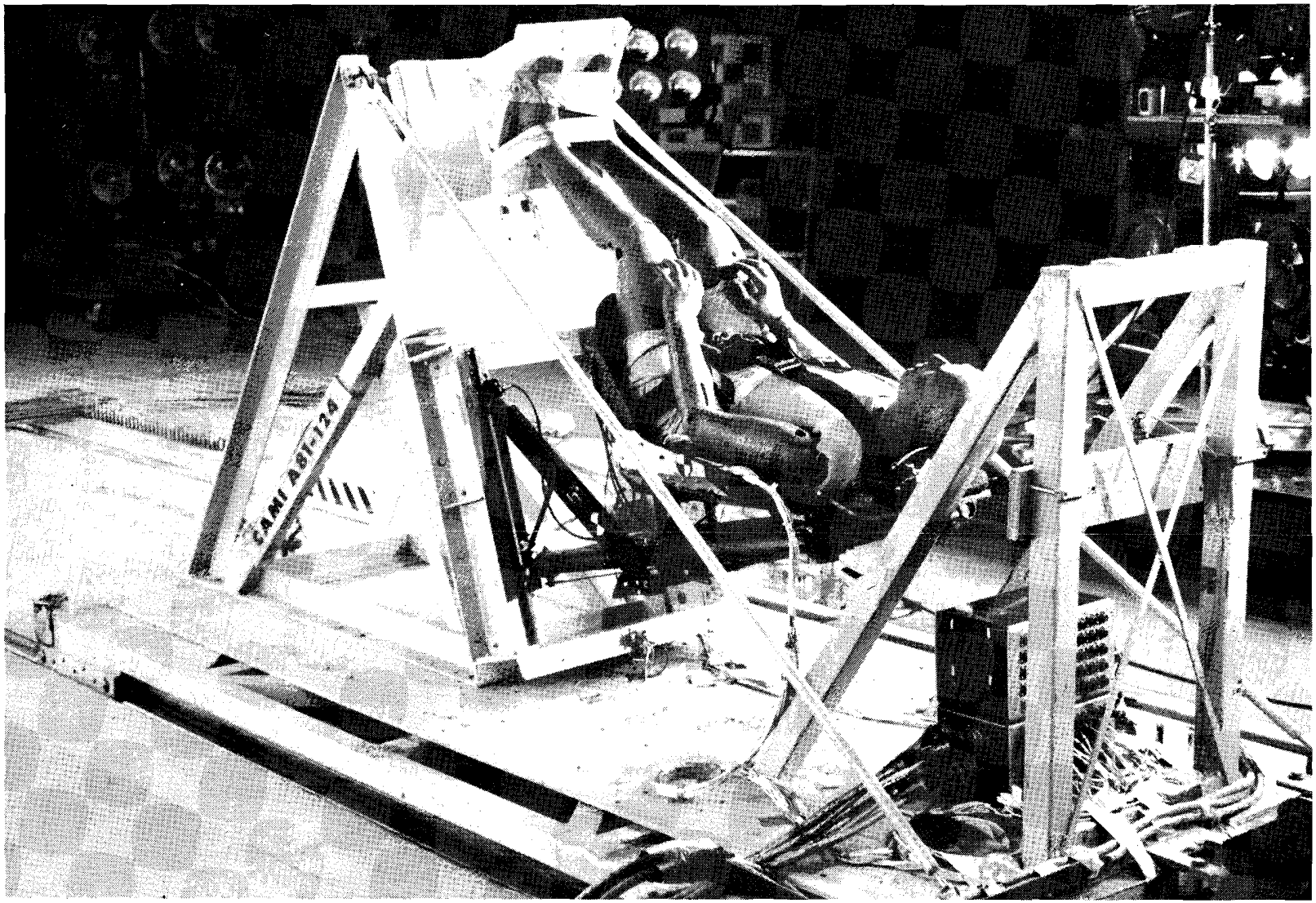

Figure 50. Part 572 dummy positioned in UH-60A Black Hawk crewseat prior to test.

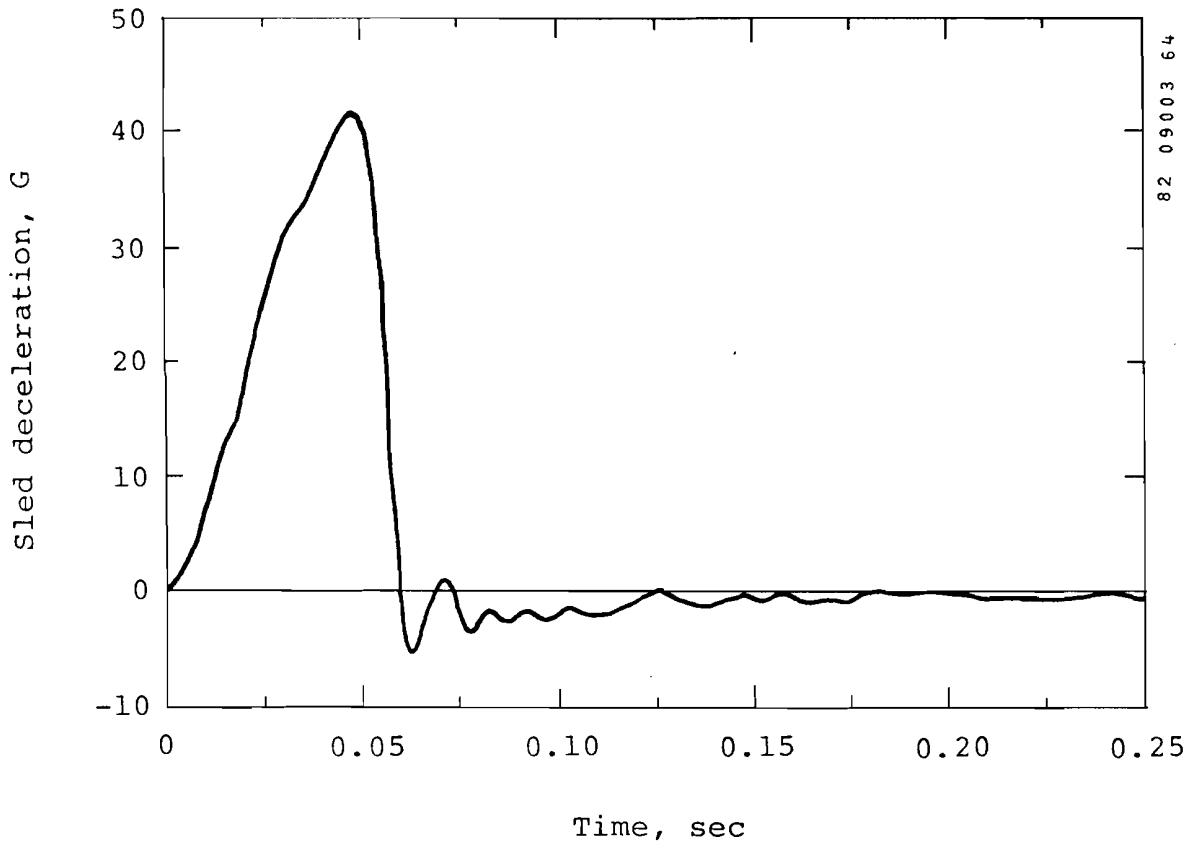

Figure 51. Sled deceleration for energy-absorbing seat test.

Accelerations were measured in the dummy, and forces were measured in the lumbar spine, footrest, and seat pan.

Simulation results and test data are compared in figures 64 through 70.

5.4 GENERAL AVIATION SEAT TESTS

To complete the SOM-LA validation, CAMI conducted several tests with production general aviation seats, which were purchased from dealers of used aircraft hardware. Twelve seats of two different designs were used in a total of four static and thirteen dynamic tests. The tests which will be described here utilized a seat with a frame of rectangular aluminum tubing. This seat produced more interesting results for validation of the seat model than the

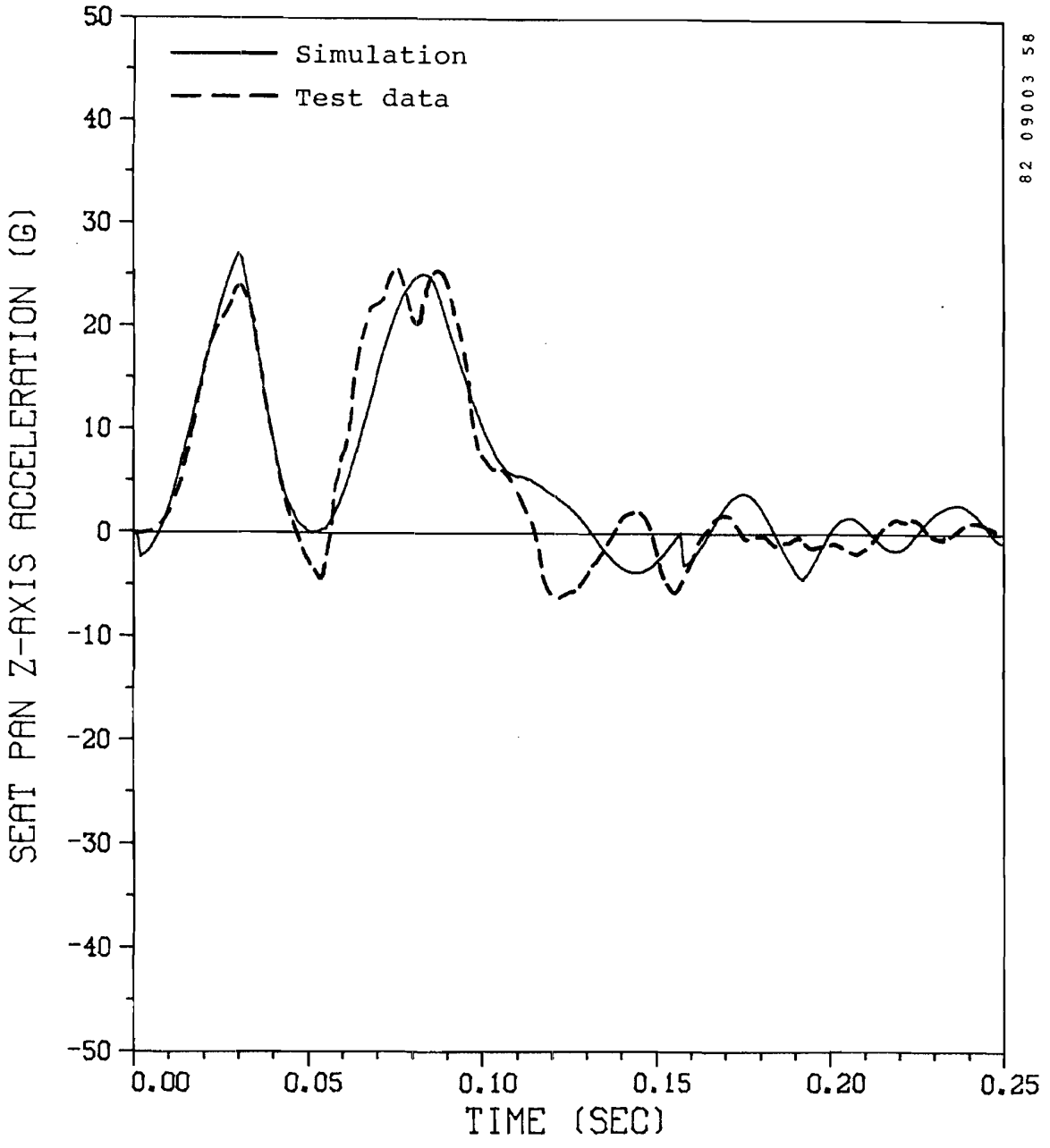

Figure 52. Energy-absorbing helicopter seat test, seat z-acceleration.

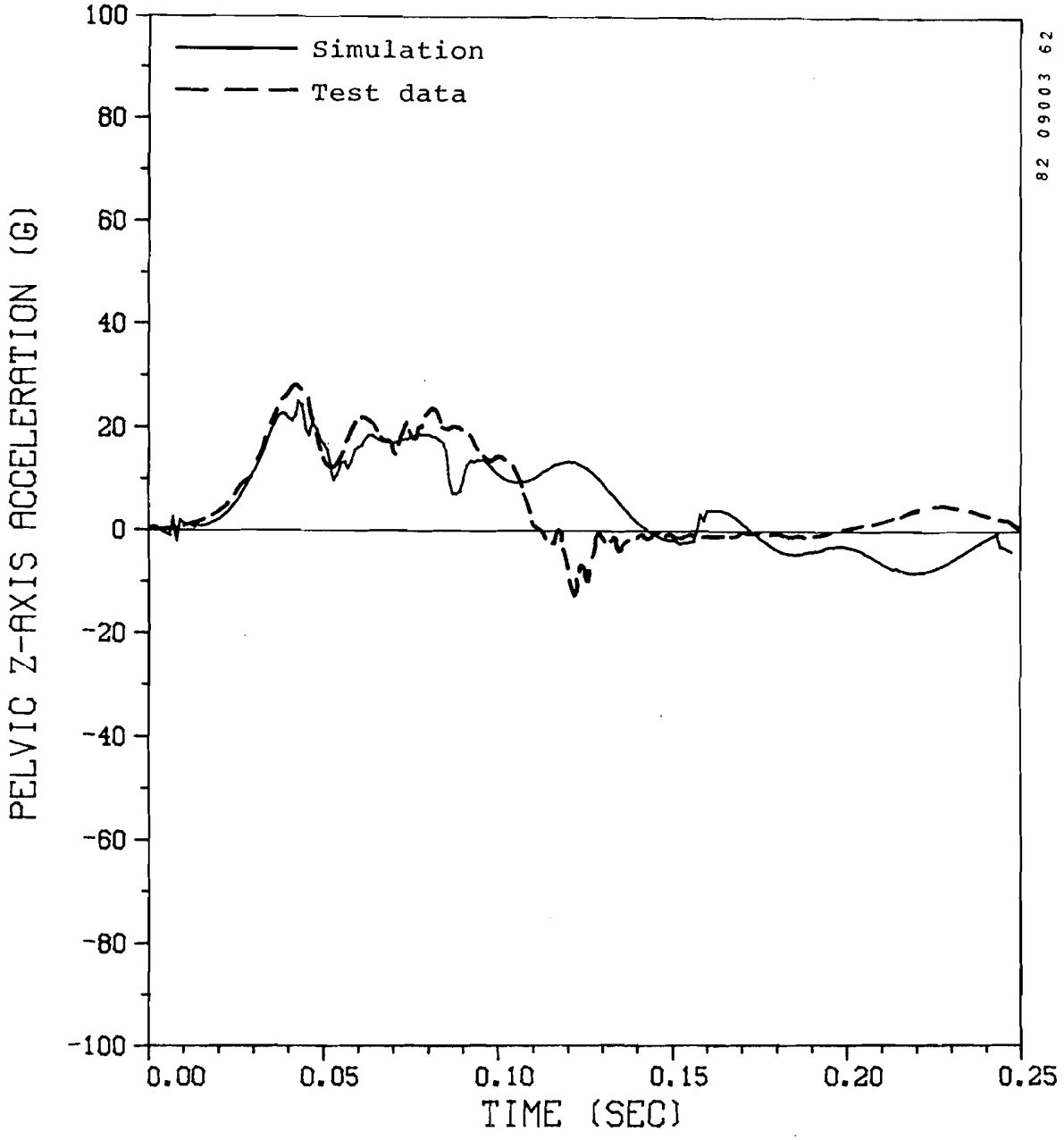

Figure 53. Energy-absorbing helicopter seat test, dummy pelvis z-acceleration.

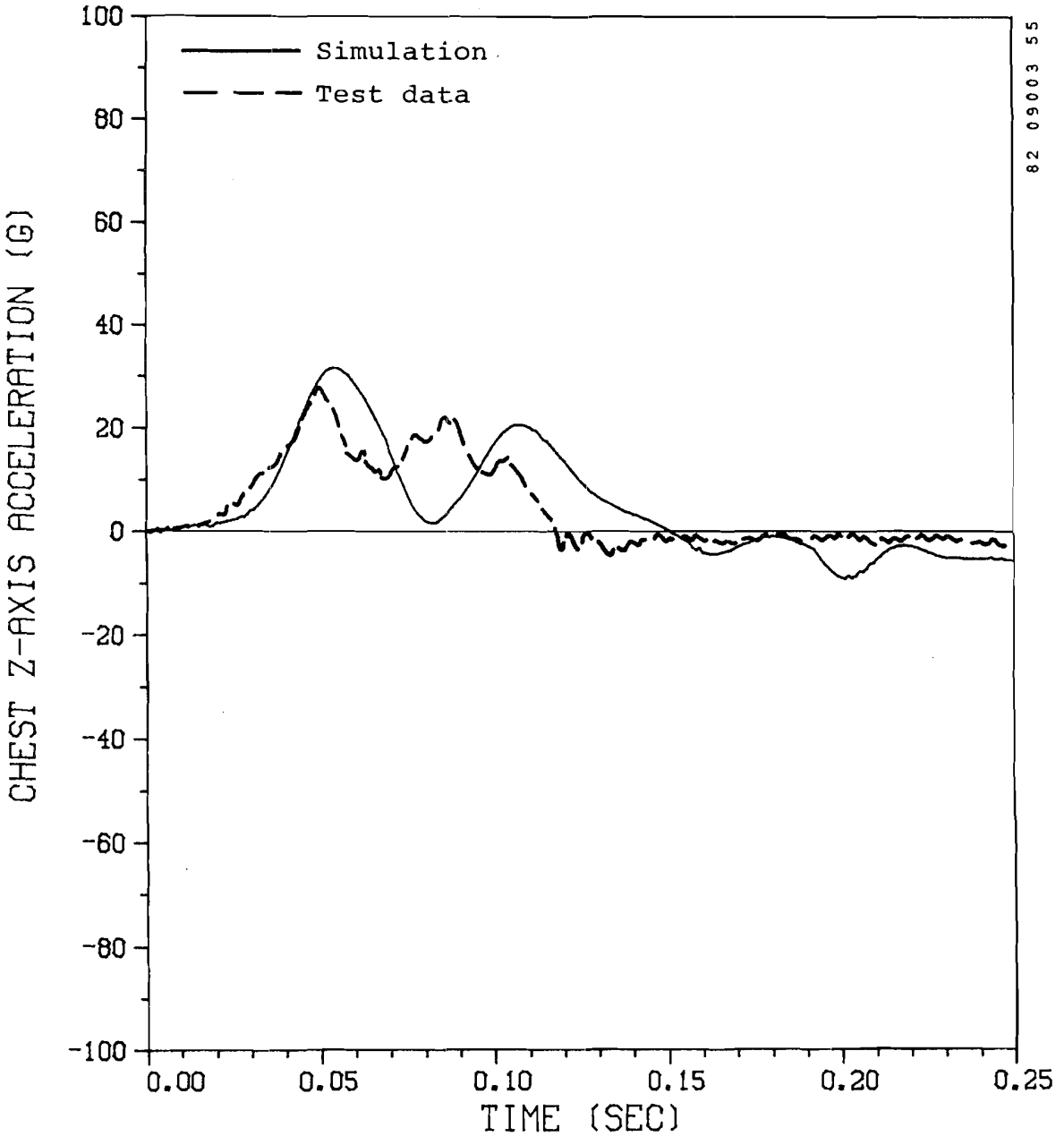

Figure 54. Energy-absorbing helicopter seat test, dummy chest z-acceleration.

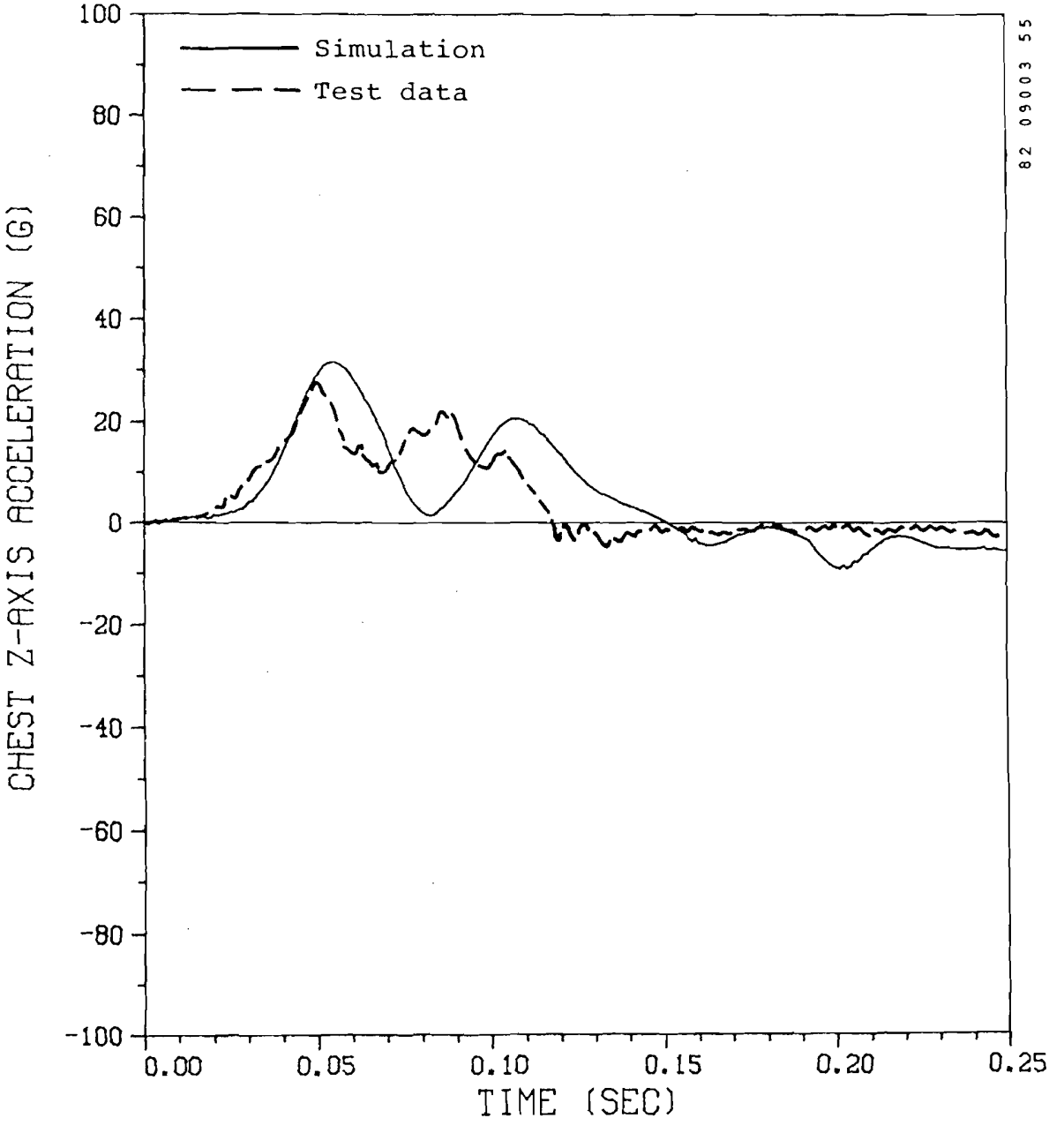

Figure 54. Energy-absorbing helicopter seat test, dummy chest z-acceleration.

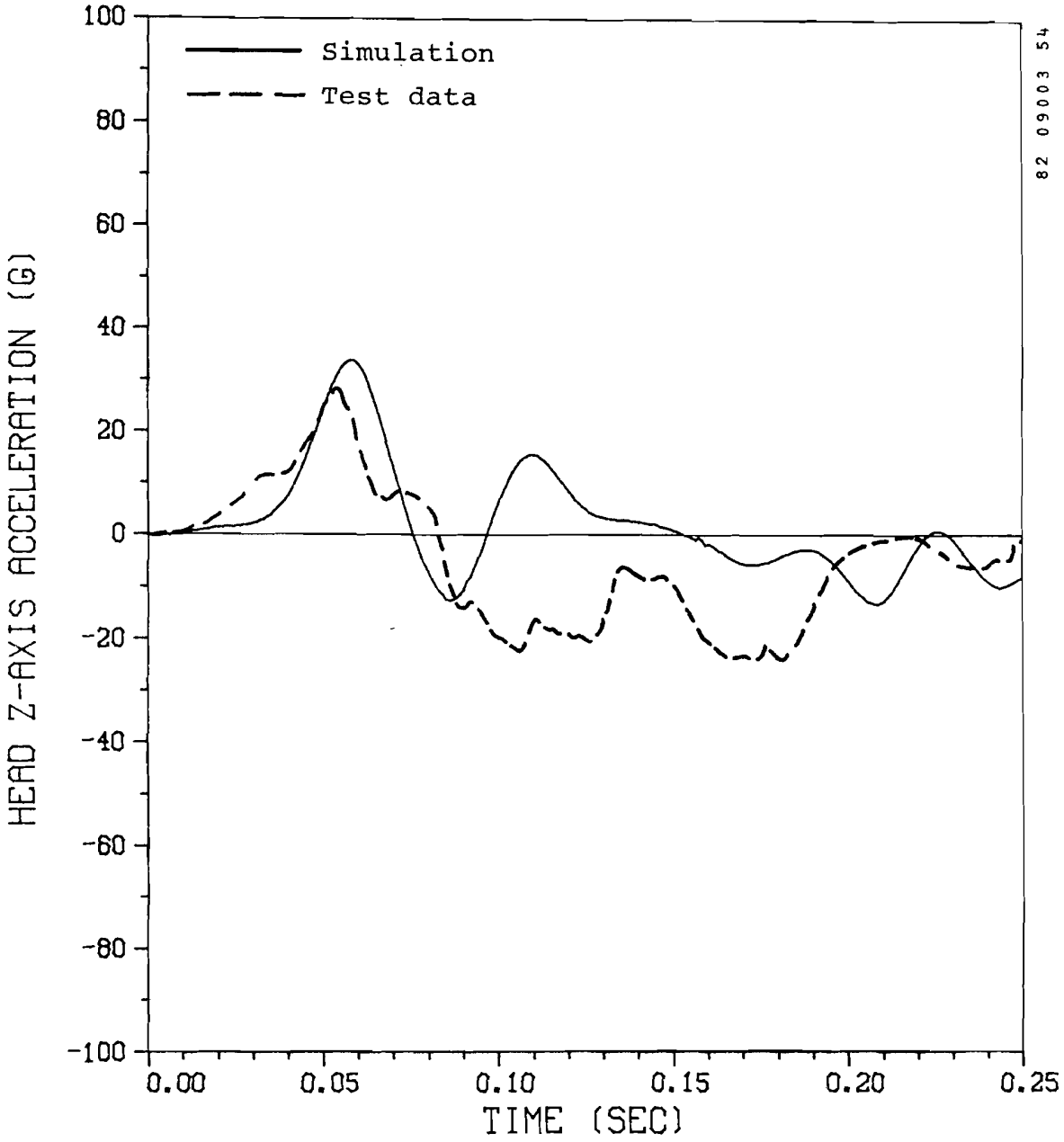

Figure 55. Energy-absorbing helicopter seat test, dummy head z-acceleration.

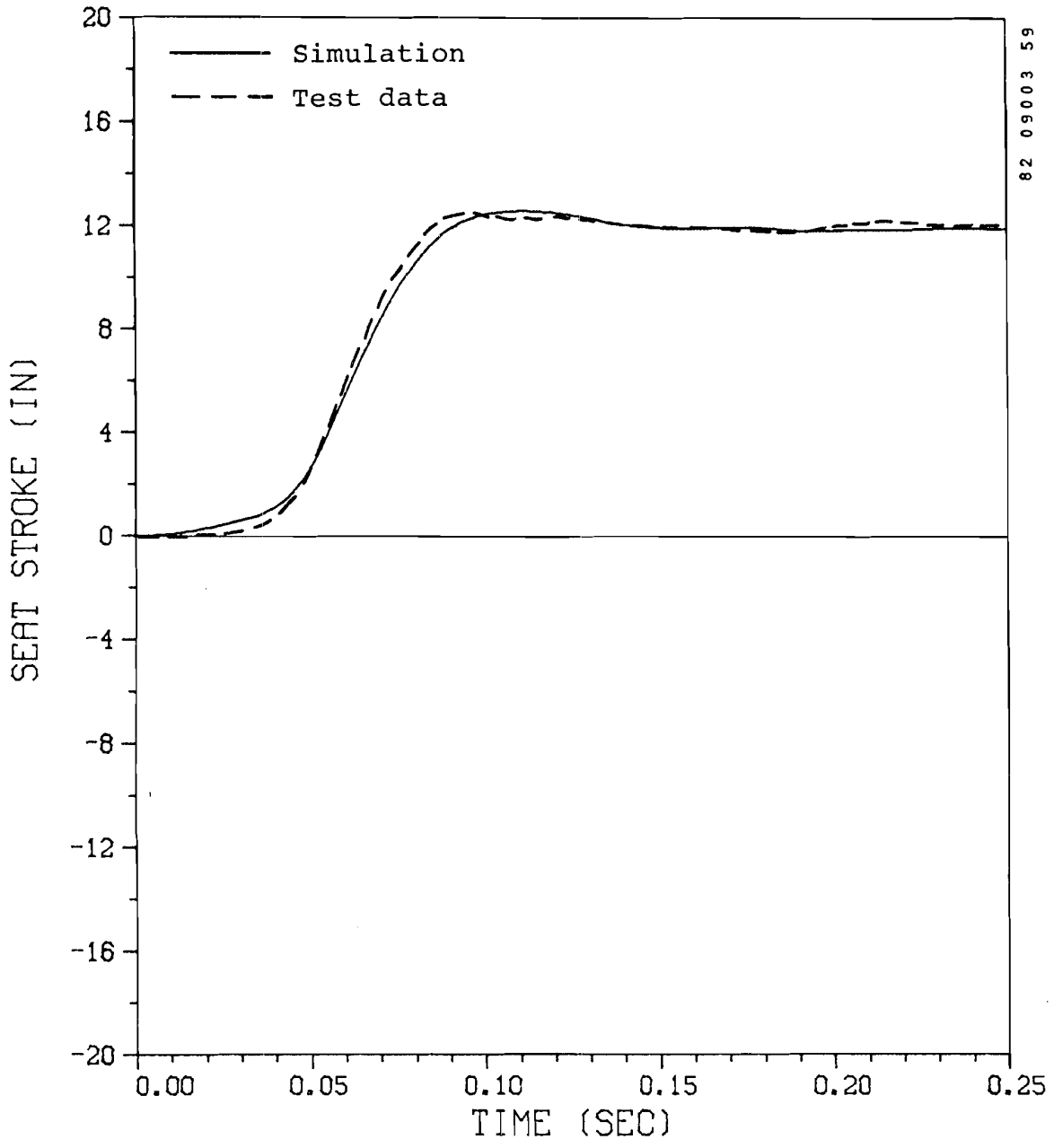

Figure 56. Energy-absorbing helicopter seat test, seat vertical displacement.

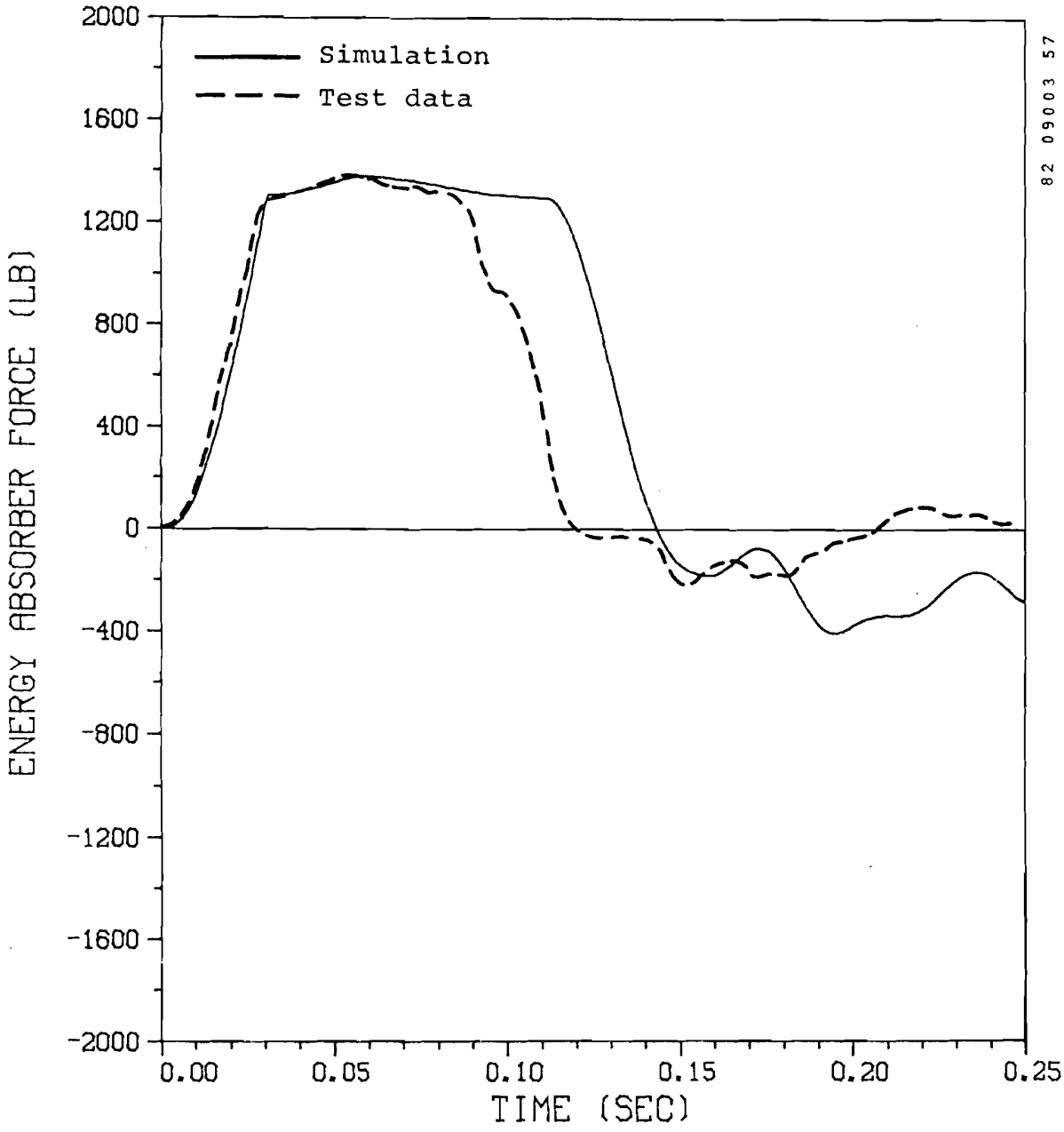

Figure 57. Energy-absorbing helicopter seat test, energy absorber force.

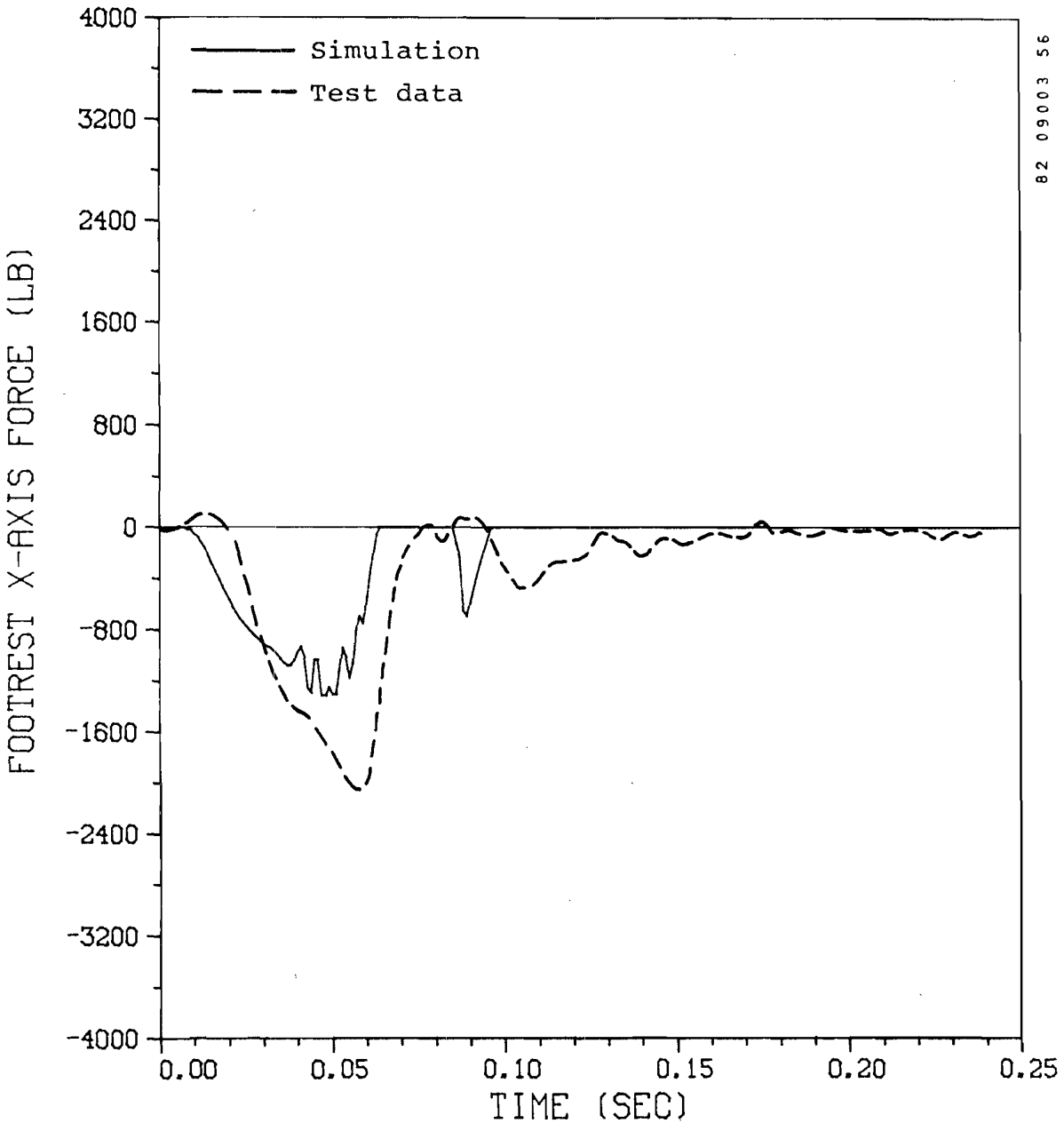

Figure 58. Energy-absorbing helicopter seat test, footrest x-force.

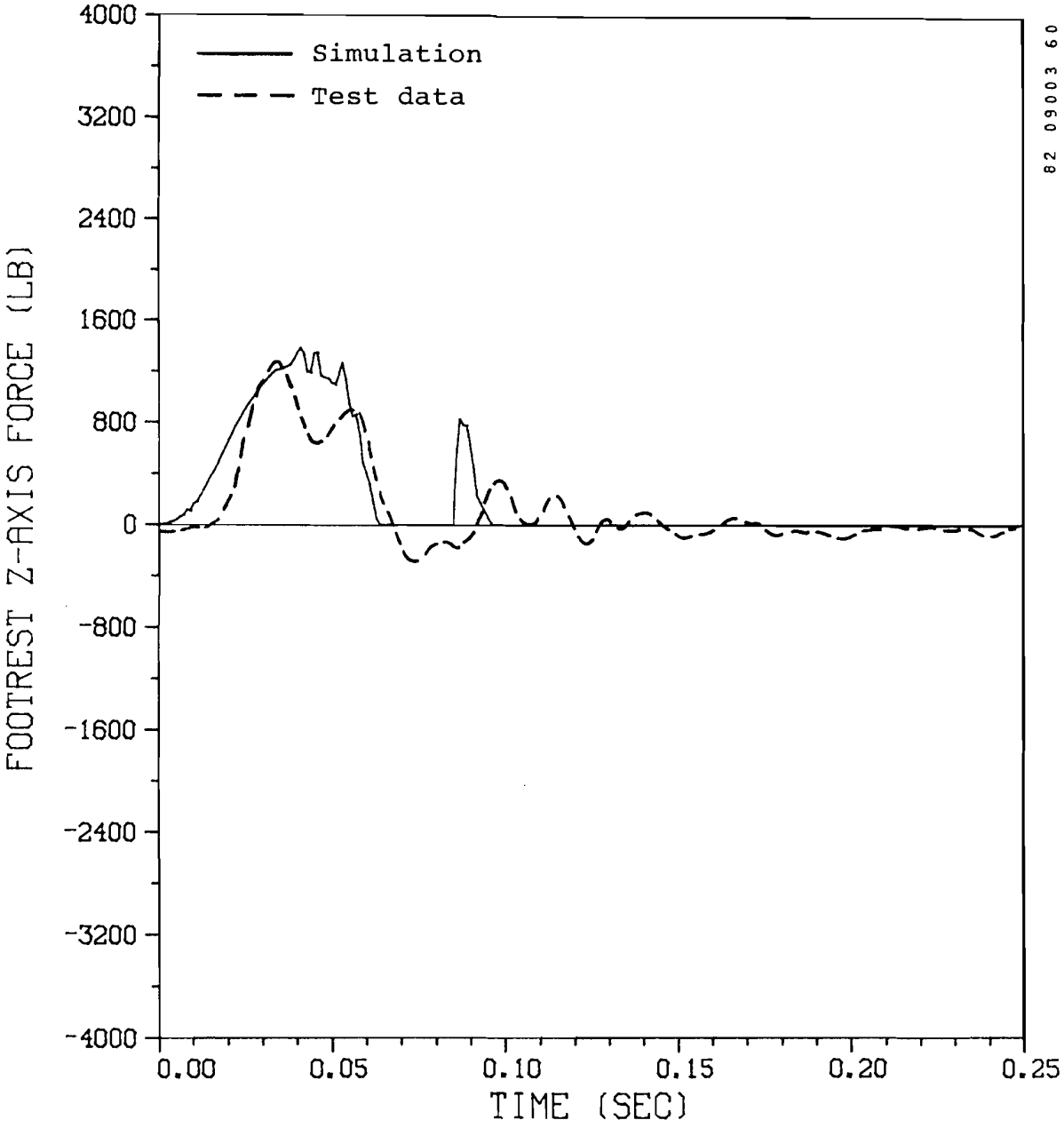

Figure 59. Energy-absorbing helicopter seat test, footrest z-force.

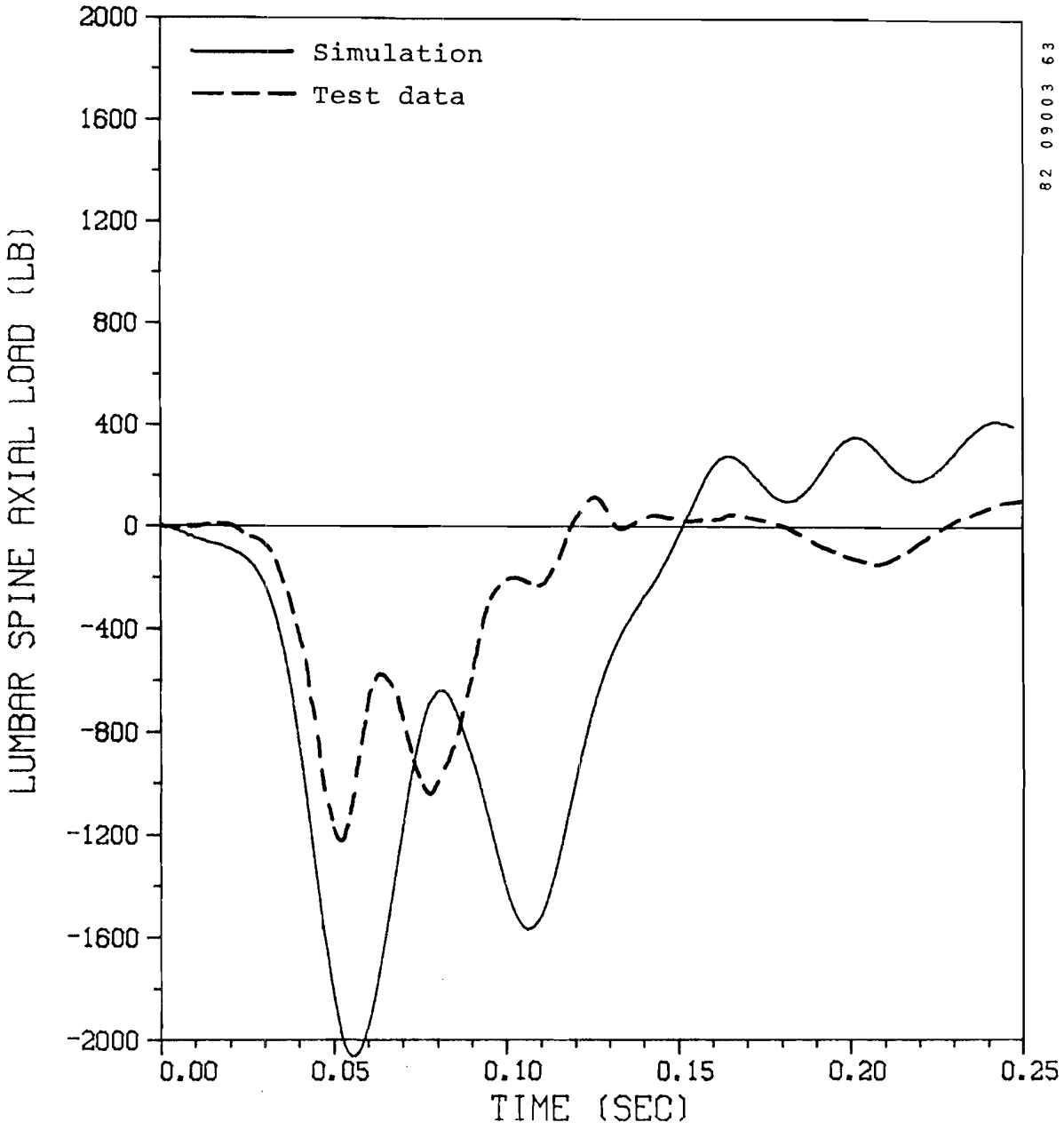

Figure 60. Energy-absorbing helicopter seat test, lumbar spine axial load.

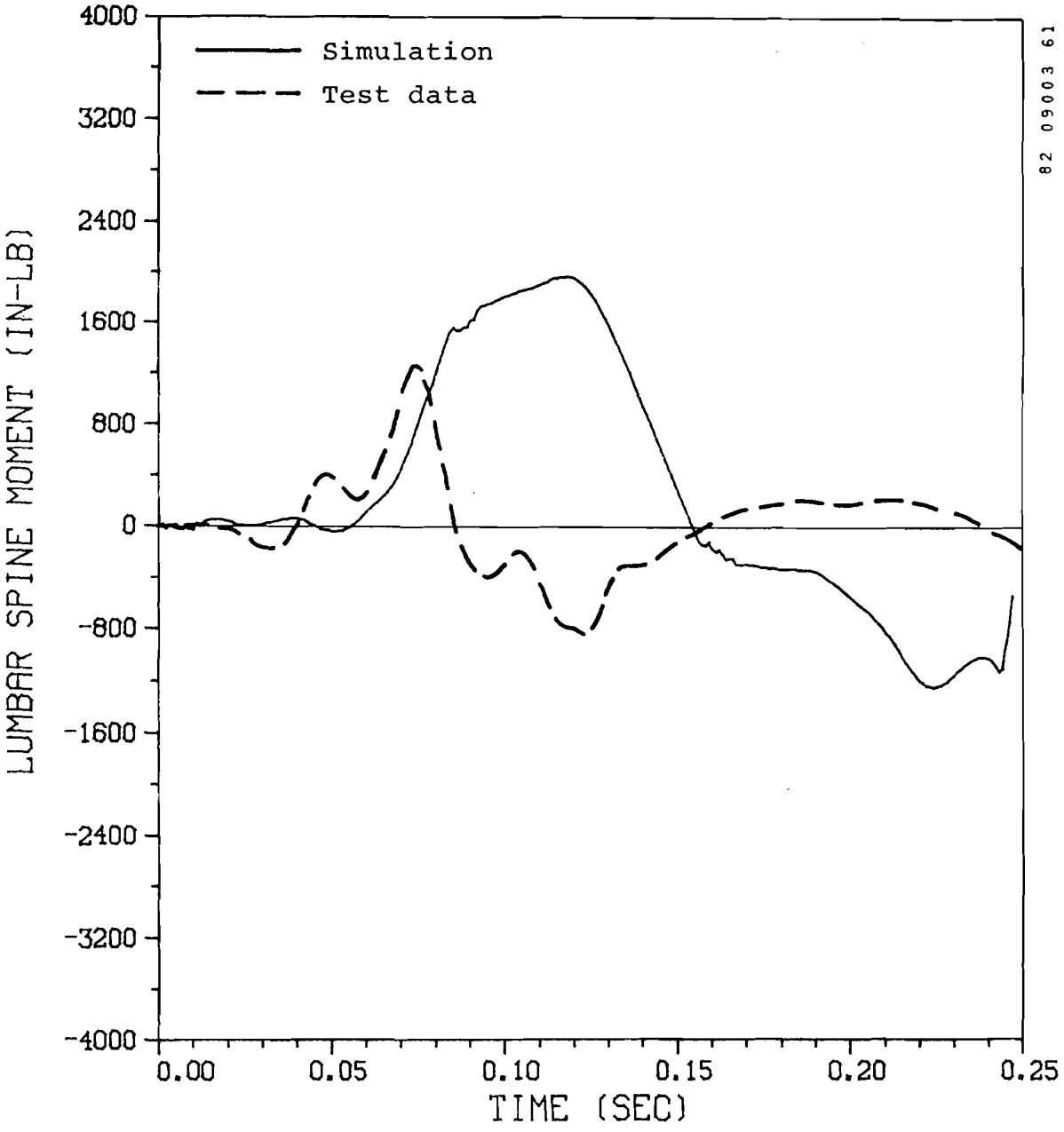

Figure 61. Energy-absorbing helicopter seat test, lumbar spine moment.

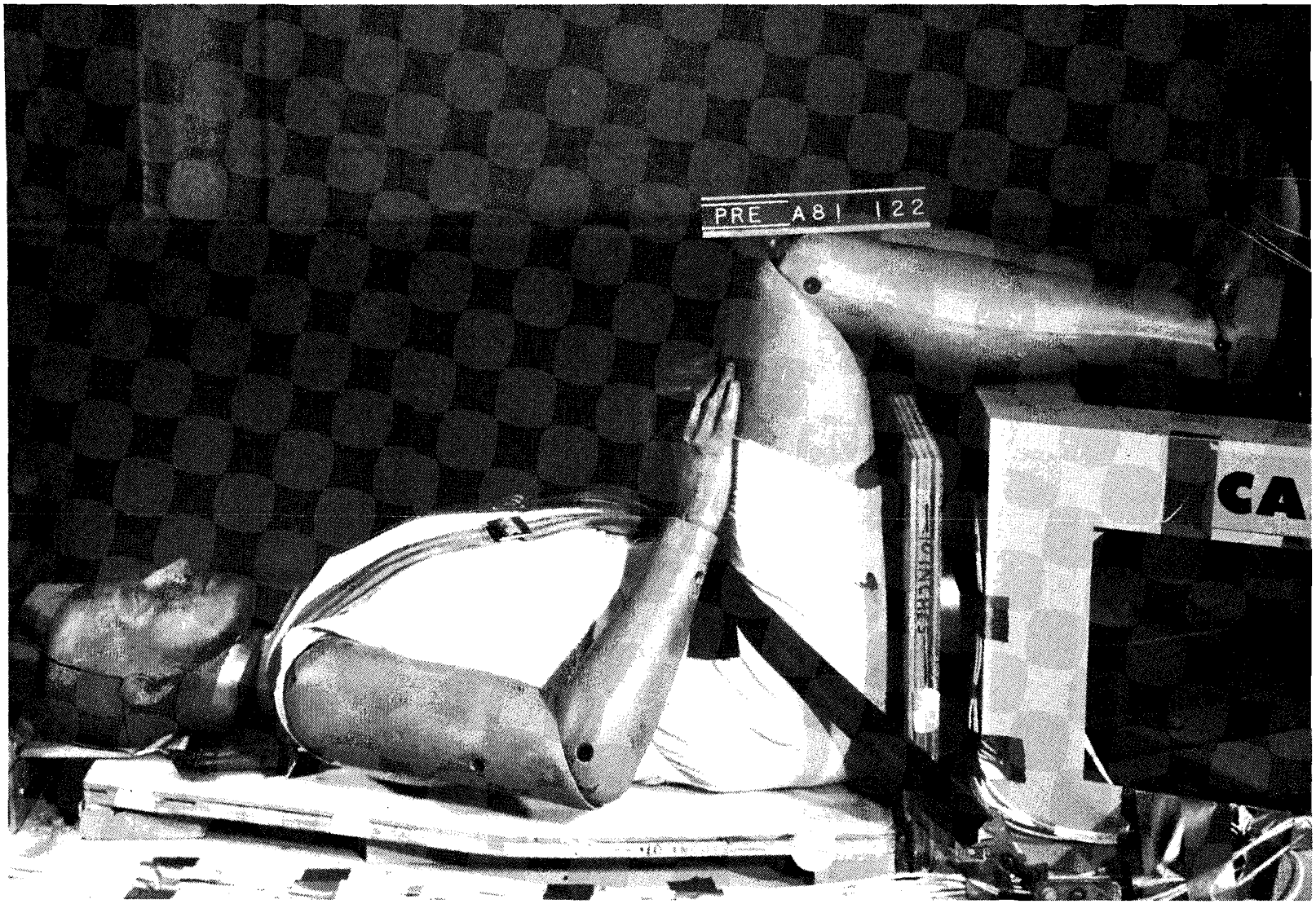

Figure 62. CAMI rigid seat (with VIP-95 dummy in place).

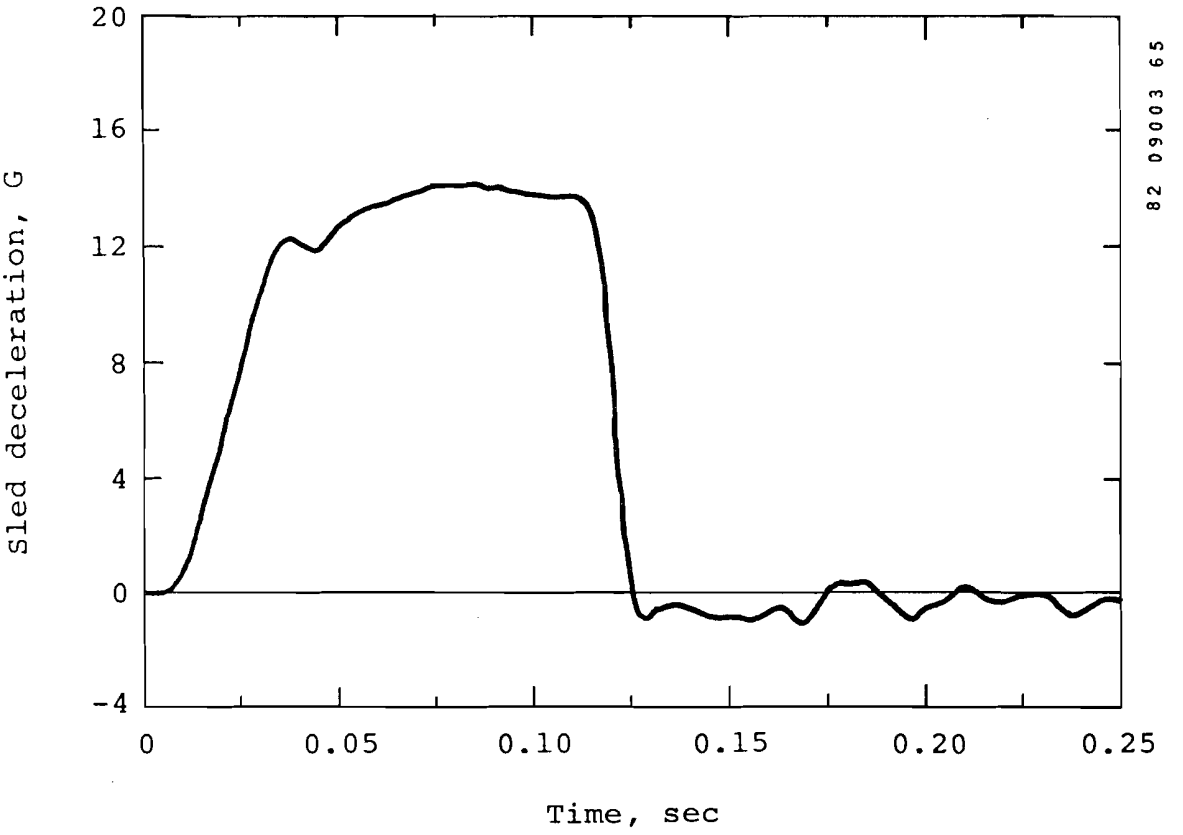

Figure 63. Sled deceleration for rigid seat test.

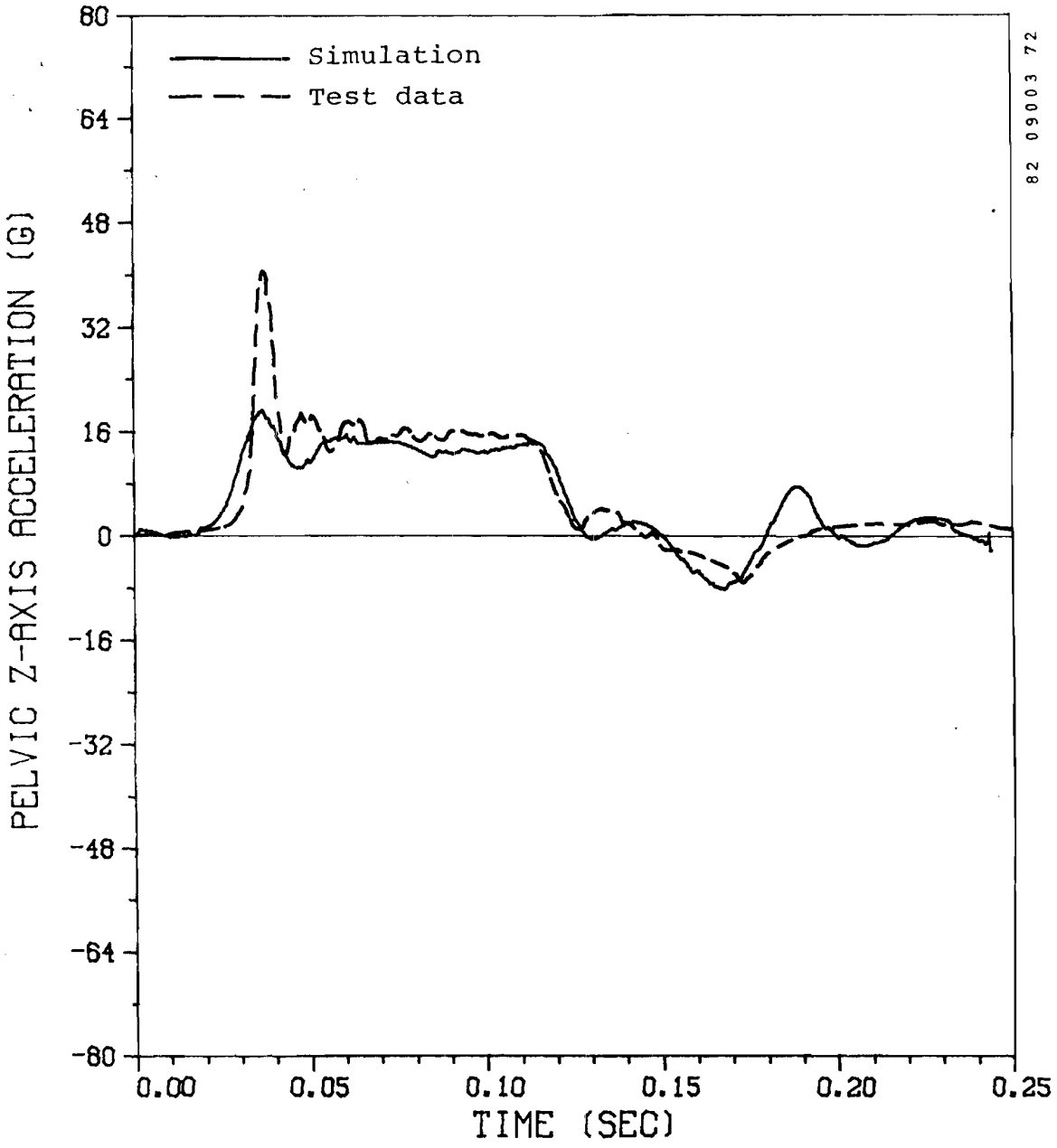

Figure 64. Rigid seat test, dummy pelvis z-acceleration.

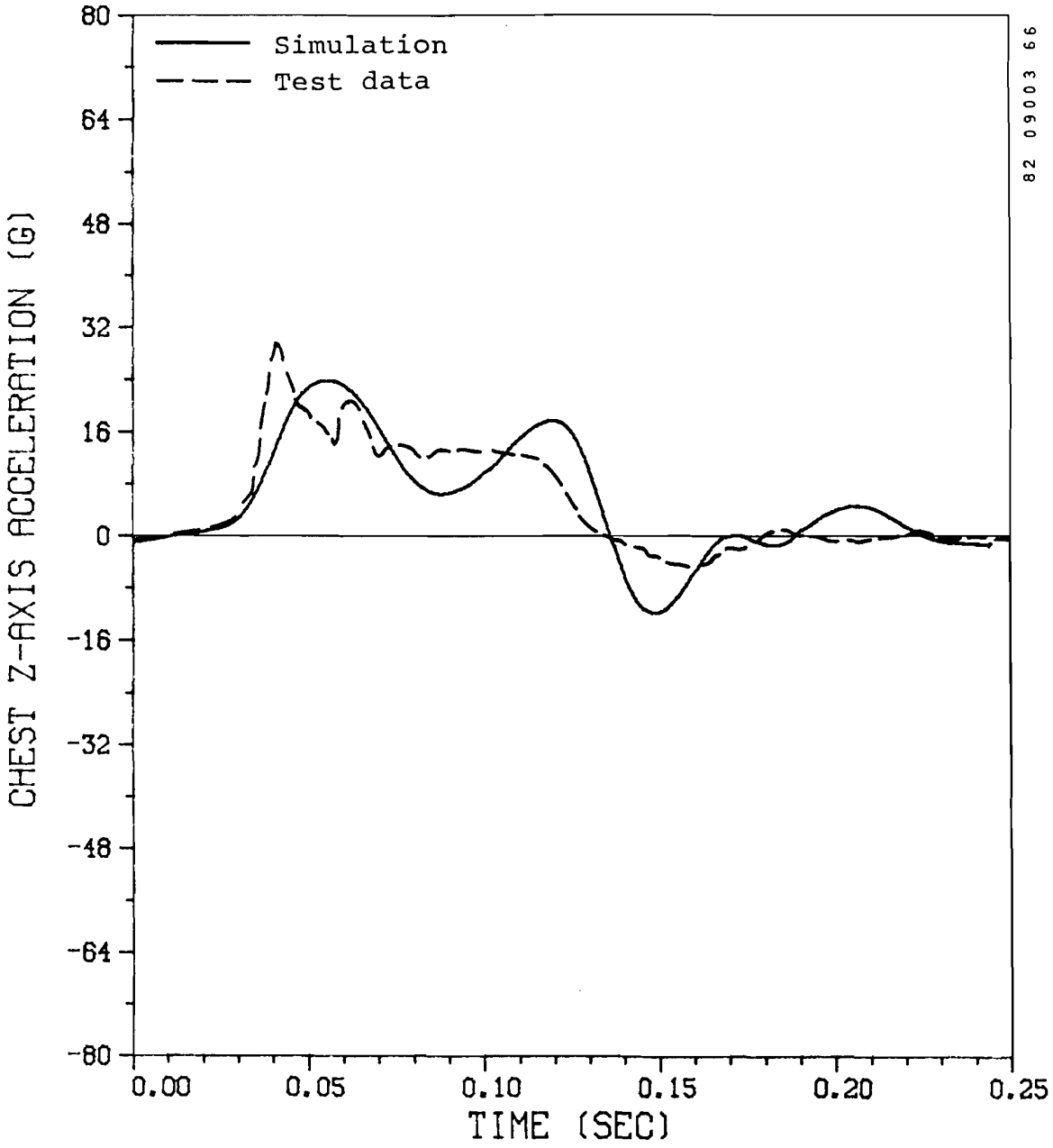

Figure 65. Rigid seat test, dummy chest z-acceleration.

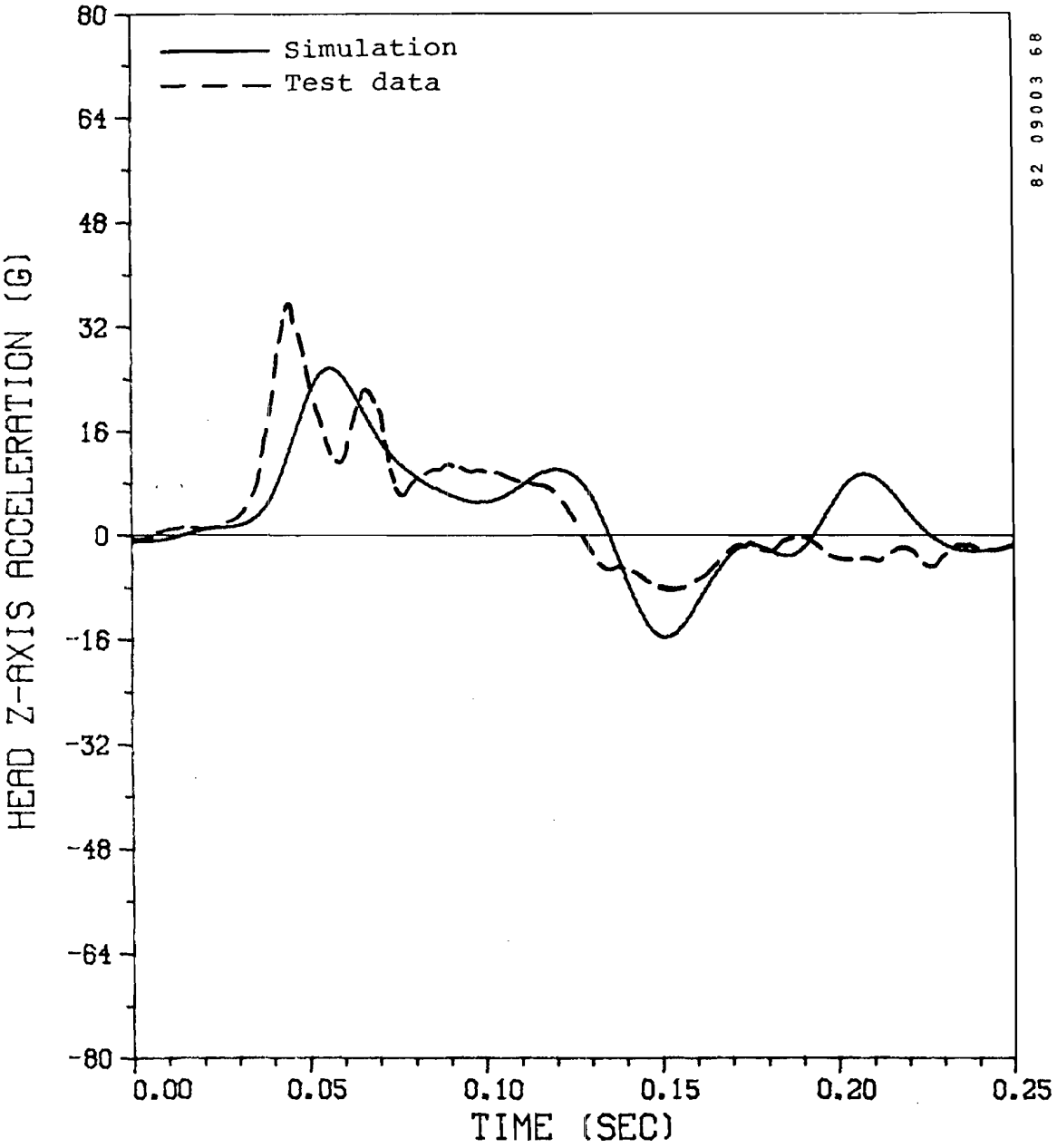

Figure 66. Rigid seat test, dummy head z-acceleration.

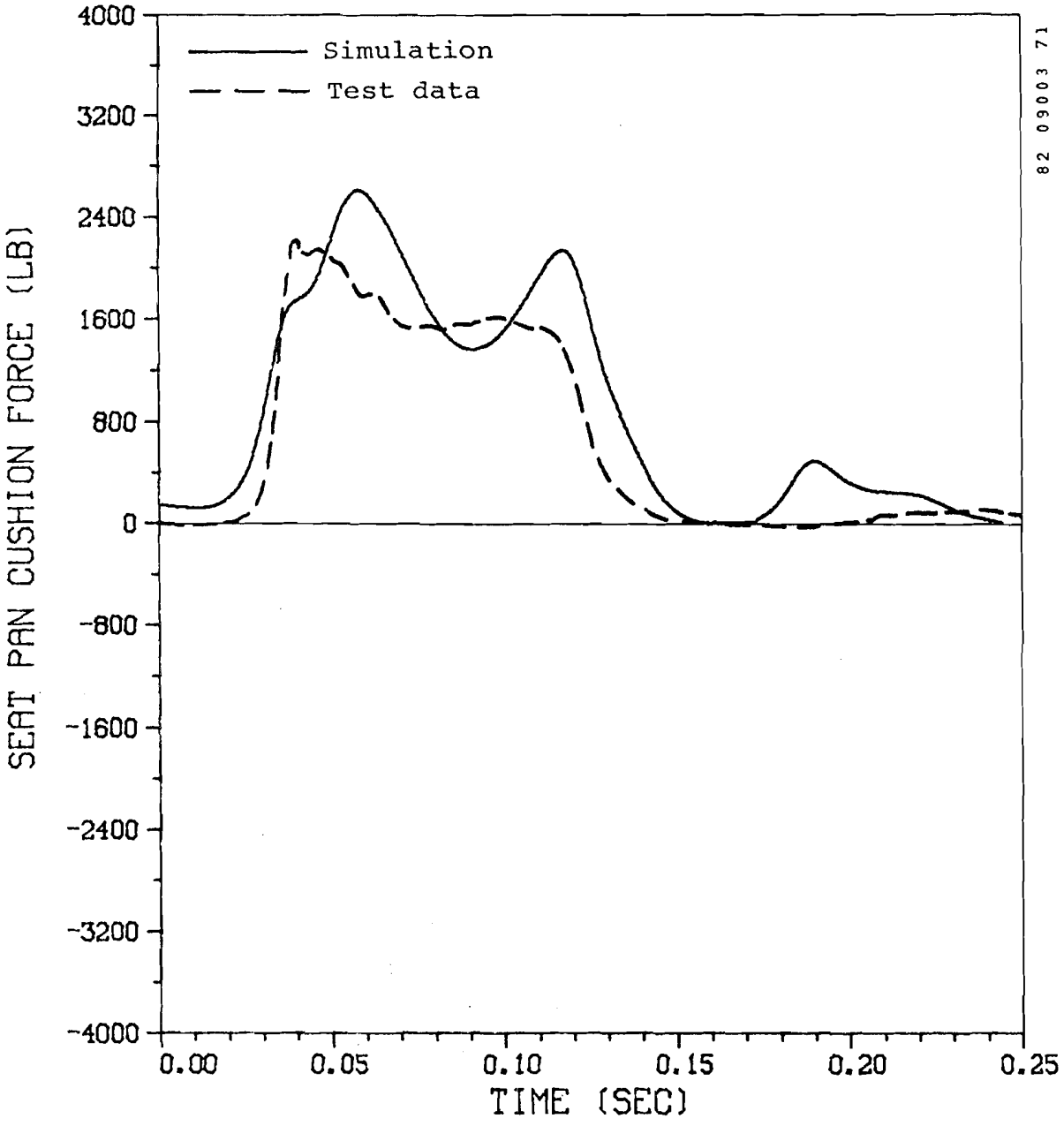

Figure 67. Rigid seat test, seat pan z-force.

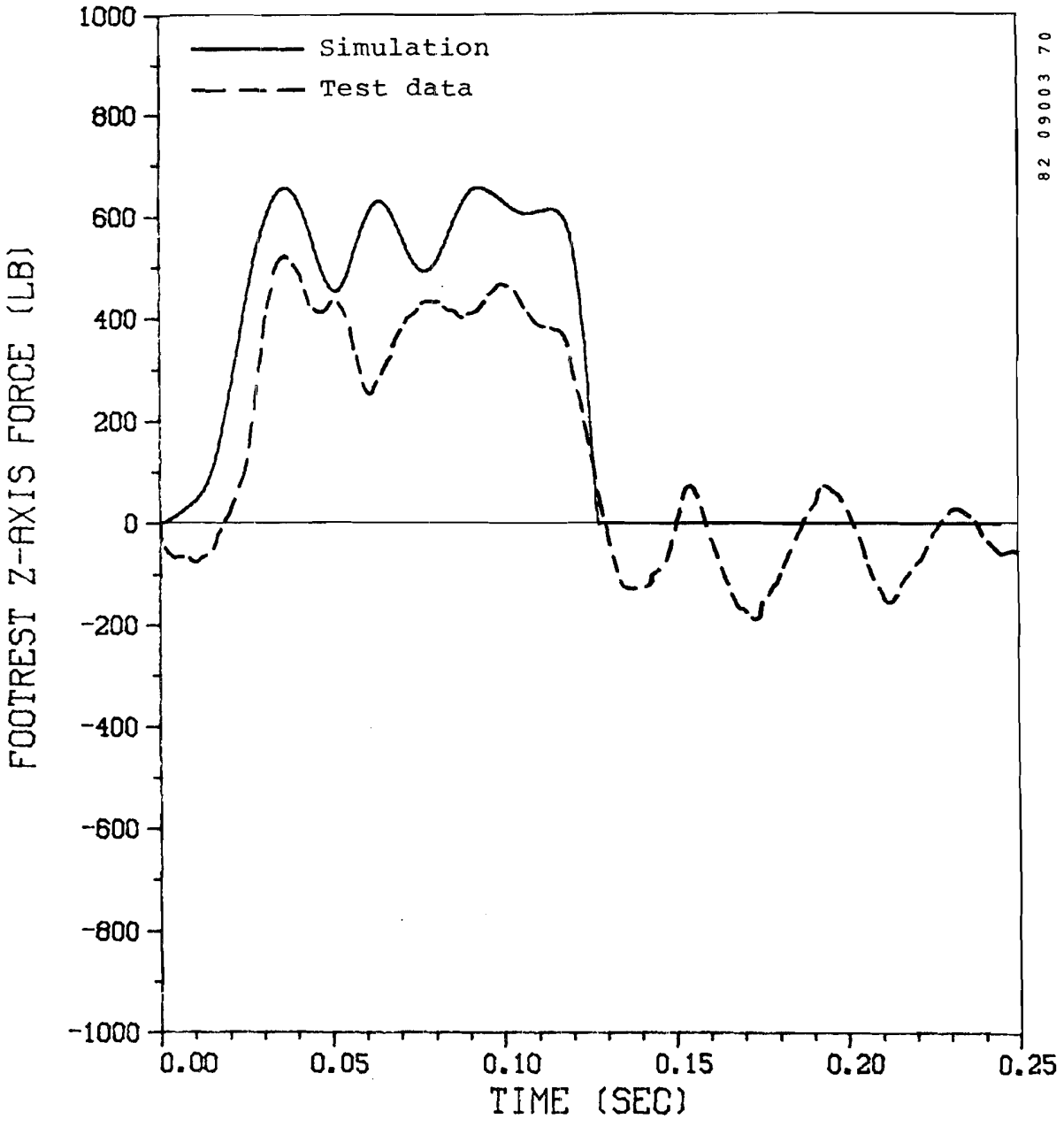

Figure 68. Rigid seat test, footrest z-force.

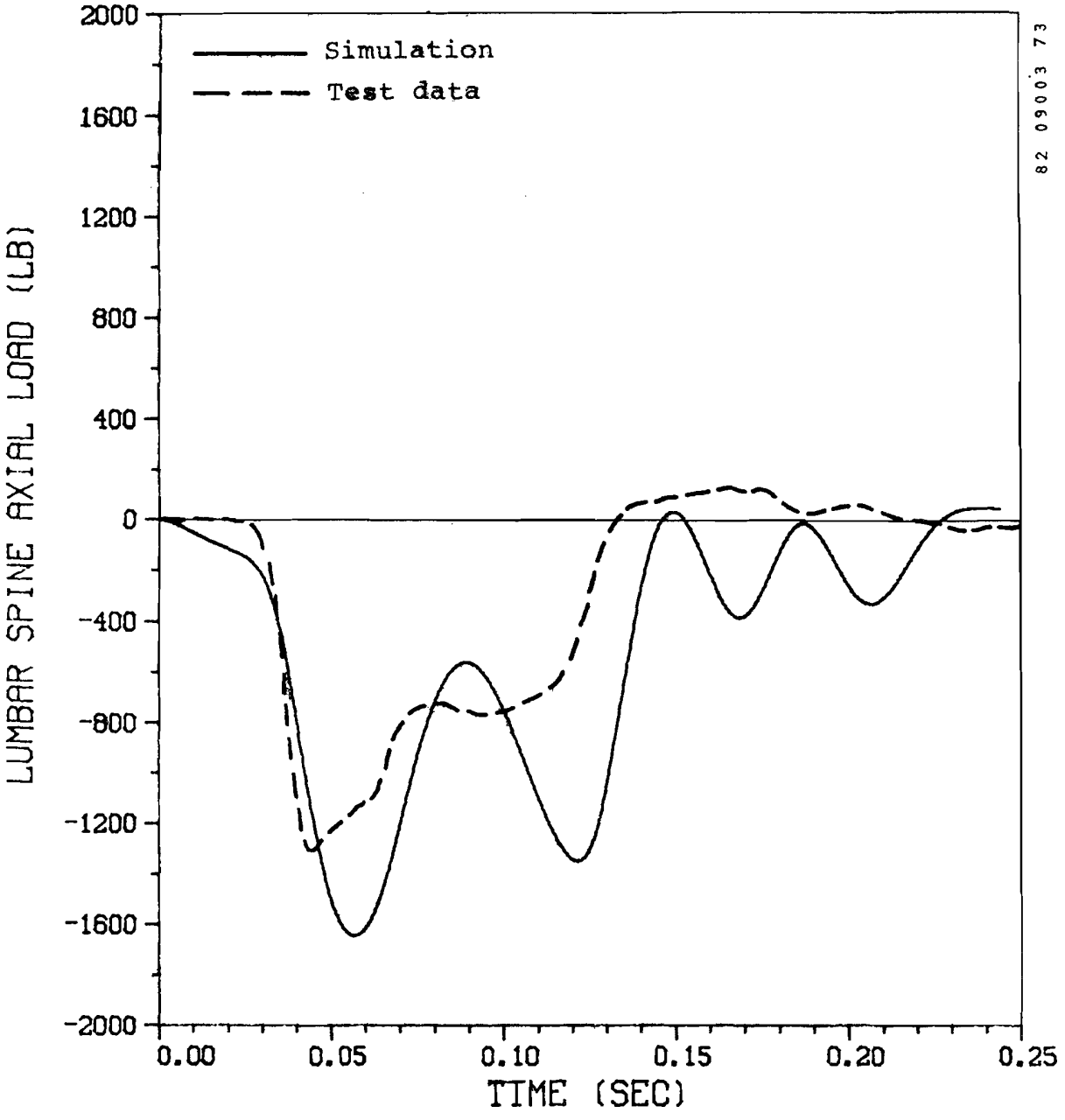

Figure 69. Rigid seat test, lumbar spine axial force.

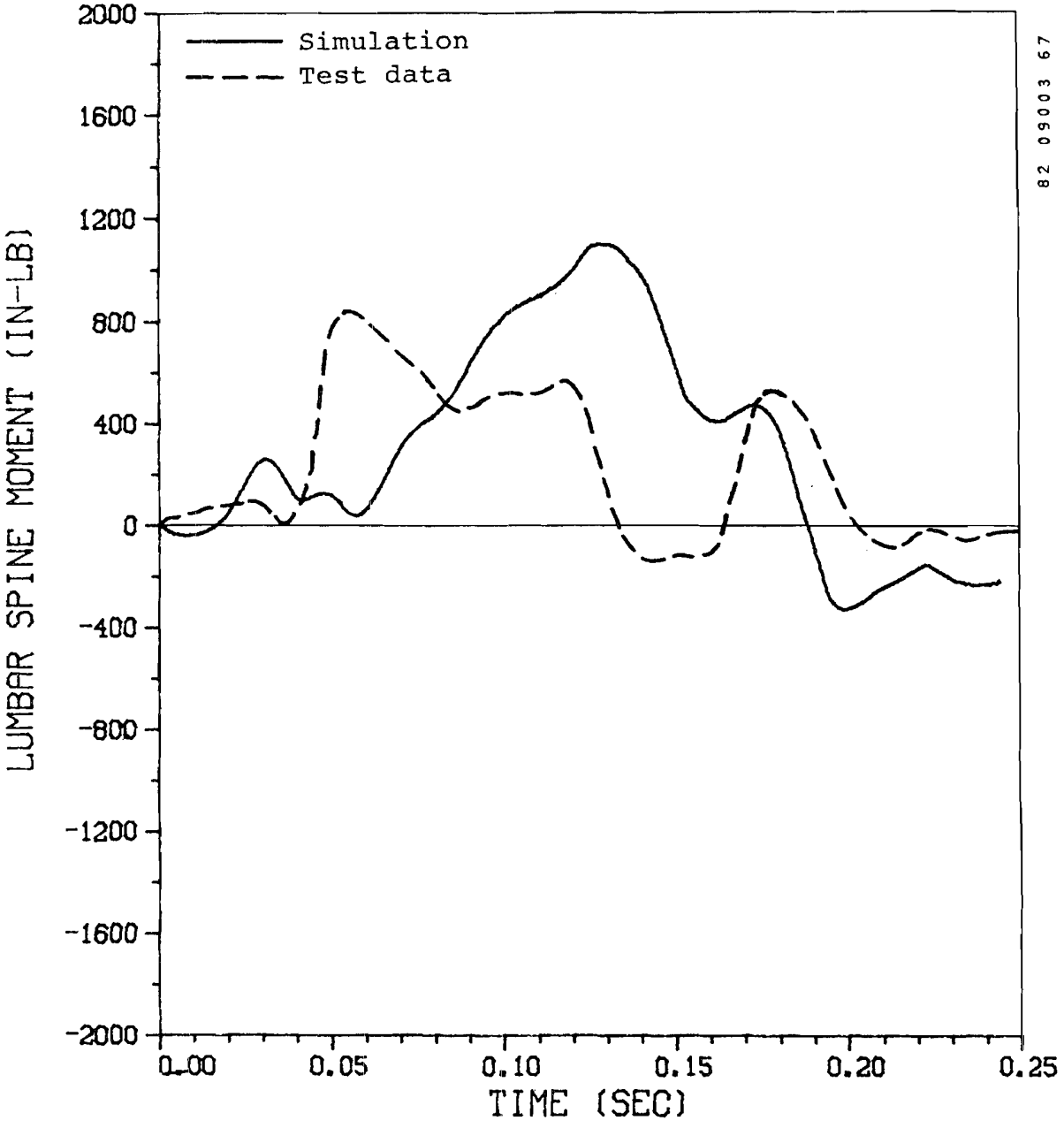

Figure 70. Rigid seat test, lumbar spine moment.

second seat because of bending in the structure. The seat and 50th-percentile (Part 572) dummy prior to the initial dynamic test are shown in figure 71.

In order to achieve sufficiently high decelerative loading to cause deformation of the seat frame, it was necessary to modify the floor (sled) attachments. The modified right-front leg of the seat is shown in figure 72, where it can be seen that the track roller has been removed and the track roller housing has been pinned to an inverted steel T-section. The web of the T-section has been notched to permit rotation of the seat leg. The two rivets that secure the roller housing to the lower end of the leg have been replaced by 0.25-in. steel bolts. All four of the seat legs were modified in this manner.

Each leg was bolted to a six-axis load cell. A general aviation-type three-point restraint system was used, with the shoulder belt passing over the dummy's left shoulder and anchored above and to the left of the seat, in a position typical of an aircraft installation. Forces were measured in both sides of the lap belt and in the shoulder belt, between the dummy and the anchor point. As shown in figure 71, a displacement transducer was installed to measure forward motion of the seat frame. For some tests a footrest was included, mounted at an angle of 45 degrees relative to the horizontal and bolted to a load cell. In tests that used a flat floor, the foot forces were not measured, as the feet leave the floor a very short time after impact. Accelerations were measured in the pelvis, chest, and head of the dummy. The dummy had been modified to include a load cell at the base of the lumbar spine, as in the tests described in sections 5.2 and 5.3.

The initial finite element model of the seat structure illustrated in figure 73 used 28 nodes, 36 beam elements, and 2 triangular plate elements. The approximation to the cross section of the 6061-T6 aluminum beam elements is shown in figure 74.

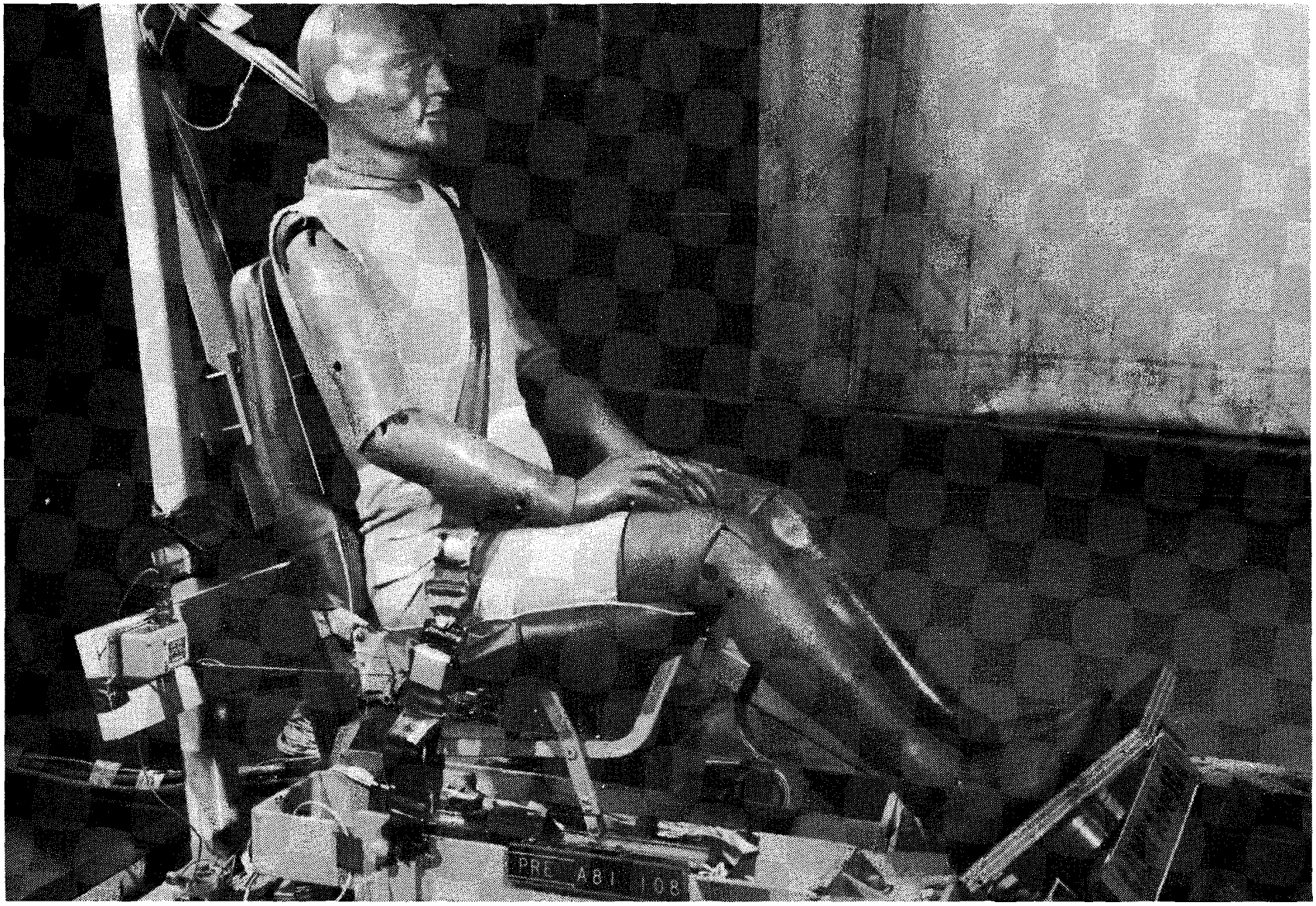

Figure 71. General aviation seat and Part 572 dummy prior to CAMI Test A81-108.

Figure 72. Modified floor attachment.

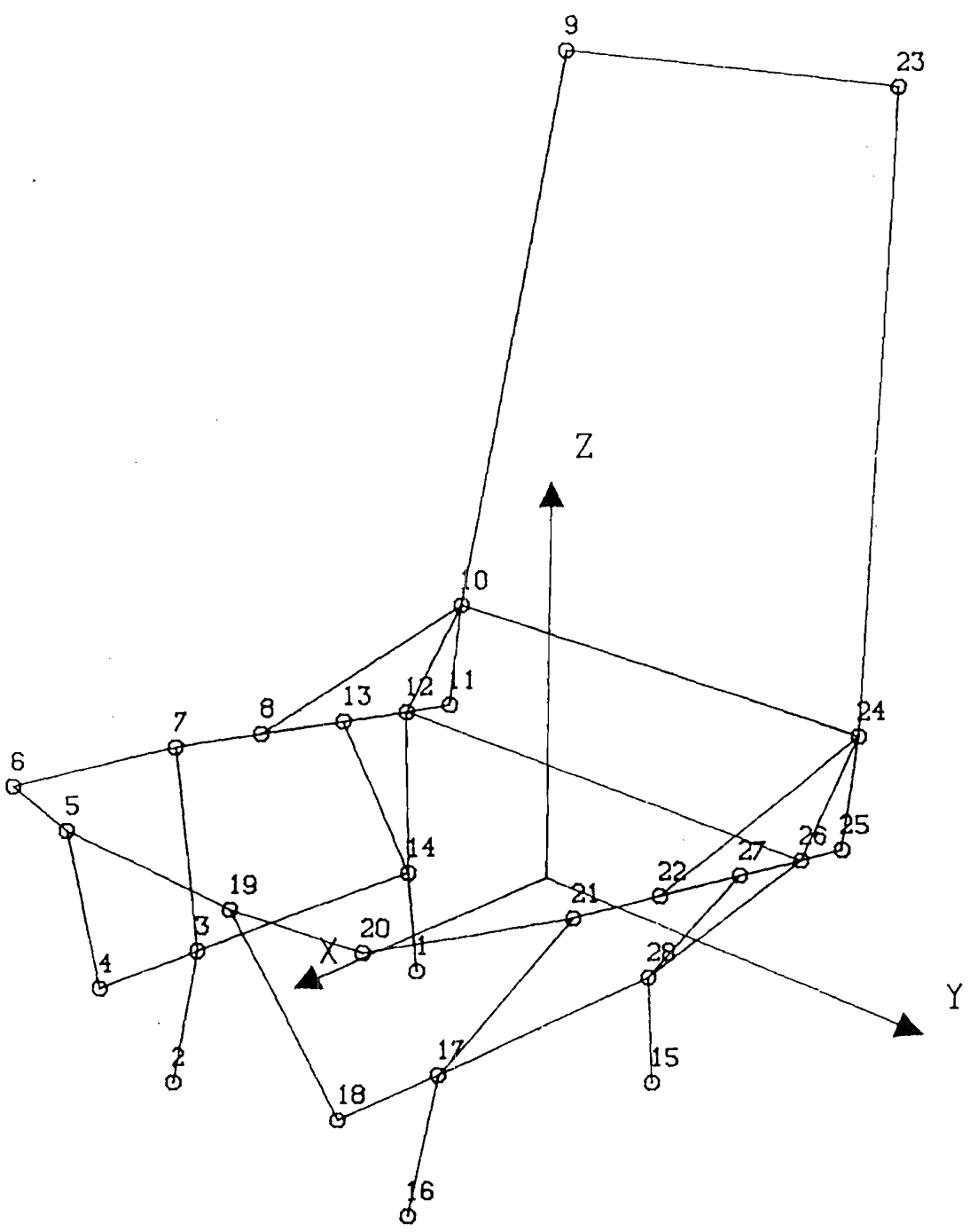

Figure 73. Initial finite element model of general aviation seat.

Actual Cross Section

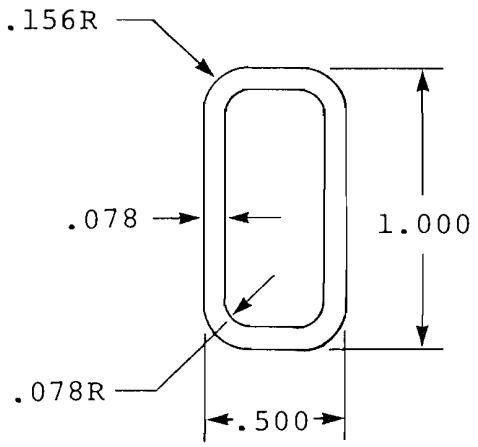

$A = 0.1940 \text{ in.}^2$

$I_y = 0.02078 \text{ in.}^4$

$I_z = 0.00672 \text{ in.}^4$

Approximate Cross Section

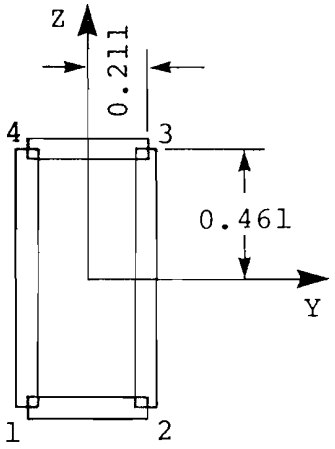

	Y	Z
1	-0.211	-0.461
2	0.211	-0.461
3	0.211	0.461
4	-0.211	0.461

81 09003 06

Figure 74. Beam element cross section for general aviation seat model.

The tests given greatest attention in the simulations because of bending in the seat structure were those conducted in a forward-facing configuration with a 12-G sled deceleration (figure 75). Two tests, A81-110 and A81-111, were conducted under similar conditions except that the former included a footrest, as shown in figure 76, and the latter did not (figure 77). Results of both tests were similar except that without the footrest dummy x-accelerations reached somewhat higher magnitudes. In test A81-111, without the footrest, the shoulder belt load reached a higher value, and the dummy, rebounding rearward, caused failure of the seat back. Because of the latching mechanism on the folding seat back, the actual seat was less able to resist rearward loading* than the finite element model, for which the frame was assumed to be continuous from the seat pan to the seat back. Examining the model in figure 73 and using the right-hand side of the seat as an example, the latch is represented by beam elements connecting nodes 10 to 11 and 11 to 12. The cross section of these elements is that of the tubing shown in figure 74, rather than the thinner material actually used in the latch. This structure is further supported by a triangular plate connecting nodes 8, 10, and 12, resulting in a structure that is much stronger than the actual hardware. In the SOM-LA simulations, the impact of the rebounding dummy into the relatively rigid seat back produces a spike in the segment accelerations, particularly the chest, as shown in figures 78 and 79. The effect of this impact with the seat back on occupant motion can be seen in the last two plots of figure 80.

The revised finite element model is shown in figure 81. The short beam elements that connect nodes 8 to 10 and 22 to 24 contain torsional releases to allow pivoting of the seat back about the lateral horizontal line from node 8 to node 22. Crushing or buckling of

*NAS 809, paragraph 4.1.2.1, requires the capability of the seat to resist a 300-lb load applied aftward 8 in. above the intersection of the seat back and bottom.

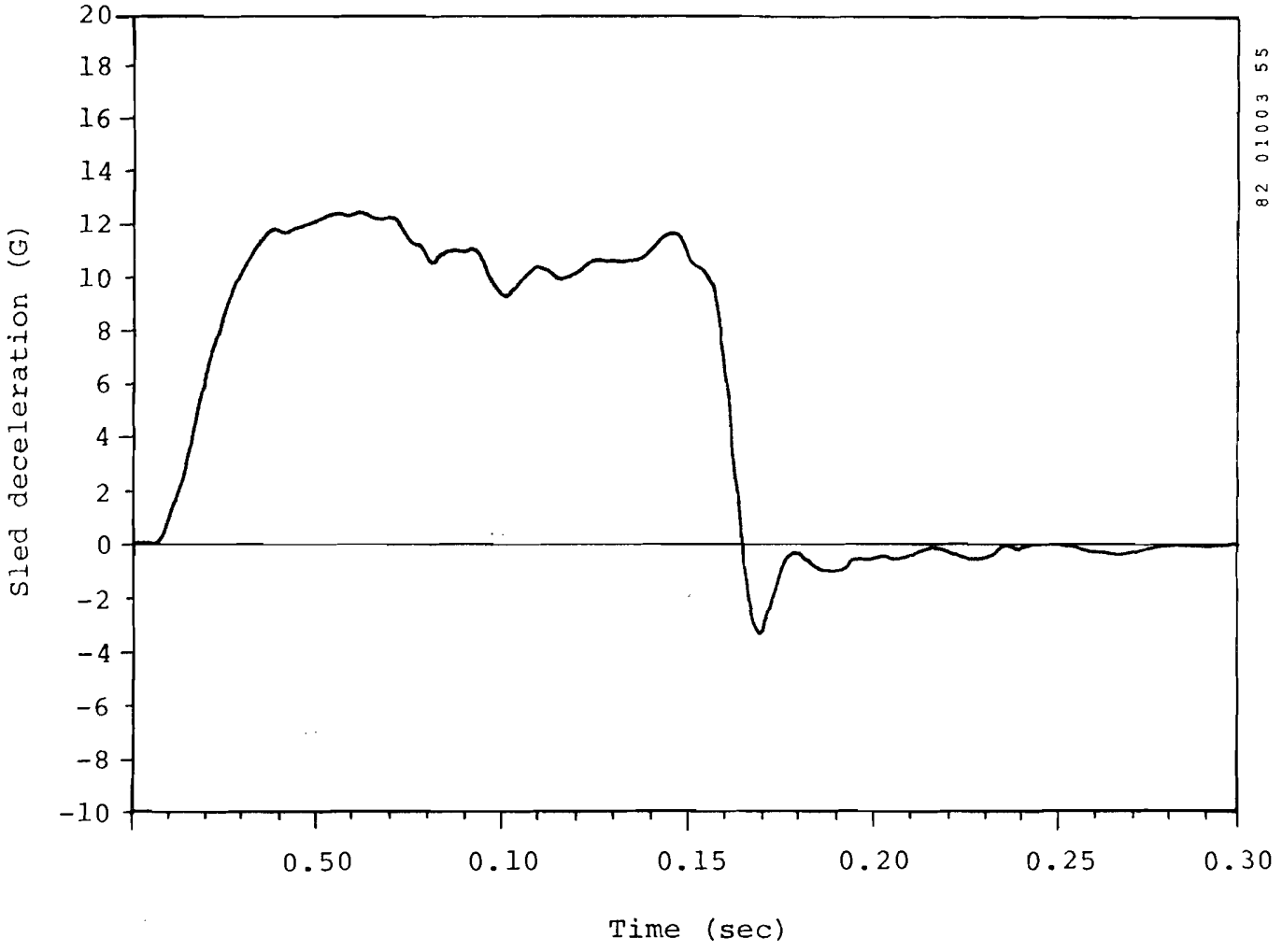

Figure 75. Sled deceleration, CAMI general aviation seat Test A81-110.

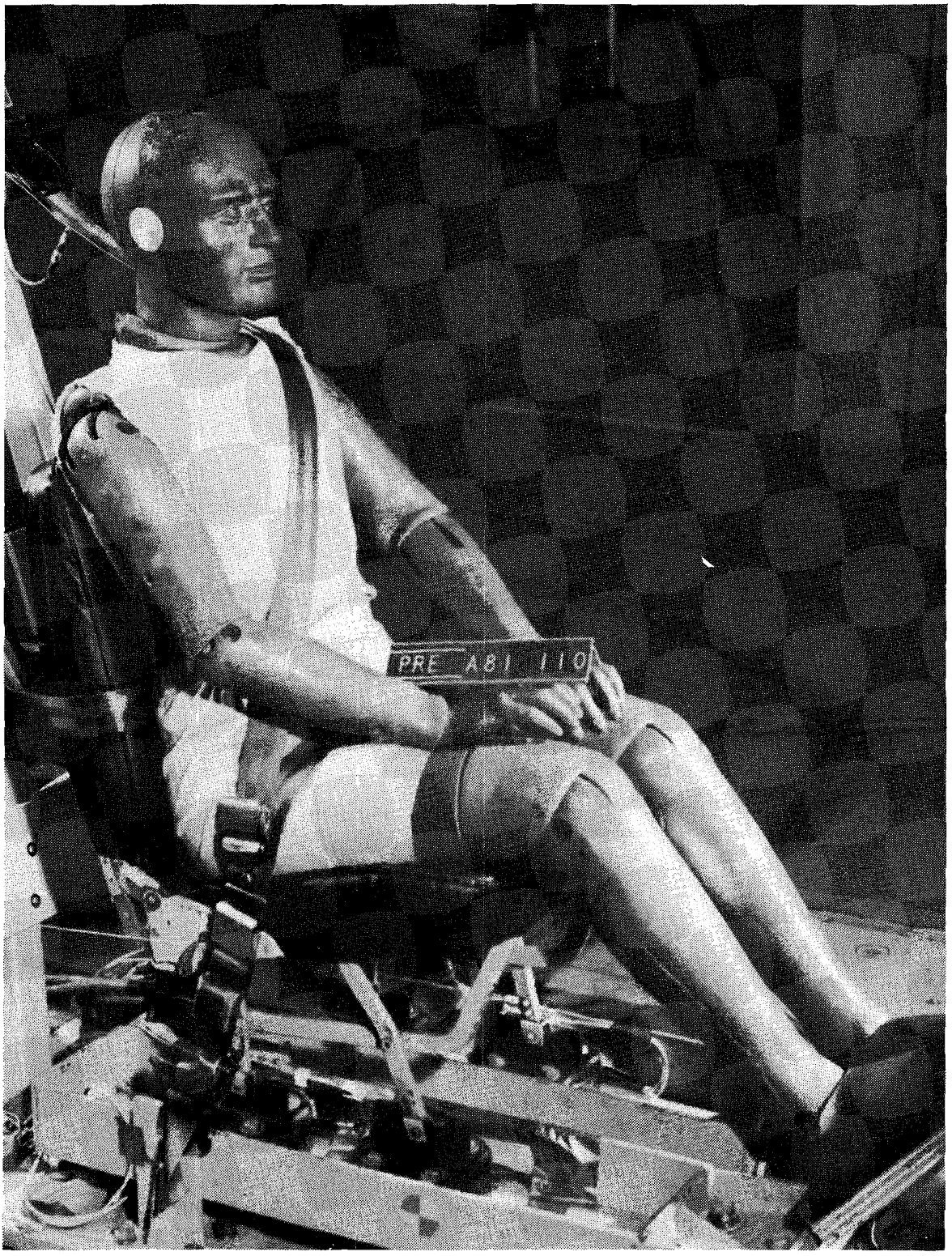

Figure 76. General aviation seat and dummy prior to CAMI Test A81-110.

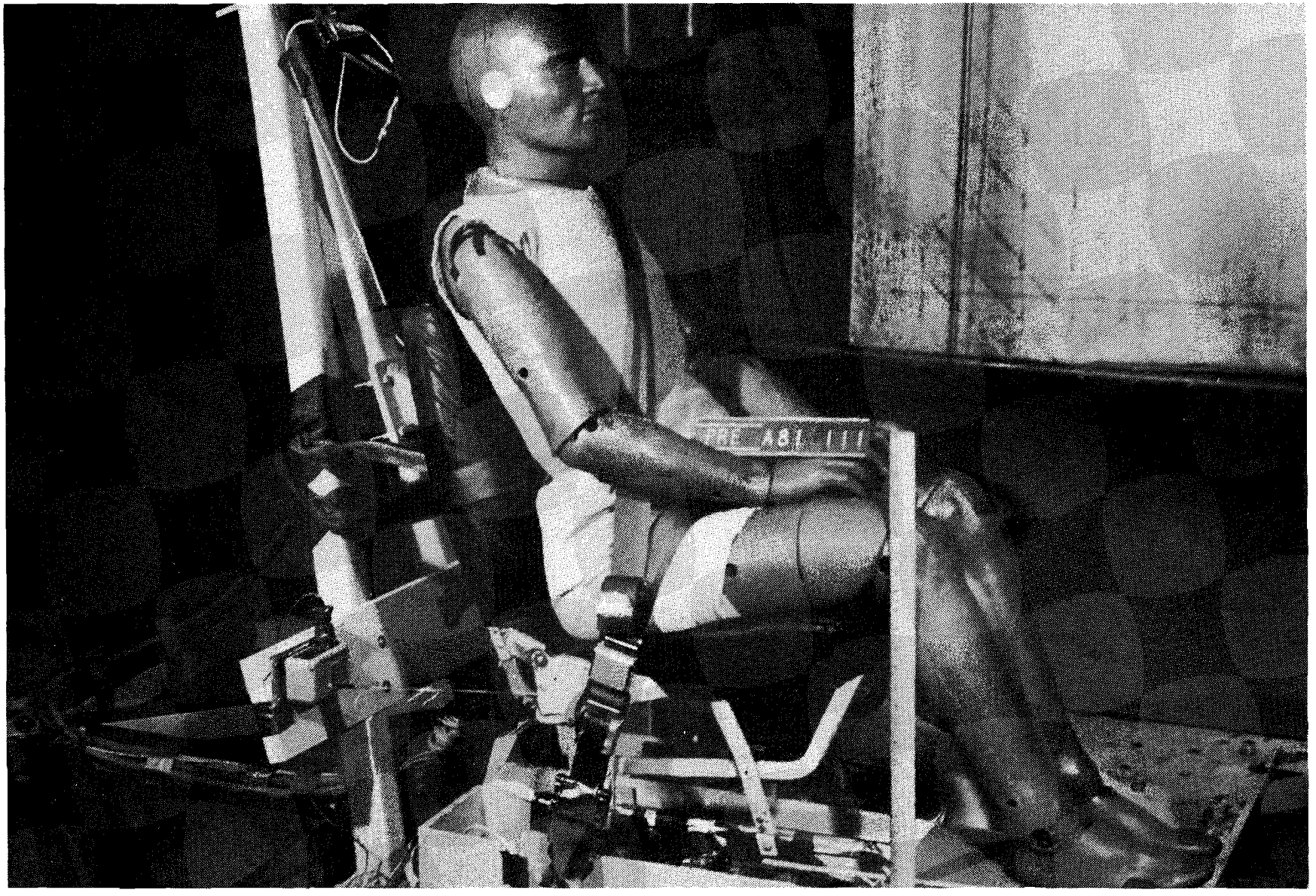

Figure 77. General aviation seat and dummy prior to CAMI Test A81-111.

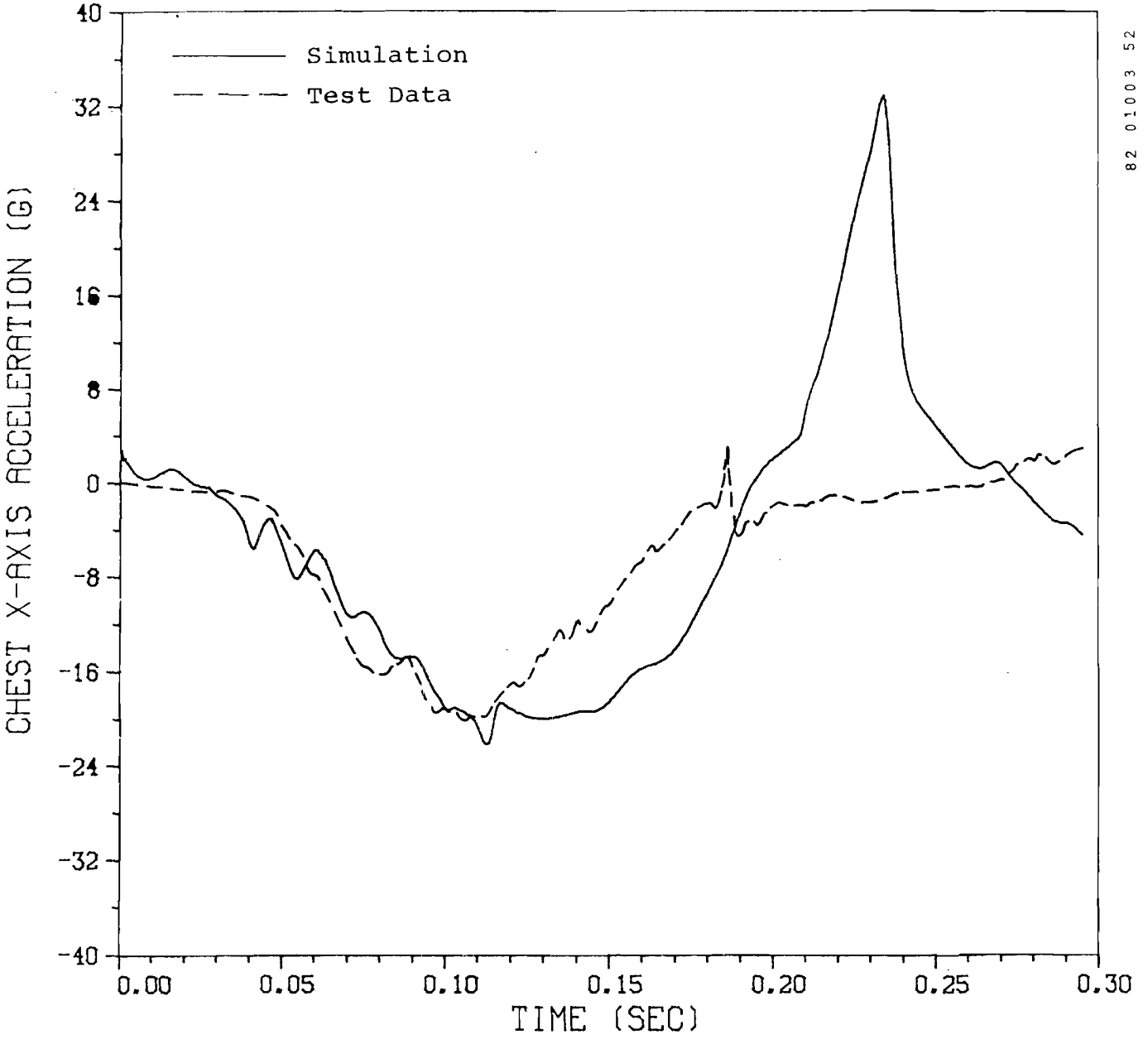

Figure 78. General aviation seat Test A81-110, dummy chest x-acceleration (initial finite element model).

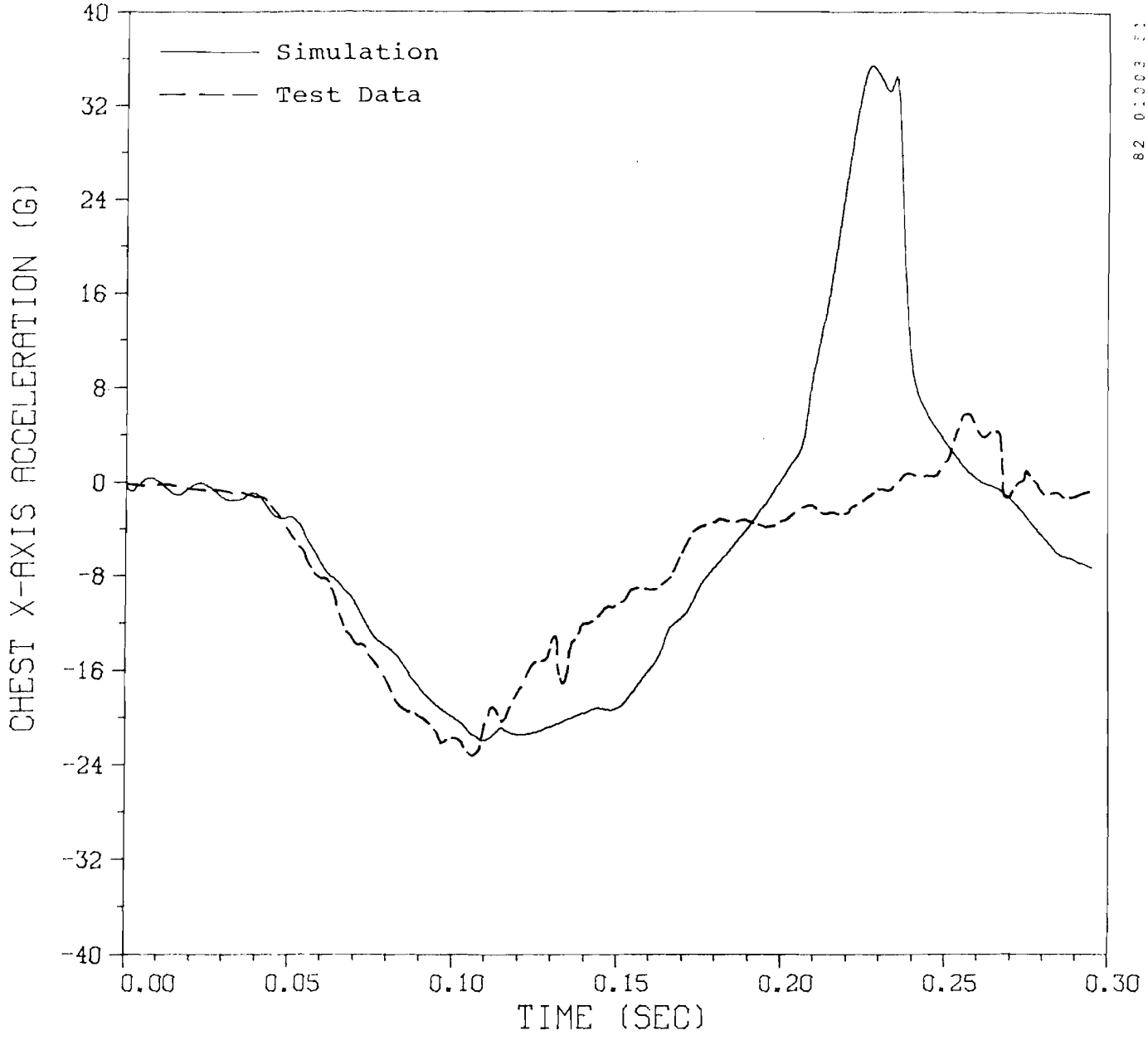

Figure 79. General aviation seat Test A81-111, dummy chest x-acceleration (initial finite element model).

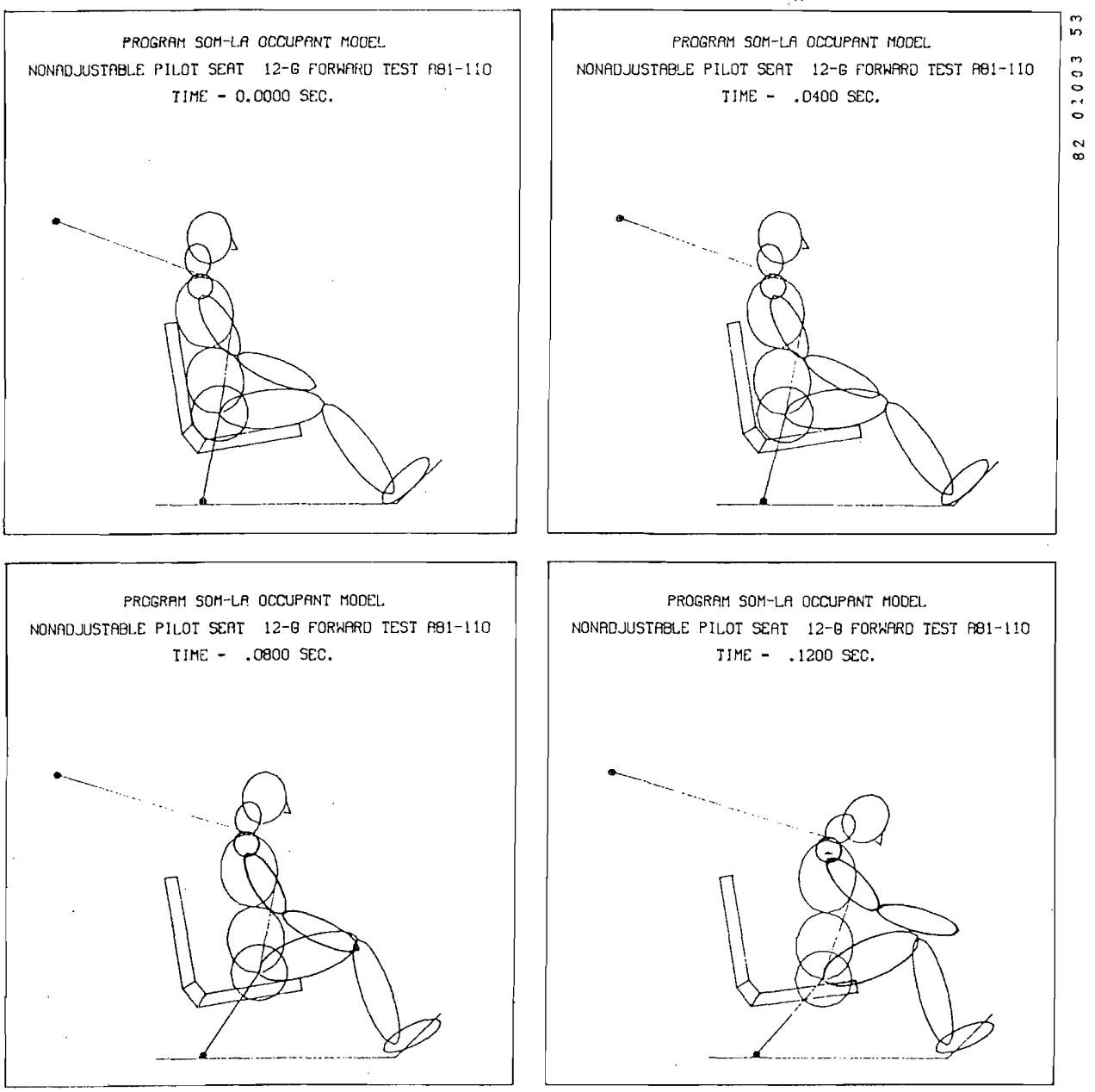

Figure 80. General aviation seat Test A81-110, predicted occupant position (initial finite element model).

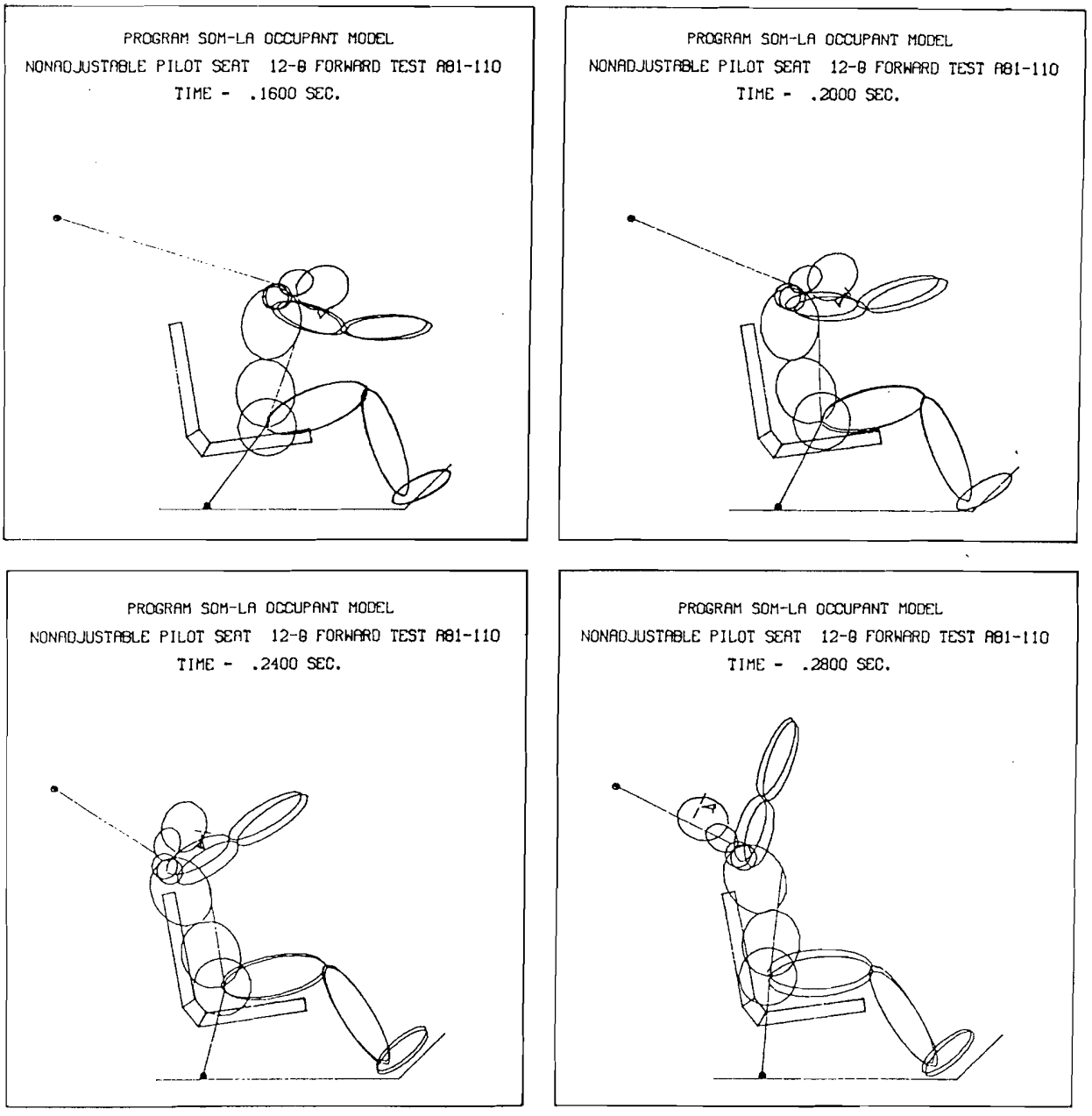

Figure 80 (contd). General aviation seat Test A81-110, predicted occupant position (initial finite element model).

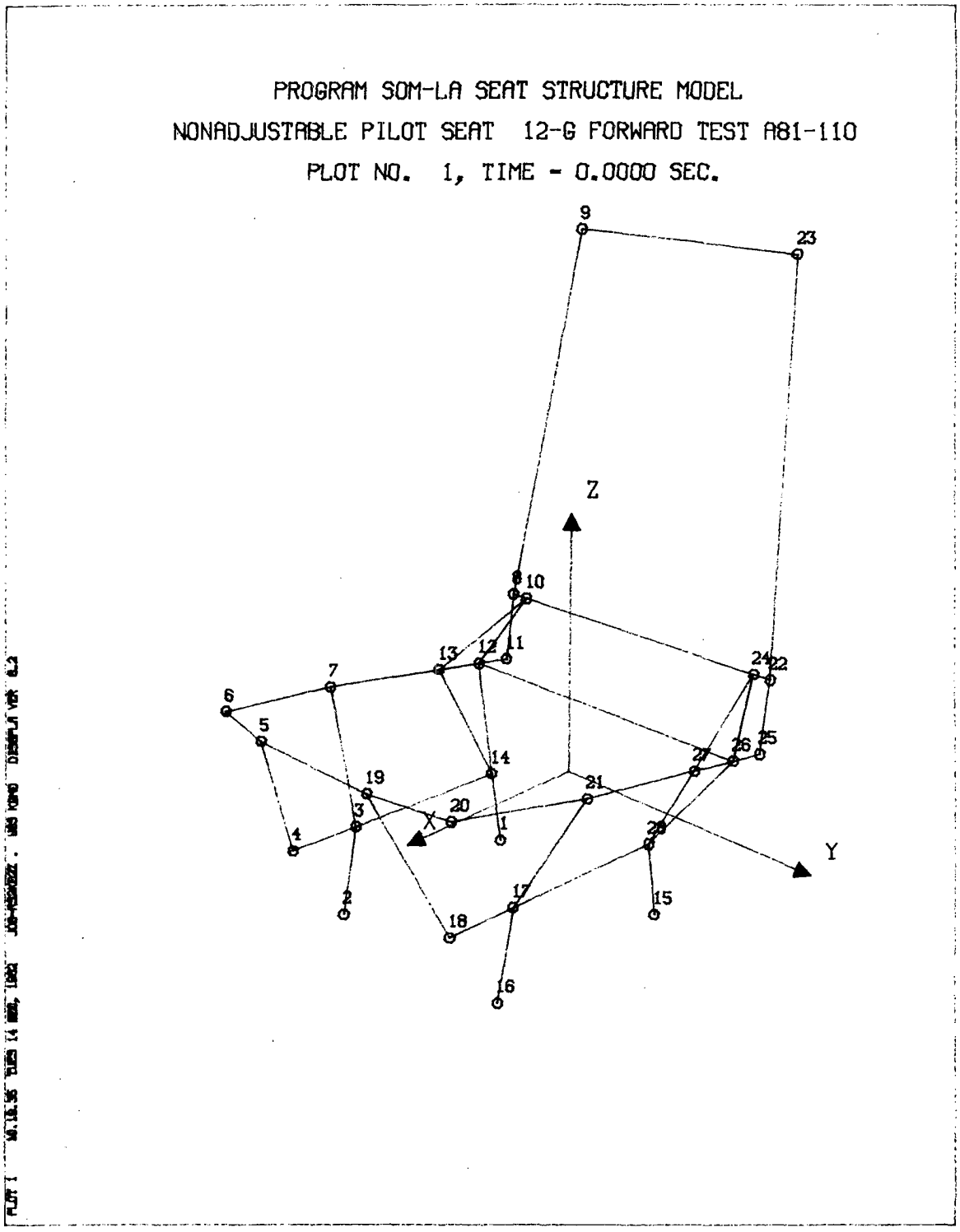

Figure 81. Revised finite element model of general aviation seat.

the seat back latch mechanisms is modeled by nonlinear spring elements that connect nodes 11 to 12 and 25 to 26. A complete listing of the input data is presented in figure 82.

The revisions to the seat model reduced the severity of the occupant's impact with the seat back by permitting deformation of the latches (spring elements). However, at 0.237 sec, after nodes 9 and 23 at the top of the seat back had been pushed more than 5.4 in. rearward, the simulation was halted due to ill conditioning in the seat stiffness matrix. Occupant position just prior to this time can be seen in figure 83, and the seat, in figure 84.

The remaining SOM-LA predictions for test A81-110 (45-degree footrest) are compared with measured data in figures 85 through 100. Footrest forces are included (figures 97 and 98), although the X- and Z- directions for simulation and test do not coincide. SOM-LA assumes the X-direction in the plane of the floor whereas for these tests the load cell was rotated 45 degrees (figure 71). A transformation between the coordinate systems would thus be required for comparison of forces. Lumbar axial force and y-moment measured in the test are included (figure 99 and 100). However, because of the nonsymmetric three-point restraint system, the three-dimensional occupant model was used, and this model does not have the capability for spinal load prediction.

5.5 DISCUSSION

The simulation results presented in this chapter were obtained using identical modeling parameters in all cases. For any single case, performance could be improved by adjustment of certain input parameters, but the standard values as presented in this report (including Volume II) are based on compromises, e.g., between vertical and longitudinal impact configurations.

The most likely parameter for optimizing seat response in a particular case is the buckling coefficient, described in section 3.6.

```
 NONADJUSTABLE PILOT SEAT  12-G FORWARD TEST A81-110        1    1    3
1    0    2    0    1    1    2    1    1    1    8    8.00050.005
    0.        .040       .080       .120       .160       .200       .220       .235
    0.          0.         0.         0.         0.         0.         0.         0.
  20.0       20.0       20.0       20.0       20.0       20.0       20.0       20.0
  45.0       45.0       45.0       45.0       45.0       45.0       45.0       45.0
1   28
1   36
 2048.      .0005      .0005        .10       .001         0.       .250      .0005
 197.2        0.7        .87          2.
 197.2        0.7        .87          2.
2    1    0    0    0    0
  550.       1300.      2250.      .0403      .1048      .1613      0.00         0.
   7.5       -9.50        .5        7.5       9.50         .5      38.0        45.
  550.       1300.      2250.      .0403      .1048      .1613      0.00         0.
  -16.       15.75        46.      13.25         0.
    0.      -0.109      -8.93      -10.9      -11.9      -11.6      -12.4      -12.2
 -10.7       -11.1      -9.29      -11.6      -9.59       3.47      0.952         0.
    0.       .0092      .0262      .0330      .0389      .0420      .0550      .0716
 .0805       .0933      .1000      .1463      .1592      .1688      .1750      .2180
```

```
   50.          0.         0.         0.         0.         0.
3    0         .25        .25
164.38       69.1       -8.4       -8.4         0.       -30.        37.       38.0
 10.85        8.35       11.3       13.3       16.5       18.0
  4.67       6.550      6.330      4.720      6.260      8.350      10.96
 34.60       35.97      10.10       4.85       4.85       21.70      9.49       1.98
  2.32        2.18       .275       .132       .017       .127       .927
  0.76        0.93       .266       .135       .185       1.22       .994       .0177
  2.32        1.70       .233       .022       .195       .873       .505
  4.50        4.50       3.44       1.95       1.85       3.10       2.30       2.30
  1.60        3.56       2.61       1.85       2.34
```

Figure 82. Input data listing for simulation of Test A81-110.

```
   3.70      6.34      0.20      0.20      2.00
   4000.      .500     2000.      0.38
   6000.      .238      1.00     3240.      .270       1.0
   375.0      1.49      150.      375.0     1.49       30.0
   4.67       7.93       9.2       8.4     15.3       15.8       29.2       12.2
28   40    2    4    6    4    2  .50
 1                 250    0    3
 16061-T6 AL
.2588E-4     10.E6     36000.      1.E6      .162     45000.        .3
                       42000.    18750.
 2SPRING
                3500.     350.0     45.0               3000.0
                          500.0     45.0
 4    0      .02078     .00672
  -.211      -.461       .078
   .211      -.461       .078
   .211       .461       .078
  -.211       .461       .078
 1    0

 1              8.0       -5.0        0.
 2             17.9       -5.0        0.
 3             17.0      -5.00       4.16
 4             20.5      -5.00       4.29
 5             23.0       -3.3       10.9
 6             22.1       -7.0      10.76
 7            15.82       -7.9       9.75
 8             4.15       -7.9      11.30
 9             1.50       -6.1       29.2
10             4.15       -7.0       11.3
11             4.67       -7.9       7.93
12             6.57       -7.9       8.24
13             9.22       -7.9       8.68
14             8.57      -5.00       3.87
15              8.0        5.0        0.
16             17.9        5.0        0.
17             17.0       5.00       4.16
18             20.5       5.00       4.29
19             23.0        3.3       10.9
20             22.1        7.0      10.76
21            15.82        7.9       9.75
22             4.15        7.9      11.30
23             1.50        6.1       29.2
24             4.15        7.0       11.3
25             4.67        7.9       7.93
26             6.57        7.9       8.24
27             9.22        7.9       8.68
28             8.57       5.00       3.87
29             8.57         0.       3.87
30             17.0         0.       4.16
31             23.0         0.       10.9
32             4.67         0.       7.93
```

Figure 82 (contd). Input data listing for simulation of Test A81-110.

```
 1    1   14                        1   29    2    1
 2    2    3                        1   30    2    1
 3   14    3                        1   29    2    1
 4    3    4                        1   30    2    1
 5    4    5                        1   31    2    1
 6    5    6                        1   31    2    1
 7    6    7                        1   31    2    1
 8    7   13                        1   31    2    1
 9   12   13                        1   32    2    1
10    3    7                        1   30    2    1
11   14   13                        1   29    2    1
12   14   12                        1   29    2    1
13    8   10          500001001     1   32    2    1
14    8   11                        1   32    2    1
15    9    8                        1   32    2    1
16   15   28                        1   29    2    1
17   16   17                        1   30    2    1
18   28   17                        1   29    2    1
19   17   18                        1   30    2    1
20   18   19                        1   31    2    1
21   19   20                        1   31    2    1
22   20   21                        1   31    2    1
23   21   27                        1   31    2    1
24   26   27                        1   32    2    1
25   17   21                        1   30    2    1
26   28   27                        1   29    2    1
27   28   26                        1   29    2    1
28   22   24          500001001     1   32    2    1
29   22   25                        1   32    2    1
30   23   22                        1   32    2    1
31    5   19                        1   32    2    1
32   12   26                        1   31    2    1
33    9   23                        1   32    2    1
34   10   24                        1   32    2    1
35   12   10                        1   32    2    1
36   26   24                        1   32    2    1
37   11   12                        2   32    3    2
38   25   26                        2   32    3    2
39   10   12   13                   1    0    1    1
40   24   26   27                   1    0    1    1
12   26    5   19
10   24    9   23

1111101
2111101
15111101
16111101
```

Figure 82 (contd). Input data listing for simulation of Test A81-110.

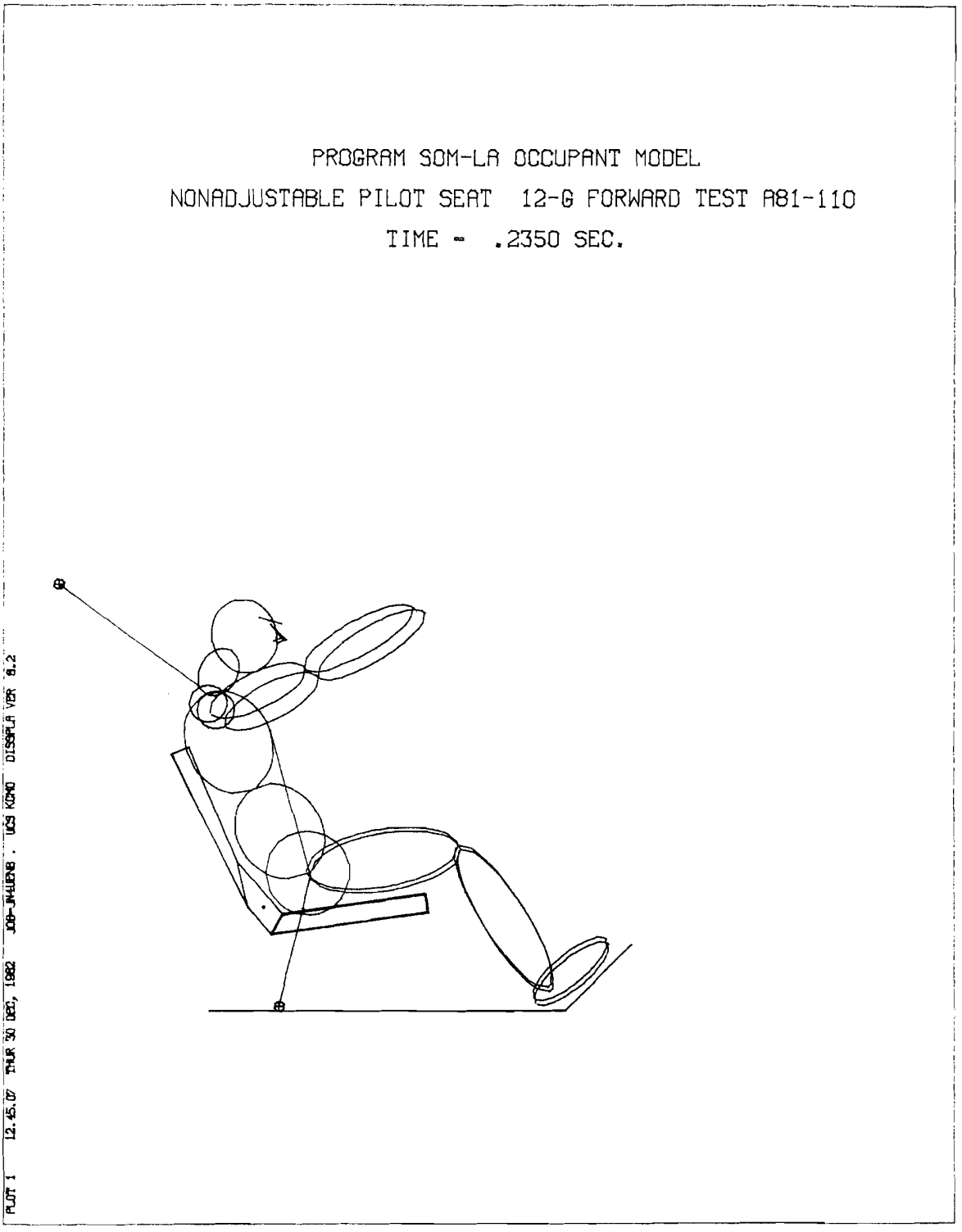

Figure 83. General aviation seat Test A81-110, predicted occupant position at t = 0.235 sec (revised finite element model).

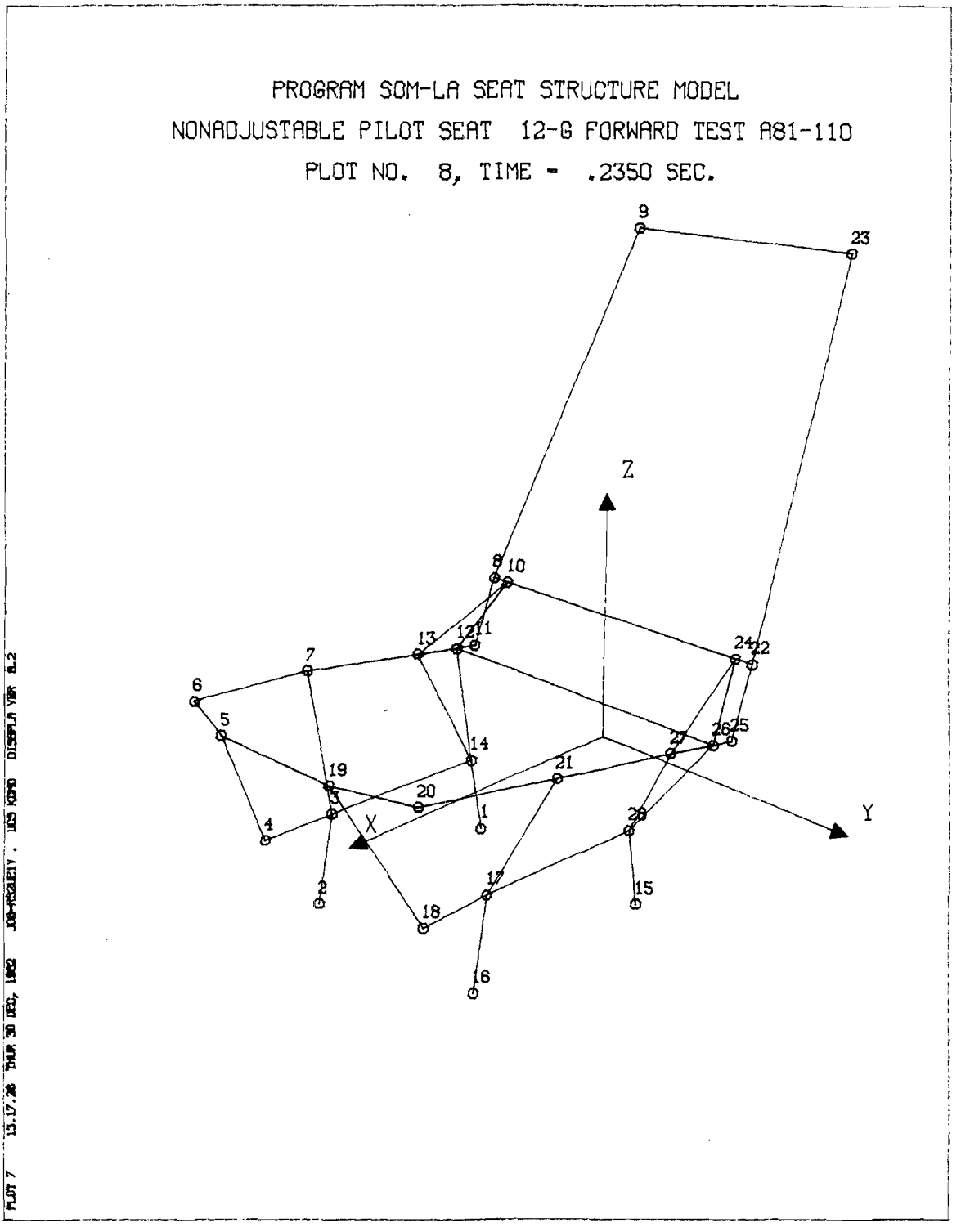

Figure 84. General aviation seat Test A81-110, predicted seat position at t = 0.235 sec (revised finite element model).

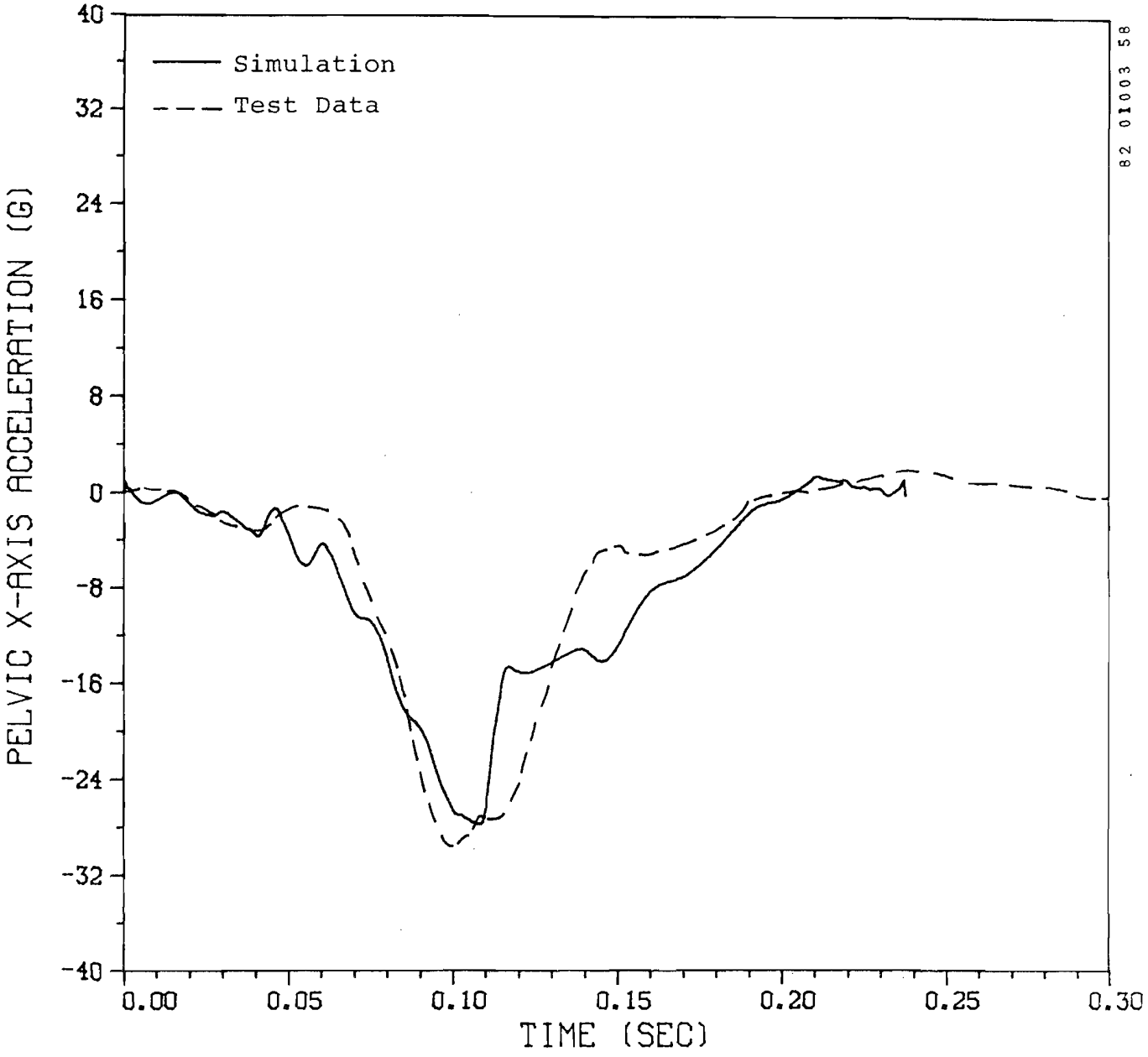

Figure 85. General aviation seat Test A81-110, pelvis x-acceleration.

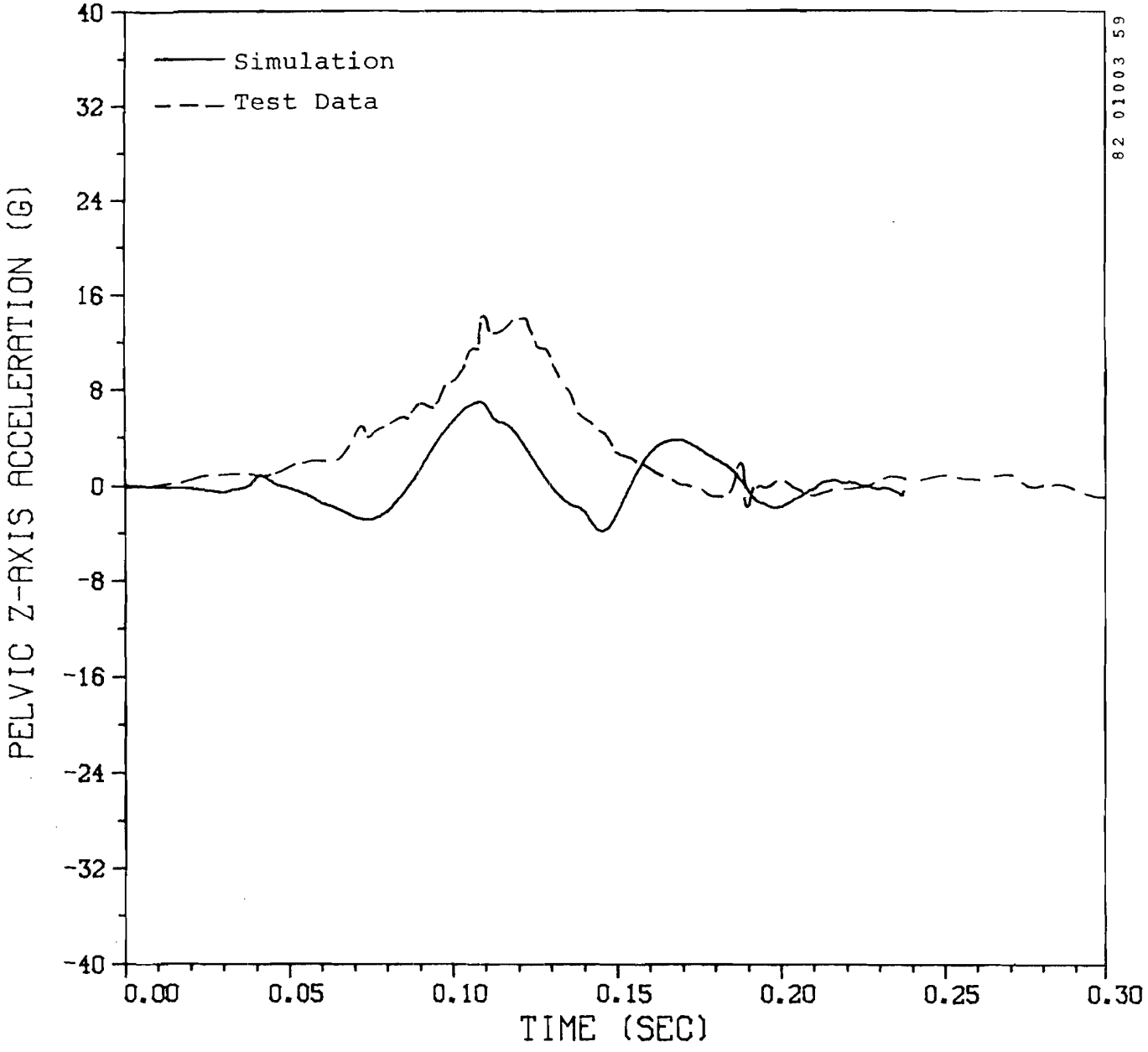

Figure 86. General aviation seat Test A81-110, pelvis z-acceleration.

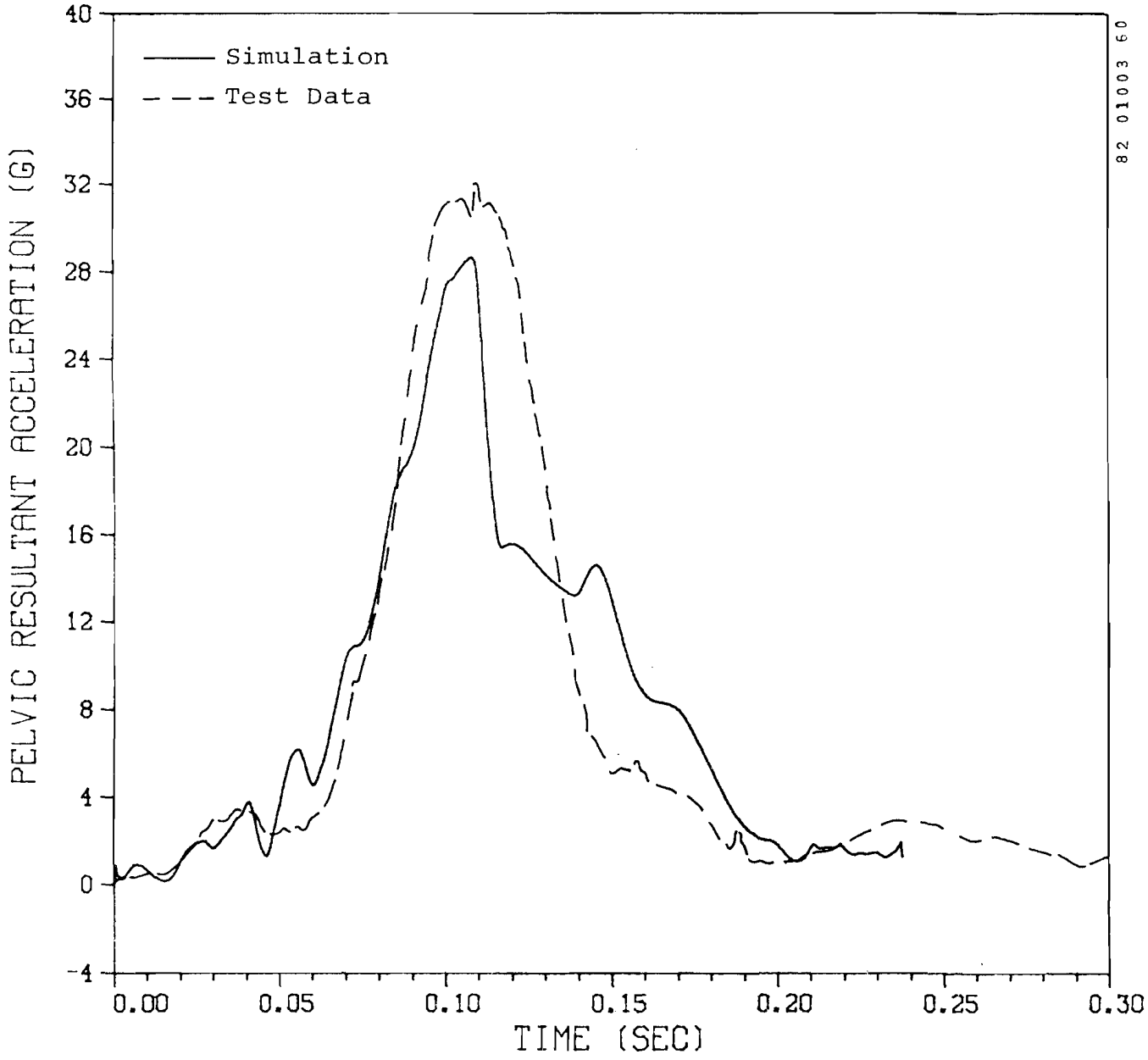

Figure 87. General aviation seat Test A81-110, pelvis resultant acceleration.

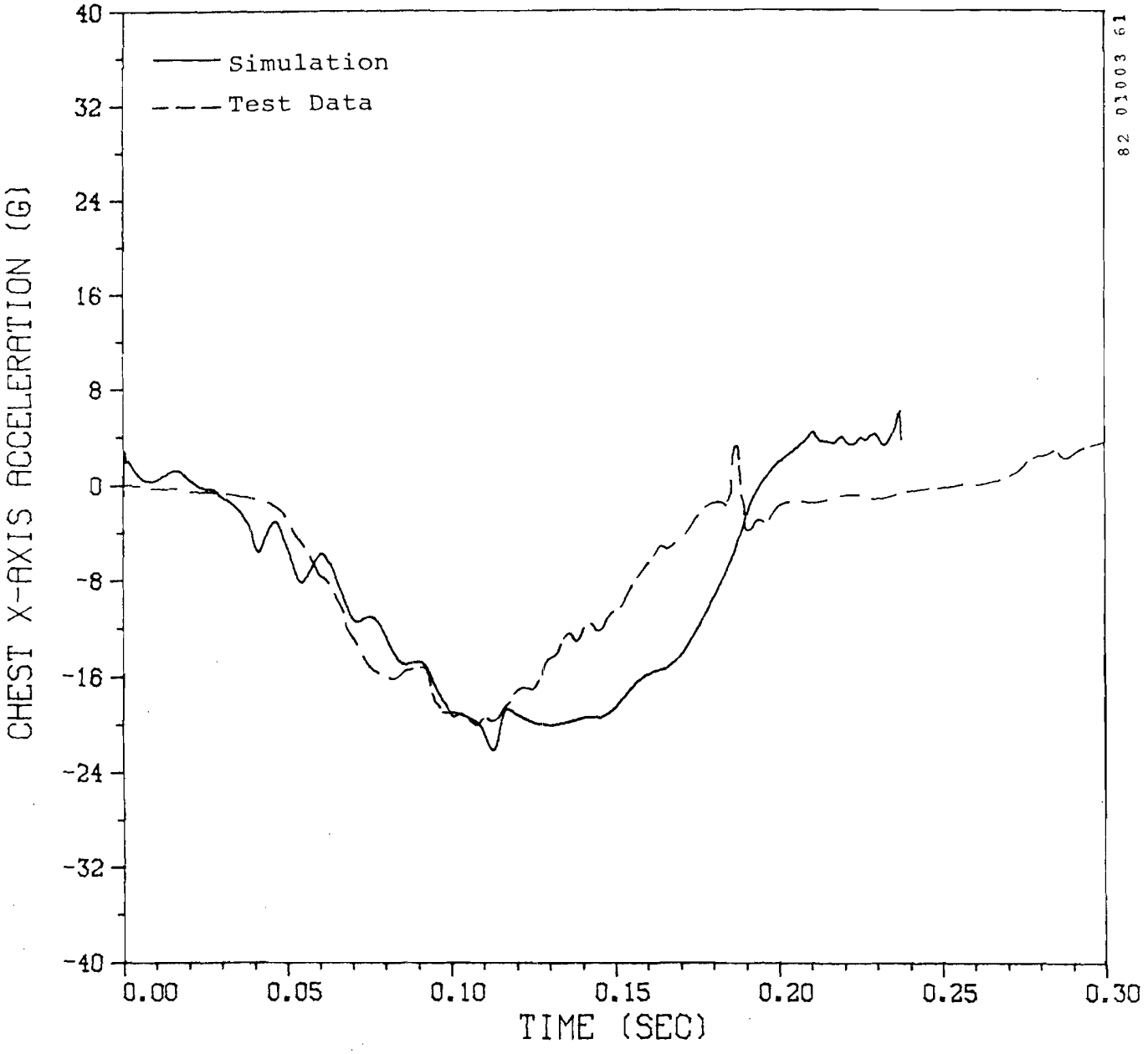

Figure 88. General aviation seat Test A81-110, chest x-acceleration.

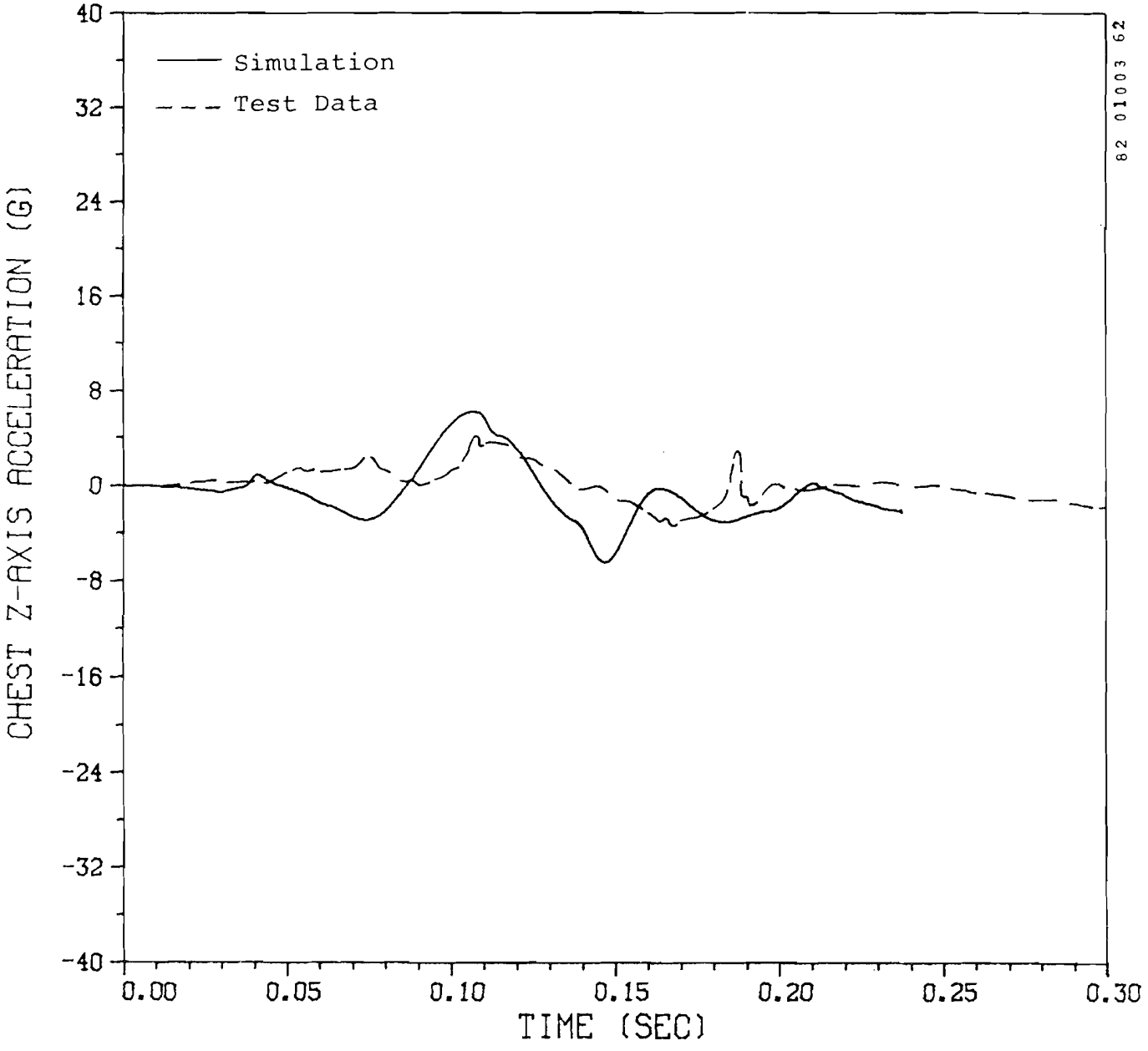

Figure 89. General aviation seat Test A81-110, chest z-acceleration.

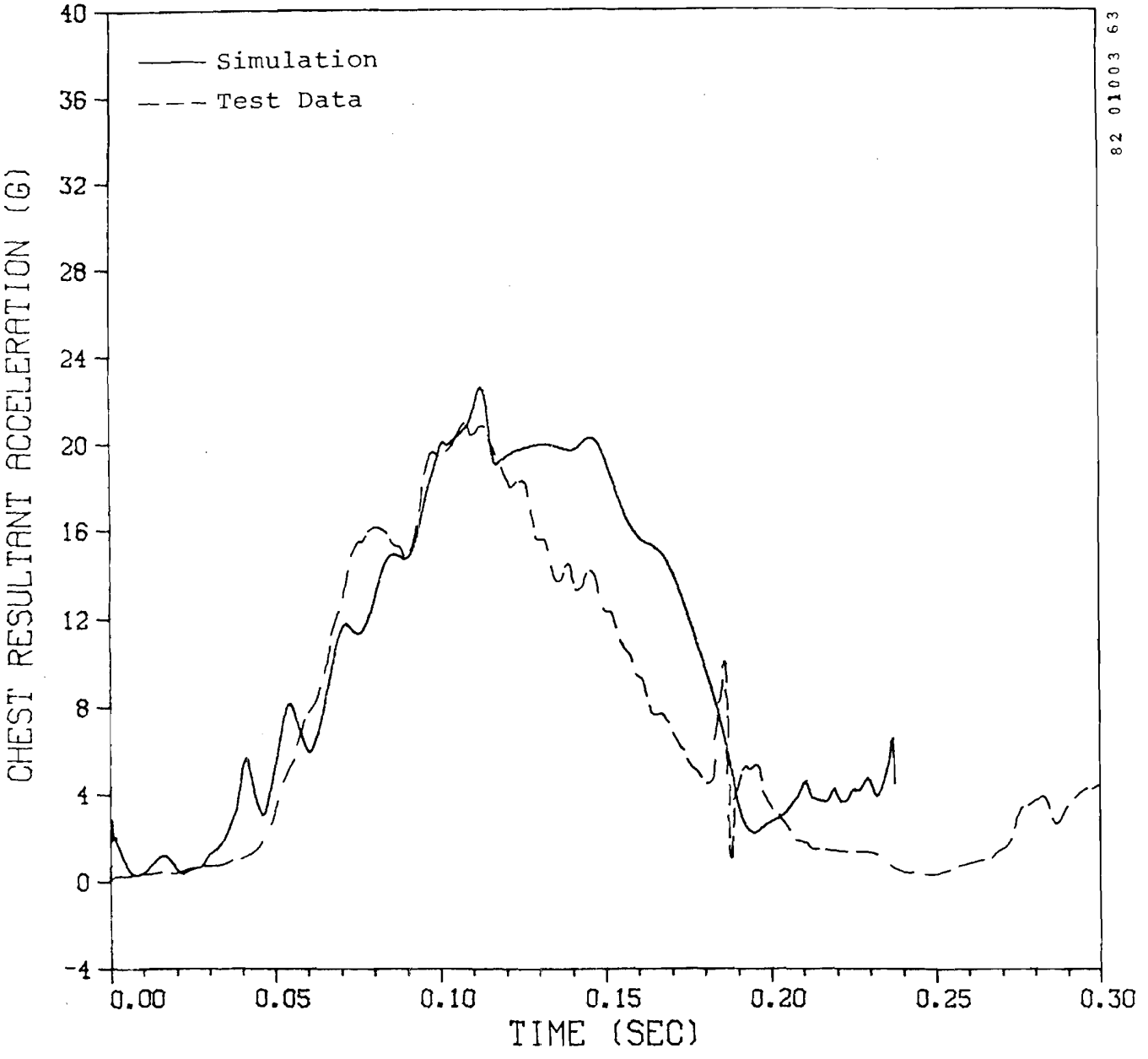

Figure 90. General aviation seat Test A81-110, chest resultant acceleration.

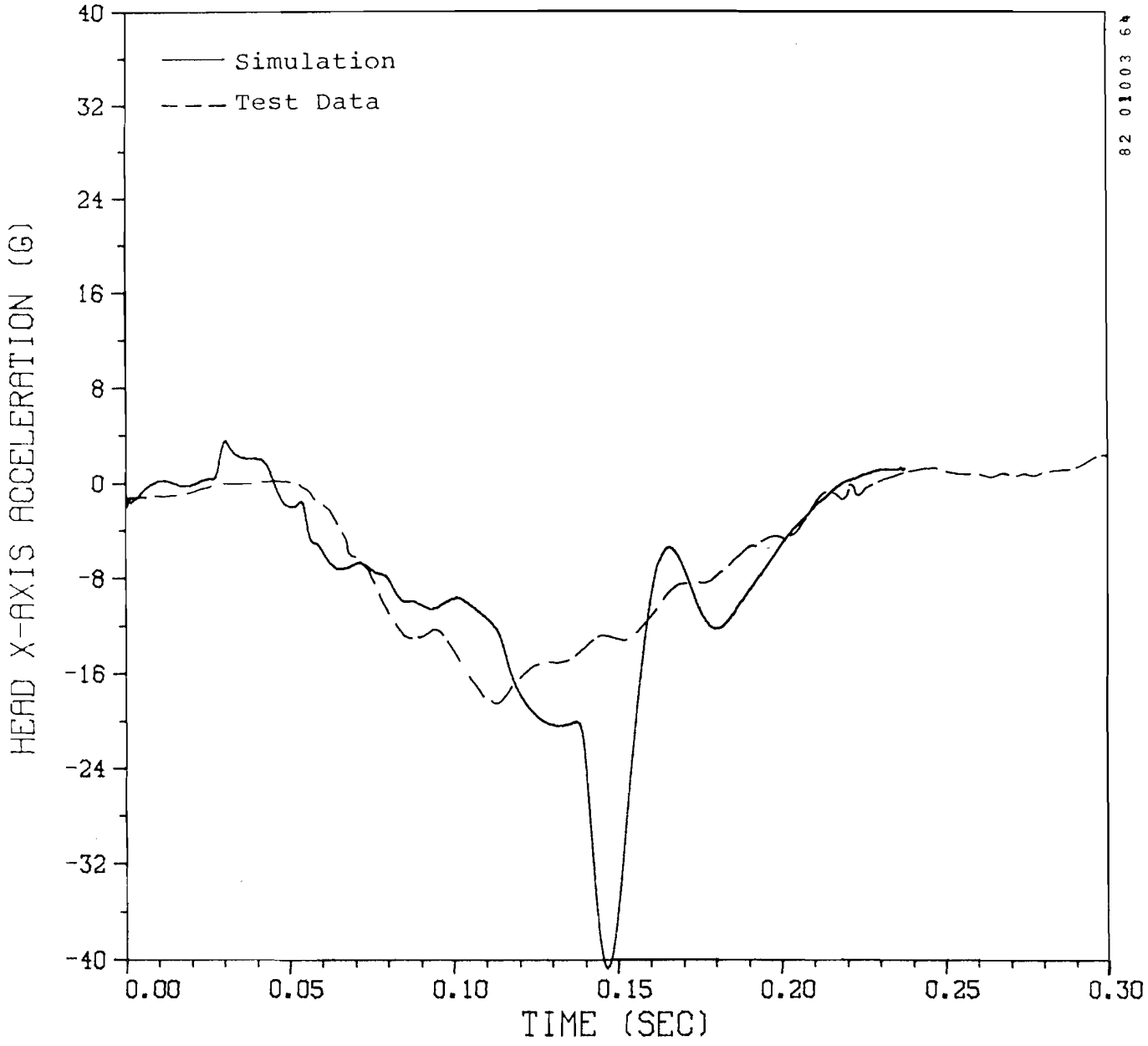

Figure 91. General aviation seat Test A81-110, head x-acceleration.

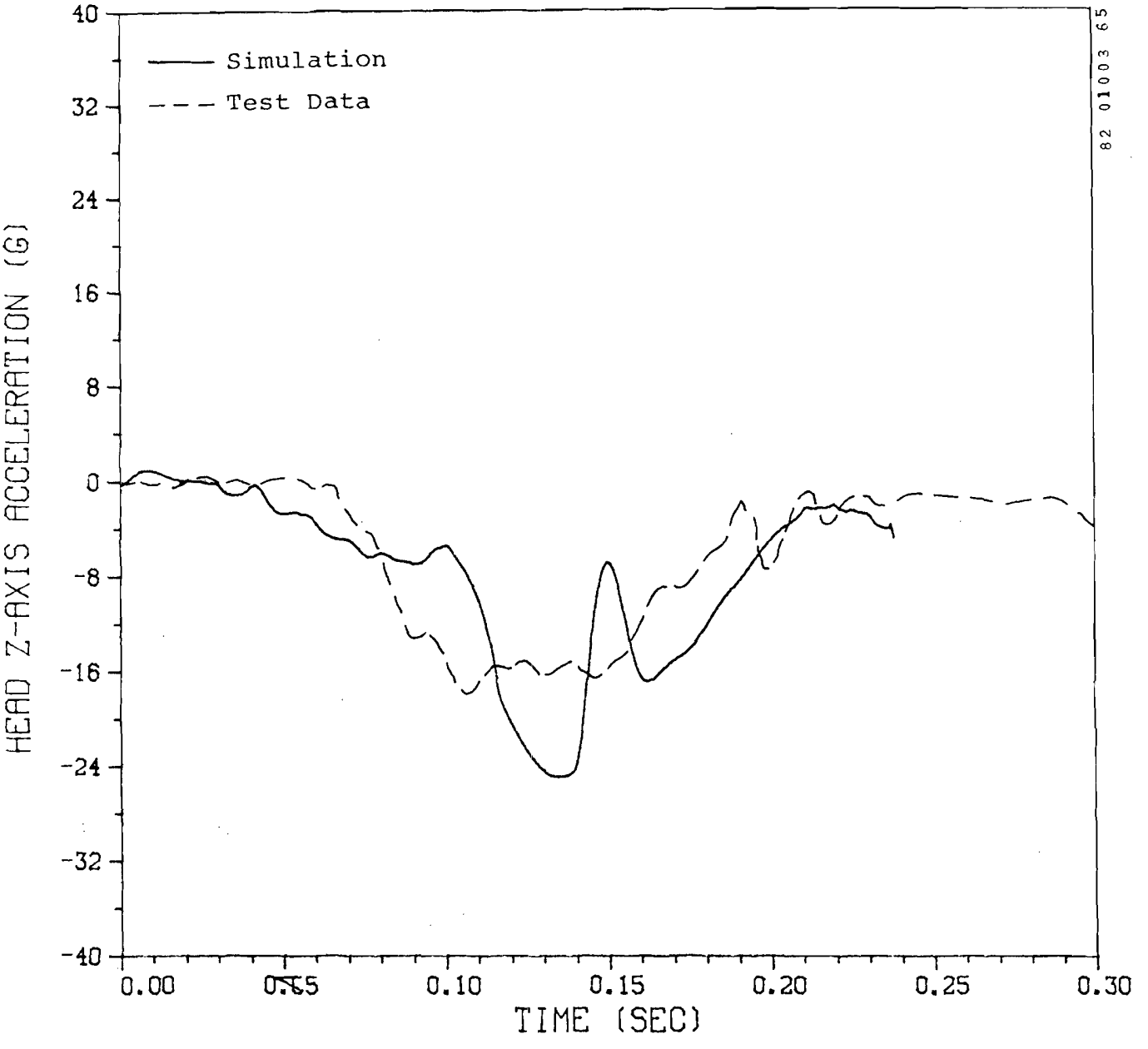

Figure 92. General aviation seat Test A81-110, head z-acceleration.

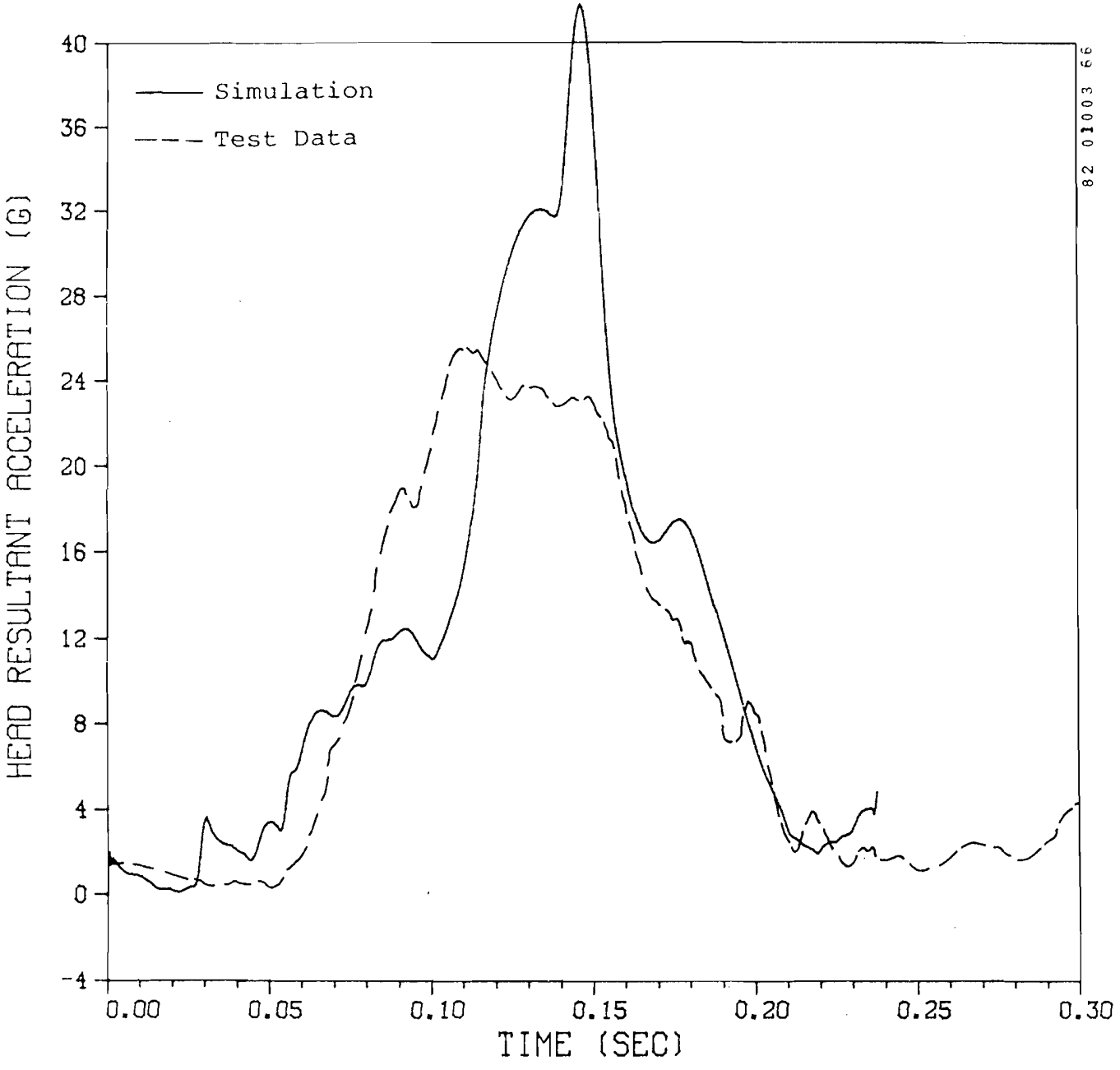

Figure 93. General aviation seat Test A81-110, head resultant acceleration.

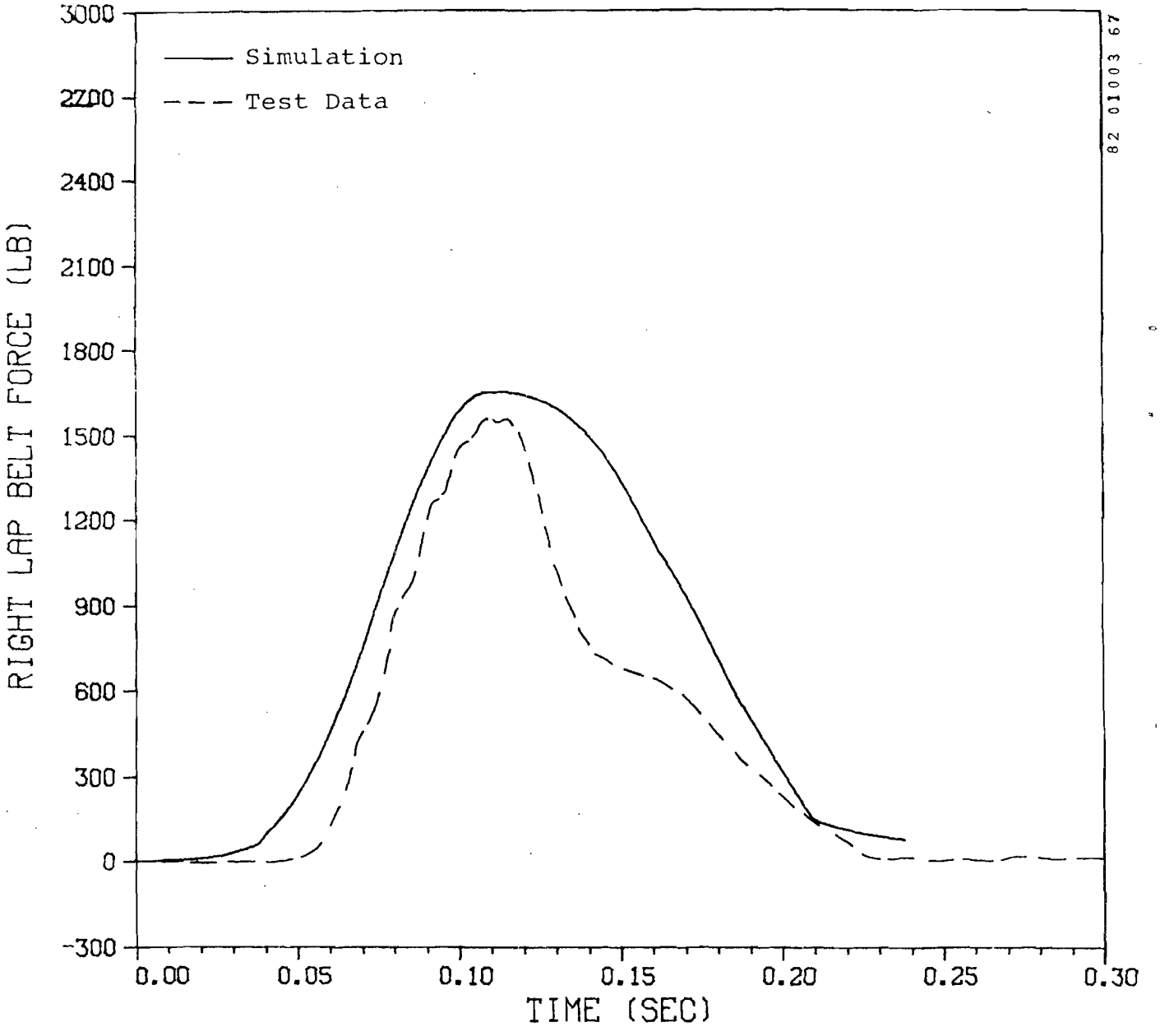

Figure 94. General aviation seat Test A81-110, right lap belt force.

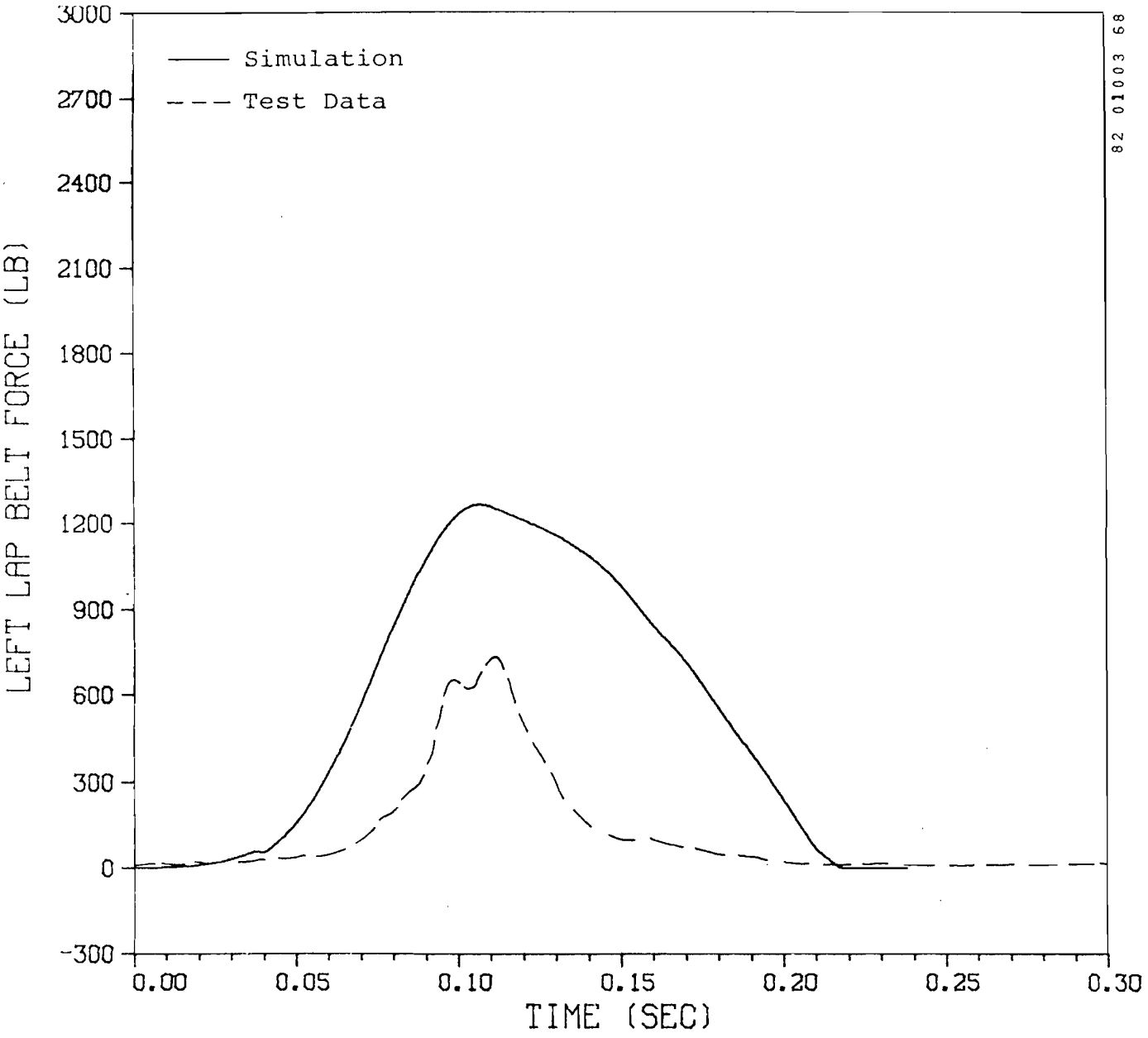

Figure 95. General aviation seat Test A81-110, left lap belt force.

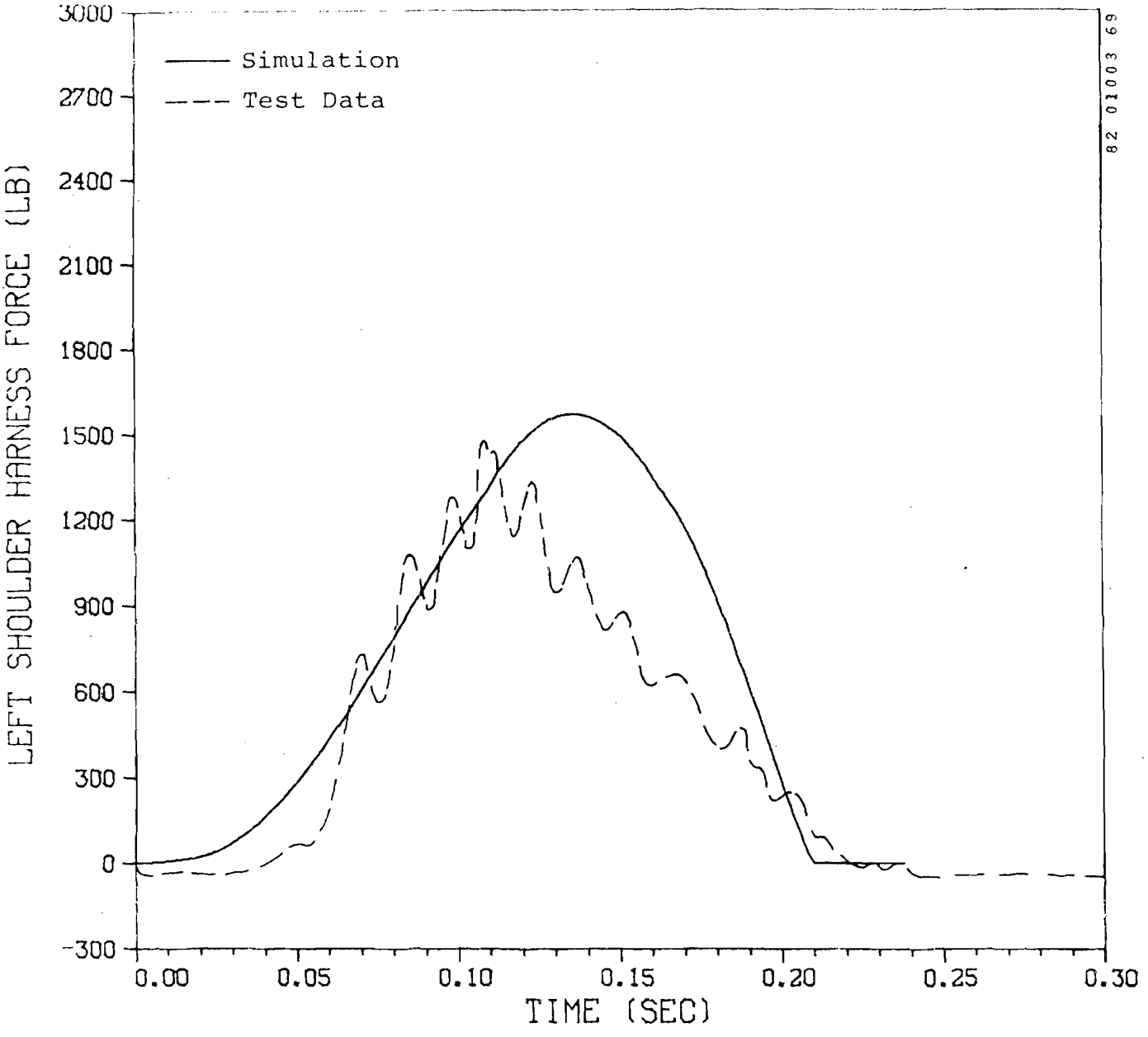

Figure 96. General aviation seat Test A81-110, shoulder belt force.

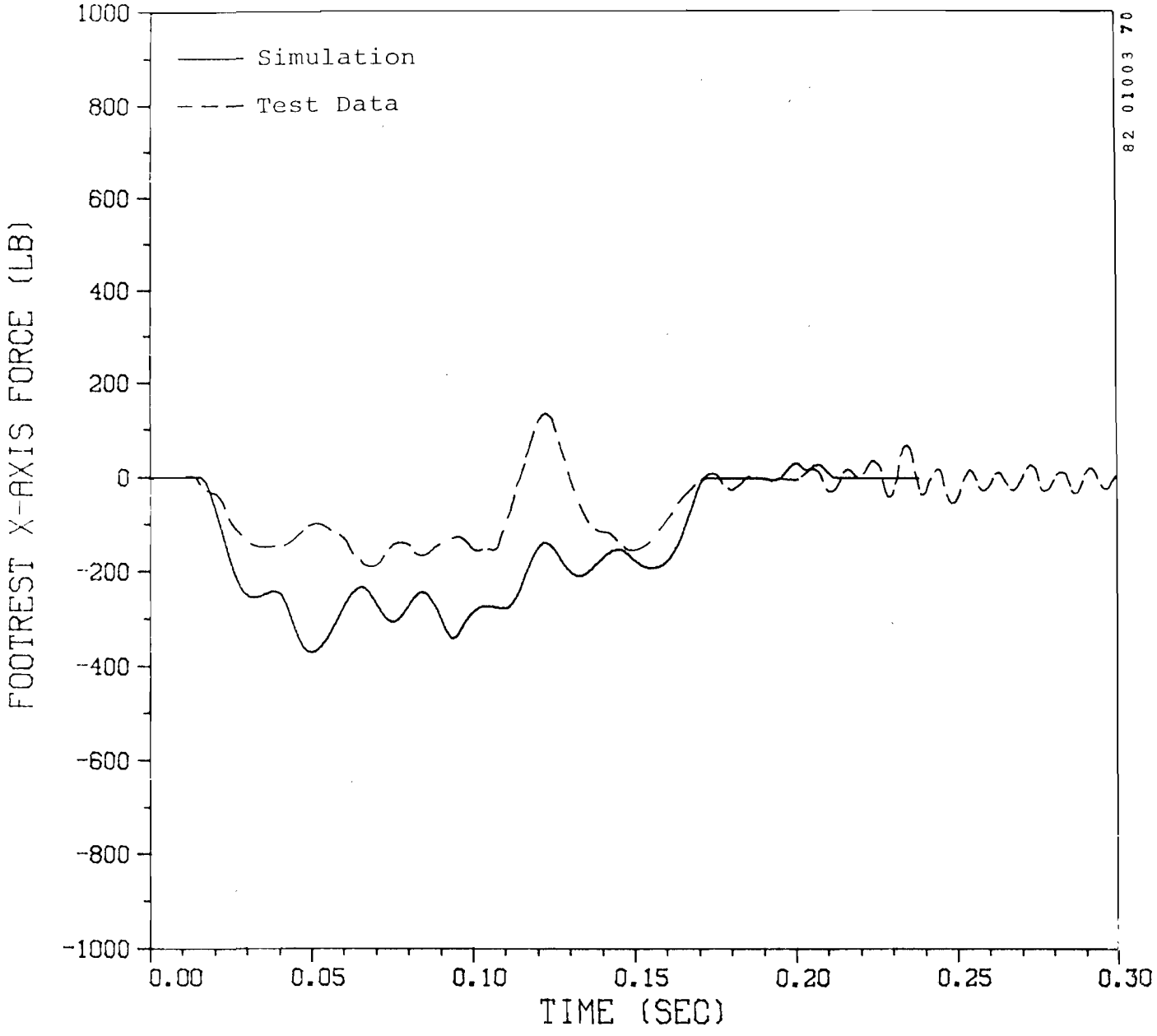

Figure 97. General aviation seat Test A81-110, footrest X-force.

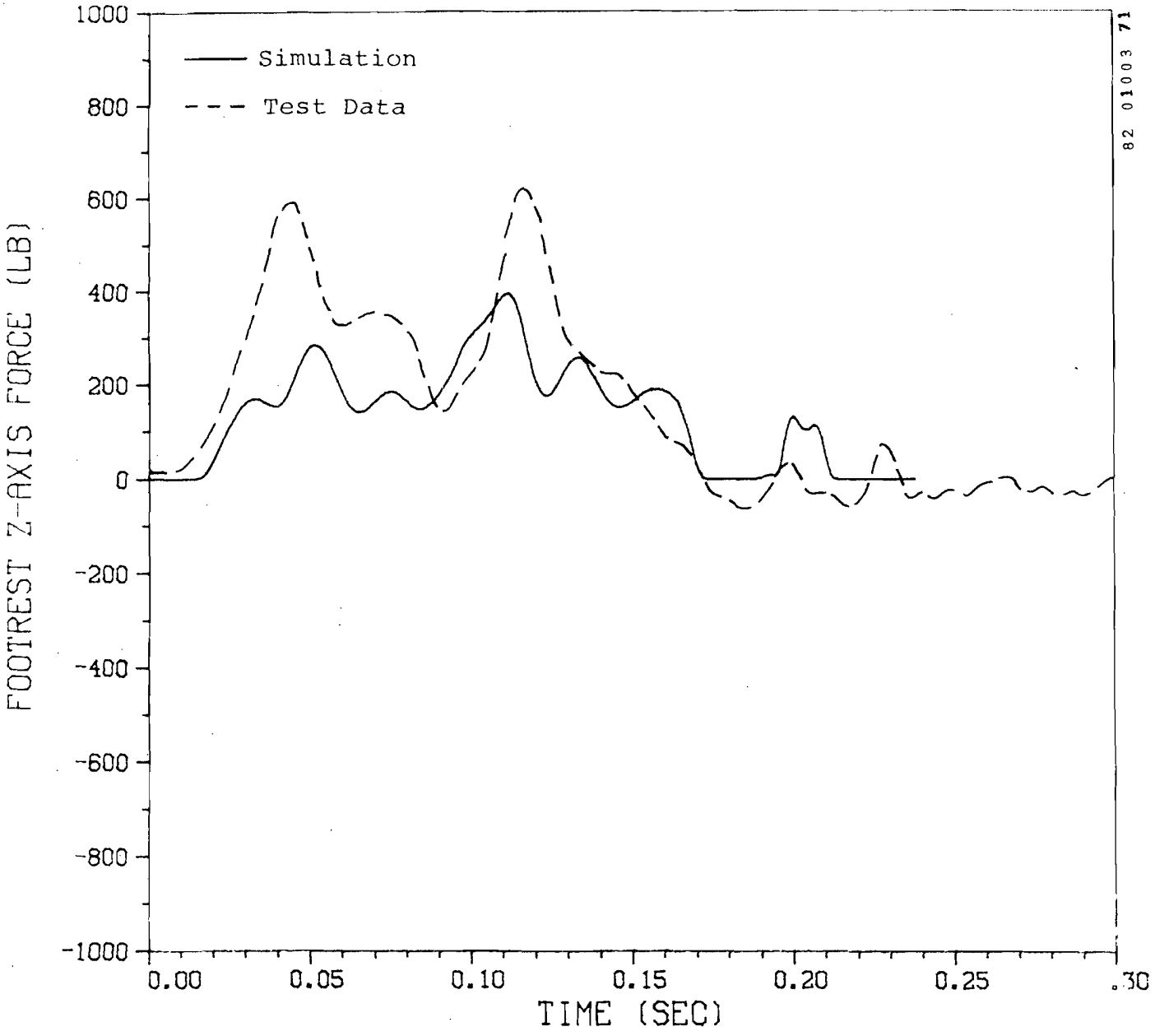

Figure 98. General aviation seat Test A81-110, footrest Z-force.

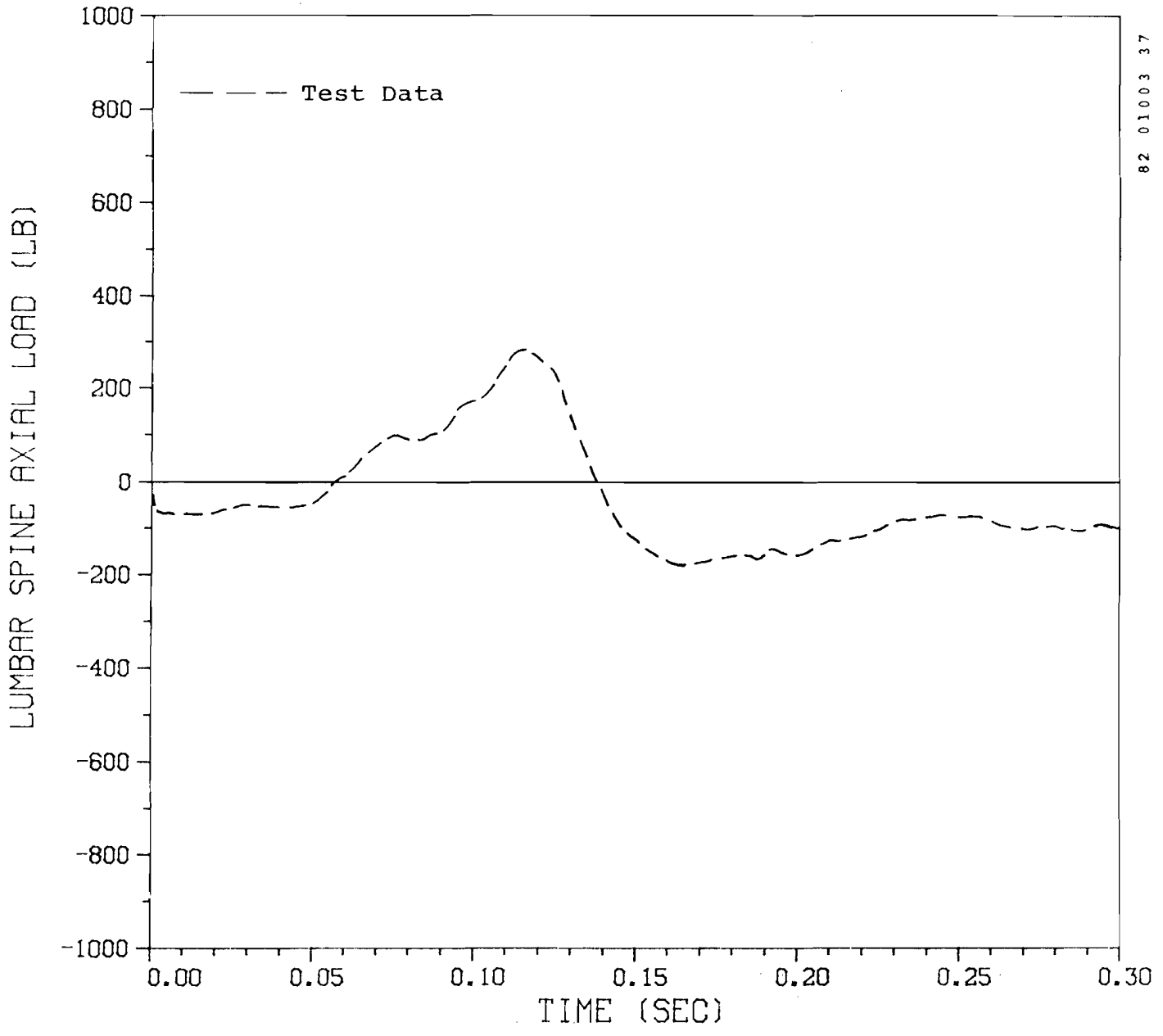

Figure 99. General aviation seat Test A81-110, lumbar axial force.

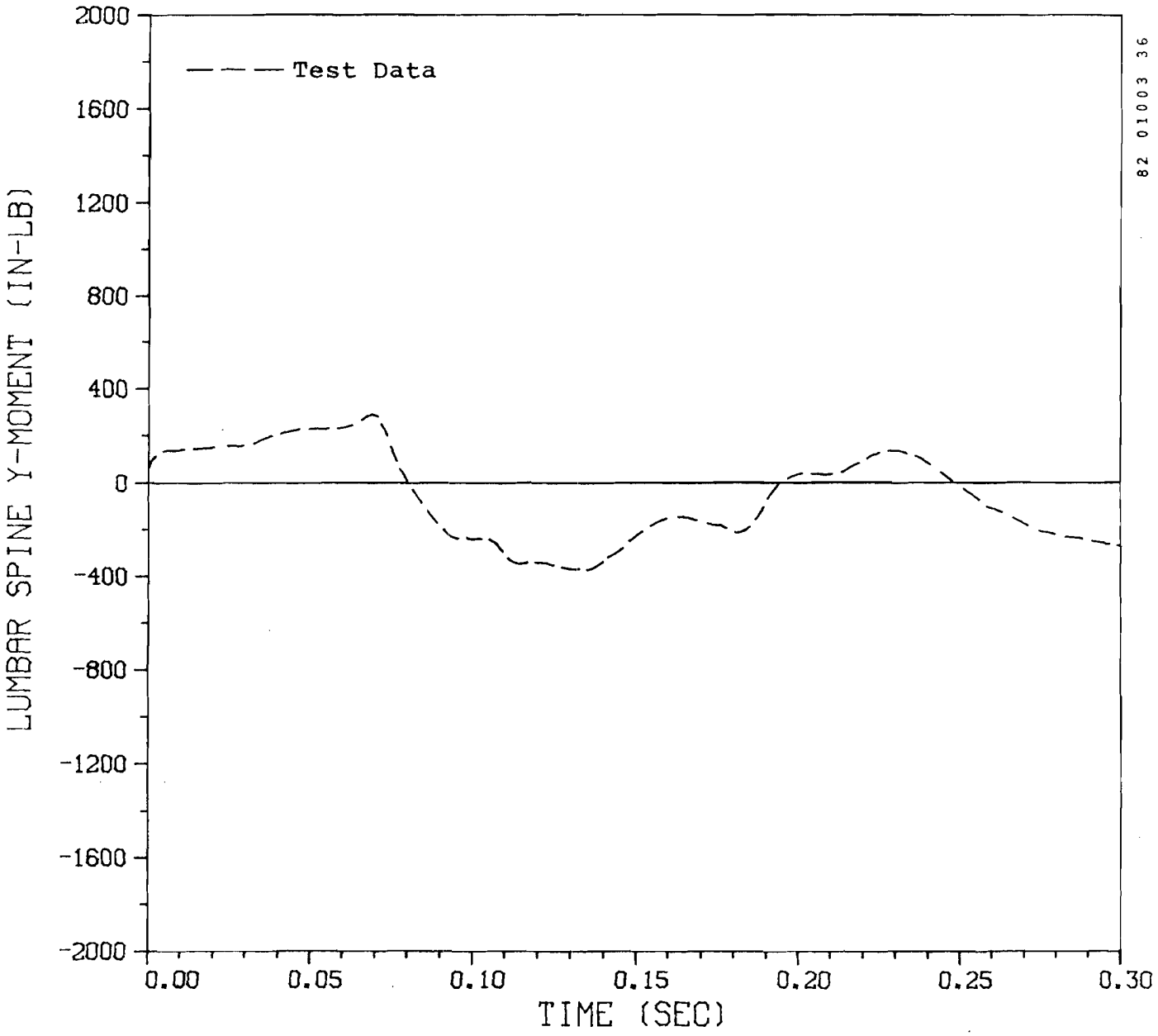

Figure 100. General aviation seat Test A81-110, lumbar y-moment.

The value of 0.5, which has a rational basis, produced seat displacement in the low-deceleration case which was within the envelope of the test data (figure 41). For the higher-deceleration case, the predicted seat displacement was low (figure 48), but could be increased by increasing the coefficient. However, another reason for the reduced seat displacement could be the model's ignoring seat inertia. In this case the seat weight was more than 50 lb, so that its contribution to the displacement measured in the test may have been significant. However, general aviation seats are expected to weigh considerably less, so that this discrepancy should be reduced in simulation of actual seat systems.

Occupant parameters which might be adjusted to improve simulation of one particular type of test configuration, such as longitudinal impacts, are the chest and abdominal compliance parameters, which are used to effectively soften the input belt characteristics. Also, if head response is of particular interest, the neck damping coefficients can be adjusted to achieve optimum response.

6.0 CONCLUSIONS

The Seat/Occupant Model - Light Aircraft (Program SOM-LA) provides a method for analyzing the performance of a seat and occupant in an aircraft crash environment. For preliminary analyses of cabin configuration or restraint system design where details of the seat structure are not known, a rigid seat can be used. Otherwise, finite element modeling capability is available for the seat structure.

Modeling parameters have been based on a compromise among various impact configurations and seat types. If a user were to desire more rigorous modeling of a particular impact configuration, certain parameters could be adjusted to optimize simulation.

7.0 REFERENCES

1. Laananen, D. H., "Aircraft Crash Survival Design Guide, Volume II, Aircraft Crash Environment and Human Tolerance," Simula Inc.; USARTL Technical Report 79-22B, Applied Technology Laboratory, U.S. Army Research and Technology Laboratories (AVRADCOM), Fort Eustis, Virginia, January 1980.

2. Bartz, J. A., "Development and Validation of a Computer Simulation of a Crash Victim of Three Dimensions," Proceedings of the Sixteenth Stapp Car Crash Conference, Society of Automotive Engineers, New York, 1972, pp. 105-127.

3. Huston, R. L., Hessel, R., and Passerello, C., "A Three-Dimensional Vehicle-Man Model for Collision and High Acceleration Studies," SAE Paper No. 740275, Society of Automotive Engineers, 1974.

4. Robbins, D. H., Bennett, R. O., and Bowman, B. M., "User-Oriented Mathematical Crash Victim Simulator," Proceedings of the Sixteenth Stapp Car Crash Conference, Society of Automotive Engineers, New York, 1972, pp. 128-148.

5. Young, R. D., "A Three-Dimensional Mathematical Model of an Automobile Passenger," Texas Transportation Institute, College Station, Texas, Research Report 140-2, 1970.

6. Laananen, D. H., "Development of a Scientific Basis for Analysis of Aircraft Seating Systems," Dynamic Science, Division of Ultrasystems, Inc.; Report No. FAA-RD-74-130, Federal Aviation Administration, U.S. Department of Transportation, Washington, D.C., 1975, AD-A004306.

7. McConville, J. T., and Laubach, L. L., "Anthropometry," Anthropometric Source Book, Volume I: Anthropometry for Designers, Chapter III, NASA Reference Publication 1024, NASA Science and Technical Information Office, Houston, Texas, July 1978.

8. Chandler, R. F., and Young, J., "Uniform Mass Distribution Properties and Body Size Appropriate for the 50 Percentile Male Aircrewmember During 1980-1990," Civil Aeromedical Institute, Protection and Survival Laboratory, Memorandum Report No. AAC-119-81-4 (draft), Federal Aviation Administration, Mike Monroney Aeronautical Center, Oklahoma City, March 1981.

9. Hubbard, R. P., and McLeod, D. G., "Geometric, Inertial and Joint Characteristics of Two Part 572 Dummies for Occupant Modeling," Proceedings of the Twenty-First Stapp Car Crash Conference, SAE P-73, Society of Automotive Engineers, Inc., Warrendale, Pennsylvania, 1977, pp. 933-71.

10. Dempster, W. T., "Space Requirements of the Seated Operator," Wright Air Development Center Technical Report 55-159, Wright-Patterson Air Force Base, Ohio, July 1955.

11. Glanville, A. D., and Kreezer, G. "The Maximum Amplitude and Velocity of Joint Movements in Normal Male Human Adults," Human Biology, Vol. 9, 1937, pp. 197-211.

12. Yeung, K. S., and Welch, R. E., "Refinement of Finite Element Analysis of Automotive Structures Under Crash Loading," IIT Research Institute, Chicago, Illinois, Report No. DOT-HS-803-466, U.S. Department of Transportation, Washington, D.C., October 1977.

13. Meek, J. L., Matrix Structural Analysis, McGraw-Hill, 1971.

14. Hartzman, M., and Hutchinson, J. R., Nonlinear Dynamics of Solids by the Finite Element Method, Computers and Structures, Vol. 2, Pergamon Press, 1972, pp 47-77.

15. Pirotin, S. D., and East, G. H., "Large Deflection, Elastic-Plastic Response of Piping: Experiment, Analysis and Application," Paper F3/1, 4th SMIRT Conference, San Francisco, California, August 1977.

16. Spunt, L., Optimum Structural Design, Prentice-Hall, 1971.

17. Gadd, C. W., "Criteria for Injury Potential," Impact Acceleration Stress, Publication 977, NAS-NRC, 1962. pp. 141-45.

18. Gadd, C. W., "Use of a Weighted-Impulse Criterion for Estimating Injury Hazard," Proceedings of the Tenth Stapp Car Crash Conference, Society of Automotive Engineers, New York, 1966.

19. Gadd, C. W., "Tolerable Severity Index in Whole-Head Nonmechanical Impact," Proceedings of the Fifteenth Stapp Car Crash Conference, Society of Automotive Engineers, New York, 1971.

20. Mertz, H. J., and Patrick, L. M., "Strength and Response of the Human Neck," Proceedings of the Fifteenth Stapp Car Crash Conference, Society of Automotive Engineers, New York, 1971, pp. 207-55.

21. Mertz, H. J., and Patrick, L. M., "Investigation of the Kinematics and Kinetics of Whiplash," Proceedings of the Eleventh Stapp Car Crash Conference, Society of Automotive Engieers, New York, 1967.

22. Brinkley, J. W., "Development of Aerospace Escape Systems," Air University Review, Vol. XIX, July-August 1968, pp. 34-49.

23. Massing, D. E., Naab, K. N., and Yates, P. E., "Performance Evaluation of New Generation 50th Percentile Anthropomorphic Test Devices: Volume I - Technical Report," Calspan Corporation, Buffalo, New York, Report No. DOT-HS-801-431, U.S. Department of Transportation, Washington, D.C., March 1975.

24. Massing, D. E., Naab, K. N., and Yates, P. E., "Performance Evaluation of New Generation 50th Percentile Anthropomorphic Test Devices: Volume II - Accelerator Sled Test Data," Calspan Corporation, Buffalo, New York, Report No. DOT-HS-801-432, U.S. Department of Transportation, Washington, D.C., March 1975.

25. Desjardins, S. P., Coltman, J. W., and Laananen, D. H., "Development of Improved Criteria for Energy-Absorbing Aircraft Seats," in Impact Injury: Mechanisms, Prevention, and Cost, Advisory Group for Aerospace Research and Development, North Atlantic Treaty Organization, Neuilly sur Seines, France, April 1982.

26. Desjardins, S. P., et al., "Crashworthy Armored Crewseat for the UH-60A Black Hawk," paper presented at 35th Annual National Forum of the American Helicopter Society, American Helicopter Society, Washington, D.C., May 1979.

27. Chandler, R. F., and Laananen, D. H., "Seat/Occupant Crash Dynamic Analysis Verification Test Program," Paper No. 790590, presented at Business Aircraft Meeting, Society of Automotive Engineers, Inc., Wichita, Kansas, April 1979.

APPENDIX A

OCCUPANT SEGMENT POSITION: THREE-DIMENSIONAL MODEL

Referring to figure A-1, and using $\bar{\rho}_n = L_n - \rho_n$ the absolute position of the mass center of each body segment is given below. The elements of the transformation matrices $[T^n]$ are functions of the generalized coordinates, as given by equations (6), (9), and (10).

Segment 1:

(X_1, Y_1, Z_1), the coordinates of the reference point on the body are the generalized coordinates (q_1, q_2, q_3).

Segment 2:

$$\begin{Bmatrix} X_2 \\ Y_2 \\ Z_2 \end{Bmatrix} = \begin{Bmatrix} X_1 \\ Y_1 \\ Z_1 \end{Bmatrix} + \begin{bmatrix} T^1 \end{bmatrix} \begin{Bmatrix} 0 \\ 0 \\ \bar{\rho}_1 \end{Bmatrix} + \begin{bmatrix} T^2 \end{bmatrix} \begin{Bmatrix} 0 \\ 0 \\ \rho_2 \end{Bmatrix}$$

Segment 3:

$$\begin{Bmatrix} X_3 \\ Y_3 \\ Z_3 \end{Bmatrix} = \begin{Bmatrix} X_1 \\ Y_1 \\ Z_1 \end{Bmatrix} + \begin{bmatrix} T^1 \end{bmatrix} \begin{Bmatrix} 0 \\ 0 \\ \bar{\rho}_1 \end{Bmatrix} + \begin{bmatrix} T^2 \end{bmatrix} \begin{Bmatrix} 0 \\ 0 \\ L_2 \end{Bmatrix} + \begin{bmatrix} T^{12} \end{bmatrix} \begin{Bmatrix} 0 \\ 0 \\ L_{12} \end{Bmatrix} + \begin{bmatrix} T^3 \end{bmatrix} \begin{Bmatrix} e_3 \\ 0 \\ \rho_3 \end{Bmatrix}$$

Segment 4:

$$\begin{Bmatrix} X_4 \\ Y_4 \\ Z_4 \end{Bmatrix} = \begin{Bmatrix} X_1 \\ Y_1 \\ Z_1 \end{Bmatrix} + \begin{bmatrix} T^1 \end{bmatrix} \begin{Bmatrix} 0 \\ 0 \\ \bar{\rho}_1 \end{Bmatrix} + \begin{bmatrix} T^2 \end{bmatrix} \begin{Bmatrix} 0 \\ -L_S \\ L_2 \end{Bmatrix} + \begin{bmatrix} T^4 \end{bmatrix} \begin{Bmatrix} 0 \\ 0 \\ -\rho_4 \end{Bmatrix}$$

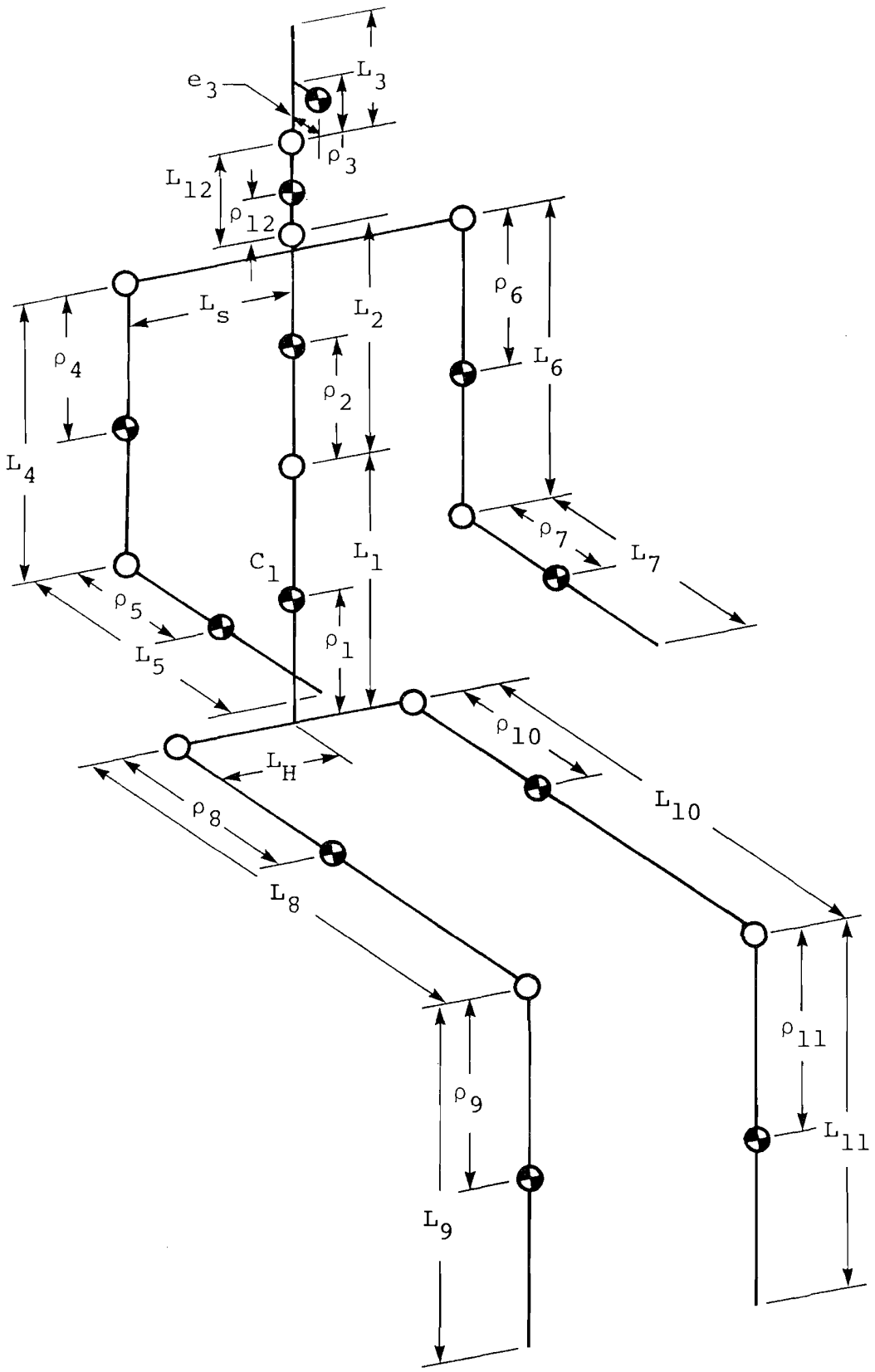

Figure A-1. Body segment lengths and mass center locations for three-dimensional model.

Segment 5:

$$\begin{Bmatrix} X_5 \\ Y_5 \\ Z_5 \end{Bmatrix} = \begin{Bmatrix} X_1 \\ Y_1 \\ Z_1 \end{Bmatrix} + \begin{bmatrix} T^1 \end{bmatrix} \begin{Bmatrix} 0 \\ 0 \\ \bar{\rho}_1 \end{Bmatrix} + \begin{bmatrix} T^2 \end{bmatrix} \begin{Bmatrix} 0 \\ -L_s \\ L_2 \end{Bmatrix} + \begin{bmatrix} T^4 \end{bmatrix} \begin{Bmatrix} 0 \\ 0 \\ -L_4 \end{Bmatrix} + \begin{bmatrix} T^5 \end{bmatrix} \begin{Bmatrix} \rho_5 \\ 0 \\ 0 \end{Bmatrix}$$

Segment 6:

$$\begin{Bmatrix} X_6 \\ Y_6 \\ Z_6 \end{Bmatrix} = \begin{Bmatrix} X_1 \\ Y_1 \\ Z_1 \end{Bmatrix} + \begin{bmatrix} T^1 \end{bmatrix} \begin{Bmatrix} 0 \\ 0 \\ \bar{\rho}_1 \end{Bmatrix} + \begin{bmatrix} T^2 \end{bmatrix} \begin{Bmatrix} 0 \\ -L_s \\ L_2 \end{Bmatrix} + \begin{bmatrix} T^6 \end{bmatrix} \begin{Bmatrix} 0 \\ 0 \\ -\rho_6 \end{Bmatrix}$$

Segment 7:

$$\begin{Bmatrix} X_7 \\ Y_7 \\ Z_7 \end{Bmatrix} = \begin{Bmatrix} X_1 \\ Y_1 \\ Z_1 \end{Bmatrix} + \begin{bmatrix} T^1 \end{bmatrix} \begin{Bmatrix} 0 \\ 0 \\ \bar{\rho}_1 \end{Bmatrix} + \begin{bmatrix} T^2 \end{bmatrix} \begin{Bmatrix} 0 \\ L_s \\ L_2 \end{Bmatrix} + \begin{bmatrix} T^6 \end{bmatrix} \begin{Bmatrix} 0 \\ 0 \\ -L_6 \end{Bmatrix} + \begin{bmatrix} T^7 \end{bmatrix} \begin{Bmatrix} \rho_7 \\ 0 \\ 0 \end{Bmatrix}$$

Segment 8:

$$\begin{Bmatrix} X_8 \\ Y_8 \\ Z_8 \end{Bmatrix} = \begin{Bmatrix} X_1 \\ Y_1 \\ Z_1 \end{Bmatrix} + \begin{bmatrix} T^1 \end{bmatrix} \begin{Bmatrix} 0 \\ -L_H \\ -\rho_1 \end{Bmatrix} + \begin{bmatrix} T^8 \end{bmatrix} \begin{Bmatrix} \rho_8 \\ 0 \\ 0 \end{Bmatrix}$$

Segment 9:

$$\begin{Bmatrix} X_9 \\ Y_9 \\ Z_9 \end{Bmatrix} = \begin{Bmatrix} X_1 \\ Y_1 \\ Z_1 \end{Bmatrix} + \begin{bmatrix} T^1 \end{bmatrix} \begin{Bmatrix} 0 \\ -L_H \\ -\rho_1 \end{Bmatrix} + \begin{bmatrix} T^8 \end{bmatrix} \begin{Bmatrix} L_8 \\ 0 \\ 0 \end{Bmatrix} + \begin{bmatrix} T^9 \end{bmatrix} \begin{Bmatrix} 0 \\ 0 \\ -\rho_9 \end{Bmatrix}$$

Segment 10:

$$\begin{Bmatrix} X_{10} \\ Y_{10} \\ Z_{10} \end{Bmatrix} = \begin{Bmatrix} X_1 \\ Y_1 \\ Z_1 \end{Bmatrix} + \begin{bmatrix} T^1 \end{bmatrix} \begin{Bmatrix} 0 \\ L_H \\ -\rho_1 \end{Bmatrix} + \begin{bmatrix} T^{10} \end{bmatrix} \begin{Bmatrix} \rho_{10} \\ 0 \\ 0 \end{Bmatrix}$$

Segment 11:

$$\begin{Bmatrix} X_{11} \\ Y_{11} \\ Z_{11} \end{Bmatrix} = \begin{Bmatrix} X_1 \\ Y_1 \\ Z_1 \end{Bmatrix} + \begin{bmatrix} T^1 \end{bmatrix} \begin{Bmatrix} 0 \\ L_H \\ -\rho_1 \end{Bmatrix} + \begin{bmatrix} T^{10} \end{bmatrix} \begin{Bmatrix} L_{10} \\ 0 \\ 0 \end{Bmatrix} + \begin{bmatrix} T^{11} \end{bmatrix} \begin{Bmatrix} 0 \\ 0 \\ -\rho_{11} \end{Bmatrix}$$

Segment 12:

$$\begin{Bmatrix} X_{12} \\ Y_{12} \\ Z_{12} \end{Bmatrix} = \begin{Bmatrix} X_1 \\ Y_1 \\ Z_1 \end{Bmatrix} + \begin{bmatrix} T^1 \end{bmatrix} \begin{Bmatrix} 0 \\ 0 \\ \bar{\rho}_1 \end{Bmatrix} + \begin{bmatrix} T^2 \end{bmatrix} \begin{Bmatrix} 0 \\ 0 \\ L_2 \end{Bmatrix} + \begin{bmatrix} T^{12} \end{bmatrix} \begin{Bmatrix} 0 \\ 0 \\ \rho_{12} \end{Bmatrix}$$

APPENDIX B

OCCUPANT SEGMENT POSITION: TWO-DIMENSIONAL MODEL

Referring to figure 6, the absolute position of the mass center of each body segment is given below. L_s and L_H are the lateral distances from the mid-saggital plane to the shoulder and hip joints, respectively.

Segment 1:

(X_1, Y_1, Z_1), the coordinates of the reference point on the body. X_1 and Z_1 are the generalized coordinates q_1 and q_2.

Segment 2:

$$X_2 = X_1 - e_1 \cos \theta_1 + \frac{S (\cos \theta_1 - \cos \theta_2)}{\theta_2 - \theta_1} + e_2 \cos \theta_2$$

$$Y_2 = Y_1$$

$$Z_2 = Z_1 + e_1 \sin \theta_1 + \frac{S (\sin \theta_2 - \sin \theta_1)}{\theta_2 - \theta_1} - e_2 \sin \theta_2$$

Segment 3:

$$X_3 = X_1 - e_1 \cos \theta_1 + \frac{S (\cos \theta_1 - \cos \theta_2)}{\theta_2 - \theta_1} + \rho_2 \sin \theta_2$$

$$+ \frac{\rho_3(\cos \theta_2 - \cos \theta_3)}{\theta_3 - \theta_2} + e_3 \cos \theta_3$$

$$Y_3 = Y_1$$

$$Z_3 = Z_1 + e_1 \sin \theta_1 + \frac{S (\sin \theta_2 - \sin \theta_1)}{\theta_2 - \theta_1} + \rho_2 \cos \theta_2$$

$$+ \frac{\rho_3(\sin \theta_3 - \sin \theta_2)}{\theta_3 - \theta_2} - e_3 \sin \theta_3$$

Segment 4:

$$X_4 = X_1 - e_1 \cos \theta_1 + \frac{S\ (\cos \theta_1 - \cos \theta_2)}{\theta_2 - \theta_1} + \rho_2 \sin \theta_2 - \rho_4 \sin \theta_4$$

$$Y_4 = Y_1 - L_s$$

$$Z_4 = Z_1 + e_1 \sin \theta_1 + \frac{S\ (\sin \theta_2 - \sin \theta_1)}{\theta_2 - \theta_1} + \rho_2 \cos \theta_2 - \rho_4 \cos \theta_4$$

Segment 5:

$$X_5 = X_1 - e_1 \cos \theta_1 + \frac{S\ (\cos \theta_1 - \cos \theta_2)}{\theta_2 - \theta_1} + \rho_2 \sin \theta_2$$

$$- L_4 \sin \theta_4 + \rho_5 \cos \theta_5$$

$$Y_5 = Y_1 - L_s$$

$$Z_5 = Z_1 + e_1 \sin \theta_1 + \frac{S\ (\sin \theta_2 - \sin \theta_1)}{\theta_2 - \theta_1} + \rho_2 \cos \theta_2$$

$$- L_4 \cos \theta_4 - \rho_5 \sin \theta_5$$

Segment 6:

$$X_6 = X_4$$
$$Y_6 = Y_1 + L_s$$
$$Z_6 = Z_4$$

Segment 7:

$$X_7 = X_5$$
$$Y_7 = Y_1 + L_s$$
$$Z_7 = Z_5$$

Segment 8:

$$X_8 = X_1 - \rho_1 \sin \theta_1 + \rho_8 \cos \theta_8$$
$$Y_8 = Y_1 - L_H$$
$$Z_8 = Z_1 - \rho_1 \cos \theta_1 - \rho_8 \sin \theta_8$$

Segment 9:

$$X_9 = X_1 - \rho_1 \sin \theta_1 + L_8 \cos \theta_8 - \rho_9 \sin \theta_9$$
$$Y_9 = Y_1 - L_H$$
$$Z_9 = Z_1 - \rho_1 \cos \theta_1 - L_8 \sin \theta_8 - \rho_9 \cos \theta_9$$

Segment 10:

$$X_{10} = X_8$$
$$Y_{10} = Y_1 + L_H$$
$$Z_{10} = Z_8$$

Segment 11:

$$X_{11} = X_9$$
$$Y_{11} = Y_1 + L_H$$
$$Z_{11} = Z_9$$